Master Thesis

Investigation of Unexpected Dynamic Vessel Response of a SSCV during DP-Operations

Lars-Christian Boll

Technische Universiteit Delft

TU Delft

MARINE CONTRACTORS

Master Thesis

Investigation of Unexpected Dynamic Vessel Response of a SSCV during DP-Operations

by

Lars-Christian Boll

to obtain the degree of Master of Science
at the Delft University of Technology,
to be defended publicly on Wednesday 18, November 2020 at 12:00 AM.

Student number:	4748204	
Thesis number:	SDPO.20.029.m.	
Project period:	February 5, 2020 - November 18, 2020	
Thesis committee:	Ir. K. Visser,	TU Delft
	Dr. ir. A. Vrijdag,	TU Delft
	Dr. H.C. Seyffert	TU Delft
	Ir. R. van Dijk,	Heerema Marine Contractors
	Ir. A. Hakim,	Heerema Marine Contractors

This thesis is confidential and cannot be made public until November 18, 2022.

An electronic version of this thesis is available at `http://repository.tudelft.nl/`.

TU Delft

MARINE CONTRACTORS

Summary

During offshore construction with a Semi-Submersible Crane Vessel (SSCV) the vessel is station keeping by means of Dynamic Positioning (DP). DP enables a vessel to keep position and heading by utilising its own propulsion, while being exposed to the environmental forces caused by waves, wind and current. In a comparison study between offshore measurements and time-domain simulations, an increased vessel/thruster response for the offshore measurement was observed. The results revealed, that in operational environmental conditions (H_s = 0-3 m, V_w < 30 kn & V_c < 3kn), the measured vessel response shows increased oscillations in Surge, Sway & Yaw, with periods of approx. 3-5 min. The goal of this thesis was to determine the causes for such an increased dynamic vessel response, which are not captured in time-domain simulations.

At present, numerical methods and time-domain simulations that assess the DP performance of a vessel (e.g. aNySIM) assume a quasi-static current of which the variation is only caused by the tides. One thesis is, that time-varying currents on a scale of 1 to 5 minutes can cause an increased vessel response. Furthermore, the DP System as it is used onboard is not captured in aNySIM simulations. This means that the characteristics of the DP System onboard are but not represented in full detail in time-domain simulations. Vortex Induced Motion (VIM) has previously been observed to affect multi column floaters. However, the influence on a SSCV during DP-operations has not yet been studied. In this thesis it was investigated, whether the unexpected increased motions originate from time-varying currents, VIM or the DP System itself.

A significant challenge was posed to find current measurement data with a small enough time step to confirm the presence of such time-varying currents. One 45 min current measurement with a sampling rate of 1Hz became available. This measurement shows that time-varying currents on a scale of 1 to 5 minutes exist and cannot be assumed to be quasi-static. More research is required to confirm their presence. However, with this limited available data it was shown that time-varying currents can cause an unexpected motion response of a SSCV during DP-operatios.

In order to obtain the DP System characteristics, a DP Response Amplitude Operator (RAO) assessment was conducted wherein the spring and damping terms were derived as demanded by the controller and as experienced by the vessel. This assessment showed that between 20% to 67% of the demanded critical damping is lost over the control loop of the DP System (including Kalman Filter, Controller, Thruster Allocation and Thrusters). These damping losses cause the vessel to overshoot and the damped natural period to decrease. For critical damping ratios below 0.7 (for surge, sway and yaw) the damped natural period shifts to the range of 3 to 5 minutes.

To determine the effects of VIM, current load tests carried out on the hull of an SSCV have been investigated. It was determined that strong currents on column type floaters can cause fluctuating forces and moments that originate from vortex shedding. Further, with real-time simulations it was demonstrated, that also VIM causes an increased, previously unknown, motion response of a SSCV. Lastly, a method was developed to extrapolate the current load test results to velocities below 2kn. Subsequently, in time-domain simulations it was shown that for current velocities above 0.5kn, the vessel experienced forces and moments that caused it to fluctuate around its setpoint.

Preface

In one of our last meetings before finishing this thesis I was encouraged ”nog even te pieken” to which I jokingly added ”maar zonder demping kwijt te raken” - it will become clearer, once you have read my report. However, I think nothing can better summarize my journey than:

”Keep peaking without losing damping.”

This project started with peaks in the vessel motions, of which the origins were unknown. Similarly, it was unknown to me whether I would be capable of climbing the mountain of successfully finishing my Master studies. Now, standing on the pinnacle of that mountain I can finally enjoy the view and proudly look back at the ascent, which far exceeded my own expectations.

I am thankful for the support I received along the way. Arthur, who helped me to maintain sight of the mountain top on this academic route and who guided me forward on this complex trail. Radboud, who threw me the rope, hard to grasp at times, to assist me in achieving the most challenging sections, when I might have taken the less-challenging detour. Arman, who went above and beyond to support me on this quest and whose encouragement kept me going. To my knowledgeable sherpas of academia, thank you!

Unlike the DP System, I received help to not loose my damping. To Sian, for her unwavering support that prevented me from overshooting. To my parents, who helped me to slow down when I was oscillating. Danke für alles!

I would also like to thank Klaas Visser for his insights and suggestions on this project and chairing this thesis; as well as Harleigh Seyffert for joining my defence committee. Additionally, I want to thank the Heerema Simulation Center Team, who remotely assisted me to use the full-scale simulator by myself and carried simulations out for me while quarantined. Finally, big thanks to my housemates for keeping me grounded with the occasional shenanigans and good food!

Euer Freund von der Spinatalm, ***Lars-Christian***

Nomenclature

Acronyms

ADCP Acoustic Doppler Current Profiler

API Application Programming Interface

CFD Computational Fluid Dynamics

COG Center of Gravity

CP Control Point

DCSM Dutch Continental Shelf Model

DCV Deepwater Construction Vessel

DGPS Differential GPS

DNVGL Det Norske Veritas Germanischer Lloyd

DOF Degrees of Freedom

DP Dynamic Positioning

DPR Daily Progress Report

EDS Energy Density Spectrum

EOM Equation of Motion

FPSO Floating Production Storage and Offloading

GNSS Global Navigation Satellite Systems

GPS Global Positioning System

HLV Heavy Lift Vessel

HMC Heerema Marine Contractors

HPR Hydro acoustic Position Reference

HSC Heerema Simulation Center

K-IMS Kongsberg Information Management System

K-POS Kongsberg Dynamic Positioning System

LIDAR Light Detection and Ranging

LPF Low-Pass Filter

LTW Light Taut Wire

MARIN Maritime Research Institute Netherlands

MPC Model Predictive Control

NBV New Build Vessel

PID Proportional-Integral-Derivative

PMS Power Management System

USBL Ultra Short Base Line

RAO Response Amplitude Operator

RMS Root Mean Square

ROV Remotely Operated Vehicle

RP Reference Point

RPM Revolutions Per Minute

SDA Significant Double Amplitude

SISO Single Input Single Output

SSCV Semi-Submersible Crane Vessel

TLP Tension Leg Platform

TMS Tether Management System

UTM Universal Transverse Mercator

VIM Vortex Induced Motion

VIV Vortex Induced Vibration

VRU Vertical Reference Unit

WFZ Wind Farm Zone

WSA Water and Shipping Authority

WTG Wind Turbine Generator

Contents

1 Introduction

When introduced in 1961, the first Dynamic Positioning (DP) vessel ”Eureka” made history for the offshore industry. Eureka was equipped with two steerable thrusters, a taut wire and a gyroscopic compass [1]. More than half a century later, Dynamic Positioning has become indispensable to the offshore industry. As for Heerema Marine Contractors (HMC), all of its vessels are equipped with a DP System. HMC is a heavy lifting market leader that keeps pushing the boundaries of what is possible during DP-operations. This is exemplified by the successful execution of the first free floating QUAD lift in October 2018 [2].

(a) Eureka

(b) SSCV Thialf & Balder performing the first QUAD Lift

Figure 1.1: Offshore Evolution

The QUAD lift aims to increase the overall lifting capacity by using 2 Semi-Submersible Crane Vessel (SSCV)s, a total of 4 cranes. This method can be used to lift loads of up to 30.000 mT, thus reducing offshore hook-up and commissioning time. The difference to previously executed offshore lifts with multiple vessels, is that the QUAD lift will be conducted with both involved SSCVs while station keeping by means of DP [2]. During lifting operation, when connected to a fixed or floating object, unwanted instabilities of the DP system may occur. When two vessels are used to lift the same load, the risk of an DP-instability increases further. Until then, solutions have proven to be inadequate for a 2 vessel synchronous move with a suspended object. For this reason, at HMC, the development of a High Kalman Filter was initiated and subsequently, in a joint effort with Kongsberg Maritime, further developed and implemented [3].
To use this method in practice, it first required approval and certification by the Det Norske Veritas Germanischer Lloyd (DNVGL). For this reason, separate tests were carried out with the SSCV Thialf in May 2017. Amongst other tests, three two-hourly station keeping tests were conducted. In those three tests, the three controller gains (Low, Medium & High) were tested respectively with the High Kalman Filter Gain activated. In a post-processing step, the measurement data of these three tests were compared to a time-domain simulation of each test respectively in order to validate these numerical tools. These results revealed a discrepancy between offshore measurements and simulations of the DP Performance and vessel response. This observation marks the initiator for this Master Thesis.

1.1. Problem Statement

The foundation of the problem is the observed discrepancy between offshore measurements and simulations of the DP Performance of the SSCV Thialf. In operational environmental conditions (H_s = 0-3 m, V_w < 30 kn & V_c < 3kn), the measured vessel response does not match the simulation as can be seen below in figure 1.4, where a larger low-frequency vessel excitation of the offshore measurements is demonstrated. As mentioned before, in the offshore test campaign and in the simulations for the comparison study the three controller gains (Low, Medium & High) were tested [4]. The results below show the Medium Gain comparison (Test 5B). The simulations were executed with the time-domain software aNySIM. The following environmental parameters in table 1.1 show the offshore observations and simulation input for Test 5B (High Kalman Filter Gain & Medium Controller Gain). Note that for the Offshore Measurements and aNySIM different coordinate systems are used, refer to figure 1.3 for clarification.

		Offshore Measurement	aNySIM Simulation
Vessel	Kalman Filter Gain	High	High
	Controller Gain	Medium	Medium
	Draft	26.5 m	26.6 m
	Heading	63 deg	0 deg
Environment	Water Depth	89 m	infinite
	Wind Velocity	5 ± 2 m/s	measured (Fig 1.2)
	Wind Direction (cf)	256 ± 15 deg	173 ± 15 deg (Fig 1.2)
	sig. Wave Height H_s	0.7 m	0.7 m
	Peak period T_p	6s	6s
	Wave direction (cf)	North	63 deg
	Spectrum		JONSWAP (γ = 2)
	Current Velocity	approx. 0.7 m/s (Fig 1.2)	constant 0.7 m/s
	Current Direction (gt)	approx. 272 deg (Fig 1.2)	151 deg

Table 1.1: Test 5B: Vessel Parameter and Environment as observed (Offshore Measurement) and simulated (aNySIM Simulation)

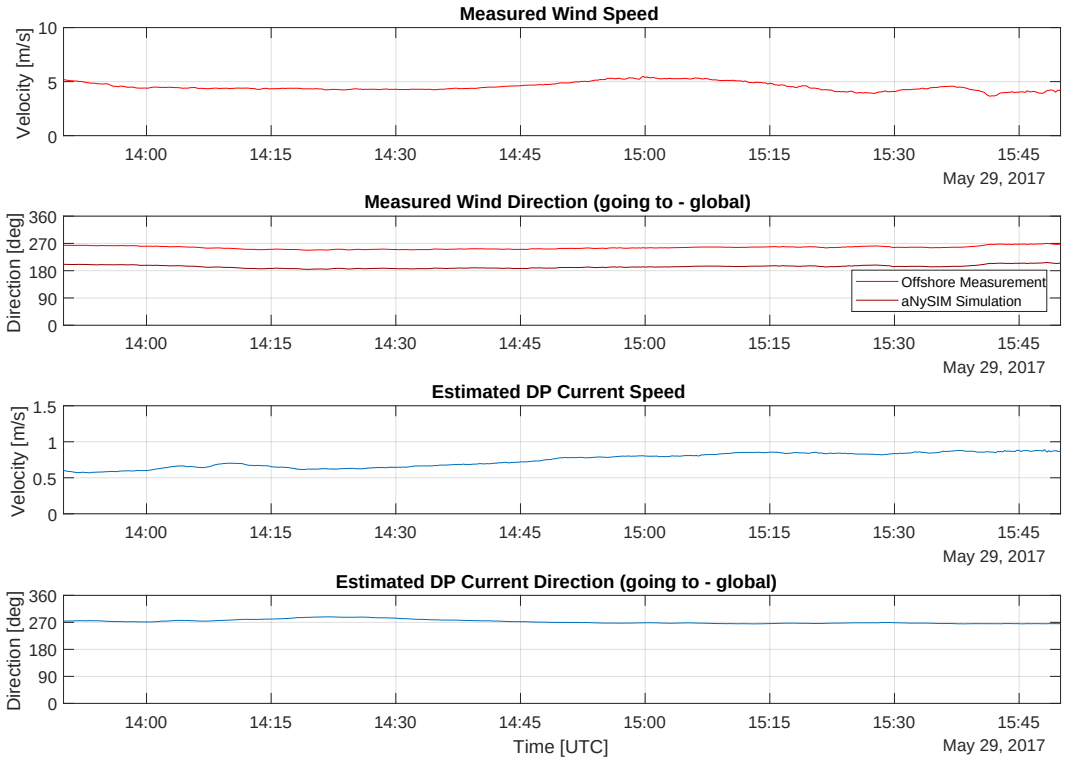

Figure 1.2: Test 5B: Wind and DP Current as obtained from DP System

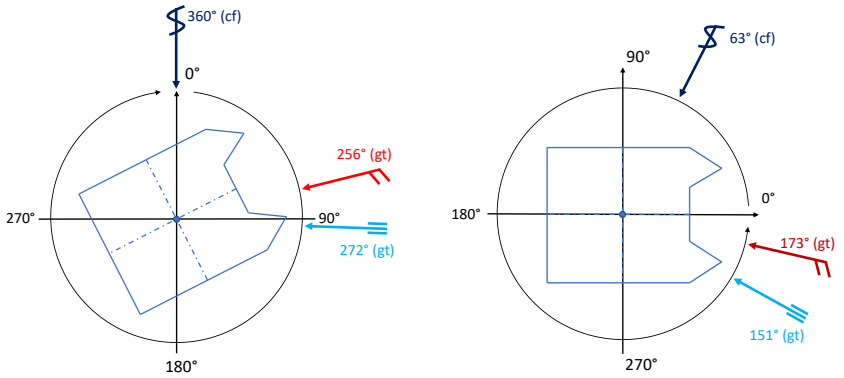

(a) Offshore Measurement (b) aNySIM Simulation

Figure 1.3: Test 5B: Coordinate Systems from Offshore Measurements and as used by aNySIM

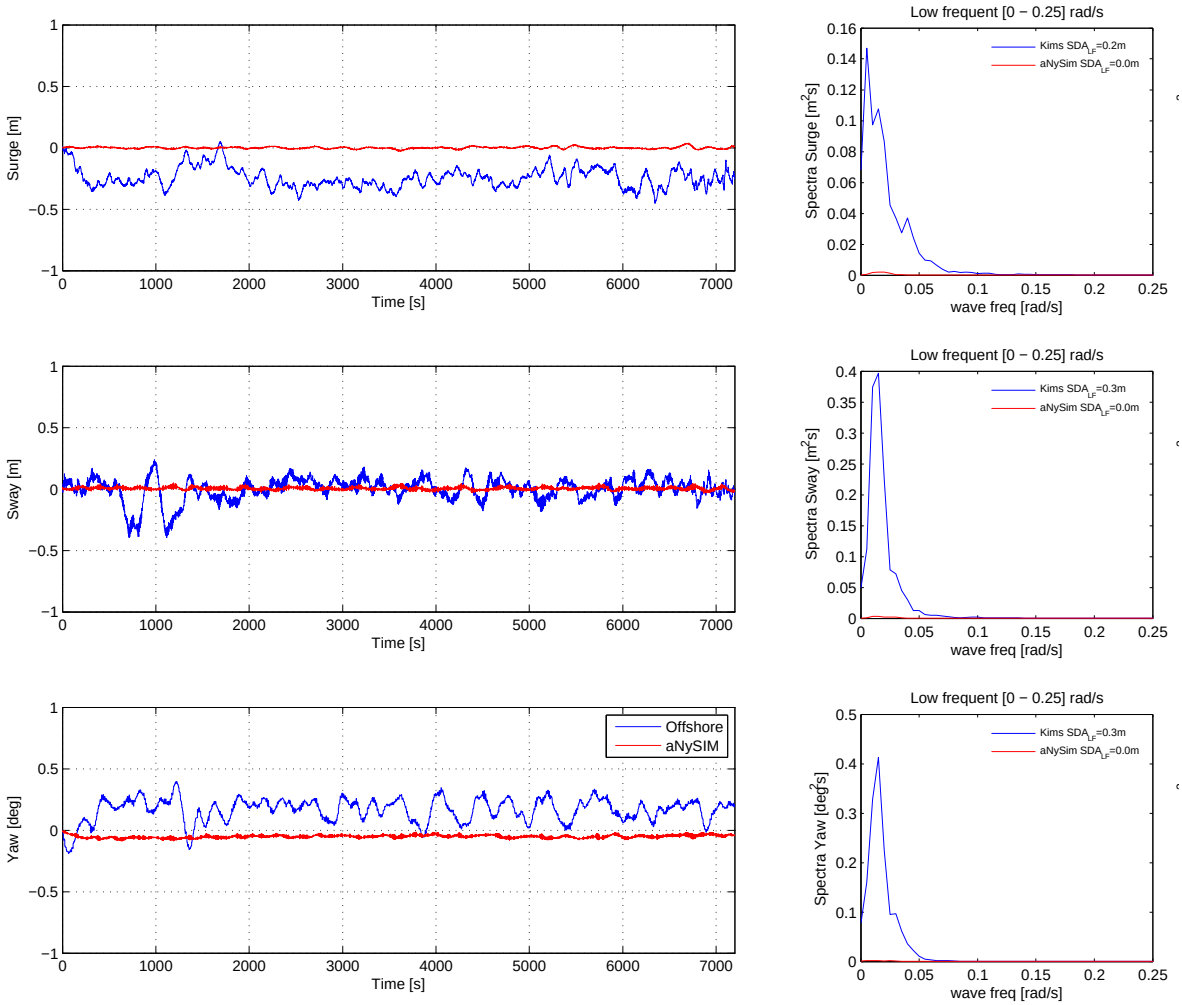

(a) Vessel Motion Time Trace (b) Vessel Motion Energy Density Spectrum

Figure 1.4: Comparison between measured offshore vessel motions and simulated vessel motions (aNySIM) with High Kalman Filter Gain and Medium Controller Gain exposed to constant current, measured wind and waves (refer to table 1.1)

Although not shown here, an unexpected response is not only observed in the vessel motions but also in the thruster response. This increased thruster response eventually causes oscillations in the vessel movements (Surge, Sway & Yaw), with periods of approx. 3-5 min.

The origin of what is causing the increased response compared to time-domain simulations, is currently unknown. At present, numerical methods and time-domain simulations that assess the DP performance of a vessel (e.g. aNySIM) assume a quasi-static current of which the variation is only caused by the tides. This is in the order of hours instead of minutes. The offshore measurements suggest an influence on the DP System and the resulting vessel response, currently not captured in time-domain simulations. This becomes even more notable as low frequent second order wave forces and wind loads are included in the time domain simulations.

This increased response can possibly originate from:

- Variability in the currents on a scale of 1-5 minutes
- DP System itself (Position Measurement, Kalman Filter, Controller, Thrust Allocation & Thrusters)
- Vortex Induced Motion (VIM) on the columns of the hull of the vessel

Position offsets, as observed of up to 0.5 m, do not yet represent a severe risk in an installation or decommissioning project. Nonetheless, the dynamic behavior of the DP-system remains not fully understood. Substantial research is required to understand this particular dynamic vessel behavior, especially as projects are becoming increasingly complex. HMC was awarded the installation of 27 *MHI Vestas V174-9.5MW* wind turbines for the Wind Park Arcadis Ost in the Baltic Sea. Specifically for this project, a floating installation method was developed [5]. In 2018, HMC demonstrated that a free floating Wind Turbine Generator (WTG) installation is possible. Yet, when a SSCV is scheduled to install 27 WTGs in water depths of 20 to 30 m, the accuracy of the DP system is of great importance. The position offsets of the DP system and its accuracy are 'given' parameters and require a different approach to be able to administer improvement. Establishing the cause of the increase to the DP footprint for specific environmental conditions is highly beneficial and can be considered in the project planning. Thus, the DP Performance and the origin of the discrepancy must be investigated.

1.2. Research Objective

The observations outlined in the problem statement and the importance of this research for the industry and HMC in particular, lead to the research question and the following sub-questions:

What causes the increased dynamic Vessel/Thruster response of a SSCV while station-keeping in operational conditions and is not captured in time-domain simulations?

- Does a variability of the currents on a scale of 1 to 5 minutes exist?
- If yes, what would be the influence on the vessel response?
- If not, what other possible causes can trigger the observed vessel response?
- How can these possible causes be assessed and simulated?

1.3. Report Structure

This Master Thesis describes the research conducted to investigate the causes of an unexpected dynamic vessel/thruster response of a SSCV. The introduction outlines the objectives of this project, identifies the areas of interest and establishes the relevance of this work in the field. The second chapter describes the background on the underlying principles of Dynamic Positioning, environmental influences and the required hydrodynamics and basis of modelling. This project is an investigation with three major considered factors. Research was undertaken to determine whether fast time-varying currents exist, if the unexpected response originates from the DP System and whether the effect of vortex induced motion causes the outlined vessel/thruster response. Therefore, chapter 3, 4 & 5 describe each aspect separately, with methodology and results. In chapter 6 a method is presented to extrapolate fluctuating current loads from current load test results to lower velocities and the effect on a SSCV in these conditions presented. Additionally in chapter 7 an overview of all determined caused and an approach to determine their relative contribution to the overall response is shown. In the last chapter, the conclusions of this thesis are drawn plus further work and research recommended.

2
Background

2.1. Dynamic Positioning

Dynamic Positioning enables a vessel to keep position and heading by utilising its own propulsion, while being exposed to the environmental forces caused by waves, wind and current. The position is measured by multiple position reference systems and the measured offset from the setpoint is then translated into required forces and moments. This is necessary to relocate the vessel to the previously selected position and heading. The required forces are then allocated to the thrusters, which initiate the vessel to move through water. Figure 2.1 depicts vessel motions (orange), environmental loads (red) and thruster forces (green) as experienced by the vessel and relevant for a DP system. Vessel motions are a result of environmental forces acting on the body as well as the forces exerted by the propulsion system. These movements in six Degrees of Freedom (DOF) are identified as: Surge, Sway, Heave, Roll, Pitch and Yaw. Surge, Sway and Heave are linear movements along the x,y & z-axis; Roll, Pitch and Yaw constitute the rotations about these axis respectively. In figure 2.1 indicated in orange are only Surge, Sway and Yaw as these are the only linear and rotational components a DP system can control.

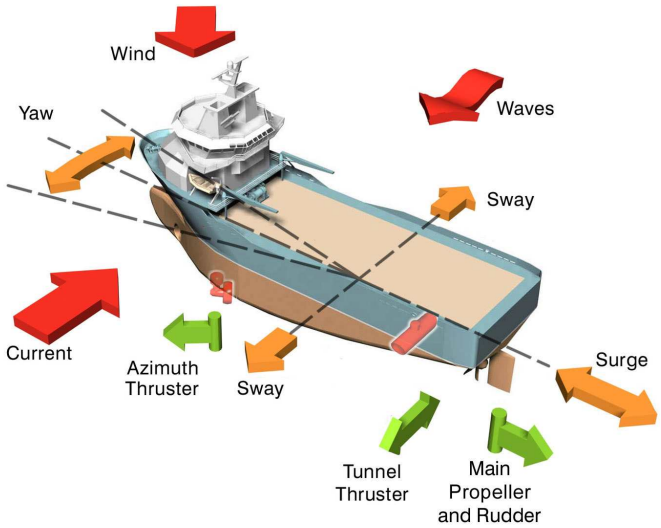

Figure 2.1: Vessel Motions, Environmental Loads & Thruster Forces of a DP System [6]

Figure 2.2 depicts a simplified DP system, which is used to outline the working principle. Disturbances, such as waves, wind, currents or external forces act upon the vessel, causing it to move. The position is measured by multiple reference systems and sensors. With the required position (and heading) selected by the operator the position error is determined. The Kalman Filter serves as a filter to remove noise in the signal and predicts the state of the vessel based on a trade-off between a dynamic model and the position measurements. The controller calculates the required forces and moments based on the position error and estimated velocity. These required forces and moments must be distributed and translated into RPM and Azimuth for each thruster individually. The thrusters provide the thrust to cause the vessel to counteract the disturbances and consequently allow the repositioning of the vessel.

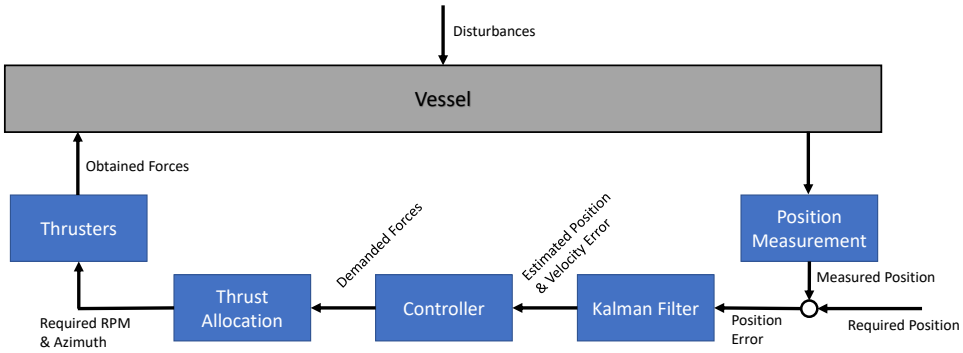

Figure 2.2: Simplified Diagram of a DP System [3]

Further information on the components of the DP system control loop is provided in chapter 4.

2.2. SSCV Thialf

The SSCV Thialf, which most of this research is based on, is a Deepwater Construction Vessel (DCV) capable of a 14.200 tonnes tandem lift. The vessel built in 1984 has 2 floaters with 4 columns each and can vary its draught from 11.8 to 31.6 m, while ballasting with up to 20.800 m^3/hour. Thialf, which can be seen in figure 2.3 below, is equipped with a Class III DP System, has an overall length of 201.6 m and a width of 88.4 m [7]. Until the delivery of its bigger sibling SSCV Sleipnir in 2019, with a maximum combined lift capacity of 20.000 tonnes, Thialf was the largest and most capable crane vessel in the world.

Figure 2.3: SSCV Thialf in transit [8]

2.3. Environmental influences

Any seagoing vessel or platform is exposed to the harsh environments due to currents, wind and waves. Especially for station keeping operations these forces determine the vessel performance.

2.3.1. Current

Currents in the ocean have different origins of occurrence. Tidal currents are caused by the cyclical change of the lunar and solar gravity. Currents are also caused by ocean circulation, wind and the difference of sea water density. For a current that is assumed to be constant with water depth, the forces and moments on a vessel, depending on the direction of a current direction can be calculated by [9]:

$$F_{x,c} = \frac{1}{2}\rho \cdot V_{rc}^2 \cdot C_{Fx,c}(\alpha_{rc}) \cdot A_T(T) \tag{2.1}$$

$$F_{y,c} = \frac{1}{2}\rho \cdot V_{rc}^2 \cdot C_{Fy,c}(\alpha_{rc}) \cdot A_L(T) \tag{2.2}$$

$$M_{z,c} = \frac{1}{2}\rho \cdot V_{rc}^2 \cdot C_{Mz,c}(\alpha_{rc}) \cdot A_L(T) \cdot L \tag{2.3}$$

Where:

$F_{x,c}$	=	Uniform longitudinal current force	[N]
$F_{y,c}$	=	Uniform lateral current force	[N]
$M_{z,c}$	=	Uniform yaw current moment	[Nm]
ρ	=	Density of water	[kg/m^3]
V_{rc}	=	Relative current velocity	[m/s]
α_{rc}	=	Relative current direction	[rad]
$A_T(T)$	=	Submerged transverse projected area dependent on T	[m^2]
$A_L(T)$	=	Submerged lateral projected area dependent on T	[m^2]
L	=	Submerged Length of vessel	[m]
T	=	Draught of vessel	[m]
$C_{Fx/Fy/Mz,c}(\alpha_c)$	=	Current load coefficient dependent on α_c	[-]

2.3.2. Wind

Wind is a mass flow of air that exists as a result of a flow from high to low pressure areas. The direction of wind is dependent on these high and low pressure areas. Winds have fluctuations in both direction and velocity, also known as gusts. For a DP System, strong gusts can cause an offset and require time for the vessel to react. This effect can be diminished by the help of Wind-Feed Forward, where the measured wind is forwarded to the DP system and, based on a model, the forces estimated.
Winds are typically represented with a direction and an average velocity at a height of 10 meters above the ground or sea level. As presented in [9], an acceptable representation of the wind speed and direction at a given height 'z':

$$\frac{V_{tw}(z)}{V_{tw}(10)} = \left(\frac{z}{10}\right)^{\mu} \tag{2.4}$$

Where:

z	=	Height in meters above surface
$V_{tw}(z)$	=	True wind speed dependent on z
$V_{tw}(z)$	=	True wind speed at 10 m above surface
μ	=	Nondimensional exponent, 0.11 (at sea) & 0.18 (on land)

Wind acts directly on the structures above sea level of a floating body causing it to move due to the flow of air around them. Similarly to the current loads, the forces and moments of the relative wind velocity are given by [9]:

$$F_{x,w} = \frac{1}{2}\rho_{air} \cdot V_{rw}^2 \cdot C_{Fx,w}(\alpha_{rw}) \cdot A_T \tag{2.5}$$

$$F_{y,w} = \frac{1}{2}\rho_{air} \cdot V_{rw}^2 \cdot C_{Fy,w}(\alpha_{rw}) \cdot A_L \tag{2.6}$$

$$M_{z,w} = \frac{1}{2}\rho_{air} \cdot V_{rw}^2 \cdot C_{Mz,w}(\alpha_{rw}) \cdot A_L \cdot L \tag{2.7}$$

Where:

$F_{x,w}$	=	Steady longitudinal wind force	[N]
$F_{y,w}$	=	Steady lateral wind force	[N]
$M_{z,w}$	=	Steady wind current moment	[Nm]
ρ_{air}	=	Density of air	[kg/m^3]
V_{rw}	=	Relative wind velocity	[m/s]
$\alpha_r w$	=	Relative wind direction	[rad]
A_T	=	Projected transverse area	[m^2]
A_L	=	Projected lateral area	[m^2]
L	=	Length of vessel	[m]
$C_{Fx/Fy/Mz,w}(\alpha_{rw})$	=	Wind load coefficient dependent on α_{rw}	[-]

2.3.3. Waves

The generation of waves in the ocean have multiple origins. Wind waves are created by the interaction between wind and the water surface. Waves can be generated by the motion of all kinds of floating vessels. Tidal waves are generated by astronomical forces. Waves are also created by landslides and earthquakes, tsunamis. This section is based on [9].

Wind driven waves are created as a result of the interaction of the sea surface and wind. The height of wind driven waves are dependent on three factors. First, the wind speed, which must be faster then the crest in order to transfer more energy. Secondly, the fetch length, which is the distance over which the wind stays constant in terms of direction and speed. Thirdly, the duration of the wind. Despite the fact that wind generated waves are highly irregular, they can be represented as multiple regular waves. This is called superposition and is clearly depicted in figure 2.4. This concept simplifies the analysis of wave systems. Wind waves can be separated in Sea and Swell Waves.

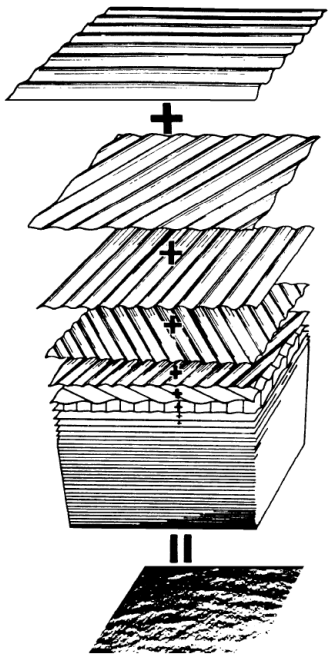

Figure 2.4: Superposition of waves [10]

The highly irregular sea waves are predominantly influenced and generated by a local wind field. The crest length of these waves is two to three times the apparent wave length. Sea waves are very short and sharp crested. Their direction spreads wider and is more deviated. Swell waves are more predictable in terms of height and have longer crests, up to even 6 - 7 times the wave length. Swell waves travel over several hundred kilometers from where they have been generated and can propagate into areas of calm winds.

First Order
First order wave loads cause an oscillating displacement of the vessel or structure, at frequencies corresponding with the frequencies of waves. Averaged over time, first order wave motions have a zero mean. These high frequent motions are filtered by the Kalman Filter, such that the DP System is not reacting upon first order wave excitation.

Second Order
Second order wave drift forces become most apparent when a floating structure is moored or station-keeping by means of DP. They consist out of two components, the mean wave drift force, which originates from non-linear wave potential effects and low-frequency wave drift forces. Combined with the spring characteristics of the DP System low-frequency wave drift forces cause an oscillating displacement of the structure.

2.4. Vortex Induced Motion

The hull of a semi submersible crane vessel consists of multiple columns with a pontoon attached at the bottom. This type of hull has the benefit of a smaller water plane area and, as a consequence, lesser wave interaction. However, those columns also introduce the possible risk of VIM. In this section, the underlying principles of Vortex Shedding and VIM is outlined, while in chapter 5 more information is presented on VIM on SSCVs.

2.4.1. Vortex Shedding

When a body is exposed to undisturbed flow, it will experience lift and drag forces acting on the body (for Rn-numbers > 65). This can result in vortices to shed behind the body and a resultant force in the direction of which the vortex detaches. For a cylindrical structure, this phenomena can be seen simplified in figure 2.5 [9].

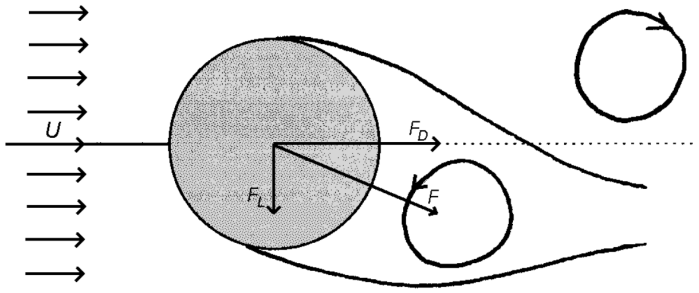

Figure 2.5: Resultant forces of vortex shedding [9]

In the figure above, the force created by the vortex can be seen decomposed in the two components of a lift and drag force. These are the components that can cause bodies to move and is referred to as vortex induced motion. As the shedding of vortices takes place alternately on each side perpendicular to the flow, so will the magnitude of the lift force. The drag force, which is parallel to the undisturbed flow direction and the alternating lift force based on vortex shedding, both per unit of cylinder length, are defined as:

$$F_D = \frac{1}{2}\rho U^2 \cdot C_D \cdot D \tag{2.8}$$

$$F_l = \frac{1}{2}\rho U^2 \cdot D \cdot C_L \cdot sin(2\pi f_s t + \epsilon_{Ft}) \tag{2.9}$$

Where:

F_D	=	Draf force per unit cylinder length	[N/m]
F_l	=	Lift force per unit cylinder length	[N/m]
ρ	=	Mass density of the fluid	[kg/m^3]
U	=	Undisturbed flow velocity	[m/s]
D	=	Cylinder diameter	[m]
C_D	=	Dimensionless drag coefficient	[-]
C_L	=	Dimensionless lift coefficient	[-]
f_s	=	Vortex shedding frequency	[Hz]
t	=	time	[s]
ϵ_{Ft}	=	Phase shift	[rad]

The frequency at which vorticies detach from a (cylindrical) body is defined by:

$$f_s = \frac{St \cdot U}{D} \tag{2.10}$$

in which:

f_s	=	Vortex shedding frequency	[Hz]
St	=	Strouhal number	[-]
U	=	Undisturbed flow velocity	[m/s]
D	=	Cylinder diameter	[m]

The non-dimensional Strouhal number, St, is dependent on the Reynolds number Rn and can be obtained for circular cylinders from figure 2.6 [11]. For $Rn > 10^2$ and $Rn < 2.10^5$ the Strouhal number can be approximated with 0.2. For larger Reynolds numbers, the Strouhal number increases and the force fluctuations become irregular,therefore the Strouhal number becomes difficult to define [9]. In this research almost square columns with Reynolds numbers ranging from $Rn = 1 \cdot 10^7$ to $Rn = 5 \cdot 10^7$ are considered. The Reynolds number is defined as:

$$Rn = \frac{V \cdot D}{\nu} \tag{2.11}$$

in which:

Rn	=	Reynolds number	[-]
V	=	Flow velocity	[m/s]
D	=	Pipe diameter / characteristic length	[m]
ν	=	Kinematic viscosity of the fluid	[m^2/s]

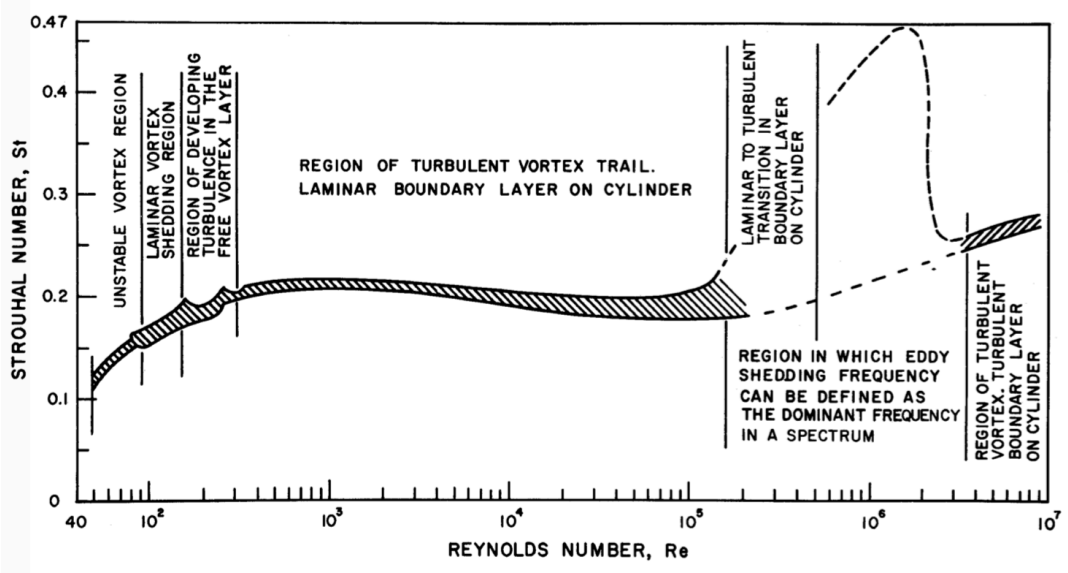

Figure 2.6: Strouhal-Reynolds number relationship for circular cylinders [11]

2.4.2. Vortex Induced Oscillation

As a result of vortex shedding, the alternating lift force as presented in equation 2.9, can cause an object to oscillate. When the vortex shedding frequency f_s and the natural frequency of the body f_n approach each other, resonance will occur. Lock-in occurs, when the vortex shedding frequency coincides with the object natural frequency. An indicator for resonance is the non-dimensional reduced velocity. Once the natural oscillation frequency of a structure is known, the reduced velocity can be obtained in order to assess the risk of resonant vortex-induced oscillations. For a cylinder lock-in usually occurs for $U_r = 5$ and will ultimately stop at $U_r > 7$ [9].

$$U_r = \frac{U}{f_n \cdot D} \tag{2.12}$$

in which:

U_r	=	Reduced velocity	[-]
U	=	Undisturbed flow velocity	[m/s]
f_s	=	Natural frequency	[Hz]
D	=	Cylinder diameter	[m]

2.5. Representation and Simulation

2.5.1. Spectral Analysis

A time record of a measured quantity (e.g. force, distance, angle) is often irregular and contains different frequencies. Vessel motions, for instance, are a result of forces and moment exerted on the vessel by outer influences as well as forces and moments caused by the propulsion system of the vessel itself. As previously mentioned, a sea state consists of irregular waves, which is a superposition of multiple regular waves. Similarly, vessel motions are irregular and are a superposition of multiple regular motion components with their own frequency characteristics. These motions in all six DOF or forces occur over time and when monitored or simulated, a time record of these motions can be obtained. This is also known as the time-domain, where a signal and its change are dependent on time. With Fourier series analysis an irregular motion can be expressed as the sum of regular motion components, each with its own frequency and amplitude in the frequency domain. This can be done with a energy density spectrum, where the energy content of a signal at each of its frequencies is represented over a specific frequency band. For a time signal $x(t)$, the energy spectrum $S_x(\omega)$ is defined as [9]:

$$S_x(\omega_n) \cdot d\omega = \frac{1}{2} x_{a_n}^2 \tag{2.13}$$

The variance σ_x^2 of the signal $x(t)$ is equal to the area under the spectrum:

$$\sigma_x^2 = \int_0^\infty S_x(\omega) \cdot d\omega \tag{2.14}$$

which is also equal to the 0th moment of the area under the spectrum m_{0x} with respect to the vertical axis at $\omega = 0$. This signifies that the Significant Double Amplitude (SDA) can be defined as follows, similar to the significant wave height:

$$SDA = 4 \cdot \sqrt{m_{0x}} \tag{2.15}$$

The relation between the frequency and time domain as well as the energy density spectrum can seen visualized in figure 2.7 below. This figure represents the analysis of recorded irregular ocean surface waves $\zeta(t)$.

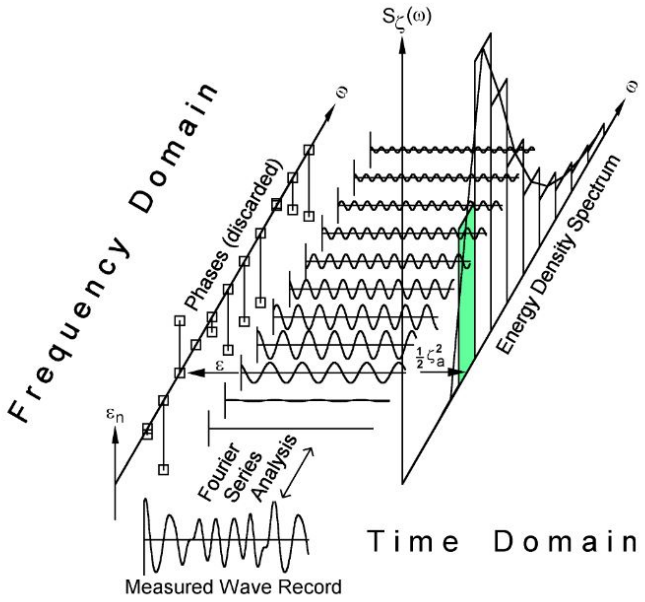

Figure 2.7: Wave Record Analysis - Relation between Time & Frequency Domain [9]

2.5.2. Time-Domain DP Simulation

This section is based on [12] and [13], which both are based on the time domain simulation software aNySIM by Maritime Research Institute Netherlands (MARIN).

aNySIM

Developed in the Netherlands, aNySIM is a multibody time-domain simulation program by MARIN, which is used in this research for DP performance analysis. With aNySIM, analysis of multi body dynamics can by carried out by calculating the response of floating bodies due to mechanic and hydromechanic forces for 6 DOF. The modules of linear and non-linear hydrostatics, wave forces (1st & 2nd order), coefficient based wind and current loads, wave radiation, Morrison loads, propellers, rudders & thrusters, DP controllers and Kalman filter are included in aNySIM XMF. Required inputs are geometry, inertia & stability, a (multi-body) hyd-file, wind, wave & current and the method for station keeping. As an output, time traces of for example vessel motions, environmental loads and thruster rpm & azimuth can be obtained.

Instead of the implemented DP Module, an alternative approach for time-domain DP simulations is the Spring-Damper model. The vessel and the DP system can be seen as a mass-spring-damper model in 3 DOF. For the 3 controller gain settings of High, Medium and Low, different spring stiffness and damping coefficients are selected. The Spring-Damper model can be regarded as a linearized ideal DP system, which is beneficial when comparing two simulation results with each other. Figure 2.8 below indicates the working principle of the Spring-Damper module of aNySIM.

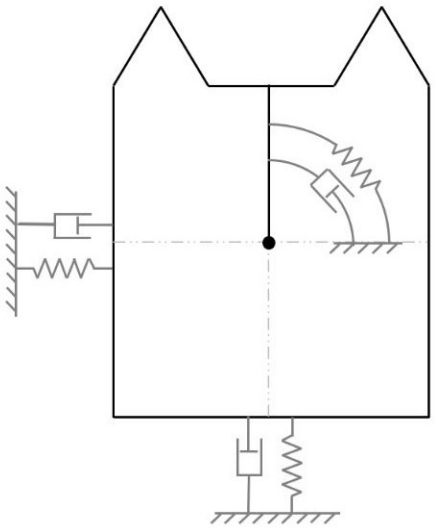

Figure 2.8: aNySIM Spring-Damper Model

2.5.3. Heerema Simulation Center

HMC has a full mission Kongsberg simulator, the Heerema Simulation Center (HSC). It is equipped with a bridge, 3 main DP consoles and 1 back-up to guarantee DP III class. In addition, 2 crane domes, a ballast control room, 2 deck position rooms, winch control room and 2 instructor stations form part of the HSC. This enables HMC to simulate the scope of work of their projects and provide training for the crew. It is possible to simulate all of HMC Heavy Lift Vessel (HLV) (Aegir, Balder, Thialf and Sleipnir). In this research, the HSC is used to assess the station keeping performance of the SSCVs Thialf in real time, using the Kongsberg DP System with access to the same DP-settings as onboard the vessel.

Figure 2.9: Main Bridge of Heerema Simulation Center

3
Variation of Currents

3.1. Existence of fast-varying currents

According to [9], the variation of currents are of a slow nature and are assumed to be constant in engineering applications. However, as the possible variation of currents may be the origin of the unexpected increased variation, this requires further investigation.

Next to the dominant variation based on the tides, currents in coastal areas are not uniform but vary in space. Current velocity along the coastline is slower than further away from the coast. This is a result of the friction that the water is exposed to. Similarly, the sea floor is a barrier and causes the currents along the seafloor to decrease in speed. Therefore, we can expect the velocities on the surface to be the fastest, as the boundary of the sea floor is the furthest away. To highlight this variability, in 2007, the Water and Shipping Authority (WSA) Bremen conducted a measurement over the width of the Weser on kilometer 28,5 during low-tide. The results can be seen in figure 3.1. A fluctuating velocity field, with decreasing velocities towards the boundaries at the side and bottom is present. The irregular fluctuation do not appear to follow any law, which is ultimately linked to the fact that currents in nature are turbulent. A flow is not formed of separate layers on top of each other. Instead, this is a process of continuous mixing between the velocity layers due to large and small eddies [14].

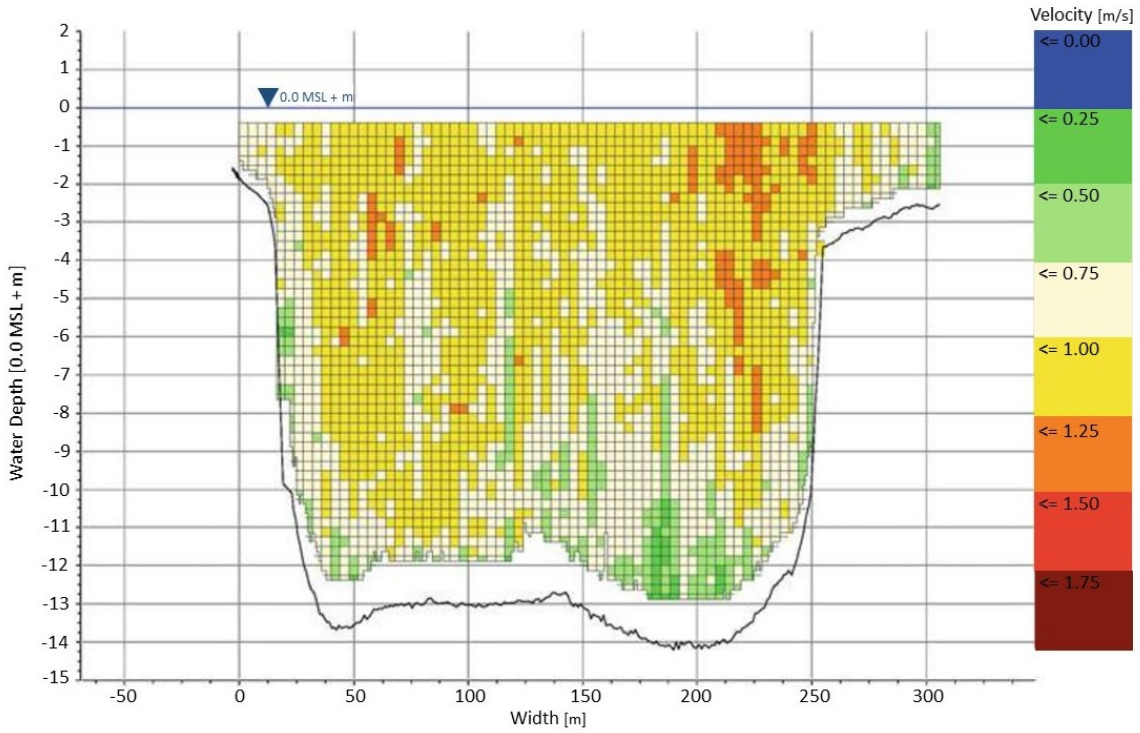

Figure 3.1: Cross section of the instantaneous velocity profile in the Weser at km 28,5 on 20.09.2007 during 10:27AM low tide measured with an ADCP (10:25:33AM to 10:28:55AM) [14]

It must be noted that the measurements obtained as seen in figure 3.1, originate from the estuary of the Weser flowing into the North Sea. In an estuary, the tidal dynamic has the largest influence on the currents. However, it is only one of the present physical processes. Together with wind induced waves, the resulting currents transport salt, solid materials and heat. In the brackish water zone, the freshwater from the river mixes with the saltwater. The fluvial sediments mix with sediments of marine origin. Temperature, salt and solid material content affect the density of the water, which, in a coupled process, influences the currents [14]. Although an estuary is not a typical project location for a SSCV, these measurements highlight the occurrence of irregular velocity fluctuations with differences of up to 1 m/s throughout the water column.

Upon recommendation of *Deltares*, public available data of a field test in the North Sea was investigated. The measurements were conducted in the Wind Farm Zone (WFZ) *Ten Noorden van den Waddeneilanden*, which is approx. 56km north of the Dutch Island Ameland. The meteorological and oceanographic data was obtained using a Seawatch Wind Light Detection and Ranging (LIDAR) Buoy, which provided data from August 2019. To measure the current velocities and direction an *AquaDopp current profiler*, also known as an Acoustic Doppler Current Profiler (ADCP), is mounted on the bottom of the hull of the buoy. An ADCP emits sound pulses that are reflected onto particles in the water. The Doppler Shift can determine the velocity of these particles. This velocity is measured along the angle of the beam, with which the transducers are mounted and the vertical and horizontal components of the velocity need to be computed. Subsequently, multiple pulses are used to calculate the current velocity with a ten minute average [15].

Figure 3.2 shows an energy density spectrum of the current velocity over the first 22 days of August 2019 at the above mentioned location. The top graph represents the very low frequencies from 0 to 0.001 rad/s, in order to better represent the contribution of the frequency range from 0.001 to 0.025 rad/s. It can be also observed that the indicated Nyquist frequency and a 5 minute mark at 0.0209 rad/s. The resolution of these measurements are in ten minute time steps, meaning that no conclusions on a possible variation of currents on a scale of one to five minutes can be drawn. However, this data does show that variations exist and current is not only quasi-static. Contacting *Fugro Norway* to obtain the raw data of these measurements proved unsuccessful. Therefore, further data is required to be able to assess the vessels behaviour under possible present varying currents.

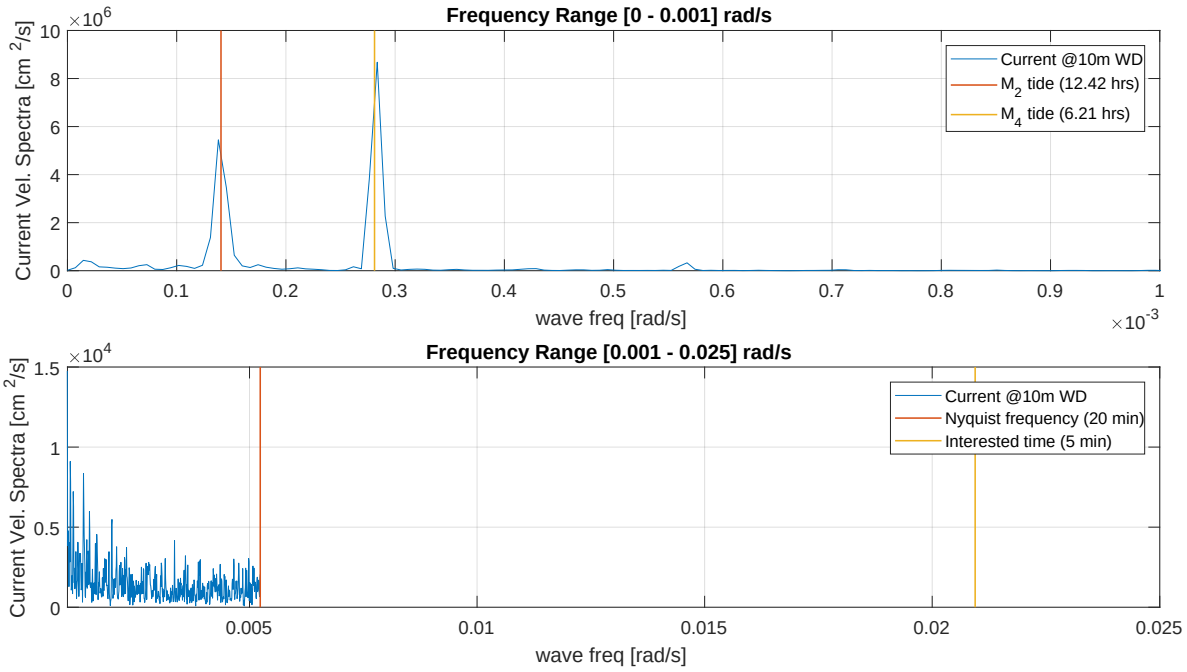

Figure 3.2: Density Spectrum of Current Velocity at 10m water depth at *Ten Noorden van den Waddeneilanden*

The project locations of HMC are infrequently in or near estuaries or the coast. The observation of the unexpected vessel response in May 2017 occurred in the North Sea at 54° 01' 00" N, 01° 50' 5" E. This area is also known as the Outer Silver Pit, which is part of a subsea crater formation with water depths of up to 100m south of the Dogger bank. For further reference, please see figure 3.3.

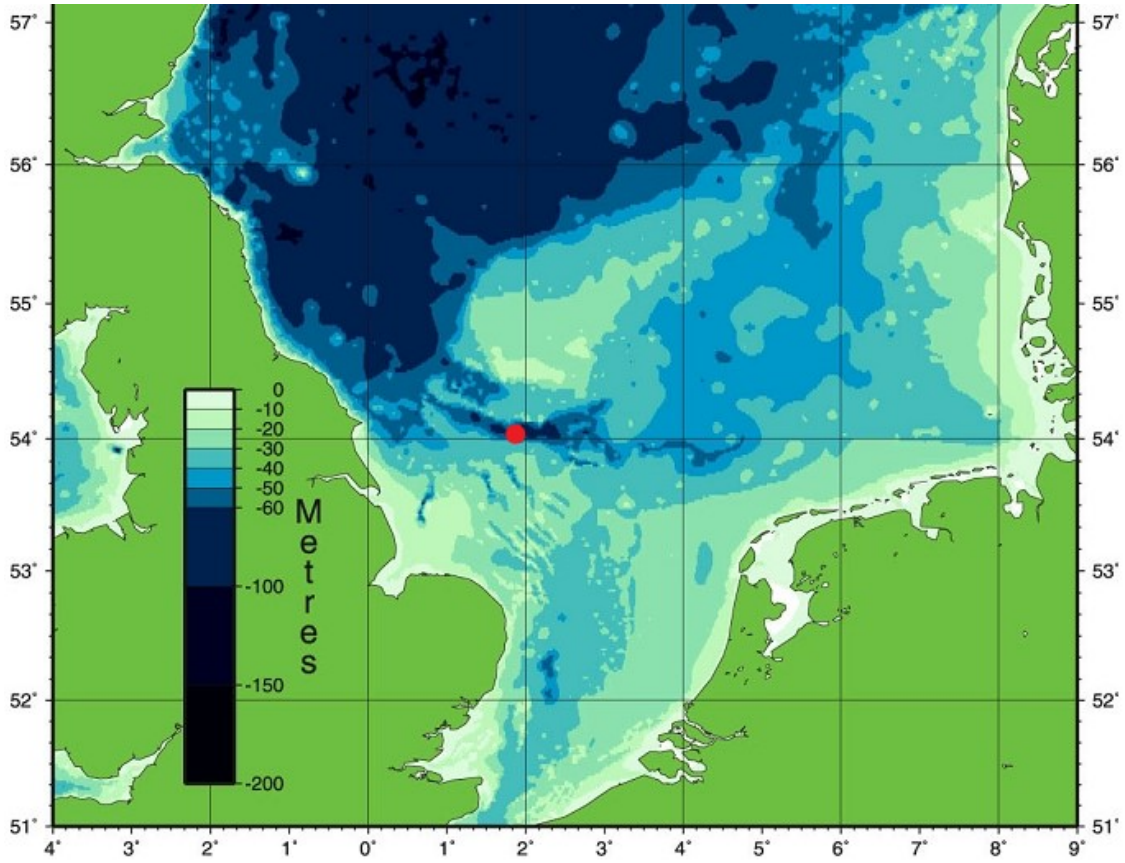

Figure 3.3: Bathymetry Chart of the North Sea and the location of the 2017 DP Trials indicated in red [16]

At this specific location, a drastic change of water depth occurs, which also has an impact on the currents. Yet, in order to prove whether a variability in the current velocity and direction is present at this specific location, measurements would need to be carried out. As described above, the time-step of accessible measurements is not detailed enough to indicate a possible variation that could effect the vessel motions.

On this matter, Dr. Sofia Caires from *Deltares* has been contacted. Unfortunately further measurement data with smaller time-steps in areas representative of the projects executed by HMC are also not available. However, Deltares provided simulation data of the Silver Pit location on the day of the DP Trials, 29th of May 2017. For this location, the velocity and direction of the current with a time-step of one minute was obtained. The data was obtained using the 2D Dutch Continental Shelf Model (DCSM) Flexible Mesh and the current are averaged over depth. Below in figure 3.4 the obtained data can be compared with the DP Current, which was obtained from the offshore data of the DP trials. Additionally indicated are the periods in which test 5A (Low Controller Gain), 5B (Medium Controller Gain) and 5C (High Controller Gain) were carried out.

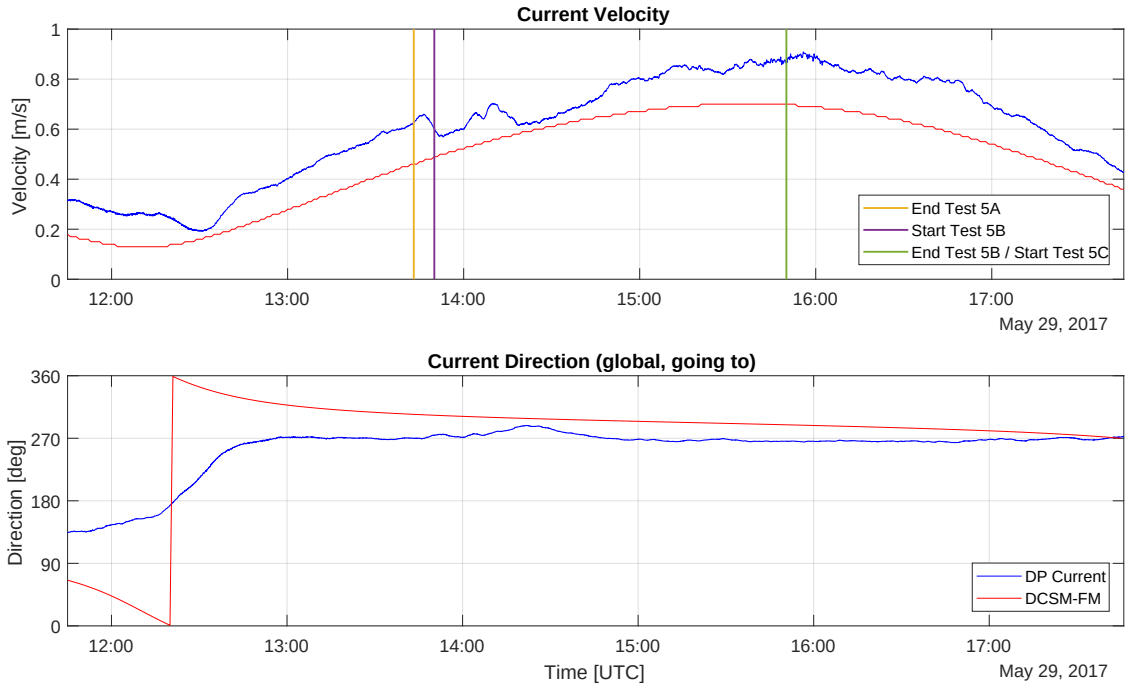

Figure 3.4: Current Velocity and Direction of DP Current and 2D DCSM-FM at DP Trials Test Location on the 29th of May 2017

It is apparent that the current velocity and direction, obtained from the DCSM-FM de- and increases monotonously, meaning that the model does not represent any fluctuation. Comparing this with the obtained DP current velocity, it can observed that a fluctuation of the DP current velocity is present and also increases. This however, also has another origin. The six hours time-span, which can be seen here, is the time in which three station keeping tests with a duration of each two hours were conducted. As mentioned in Chapter 1, these three tests were run while using a High Kalman Filter Gain and a Low, Medium & High Controller Gain. The final two hours of the time trace in figure 3.4 show more fluctuation in the DP current velocity due to the more highly reactive High Controller Gain.
This data also reveals a discrepancy in the initial direction of the currents but shows an acceptable match afterwards. For both the DP Current and the DCSM, the direction of the current is going to, true North clockwise. The origin of that particular mismatch for the current direction in the first 2 hours is unknown.

3.2. Aegir TMS Measurement

During the year 2020, HMC installed 21 wind turbine foundations with Aegir. The project location is approx. 8 km west of the cost of province of Changua in Taiwan. It was possible to conduct an ADCP measurement throughout the project. The sensor was installed on the Tether Management System (TMS) of the Remotely Operated Vehicle (ROV). The configuration used onboard Aegir is a tophat system, which houses the tether and connects to the top of the ROV by means of a lock-latch for launch and recovery. During subsea operations, the ROV detaches and moves freely while the TMS hangs suspended of the side of the vessel. Unlike garage TMS', the tophat system is not designed to sit on the seafloor. For this reason during the ADCP measurements, the TMS was hanging in the water column at a water depth of 13 m, while the vessel was in station keeping with DP.
The duration of the measurement was 45 minutes with a sampling time of 10 seconds, resulting in a sampling frequency of $\omega_{sampling} = 0.628 rad/s$. This results in a Nyquist frequency of $\omega_{Nyquist} = \frac{1}{2} \cdot \omega_{sampling} = 0.314 rad/s$. Furthermore, the frequencies relating the periods of 1 to 5 minutes are indicated in the Energy Density Spectrum (EDS) of the current measurements. The current velocity and direction timetraces, plus the according EDS can be seen in figure 3.5. From both EDS it can be seen that energy is present on the scale of 1 to 5 minutes, suggesting that currents show variations in velocity and direction on this time scale. The content of this energy, especially of velocity is limited, as

the overall current velocity is considerably low. For the current direction, large variations are present, which can be seen to also occur on the scale of 1 to 5 minutes and lower than 1 minute. What critically needs to be noted is the duration of the measurement. In a 45min measurement only 9 cycli for 5min periods and 45 cycli for 1min periods are present. Therefore, the accuracy of these EDS are limited.

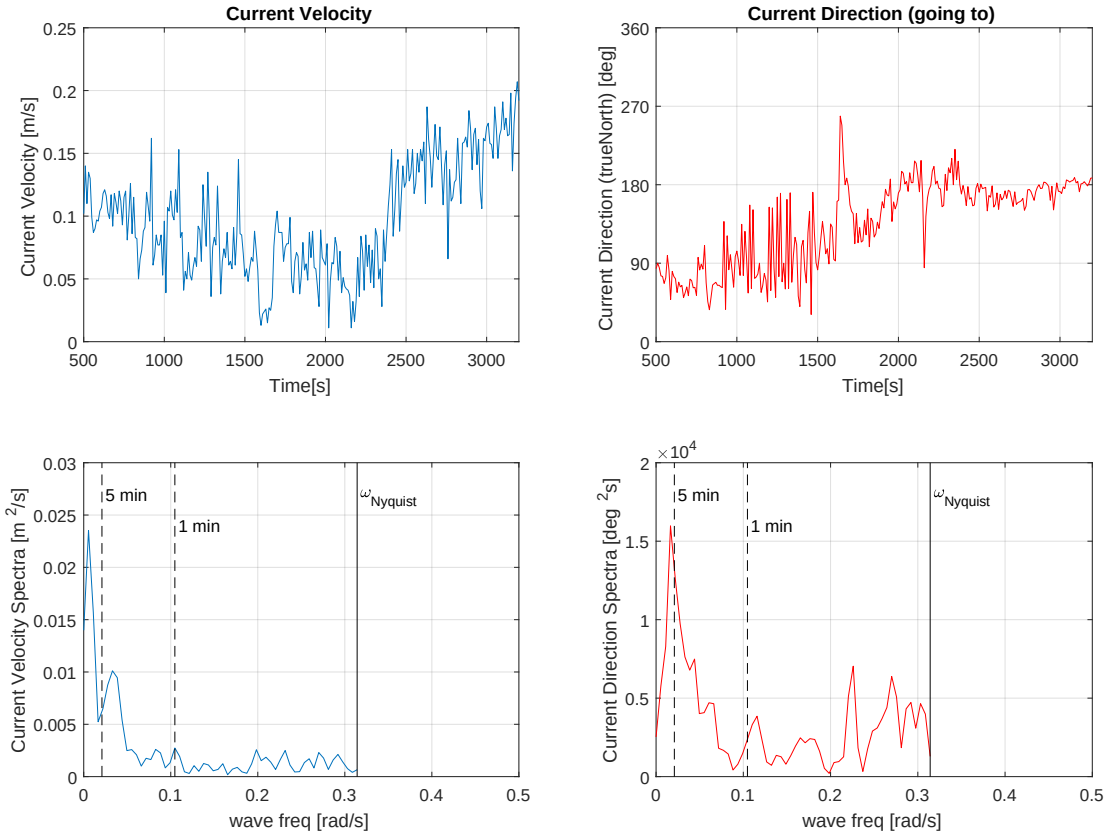

Figure 3.5: ADCP Current Measurements at Changhua with TMS in water column

An emerging question is the accuracy of the set-up of the measurement. The vessel, in DP operation, will introduce motions and thruster wash that cannot be back-traced. The TMS as a submersed pendulum will experience the motions of the vessel in all 6 DOF. As the influence of these disturbing factors cannot be quantified, the measurement cannot be applied for further research.

3.3. Sleipnir ROV Measurement

During a jacket installation with Sleipnir for the windpark Hollandse Kust Zuid in September 2020, it was possible to conduct current measurements. The windpark is located 18 kilometers off the Dutch coast between Den Haag and Zandvoort.

The measurements were carried out with an upward looking ADCP, which was mounted on the top of the ROV. To prevent additional motions that would influence the measured current velocity, the ROV was placed stationary at a water depth of 22m on the seafloor for the duration of the measurement. Unfortunately, this measurement was only executed once, as the ADCP was damaged the same day. However, a 45min time trace with a sampling rate of 1 Hz was obtained. The results can be seen below in figure 3.6. Both signals (velocity and direction) have been low-pass filtered with a frequency of $\omega_{LPF} = 0.5 rad/s$. As in the previous section, the frequencies relating the periods of 1 to 5 minutes are indicated in the EDS of the current measurements. Contrary to the TMS measurement, the outer influences have been minimized by placing the ROV on the seafloor. From this data it can be seen that variations of the current velocity (SDA = 0.15 m/s) and direction (SDA = 16 deg) in the period range of 1 to 5 minutes are present.

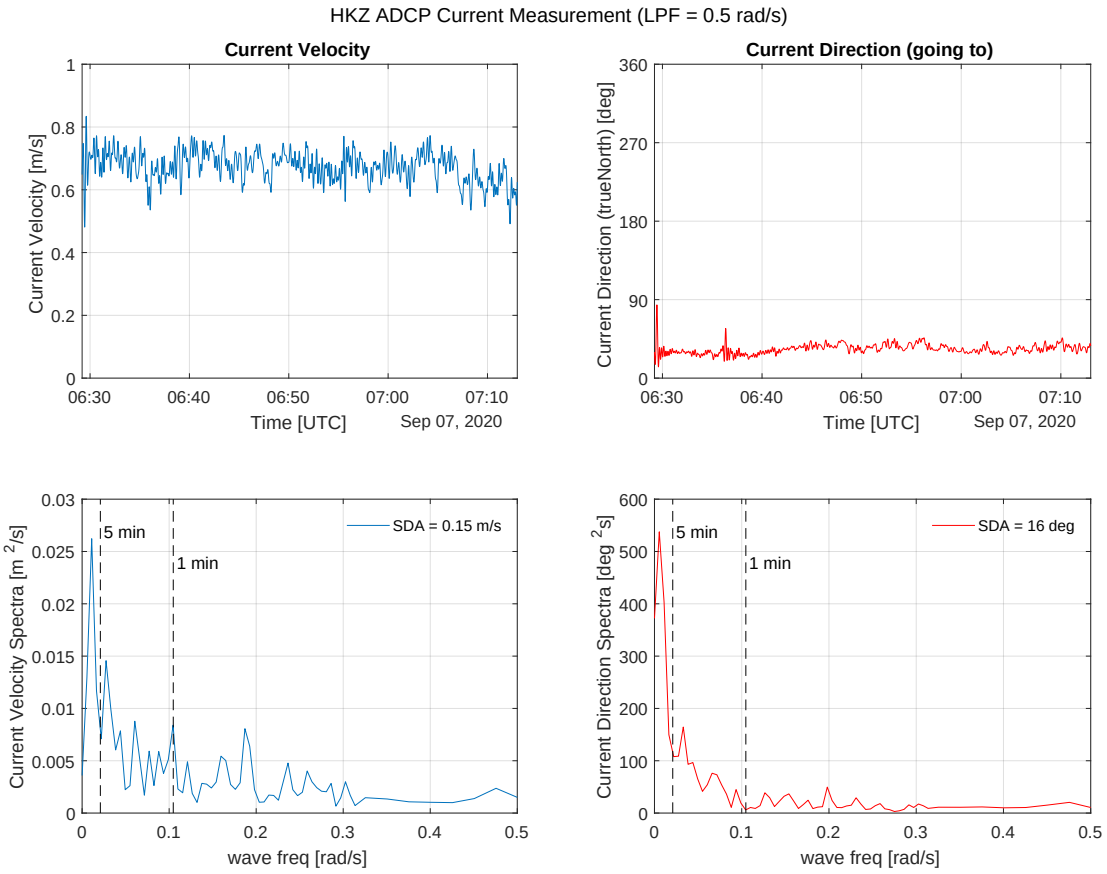

Figure 3.6: ADCP Current Measurements at Windpart Hollandze Kust Zuid with ROV on sea floor

3.4. Conclusion

After having reached out to experts in the field from Deltares, Fugro, the Hydrographic Service of the Royal Netherlands Navy, the Royal Netherlands Institute for Sea Research (NIOZ), the Alfred-Wegener-Institut Bremerhaven, Department of Civil and Environmental Engineering of the University of Washington and the Department of Environmental Fluid Mechanics and Hydraulic Engineering from the Delft University of Technology, no data with a high enough resolution or further knowledge of the existence of such fast varying currents was obtained. This leads to the unfortunate outcome that the sub research question, whether fast time-varying currents on a scale of 1-5 minutes exist, cannot be explicitly answered. The most significant challenge was obtaining suitable measurement data with a high resolution in terms of time steps. For oceanographic purposes, current measurements are typically conducted with sampling rates lower than what is required to answer the hypothesis of time-varying currents, causing an unexpected dynamic vessel response during station keeping operations.
Many arrows are pointing in the direction that such fast-varying currents do indeed exist. This is highlighted by the measurements carried out by a ROV at the Hollandse Kust Zuid project in September 2020, where fluctuations are present on a time scale of 1 to 5 minutes. To further demonstrate their presence and the effect varying currents can have on a SSCV during station keeping operations, further research on these fast varying currents is required and longer in-situ measurements need to be conducted.

4

Dynamic Positioning System

Presently, the time-domain simulation tool aNySIM represents the DP system as it is installed on the vessel. aNySIM has a DP module that aims to mimic the system as used onboard and in the HSC. Application has shown that there remains a discrepancy between real-time and time-domain simulations. In reference to the research question regarding the kind of parameters and/or environmental conditions that are not captured in the current time-domain simulations resulting in an increased vessel response, it must be taken into account that the origin of the unexpected dynamic vessel response could lie within the DP System. This chapter provides more insight to the DP system and the research carried out to investigate the origins of the unexpected vessel response is presented.

4.1. Additional Background on the DP System

The SSCV Thialf is equipped with a triple modular redundant and 1 backup DP system K-POS by Kongsberg Maritime, which exists out of four identical operator stations. At the HSC the same system is installed, as can be seen in figure 2.9. In section 2.1, the working principle of the DP system was introduced and a simplified block diagram presented. Detailed information on the main components of the DP system, namely Position Measurement, Kalman Filter, Controller, Thrust Allocation and Thrusters are provided below.

4.1.1. Position Measurement

The DP system requires the instantaneous position of the vessel to calculate the offset relative to the setpoint and required thruster forces. To operate in DP3-class it is required to use a minimum of 3 position reference systems, of which 2 should be of independant operating principle. A selection of multiple position reference systems are used onboard a DP vessel [17] [18]:

- **Satellite navigation systems**
  The most well known satellite reference system is the Global Positioning System (GPS) of the United States. GALILEO, the Global Navigation Satellite Systems (GNSS) of the European Union is used in conjunction with GPS and GLONASS, the GNSS of Russia. Differential GNSS represents an improvement on the conventional GNSS by using fixed ground based reference stations in order to correct the signal and thus enhance position accuracy.

- **Hydro acoustic Position Reference (HPR)**
  HPR systems require the prior deployment of beacons or transducers typically on the seabed. Whereas the long baseline system uses a minimum of 3 fixed transducers, the short and ultra short baseline only require one beacon. The short baseline reference system utilizes two transceivers on the vessel hull and the ultra short baseline multiple transducers on one single beacon. In addition, ROVs and divers can be equipped with such a beacon so that their position relative to the vessel is known.

- **Mechanical reference**
  The taut wire is a mechanical reference system that is lowered down to the seafloor. A depressor weight connected with the wire and the taut wire itself is kept under constant tension. Due to an offset of the vessel, the wire will deflect on an angle from the point of attachment. This angle can be measured and, with the known wire length, the position offset calculated. Water depth and deflection of the wire due to strong currents can limit the applicability.

- **Relative positioning reference**
  The position of the vessel can be determined relative to a fixed or moving object. Laser or microwave apertures installed on the vessel measure the range and direction to a reflector installed on the reference.

Below the position reference systems as installed on SSCV Thialf:

System Type	**SSCV Thialf**
Radar	1 x Artemis
Satellite	3 x DGPS
Hydroacoustic	2 x HiPAP AP-350 SSBL + LBL
Mechanical	1 x Taut wire (water depth <300m)
Relative Position	1 x Fanbeam at vessel stern

4.1.2. Kalman Filter

One challenge that the DP control system faces is the accurate estimation of the position and state of the vessel. Estimates of a mathematical model and noisy measurements create a trade-off. To obtain the most accurate estimates, a Kalman filter is introduced. Equipped with a dynamic model, the Kalman filter predicts the position and velocity of the vessel based on previous position measurements, which in turn can be inaccurate and contain noise.
A Kalman filter is set up in two steps, a prediction and correction step. In the prediction step, the filter makes a prediction of the vessel based on the present state of the ship and the dynamic model. In the correction step, the Kalman filter corrects the previous prediction based on measurements obtained by the position reference system and the calculated Kalman gain. Depending on the Kalman gain, the filter assigns more weight to the measurement (high Kalman gain) and more weight to the estimate for a low Kalman gain. Afterwards, the estimated error is forwarded to the Controller and the filter process starts again with a new prediction [19]. The time update (prediction) and the measurement update (correction) can be seen below with the respective equations, based on [20].

Time Update ("Predict")

$$\hat{x}_k^- = A\hat{x}_{k-1}^- + Bu_{k-1} \tag{4.1}$$

$$P_k^- = AP_{k-1}A^T + Q \tag{4.2}$$

Measurement Update ("Correct")

$$K_k = P_k^- H^T (HP_k^- H^T + R)^{-1} \tag{4.3}$$

$$\hat{x}_k = K_k(z_k - H\hat{x}_k^-) \tag{4.4}$$

$$P_k = (I - K_k H)P_k^- \tag{4.5}$$

In which:

$\hat{x}_k^-$	=	*apriori* state estimate of current time step
A	=	Matrix relating state at previous time step to the state at the current time step
$\hat{x}_{k-1}^-$	=	*a priori* state estimate at previous time step
B	=	Matrix relating optional control input u to the state x
u_{k-1}	=	Control input u at previous time step
P_k^-	=	*a priori* estimate error covariance
P_{k-1}	=	*a posteriori* estimate error covariance at previous time step
Q	=	Process noice covariance
K_k	=	Kalman Gain
H	=	Matrix relating the state to the measurement z_k
R	=	Measurement noise covariance
$\hat{x}_k$	=	*a posteriori* state estimate
z_k	=	Actual measurement
P_k	=	*a posteriori* estimate error covariance
I	=	Identity matrix

Heavy Lift Kalman Filter
Harmsen, van Dijk and Stuberg [3] present the procedure that lead to the implementation of a modified Kalman filter into the Kongsberg DP System onboard Thialf. To prevent DP instabilities caused ”by the inability of the DP system to handle the relatively stiff external spring of the hoist wire correctly”, the Kalman filter has been modified such that the Kalman filter ”would give higher priority to the position measurements and less priority to the ship model” [3]. Kongsberg has been involved, which lead to the implementation of this Heavy Lift Kalman filter in the DP System and is referred to as the High Kalman Filter. In order to analyze the capability of the updated DP-system to manage a wide range of specific heavy lift conditions, the modified DP-system has been assessed with a significant number of desktop and full mission simulations. In the final stage of testing, the system undergoes a dedicated DP-trial program onboard Thialf. Due to the successful performance during the tests, the new High Kalman filter is permanently available onboard Thialf alongside the original functionalities. [3]

Onboard *Thialf* the Kalman gain settings ’Normal’ and ’High’ are available. In the HSC, however, four different Kalman gain settings are available. They consist of Extreme, High, Normal and SDP. SDP originates from Simrad Dynamic Positioning, which was installed before K-POS. The filter setting was also included in the K-POS system of the HSC and can be referred to as a low Kalman gain setting. As those filter settings are already implemented and have been previously subjected to testing, the unexpected vessel response is unlikely to originate from the setting of the Kalman filter. Nevertheless, in the DP Trials, where the unexpected vessel response was observed, only the High Kalman Gain was initiated. Therefore, it is important to compare the different Kalman filter gain settings in the same environmental conditions.

4.1.3. Controller
The function of the controller is to calculate a required force output based on the position error and velocity. Most DP systems are based on a space-state controller. This can also be be treated as a Proportional-Integral-Derivative (PID) controller. A PID controller is a feed-back loop that measures the output of a system and controls the input. The controller determines the error based on the measurement and the setpoint and treats the error in 3 different ways [17]:

- Proportional $F_P = -P \cdot \Delta x$ *acts on present offset*
  The error Δx is multiplied by a proportional constant P, which results in an instantaneous system output, reducing the offset.

- Integral $F_I = -I \cdot \int \Delta x \cdot dt$ *acts on past offset*
  Integrating the error over a period of time results in the vessel gradually moving towards zero offset from the setpoint and thus reducing steady-state errors.

- Derivative $F_D = -D \cdot \frac{\delta x}{\delta t}$ *acts on future offset*
  The rate of change of the error with respect to time is calculated and multiplied with the constant D resulting in resistance against time, also known as damping.

Controller Gain Settings
The accuracy of the DP Performance can be influenced by changing the Controller Gain, which can be set to Low, Medium & High. The intentions of changing the controller gain has different reasons. In calm environments or when less position accuracy is required, the low controller gain can be used. The exact selection of controller gain is also dependent on the preference of the marine crew and vessel behavior. When high accuracy is required, the high controller gain is appropriate. This comes with a cost of increased fuel consumption and additional wear of the thrusters, a result of fast reacting and consequently more aggressive vessel behavior.

4.1.4. Thrust Allocation
The forces derived by the Control System to maintain or restore the vessels position, also known as the demanded force, need to be distributed amongst the available thrusters. To keep position, the environmental forces acting on the vessel must be equal to the forces that the vessel exerts with its thrusters, where n represents the number of thrusters:

$$F_{x,environment} = \sum_{i=1}^{n} F_{x,thruster_i} \tag{4.6}$$

$$F_{y,environment} = \sum_{i=1}^{n} F_{y,thruster_i} \tag{4.7}$$

$$M_{z,environment} = \sum_{i=1}^{n} F_{x,thruster_i} \cdot l_{x,i} + \sum_{i=1}^{n} F_{y,thruster_i} \cdot l_{y,i} \tag{4.8}$$

It is common for marine systems to be over actuated, meaning that the number of thrusters exceeds the DOF in order to ensure reliability. For the case of a DP system, the DOF are surge, sway and yaw. The task of the thruster allocation is the distribution of that demanded force in terms of thrust and direction for each individual thruster [21]. To avert thruster-thruster interaction, constraints regarding the azimuth angle for each thruster are introduced [22].

4.1.5. Thruster

To provide maneuverability for sailing and/or station keeping, a vessel needs to be equipped with a propulsion system. The selection of propulsion arrangements depend on the architecture of vessel itself and its operational profile.

- **Main Propeller and Rudder**
  The setup of a main propeller and rudder is specifically optimized for certain operational condition of a vessel, for example the operational speed of a container ship under its operational draught, load, etc. The main propeller(s) and rudder(s) are not always a part of the propulsion setup of a DP vessel due do their slow response. On smaller vessels they are often part of the DP propulsion setup.

- **Azimuth Thruster**
  Azimuth thrusters are used for most DP operations as they can produce thrust in any direction by rotating full 360 degrees. To increase thruster efficiency and reduce cavitation, they are equipped with nozzles. Additionally, a vessel can be equipped with a retractable version of azimuth thrusters. These can be lowered for DP operations or required maneuverability and then retracted for maintenance or transit in order to reduce vessel resistance.

- **Tunnel Thruster**
  These are often seen on merchant ships with a main propeller and rudder setup. They are installed in the bow or aft of the ship and provide a large lever arm and transverse maneuverability on the front of the vessel.

The thruster arrangement differs per vessel and operational profile. For example, the monohull HLV Aegir of HMC is equipped with two 6.5 MW azimuth thrusters for main propulsion and DP, four 3.2 MW retractable azimuth thrusters for DP and one 2.5 MW tunnel bow thruster for DP and maneuvering [7].

4.2. Methodology

With reference to the research sub question, where it is asked what other possible causes can trigger the observed vessel response the answer may lay within the DP system itself. This includes gaining in-depth knowledge on the background of each component, as previously presented. More importantly, vessel specific data must be obtained in order to assess the vessel behavior. With the obtained specific data, scenarios can be compared and analyzed.

4.2.1. Offshore Data

The data of the DP system is logged by the K-POS consoles onboard the vessel. For *Thialf*, this data can only be obtained when directly accessed from the DP console. However, for some past projects and more importantly the DP Trials 2017, the K-POS is accessible within HMC. Another possibility is to access data via Kongsberg Information Management System (K-IMS), where data from different sensors and systems onboard is collected. K-IMS can be accessed online and the data can be downloaded from the vessel directly. The K-IMS database does not include the complete information about the DP system than K-POS does. Data obtained from either of the system is exported as a 'csv' file that can subsequently processed with Matlab.

4.2.2. Real-time Simulations

A powerful tool to produce 'offshore data' for particular needs, such as this research, is the HSC. In the HSC the environment can be selected as desired for each simulation run.

Procedure

First, it is necessary to launch the instructor station as well as the K-POS units. The exercise can then be opened via the instructor station and the desired vessel, location, environmental parameters, ballast (in order to change the draft) and position reference systems selected. Once the simulation is set up, it is then assigned to the K-POS console and the simulation can be started. The environment then starts acting on the vessel, which can then be controlled via the K-POS console.

The operator initiates the thrusters and position reference systems. Once the position reference systems are engaged, the Auto positioning mode can be selected, which means the vessel is now keeping its position by means of DP. The vessel can now be moved to the desired position and the heading chosen. A selection of the controller gain can be made, choosing between 'High', 'Medium' & 'Low'. Plus, the Kalman filter gain can be selected with the available options in the HSC of:'Extreme', 'High', 'Normal' & 'SDP'.

Throughout all simulations carried out in the HSC, it is crucial to log the time of the K-POS console. This must be completed at each of the previously outlined steps as well as at the timestamp when a settings on the DP console has been changed. Unlike a desktop simulation, the K-POS system continues to log the variables once switched on. Therefore, in order to be able to use and extract the data for further analysis, the timestamp is essential.

Another important factor to consider is the stabilizing time of the simulation. This is required for two reasons. One aspect is that the environment requires full development in such a real-time simulation. The second aspect, in conjunction with the first, is the run-up time of the DP system, before it can be considered to be 'stable'. Drawn from the experience of the HSC team, a run-up time of 15 minutes is considered to be sufficient. This time has not only been considered at the begin of a simulation run, but also inbetween, when in the same environmental condition a controller or Kalman Gain has been changed.

An additional option is an Application Programming Interface (API) in the HSC. From this interface, amongst other options, moorings and external forces acting on the vessel can be included. With the mooring option, an object, in this case the SSCV Thialf, can be moored or even fixed in all 6 DOF. During a running simulation, a force time trace with forces and moments in all 6 DOF can be applied. These forces can then be selected to act onto the object, either body fixed or earth fixed. The location of force and moment application can also be selected. In this research it has been selected to the Center of Gravity (COG) of the vessel.

After the simulation has been executed, the variables logged by the K-POS system must be exported to a csv-file and can consequently be used for post-processing and analyzing the station keeping behavior. The output, the selected time window of the simulation, obtained from the K-POS system, is set up in two different files. One file describes the events when selections or settings have been made, for example and the other file contains the logged variables with a timestep of 1 second.

4.2.3. Post-processing of K-IMS/K-POS data

To make use of the obtained data, certain steps must be undertaken in order to compare the results of different simulations with each other. This is achieved using Matlab.

Vessel Motions

The vessel motions, which the DP system can compensate are also the desired motions to be investigated, namely Surge, Sway and Yaw. They will be presented as time-dependant in meter for Surge and Sway and degree for Yaw. From the vessel data, the instantaneous Universal Transverse Mercator (UTM) Easting and Northing can be obtained, as well as the heading. UTMN and UTME are already given in meters relative to the equator and the meridian of the UTM zone, respectively. The heading is retrieved via gyro sensors and is translated to degree North (global) and clockwise positive. Figure 4.1 shows the relation between the global and local coordinate system by means of the heading ψ. The variables used and how to obtain the Surge and Sway is explained below in equations 4.11 to 4.12.

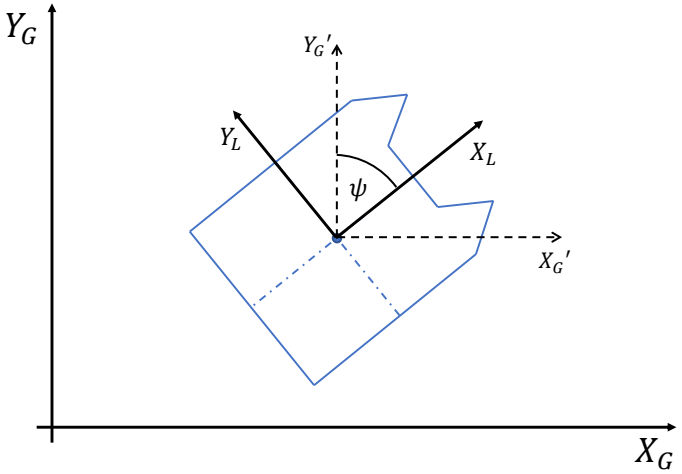

Figure 4.1: Global and Local Coordinate System

$$X'_G(t) = X_G(t) - X_G(t_1) \tag{4.9}$$

$$Y'_G(t) = Y_G(t) - Y_G(t_1) \tag{4.10}$$

$$X_L(t) = X'_G(t) \cdot sin(\psi(t)) + Y'_G(t) \cdot cos(\psi(t)) \tag{4.11}$$

$$Y_L(t) = X'_G(t) \cdot cos(\psi(t)) - Y'_G(t) \cdot sin(\psi(t)) \tag{4.12}$$

In which:

t	=	Time	[s]
t_1	=	First timestamp of desired position (timestamp of set-point selection)	[s]
ψ	=	Vessel heading	[deg]
X_G	=	Global X-coordinate (UTME)	[m]
Y_G	=	Global Y-coordinate (UTMN)	[m]
X'_G	=	Relative global X-coordinate	[m]
Y'_G	=	Relative global Y-coordinate	[m]
X_L	=	Relative local X-coordinate (Surge)	[m]
Y_L	=	Relative local Y-coordinate (Sway)	[m]

Thruster Response

The thruster response of a DP vessel provides insight on the reaction of the vessel to outer influences. The Azimuth angle and Revolutions Per Minute (RPM) is obtained from the thruster feedback data. The Azimuth angle of each thruster is represented in degrees from -180° to +180° in the local coordinate system of the vessel, where 0 degree is midship towards the bow. This means that the angle relative to the vessel indicates the direction to which thrust is exerted.

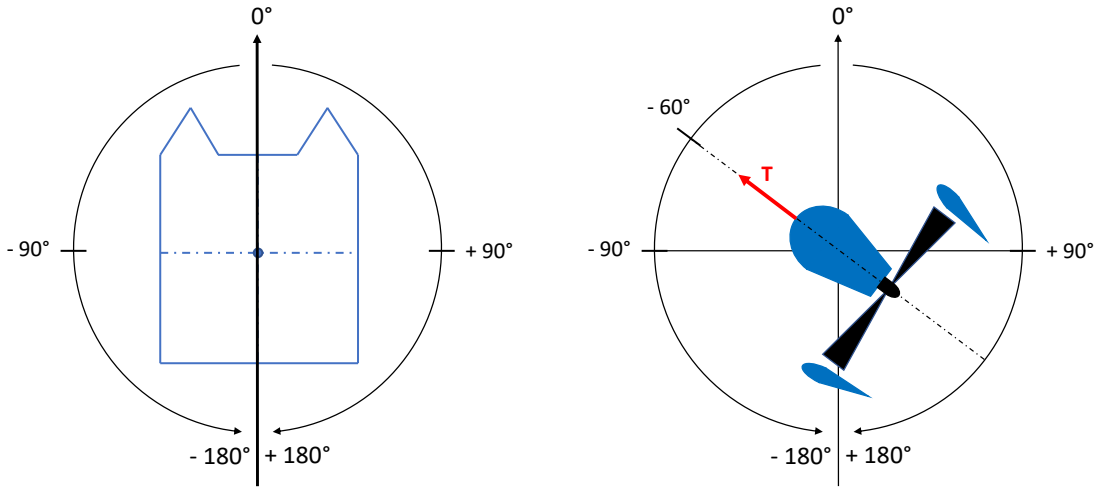

Figure 4.2: Azimuth orientation and direction of generated thrust

The maximum thrust of one thruster has been measured during DP Trials resulting in 70 ton thrust at 199 rpm. Due to the investigation of station-keeping operations, the advance ratio J is assumed to be zero. This results in a constant thrust coefficient K_T. The thrust force can be defined as:

$$T = K_T \cdot \rho D^4 n^2 \tag{4.13}$$

Where:

T	=	Thrust	[N]
K_T	=	Thrust Coefficient	[-]
ρ	=	Density of water	[kg/m^3]
D	=	Propeller Diameter	[m]
n	=	Revolution speed	[1/s]

The RPM feedback of each thruster is given as percentage of maximum rpm. With this information, the instantaneous thruster force can be estimated. It should be noted that due to the assumption $J = 0$ alongside other effects, this estimation will contain inaccuracies of determining the produced thrust per unit. As the density and propeller diameter are also considered to stay constant, it can be observed for this case that the thrust scales quadratic with respect to rpm, which yields equation 4.14, where $T_{max} = 70t \cdot 9.81m/s^2 = 686.7kN$.

$$T(t) = \left(\frac{RPM(t)}{RPM_{max}}\right)^2 \cdot T_{max} \tag{4.14}$$

4.3. Results

In this section, the results obtained through the help of the real-time simulations that were carried out in the HSC are presented and discussed. The results shown, represent the selected cases highlighting the findings relevant for this research.

4.3.1. Effect of Kalman Filter & Controller Gain

To investigate the effect of the Kalman Filter Gain and Controller Gain, an environmental scenario was chosen where varying forces are present, in order to obtain a vessel response which the DP system must act upon. This was completed with an only waves environment and was set up as presented in table 4.1. Both Filter Gains ('Normal' & 'High') were compared with the Controller Gains High, Medium and Low, resulting in 6 simulations. Below, the results will be shown for High and Normal Kalman Filter Gain and compared with Medium Controller Gain. The results of the comparison between each Kalman Filter Gain compared with 3 Controller Gains, can be found in Appendix B

Note that, for the presentation of the thruster azimuth, the coordinate system has been adapted for readability, see figure 4.3b, else jumps between -180° and 180° would be present.

		HSC Real-time Simulation
Vessel	Kalman Filter Gain	High & Normal
	Controller Gain	Medium
	Draft	26.6 m
	Heading	90° (true North)
	Position Reference System	Fanbeam 1 & 2 and LTW
Waves	Direction (coming from)	300° (global) - see figure 4.3a
	Peak Period	T_p = 9s
	Sig. Wave Height	H_s = 2m
	Spectrum	JONSWAP
	gamma	γ = 3.3
	Wave Spreading	minimal (K-SIM: 50)
Duration		2 hrs (excluding stabilizing time)

Table 4.1: Vessel and environmental parameters

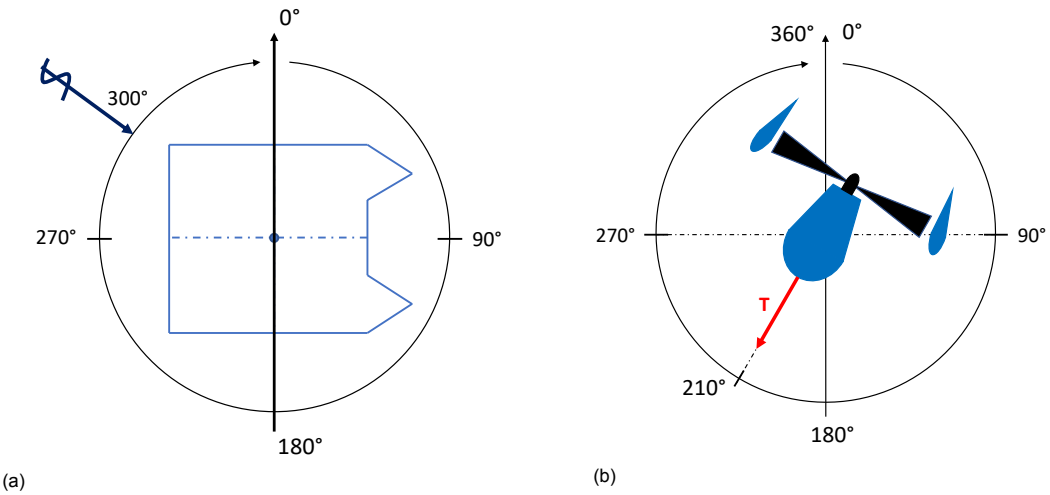

Figure 4.3: Environmental Direction and adapted Azimuth coordinate system

Medium Controller Gain Normal & High Kalman Filter Gain

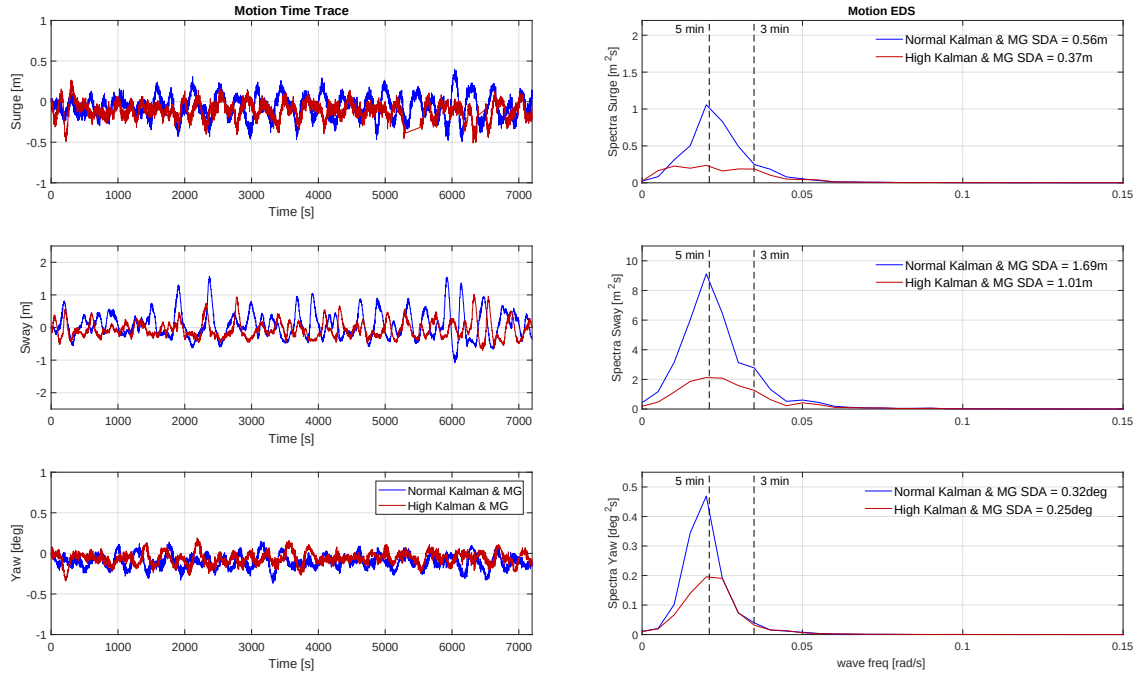

(a) Time Trace (b) EDS

Figure 4.4: HSC run with SSCV Thialf - Motions - Heading: 90 deg, Draft 26.6 m, Waves (Dir=300(coming from), $T_p = 9s$, $H_s = 2m$, JONSWAP, $\gamma = 3.3$), Kalman Gain: High & Normal Controller Gain: Medium

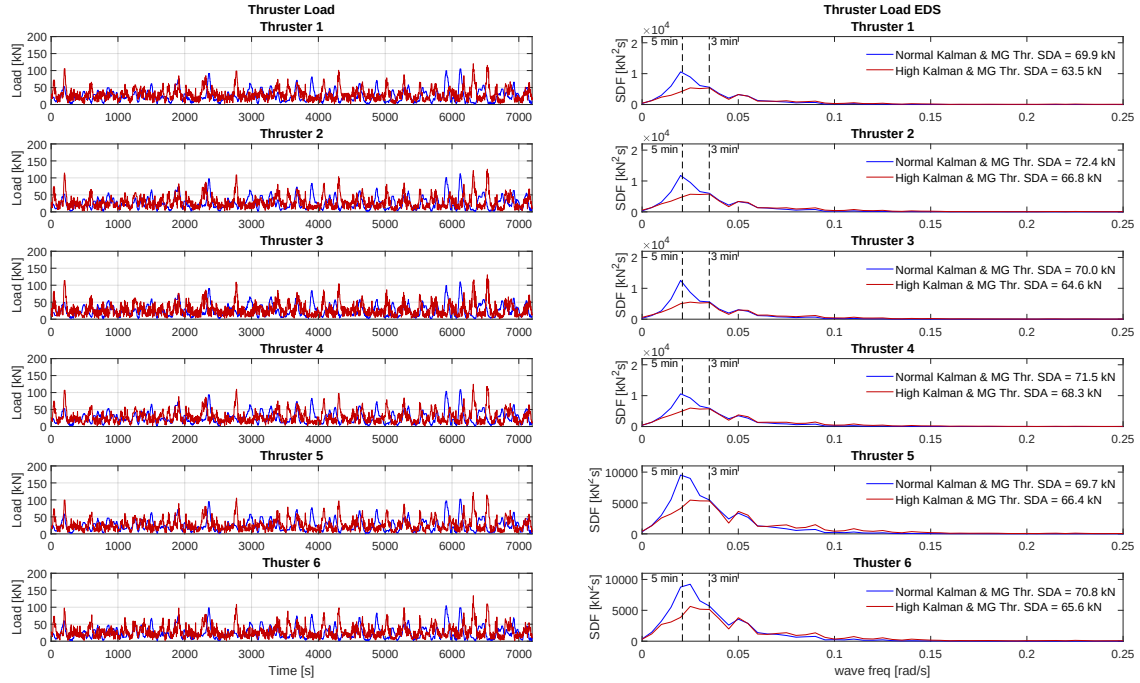

(a) Time Trace (b) EDS

Figure 4.5: HSC run with SSCV Thialf - Thruster Load - Heading: 90 deg, Draft 26.6 m, Waves (Dir=300(coming from), $T_p = 9s$, $H_s = 2m$, JONSWAP, $\gamma = 3.3$), Kalman Gain: High & Normal Controller Gain: Medium

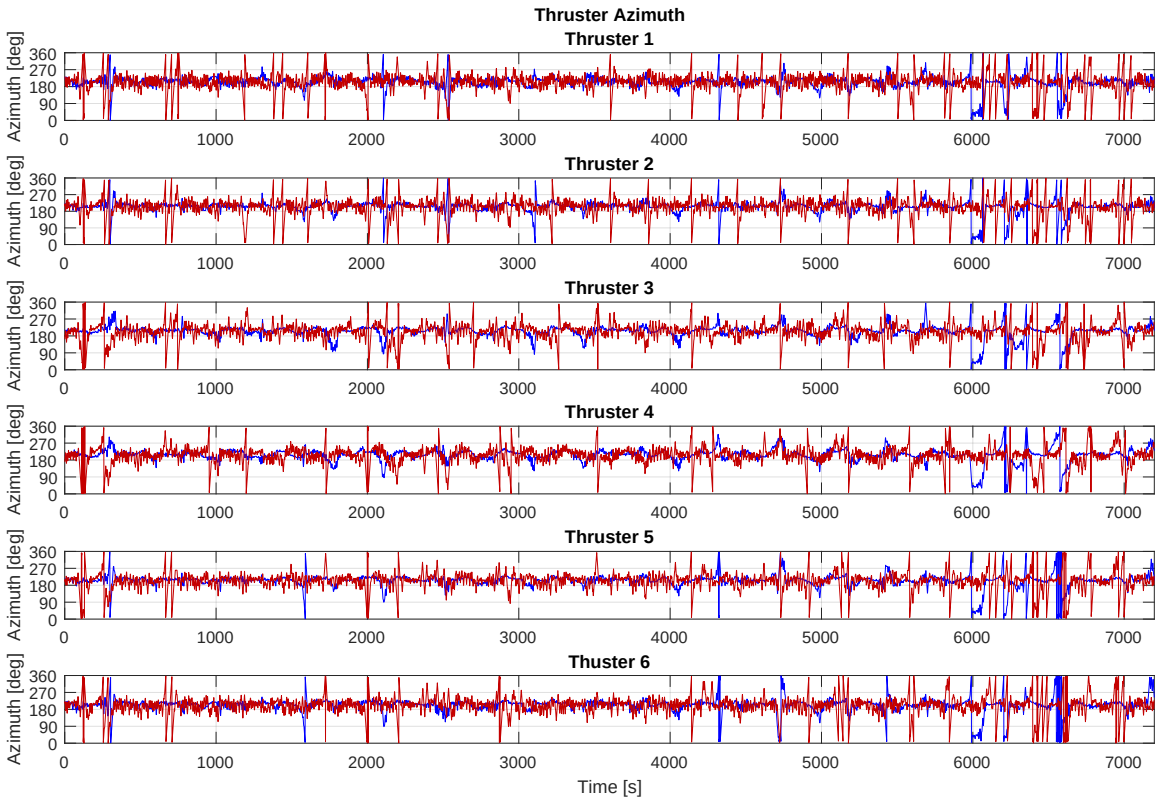

Figure 4.6: HSC run with SSCV Thialf - Thruster Azimuth - Heading: 90 deg, Draft 26.6 m, Waves (Dir=300(coming from), $T_p = 9s$, $H_s = 2m$, JONSWAP, $\gamma = 3.3$), Kalman Gain: High & Normal Controller Gain: Medium

Discussion

The SDAs for surge, sway and yaw of the presented simulations are summarized in table 4.2. For a better assessment and understanding, an aNySIM simulation with an ideal DP system and the spring damper configuration, representing Medium Controller Gain at a Normal Kalman Filter Gain in the same environmental condition has been carried out.

	Kalman Filter Gain						**aNySIM**
	Normal			**High**			
Controller Gain	High	Medium	Low	High	Medium	Low	Medium
SDA Surge [m]	0.49	0.56	0.82	0.33	0.37	0.54	0.18
SDA Sway [m]	1.40	1.69	2.55	0.92	1.01	1.71	0.29
SDA Yaw [deg]	0.27	0.32	0.36	0.24	0.25	0.25	0.14

Table 4.2: Significant Double Amplidutes (SDA) of HSC and aNySIM simulation runs

From the table and the EDS, it can be observed that indeed the High Controller Gain shows smaller offsets in comparison to Medium and Low. Although the difference between High and Medium is minor, the difference between High and Low, as well as Medium and Low is significant.
For all Controller Gains, the High Kalman Filter Gain shows fewer offsets for the 3 DOF. The best performance in this environment can be seen for High Controller Gain and High Kalman Filter Gain.

The thruster response shows only small difference in the SDA of the provided thrust per thruster (figure 4.5b. From these EDS', it is evident that when High Kalman Filter Gain was selected, that for all Controller Gains, the thrusters show more energy content for periods lower than 3 min. This signifies that

the reaction of the thrusters in terms of provided thrust, is faster than for Normal Kalman Filter Gain, which is logical, as the High Kalman Filter Gain makes the system more 'aggresive'. This 'aggressive' behavior is clearly desmonstrated in the thruster azimuth angle, depicted in figure 4.6. Here it should be noted that the Thruster Azimuth representation has been adapted for these results, see figure 4.3b. It is apparent that the thrusters show their main thrust being directed towards 210°, counteracting the waves. An aspect that clearly emerges, is that for the High Kalman Gain a significant amount of full 360° rotations per thruster is present. This is a result of the fact that the more aggressive Kalman Filter causes the system overshoot and subsequently corrects that overshoot. One explanation for this increased performance of the High Kalman filter in terms of excitation, even with the present overshoots and 360° rotations, is the extimation of the vessel velocity - see section 4.4.5.
Additionally, the simulations with the ideal spring-damper DP system, show small SDAs for Medium Gain and a Normal Kalman Filter Gain, while the HSC simulation shows more than double of those values.

An aspect that stands out for all the presented results are the peak periods of the vessel response of approx. 5 min with large SDAs. Nonetheless, the present low frequent vessel motions are also to be notable in aNySIM time-domain simulations. The origin of these increased low frequent vessel motions are second order wave drift forces. These forces, as simulated by aNySIM, can be seen in figure 4.7, with an SDA of 254kN in y - / sway - direction at peak periods between 3 to 5 min.

At this point, it should be mentioned that the environmental condition of only waves with a significant wave height of $H_s = 2m$ and a peak period of $T_p = 9s$, is unrealistic.

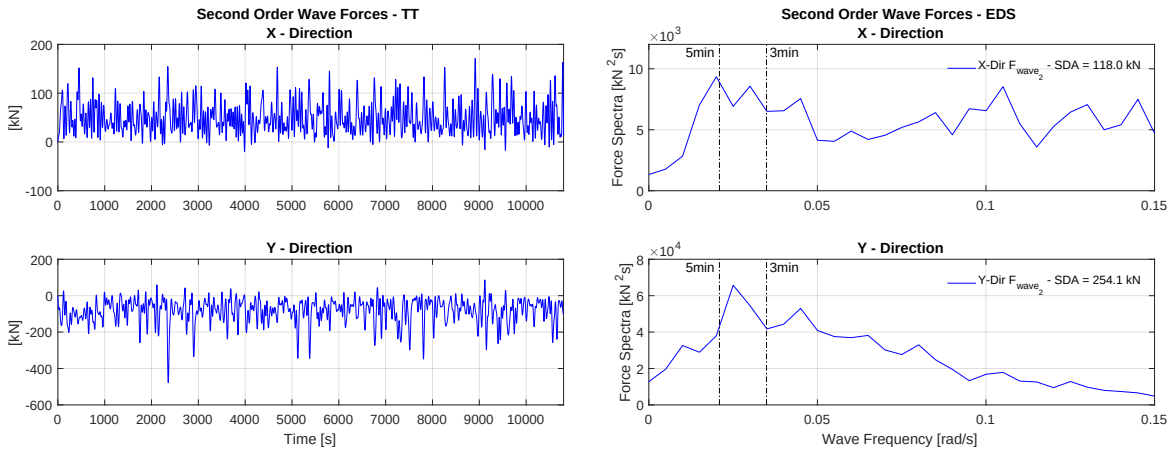

(a) Time Trace (b) EDS

Figure 4.7: Second order wave forces as simulated in aNySIM in x- and y- direction

4.3.2. Subconclusion

From the comparison between the Kalman Filter Gain and Controller Gains, in an environment where by coincidence low frequent varying forces are present, provide a useful representation on the influence of both selected gains. From this, it can be concluded that the High Kalman Filter Gain does not cause an increase of the vessel response, but in fact, reduces it. This signifies that while in the DP Trials 2017 only the High Kalman Filter Gain was tested, the selection of the Kalman Filter Gain does not influence the occurrence of the unexpected low frequent vessel response. Furthermore, as expected, it has been demonstrated that the High Controller Gain provides the most accurate performance, whether in combination with High or Normal Kalman Filter.

Finally, from the aNySIM simulation it can be concluded that the effect of second order waves is indeed captured in time-domain simulations. Regarding the increased magnitude of the excitation, as observed in the HSC in comparison to aNySIM, section 4.4 represents an approach to assess this discrepancy.

4.4. DP System RAOs

In ”DP-stability during heavy lift operations using a modified Kalman filter” Harmsen and van Dijk [3] first introduce DP system Response Amplitude Operator (RAO)s. This paper presents the research of the behavior of the DP system during heavy lift operations and the implementation and validation of a modified Kalman filter onboard Thialf to prevent DP instabilities. The analysis of the DP system itself was carried out by identifying RAOs of different stages of the control loop of the DP system.

4.4.1. DP System Analysis

In figure 4.8, the important RAOs for the system analysis are indicated and can schematically be seen in figure 4.9. ”The meaning of the presented RAO should be interpreted as follows: if the position of the vessel is experiencing a sinusoidal oscillation with a certain period and an amplitude of 1m, the DP system is delivering a certain trust to the vessel with that same period and with a certain phase angle (ahead of the position).” [3]

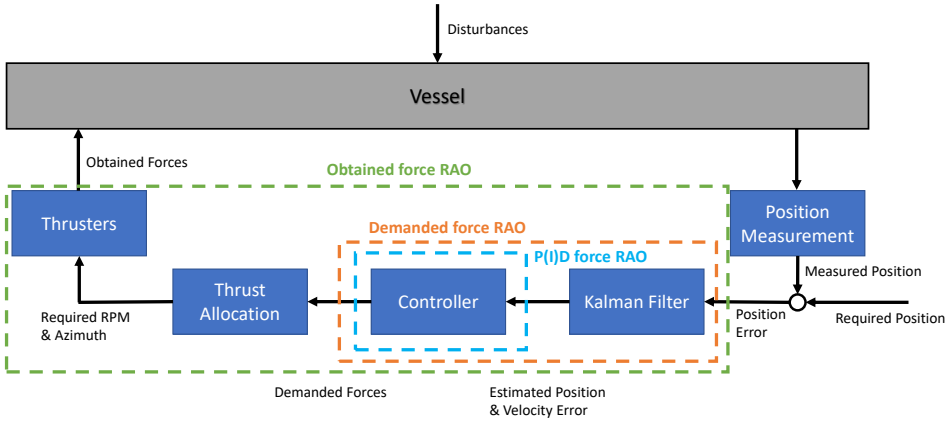

Figure 4.8: Block diagram of simplified DP System with DP system RAO - from [3]

In a Single Input Single Output (SISO) system, with one known input and one known output of one component of the system, a transfer function (RAO) can be calculated. By cross-correlating the input with the output, the frequency dependent relation between them can empirically be determined.[23]

$$H(i\omega) = \frac{S_{xy}(i\omega)}{S_{xx}(\omega)} \tag{4.15}$$

in which:

$H(i\omega)$ = Complex transfer function of system
$S_{xy}(i\omega)$ = Cross power spectrum of input ’x’ and output ’y’
$S_{xx}(\omega)$ = Power spectrum of input ’x’

and results in a complex transfer function:

$$H(i\omega) = A(\omega) \cdot e^{i\Phi} \tag{4.16}$$

The amplitude and phase components of the RAO can then be obtained by:

- Amplitude $A = \sqrt{Re(H)^2 + Im(H)^2}$
- Phase $\Phi = atan2(Im(H), Re(H))$

The smoothed amplitude and phase for the indicated decisive components of the DP control loop can be seen in 4.9. It is clear that for very short periods, which result in high velocities, the Damping term dominates the amplitude of the P(I)D RAO. For very long periods, the D term can be neglected due to very low velocities at such long oscillating periods. This is similarly represented in the phase. For very long periods, the phase is 180°, as the P force acts opposite the position error. Furthermore, for very

low periods the phase has an offset of 270° (180° + 90°), which, based on the fact that velocity has a 90° phase shift ahead of position. Therefore, at low periods and a resulting high velocity, the D-term dominates the total P(I)D force.
After the Kalman Filter has been considered in the RAO, it can be noted that the force amplitude reduces for very low periods . This is to be expected, as the DP System is not intended to react on high frequent motions caused, for example, by first order wave forces. With reference to figure 4.9b, it can be seen that the Kalman Filter introduces a phase lag. This means that the force as predicted by the controller to counteract the position and velocity error, is later delivered than intended by the controller.
Including the Thrust Allocation and the Thrusters to the RAO (refer to figure 4.8 - Obtained force RAO) it can clearly be seen that, as a result of the allocation of forces and the reaction of thrusters in terms of Azimuth and RPM, the phase lag increases even more. [3] [24]

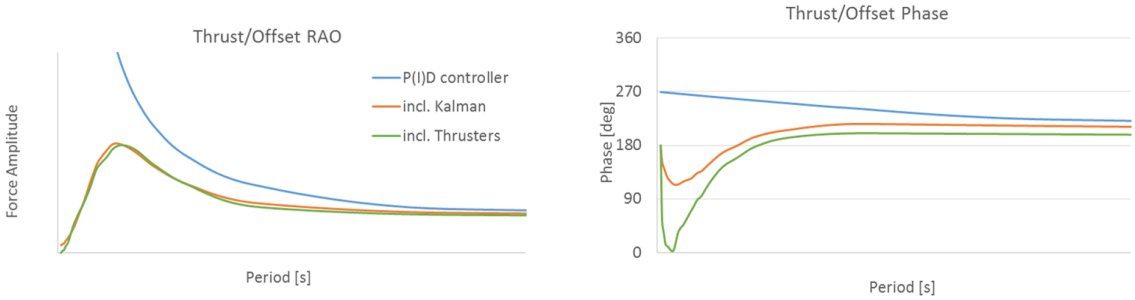

(a) Amplitude

(b) Phase

Figure 4.9: DP System RAOs [3]

The previously obtained RAO can now be further used to determine the spring and damper term for surge, sway and yaw, respectively. Damping is the part of the DP force acting opposite to the velocity, while the spring term acts opposite to the position error. The velocity from displacement in time domain is ascertained by taking the derivative with respect to time $\frac{\partial x}{\partial t}$. In the frequency domain this can be done by applying the factor $i \cdot \omega$ [25]. The spring and damper diagrams can now be obtained by[24]:

- Spring $= -Re(H)$
- Damper $= -Re(\frac{H}{i\omega})$

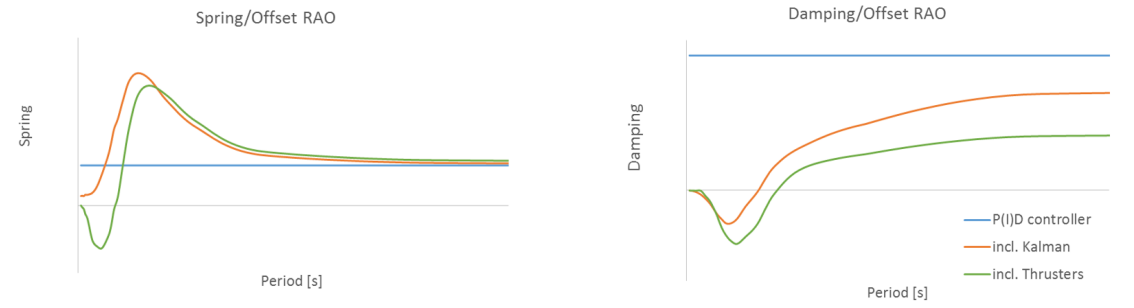

(a) Effective Spring

(b) Effective Damping

Figure 4.10: DP System effective spring and damping RAOs [3]

Figure 4.10b shows that the effective damping is negative for low periods, which causes the DP system to become unstable. This period, where the damping becomes negative is defined as the 'DP critical period' (not considering additional damping). This was one motivation for HMC to determine these DP system RAOs, as the critical period, the cause for DP-instability, can be determined. [3] In the present research, the DP RAOs will be utilised to determine the effective spring and damping coefficients.

4.4.2. Spring and Damping of DP system

From the previous results, where the Controller and Kalman Filter Gains were compared, it was observed that a large discrepancy was present between the aNySIM simulations and the real-time simulations. Using DP RAOs the effective spring and damping coefficients of the vessel can be obtained. This provides additional insight to the DP system and provides the possibility to conduct time-domain simulation with the obtained coefficients.

The procedure of how to obtain the spring and damping terms of the DP system will be shown for the Normal Kalman Filter Gain and Medium Controller Gain from the simulation of the only waves environment, as presented in section 4.3.1 (Direction (coming from - trueN) 300°, $T_p = 9s$, $H_s = 2m$, JONSWAP $\gamma = 3.3$).

The first step is a regression analysis, as presented in figure 4.11. The demanded proportional force $F_{proportional} = -P \cdot \Delta x$, where x represents the position error, is plotted against the estimated offset for surge, sway and yaw respectively. A similar process is undertaken for the damping force $F_{damping} = -D \cdot \frac{\partial x}{\partial t}$, however, here plotted against the estimated velocities. Note, that these velocities are estimated by the Kalman Filter and differ from the real vessel velocity $\frac{\partial x}{\partial t}$ (see section 4.4.5). With a regression of the demanded values the 'P' and 'D' gain as demanded by the controller can be determined. [24]

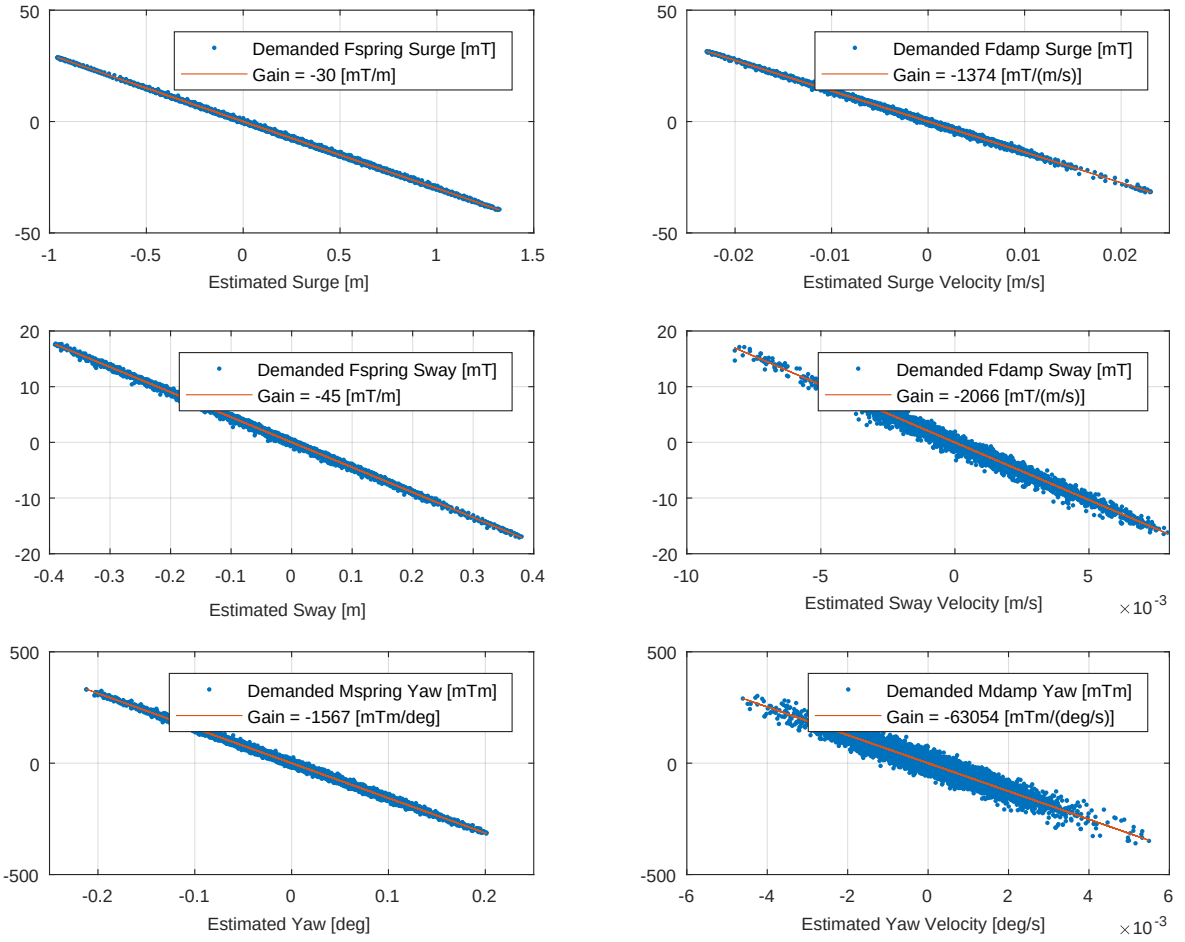

Figure 4.11: DP-controller demanded Spring and Damping Forces - Normal Kalman & Medium Gain - Waves (Direction (coming from - trueN) 300°, $T_p = 9s$, $H_s = 2m$, JONSWAP $\gamma = 3.3$), Heading 90° (trueN), Draft 26.6

When the frequency dependent spring and damping on basis of the transfer function $H(i\omega)$ is determined, the demanded 'P' and 'D' gains are plotted as indication, see below. Here, the critical period for the DP system is also indicated.

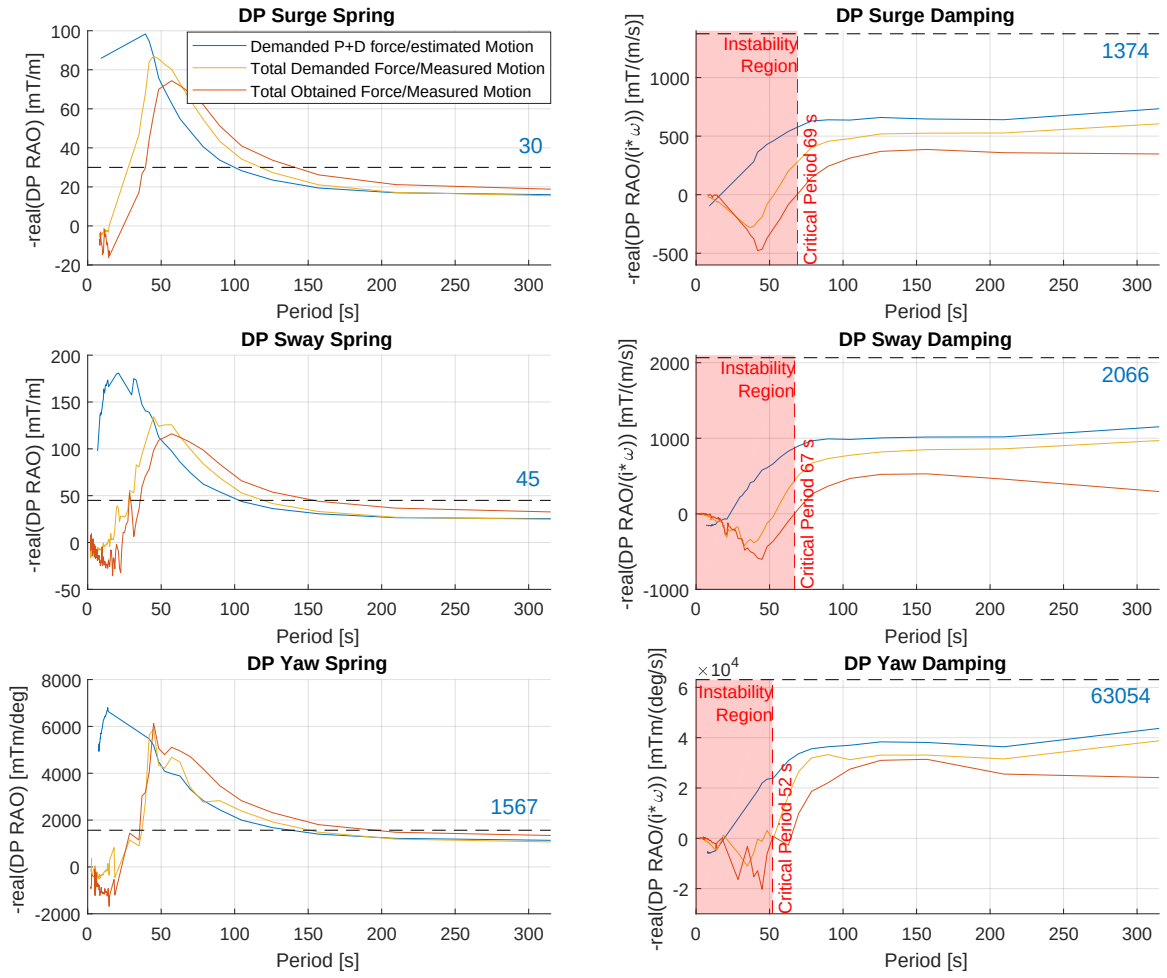

Figure 4.12: DP RAO - Spring and Damping Terms - Normal Kalman & Medium Gain - Waves (Direction (coming from - trueN) 300°, $T_p = 9s$, $H_s = 2m$, JONSWAP $\gamma = 3.3$), Heading 90° (trueN), Draft 26.6

Besides the negative damping, resulting in an unstable control system, it can be seen that the damping the system experiences (including Kalman Filter, Thrust Allocation and Thrusters), is for all 3 DOF, less than half of the demanded damping gain. Furthermore, for the low periods, the spring term is larger and delays from the Kalman filter and Thrust Allocation plus Thrusters are introduced. For longer periods, the spring term approaches the demanded value.
DP spring terms of approx. 30 to 45 mT/m result in natural periods of approx. 170s in surge and sway for Thialf. To be within the range of the natural period, the spring and damping terms for the following assessment will be selected for the period range from 157s ($\omega = 0.04rad/s$) to 210s ($\omega = 0.03rad/s$). The assessment will also include the simulation in the same environmental condition, with the same Controller Gain, but with High Kalman Filter Gain, see table 4.3. The regression analysis and the Spring and Damping Terms can be found in Appendix D

	Spring			**Damping**		
Unit	Surge *mT/m*	Sway *mT/m*	Yaw *mTm/deg*	Surge *mT/(m/s)*	Sway *mT/(m/s)*	Yaw *mTm/(deg/s)*
Normal Kalman - Med. Contr.	24	40	1643	373	494	28467
High Kalman - Med. Contr.	31	49	1972	629	853	30460
Unit	*kN/m*	*kN/m*	*kNm/deg*	*kNs/m*	*kNs/m*	*kNms/rad*
Normal Kalman - Med. Contr.	235	392	9.23×10^5	3.66×10^3	4.85×10^3	1.60×10^7
High Kalman - Med. Contr.	304	481	1.11×10^6	6.17×10^3	8.37×10^3	1.72×10^7

Table 4.3: Spring and Damping Coefficient obtained via DP RAO

	Mass & Inertia		Added Mass @ $\omega = 0.03 rad/s$		
Unit	M *t*	I_{zz} *tm²*	A_{11} *t*	A_{22} *t*	A_{66} *tm²*
SSCV Thialf @ T=26.6	174,722	7.38×10^8	52,732	171,359	3.11×10^8

Table 4.4: Mass, Inertia and Added mass

With the obtained spring term and the mass, inertia and added mass for the 3 DOF the natural period and the critical damping can be determined, based on:

$$T_n = 2\pi \sqrt{\frac{M + A}{k}} \tag{4.17}$$

$$B_c = 2\sqrt{k(M + A)} \tag{4.18}$$

Where:

T_n	=	Natural (undamped) Period	[s]
B_c	=	Critical damping coefficient	[kNs/m]
M	=	Mass	[kg]
A	=	Added Mass	[kg]
k	=	Spring Constant here obtained spring	[N/m]

	Natural Period			Critical Damping		
Unit	$T_{0_{Surge}}$ *s*	$T_{0_{Sway}}$ *s*	$T_{0_{Yaw}}$ *s*	$B_{c_{Surge}}$ *kNs/m*	$B_{c_{Sway}}$ *kNs/m*	$B_{c_{Yaw}}$ *kNms/rad*
Normal Kalman - Med. Controller	195	187	212	2.33×10^4	6.22×10^7	1.60×10^7
High Kalman - Med. Controller	172	169	193	2.58×10^4	6.82×10^7	1.72×10^7

Table 4.5: Natural Period and Critical Damping

Now, the critical damping coefficient β can be determined.

$$\beta = \frac{b}{B_c} \tag{4.19}$$

in which:

β	=	Critical damping coefficient	[-]
b	=	Actual damping	[kNs/m] or [kNms/rad]
B_c	=	Critical damping	[kNs/m] or [kNms/rad]

and for the following values the system can be considered:

β	=	0	- undamped
β	<	1	- underdamped
β	=	1	- critically damped
β	>	1	- overdamped

	Critical Damping Coefficient		
Unit	β_{Surge} *[-]*	β_{Sway} *[-]*	β_{Yaw} *[-]*
Normal Kalman - Med. Controller	25 %	21 %	26 %
High Kalman - Med. Controller	37 %	32 %	25 %

Table 4.6: Critical Damping Coefficient with actual damping

As a final step, the critical damping coefficient between the critical damping and the damping that the controller demanded, which was obtained form the regression analysis.

	Critical Damping Coefficient		
Unit	β_{Surge} [-]	β_{Sway} [-]	β_{Yaw} [-]
Normal Kalman - Med. Controller	92 %	87 %	57 %
High Kalman - Med. Controller	79 %	73 %	45 %

Table 4.7: Critical Damping Coefficient with damping as demanded by controller

4.4.3. Discussion

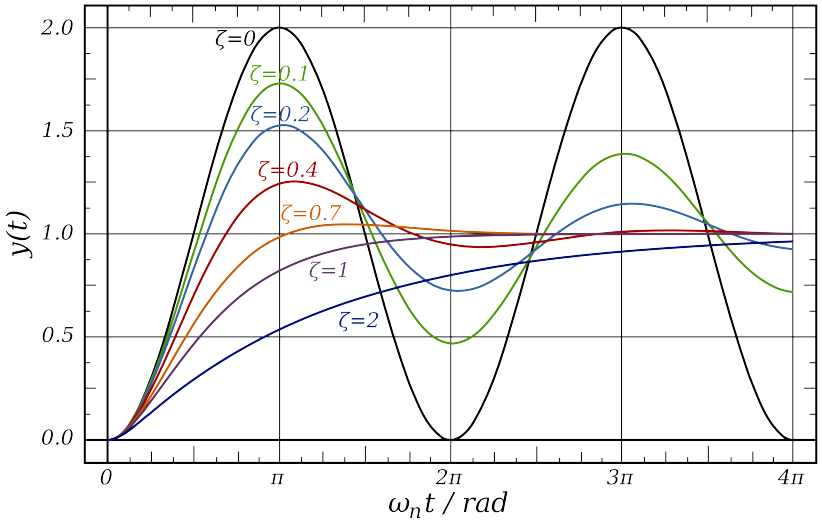

Figure 4.13: Effect of vaying damping ratio β here ζ

In figure 4.13, the effect of the damping coefficient β here referred to as ζ, is depicted for a second order system. It can be noted that $\zeta = 0$ results in an undamped motion and the oscillation continues. From the settings of the Kongsberg DP system, it can be ascertained that the theoretical damping for surge and sway is 90% of its critical damping for that motion and for yaw 70%. With reference to figure 4.13, these values represent the best trade-off between reaction time and overshoot.

The demanded critical damping coefficient (table 4.7) for Normal Kalman Filter Gain and Medium Controller Gain with $\beta_{surge} = 92\%$ and $\beta_{sway} = 87\%$ represent that, while for yaw it is $\beta_{yaw} = 57\%$ instead of the theoretical 70%. Upon studying the simulation using the High Kalman Filter gain, it can be seen that the demanded dampings are between 11% to 25% less than demanded.

The critical damping coefficients with the actual obtained damping for the Normal Kalman Filter Gain reduce to $\beta_{surge} = 25\%$, $\beta_{sway} = 21\%$ and $\beta_{yaw} = 26\%$, while for the High Kalman Filter Gain $\beta_{surge} = 37\%$, $\beta_{sway} = 32\%$ and $\beta_{yaw} = 25\%$ (table 4.6). A prominent factor is that the demanded critical damping coefficient of the High Kalman Gain simulation is lower than for the Normal Kalman Gain, which itself is closer to the theoretical damping. However, the damping coefficients for the obtained actual damping (High Kalman Gain simulation) are larger for surge & sway and similar for yaw. Looking at figure 4.13, such small damping ratios will cause the vessel to overshoot and cause it to oscillate more.

4.4.4. Effect of Reduced Damping

To highlight the influence of lost damping a test series with decreasing critical damping values is presented here. Furthermore, with this series it was also aimed to mimic the vessel motions as observed in the HSC. The comparison will be done against the Normal Kalman Filter Gain & Medium Controller Gain simulation as presented in section 4.3.1 under the same environmental conditions. From this measurement the spring coefficient and the critical damping was obtained via DP RAOs. The same

Spring terms will be applied (table 4.3: Normal Kalman - Med. Contr.), while the damping will be altered for cases A - K as percentage of the critical damping, see table 4.8.

Case	Critical Damping Coefficient		
	β_{Surge} [-]	β_{Sway} [-]	β_{Yaw} [-]
A	90 %	90 %	70 %
B	80 %	80 %	65 %
C	70 %	70 %	50 %
D	60 %	60 %	55 %
E	50 %	50 %	50 %
F	40 %	40 %	40 %
G	30 %	30 %	30 %
H	20 %	20 %	20 %
I	15 %	15 %	15 %
J	10 %	10 %	10 %
K	5 %	5 %	5 %

Table 4.8: Critical Damping Coefficient - Damping Series

Results

Figure 4.14 displays the results for case A , where 90% critical damping for surge and sway and 70% for yaw was applied. Below, in figure 4.15, the results for the test case H with 20% critical damping for surge, sway and yaw are shown. The complete results (case A to K) can be found in Appendix E. For all figures the obtained result from the HSC is shown, where $\beta_{surge} = 25\%$, $\beta_{sway} = 21\%$ and $\beta_{yaw} = 26\%$ (table 4.6). Additionally, the natural damped frequency per motion of the vessel are depicted in the EDS' with the according natural damped period T_{0_d}.

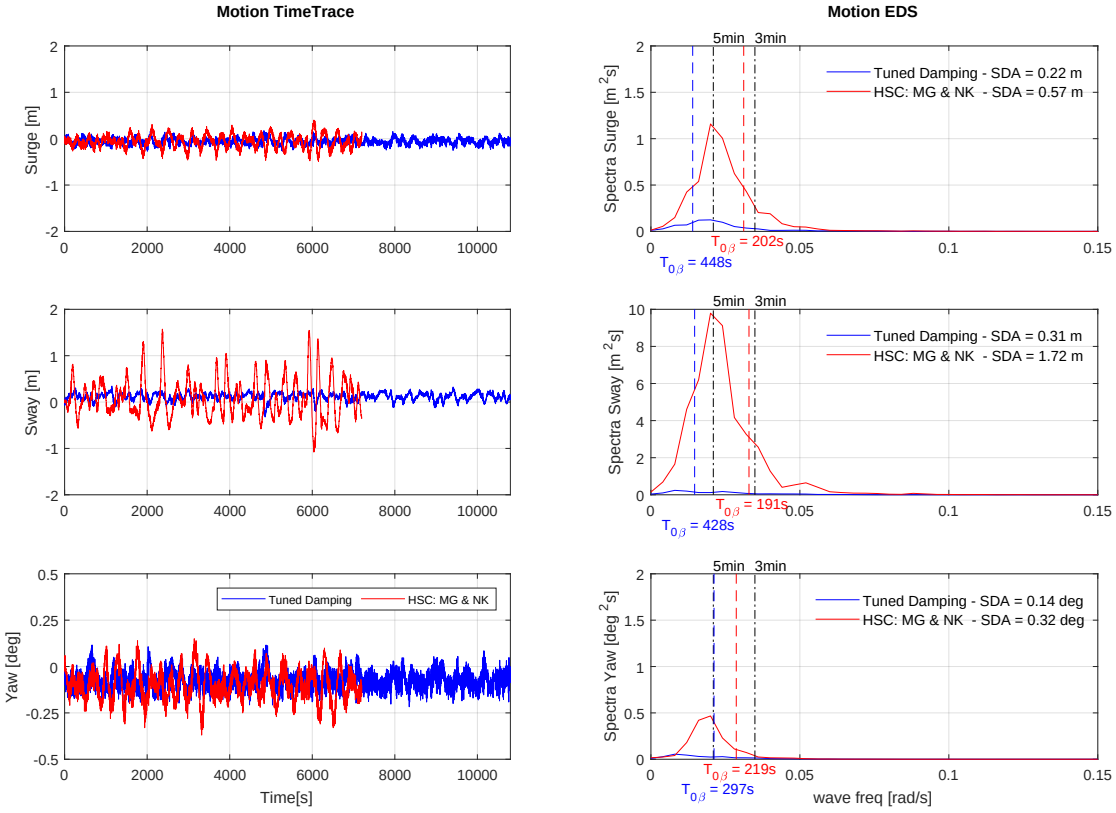

Figure 4.14: Case A - Damping Series Comparison with HSC Simulation SSCV Thialf - Heading: 90 deg, Draft 26.6 m, Waves (Dir=300(coming from), $T_p = 9s$, $H_s = 2m$, JONSWAP, $\gamma = 3.3$), Kalman Gain: Normal, Controller Gain: Medium

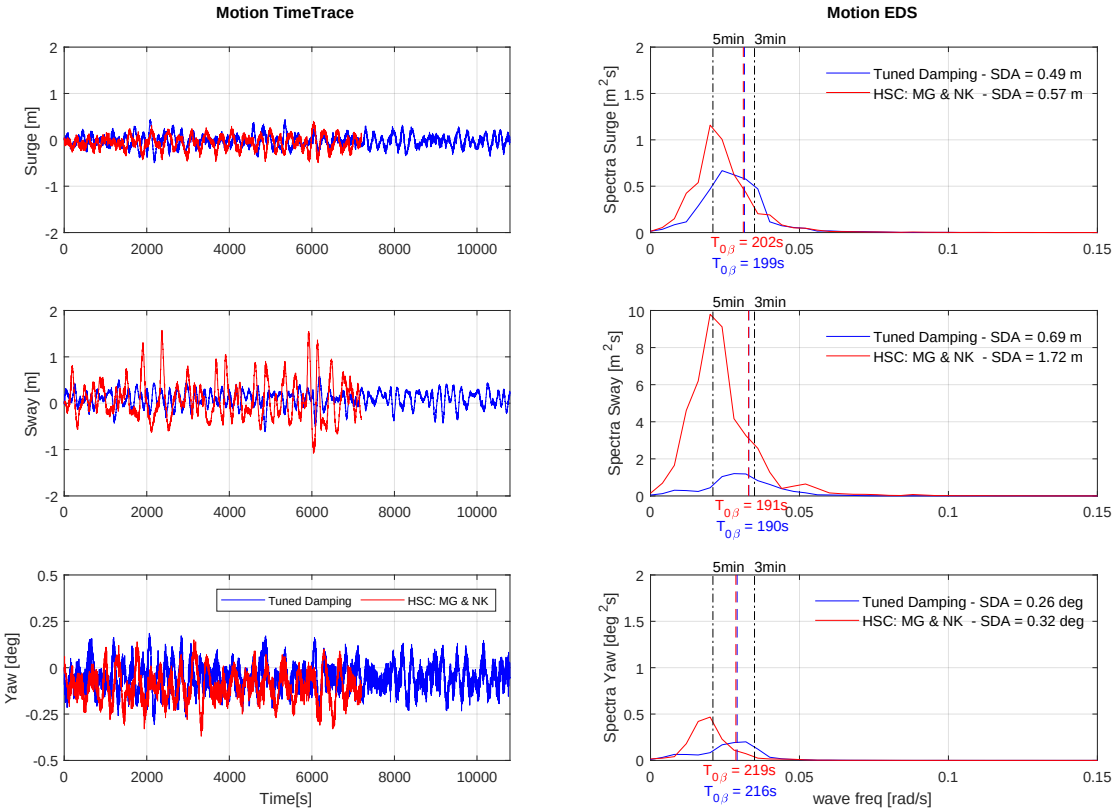

Figure 4.15: Case H - Damping Series Comparison with HSC Simulation SSCV Thialf - Heading: 90 deg, Draft 26.6 m, Waves (Dir=300(coming from), $T_p = 9s$, $H_s = 2m$, JONSWAP, $\gamma = 3.3$), Kalman Gain: Normal, Controller Gain: Medium

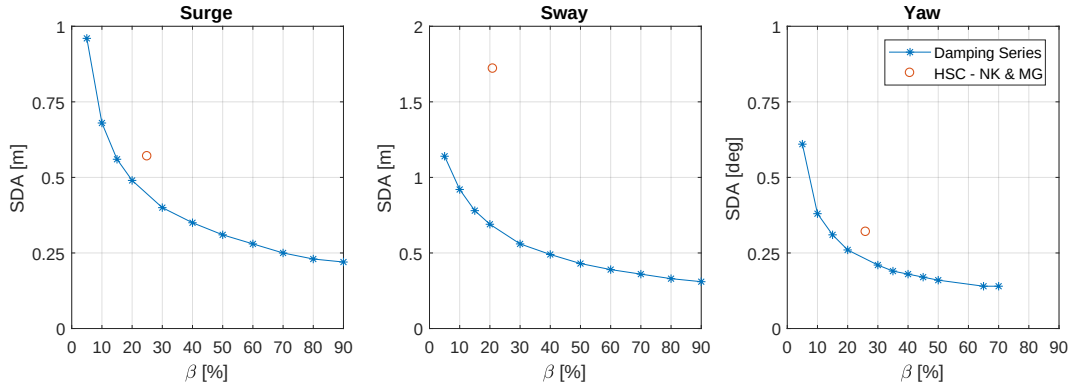

Figure 4.16: SDA Assessment of Damping Series Case A to K and HSC Simulation SSCV Thialf - Heading: 90 deg, Draft 26.6 m, Waves (Dir=300(coming from), $T_p = 9s$, $H_s = 2m$, JONSWAP, $\gamma = 3.3$), Kalman Gain: Normal, Controller Gain: Medium

Discussion

The damped natural frequency ω_d and natural damped period T_{0_d} is defined as:

$$\omega_d = \omega_n \sqrt{1 - \beta^2} \tag{4.20}$$

$$T_{0_d} = \frac{2\pi}{\omega_d} \tag{4.21}$$

Where:

ω_d	=	Natural damped frequency	[rad/s]
ω_n	=	Natural (undamped) frequency	[rad/s]
β	=	Critical damping coefficient	[-]
T_{0_d}	=	Natural damped period	[s]

From this one can conclude that with decreasing damping, the natural damped frequency increases. For the DP System with ideal damping, a natural damped period for surge of $T_{0_d} = 448s$ is obtained (figure 4.14). However, for the DP System with only 20% critical damping, a natural damped period for Surge of $T_{0_d} = 199s$ is obtained (figure 4.15). This can be similarly be observed for sway and yaw. Comparing the peak periods for case A and case H the following becomes clearer. As less damping is present, the damped natural periods shift towards the range of 3-5 minutes. Due to the reduced damping the vessel overshoots and motions with large excitation take place, which is then observed in the EDS.

Furthermore, in figure 4.16 the SDAs for surge sway and yaw per critical damping β from the simulation cases of A to K are plotted. The SDA, as obtained from the HSC simulation is also depicted. It can be seen, that with decreasing β the SDAs incrase. While the SDAs for surge and yaw of the HSC are close to the aNySIM simulation, the SDA of sway is larger than the SDA with even 5% critical damping.

A possible cause for this behavior can be the direction of generated thrust. As the waves are predominantly acting in longitudinal direction of the vessel, the majority of thrust is generated opposite that direction to counteract - refer to figure 4.3 and 4.6. When transverse offsets now occur, the DP system cannot react quickly enough to rotate the thrusters and deliver an opposing force. This observation is explained further in section 5.6.1.

4.4.5. Estimation of Vessel Velocity

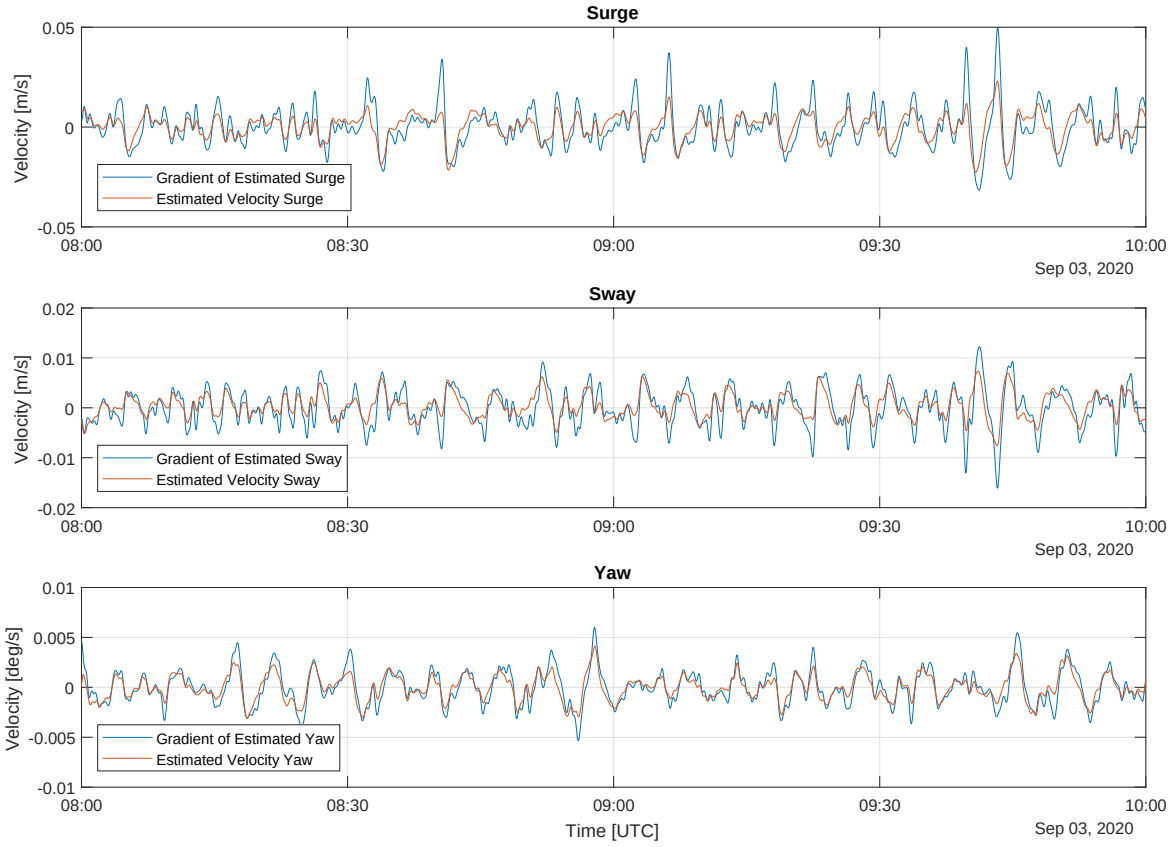

Figure 4.17: Estimated Velocity vs Vessel Measured Velocity from HSC run with SSCV Thialf - Heading: 90 deg, Draft 26.6 m, Waves (Dir=300(coming from), $T_p = 9s$, $H_s = 2m$, JONSWAP, $\gamma = 3.3$), Kalman Gain: Normal, Controller Gain: Medium

One explanation as to why damping is lost over the control loop, is the estimation of the velocity. The instantaneous velocity of the vessel can only be estimated based on the previous prediction and position. This means that estimation errors of the vessel velocities are made and based on that a different damping demanded. This can be seen in figure 4.17, where the estimated and real velocity are shown. The real velocity is obtained by calculating the gradient of the position signal, which is the velocity as the vessel experienced. From there, it is evident that indeed estimation errors are present, especially for the higher values that can then cause insufficient damping.

4.4.6. Subconclusion

Before any conclusions can be drawn, it must be noted that the DP RAO assessment method is still under development. Another factor to consider is the duration of the measurement/simulation. While the present simulations were 2 hours, for periods of 210s, this does only represent 34 cycli. Especially for the long periods to be investigated around the natural frequency, longer measurements are required in order to obtain an accurate RAO. Nevertheless, this method has still shown to be valuable for this research and highlighted certain DP system behaviors.

First, it can be claimed that over the entire control loop, from Kalman Filter, to Controller, to Thrust Allocation and the Thrusters, the damping decreases. According to the DP RAOs for Normal Kalman Filter Gain, for a demanded surge damping of $\beta_{surge} = 92\%$ only $\beta_{surge} = 25\%$ is actually obtained. While the discrepancy between the estimated and actual velocity is one contributing factor, it seems that the Kalman Filter itself and the Thrust & Thrust Allocation cause the effective damping to decrease more - see figure 4.12. Furthermore, from the obtained data it can be seen that when High Kalman Filter Gain is selected less damping is demanded by the controller - see table 4.7. Yet over the whole control loop, when the High Kalman Filter is selected, less damping is lost - table 4.6. One reason for this could be a more acurate estimation of the vessel velocity by the High Kalman Filter in comparison to the Normal Kalman Filter. This requires further investigation.

Presently, only one factor for the 'losses' of damping, the difference between estimated and actual velocity can be mentioned. This highlights the importance that this matter requires further investigation. The DP system analysis was carried out at a late stage of the project and additional research could not be carried out. Instead, this will be advised in the recommendations in chapter 8.2.

Ideal / Not-Ideal DP System

Based on these findings, for further research in this thesis an Ideal and Not-Ideal DP System is defined (table 4.9). For both system settings, the spring terms as defined by Kongsberg for Medium Gain are used. The damping is represented with the critical damping coefficient β.

	Spring			**Damping**		
	Surge	Sway	Yaw	Surge	Sway	Yaw
Unit	*mT/m*	*mT/m*	*mTm/deg*	-	-	-
Ideal	30	45	1570	90 %	90 %	70 %
Not-Ideal	30	45	1570	30 %	30 %	30 %
Unit	*kN/m*	*kN/m*	*kNm/rad*	*kNs/m*	*kNs/m*	*kNms/rad*
Ideal	294	441	8.8×10^5	1.42×10^4	2.14×10^4	4.13×10^7
Not-Ideal	294	441	8.8×10^5	4.75×10^3	7.12×10^3	1.77×10^7

Table 4.9: Spring and Damping Coefficient for Ideal & Not-Ideal DP System

5

Vortex Induced Motion on SSCV

Previous research indicates that VIM affects multi column floaters. Much research considers semi submersibles that are fixed with a mooring system to the seafloor, typical in the oil & gas industry. However, for this project, the SSCV is free floating and maintains its position by means of DP. In order to assess the effect of VIM on a SSCV during station keeping operations, the forces and moments caused by vortex shedding must be established. Subsequently, simulations can be carried out and the effect assessed.

5.1. Additional Background of VIM on Semi Submersibles

In the background chapter the Strouhal number, vortex shedding and their frequencies are briefly introduced. With reference to figure 2.6, the graph relating the Reynolds number with the Strouhal number is only applicable for circular cylinders. However, the columns on the hull of semi submersible crane vessels (e.g. *Thialf, Sleipnir, Balder*) are square or even rectangular shaped and are also arranged in an array of multiple columns. This section highlights the difference in Stouhal numbers for square cylinders with rounded edges and the effect of VIM on multi column floaters.

5.1.1. Strouhal Number

In the work of Sarioglu and Yavuz, [26], the Strouhal numbers for rectangular cross sections were determined via horizontal wind tunnel experiments and hot-film measurements. The findings can be best summarized in the following passage: ”Strouhal numbers determined for the circular cylinder are about 0.2 in the Reynolds number range $1 \cdot 10^4$ - $2 \cdot 10^5$ whereas the Strouhal numbers obtained for the square cylinder (w/h = 1.0) having the same hydraulic diameter as that of the circular cylinder at 0° incidence were between 0.12 and 0.16. The Strouhal numbers determined for the rectangular cylinders decreased with increasing width-to-height ratios. [26]”.

The recent work of Gambarine, Koop, Asso, Tampazzo and Gonçalves [27] the flow around single columns are studied specifically to gain understanding of the behaviour of multi-column floaters such as semi submersibles or floating offshore wind turbines. In their research two DOF force measurements for square cylinders with and without rounded edges were carried out to assess the forces for these two cylinders in different flow incidence (0° to 45° in steps of 7.5°). The experiments were carried out in a recirculating water channel at a Reynolds number of $Rn = 4 \cdot 10^4$. The rounded edges of the cylinder had a radius of 6.25mm at a length of 125mm. It was discovered that, for the 7 incidence angles, the rounded edge caused an approximate 10% reduction of the drag coefficient. More important for this research are the results of the performed Strouhal number study (figure 5.1). For the sharp and rounded edge configuration an increase of St at the incidence angle of 15° takes place. Furthermore, the observed Strouhal number range of the rounded edge cylinder is $0.15 \leq St \leq 0.19$, while for the sharp edge cylinder $0.15 \leq St \leq 0.18$ [27].

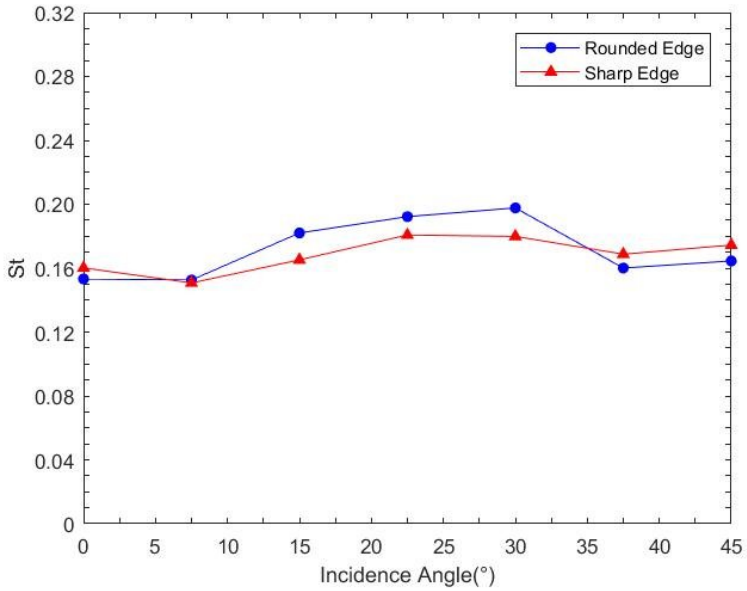

Figure 5.1: Strouhal Number versus angle of flow incidence for a square section cylinder with sharp and rounded edges [27]

5.1.2. VIM of multi column floaters

VIM has previously been observed and investigated on Truss Spars and based on these findings, the strake configuration optimized in order to minimize VIM [28]. The research of VIM and Vortex Induced Vibration (VIV) on semi submersibles and Tension Leg Platform (TLP)s has gained importance over the past two decades.The conference paper ”Flow Induced Motions of Multi Column Floaters”, by Waals, Phadke and Bultema, discusses ”the behavior in current of multi column floaters and the associated complex flow patterns” [29]. This paper makes reference to the work of Rijken, Leverette and Davies, ”Vortex Induced Motions of Semi Submersible with Four Square Columns” in which they observe VIM on the vessel [30].

One parameter to assess VIM, as outlined in section 2.4.2 is the reduced velocity Ur, which the previous mentioned research made use of. VIM occurs when the vortex shedding frequency nears the response frequency of the structure. The motion of a structure is largest at the lock-in condition, where the vortex shedding frequency is equal to the response frequency of the structure.[9]. This was also observed in [31]: ”In General the VIM of a deep draft semi is characterized by three degree-of-freedom motions, namely the surge (in-line), sway (transverse), and yaw motions, with the sway motion as the main concern in VIM. [...] Most model tests revealed that the largest sway motion, namely the lock-in condition, was observed at reduced velocity around 6-8 for a semi towed in a 45° direction”. This is also in line with the observation of [29], that ”the largest motions were observed for the 45 degree towing direction”. Likewise, the observation of [30] ”The largest VIM response amplitudes occurred when the platform was at a 45° angle to the tow direction. [...] The maximum observed normalized sway response as found for a reduced velocity between 6 and 7.” Rijken, Leverette and Davies also advise a careful approach when applying these findings to related structures due to unidentified factors in their research, such as draft, column and pontoon shape, model details, et cetera. [30]

5.2. Current Load Test

Following up on *their* advice, specific data on SSCVs is required to investigate the effect of VIM - luckily this was the case for this project.

In 2008, MARIN was appointed to conduct model tests with a semi submersible crane vessel concept and the presented information is based on the test report [32]. The vessel itself was designed with two ship-shaped pontoons, each connected with 4 columns to the deck box. The model, which has been built and used for these tests can be seen below in figure 5.2 and the full scale dimensions in figure 5.5a. The wooden model of the semi-submersible crane vessel, which will further on be referred to as New Build Vessel (NBV) has a geometric scale ratio of 1 to 40.

Figure 5.2: Model of concept design vessel [32]

The current load tests were carried out for the full scale draft conditions of 13.0 and 24.0 m and velocities of 2 and 4 knots. The towing direction was varied from 90° to 180° and 270° to 360° in steps of 15°. Due to the symmetry of the vessel, the results are applicable for the full 360° of incoming currents. The presentation of these results is a function of the heading from 0° to 180°, refer to figure 5.3. This figure depicts the position of the measurement frame to which the vessel was fixed during the tow tests. The measurement frame was attached to the bow and stern of the vessel with vertical bearings to allow for heave and pitch [32]. In addition, figure 5.4 provides further information on the direction convention for the environmental loads. In this case, the arrows are indicating the environmental influence as 'going-to', signifying that a vessel heading of 0° represents a current direction of going to 180°. The forces and the moment around the reference point are indicated. The current load test results that will be used in this research are from the 24.0 m load condition, as this is the so called 'column-draft', very similar to the *Thialf* draft of 26.6 m.

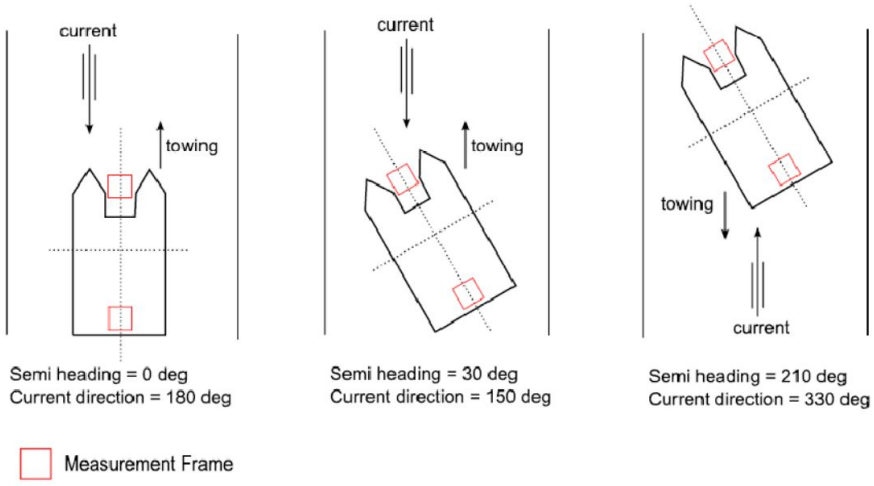

Figure 5.3: Orientation of the vessel in the basin during the current load tests [32]

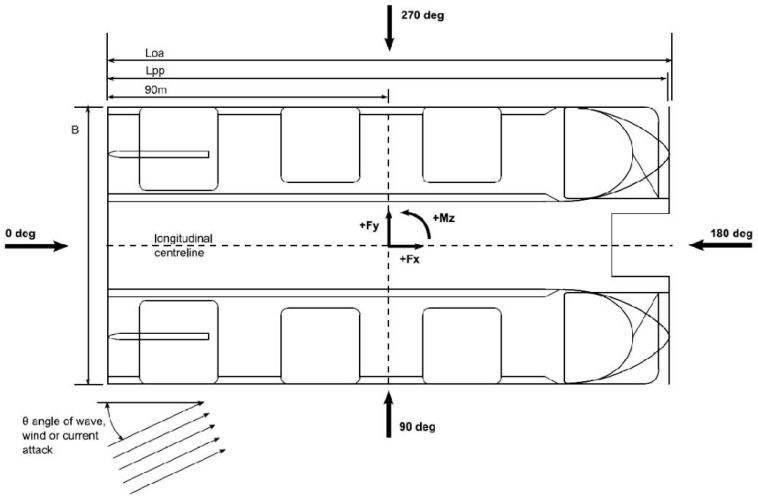

Figure 5.4: Sign convention and definition of environmental directions [32]

The relation between the vessel heading of the NBV model in the tank and the current direction is defined as:

CURRENT DIRECTION = 180° - VESSEL HEADING

5.3. Strouhal Number and Vortex Shedding Frequency

Figure 5.4 shows that for *NBV* the columns per pontoon have three different shapes. This has a direct influence on the vortex shedding frequency per column and on the investigation of the frequencies of the obtained forces & moment time traces of the current load test. These columns will be further referred to as the forward, middle (of which two are present) and aft column. From figure 5.5b, it can further be seen that *Thialf* has four columns per pontoon with two different shapes. The aft column being the largest and the three columns facing forward from there having the same dimensions. The latter mentioned columns will be referred to as ”other” for *Thialf* specifically. The effective diameter (full scale) of each of the columns for both vessels at the heading in relation to the current load tests can be obtained from table 5.1 below. This table also shows the full vessel dimension as a rectangle, as the current may not only act on each columns individually (in terms of vortex shedding) but also on the whole structure.

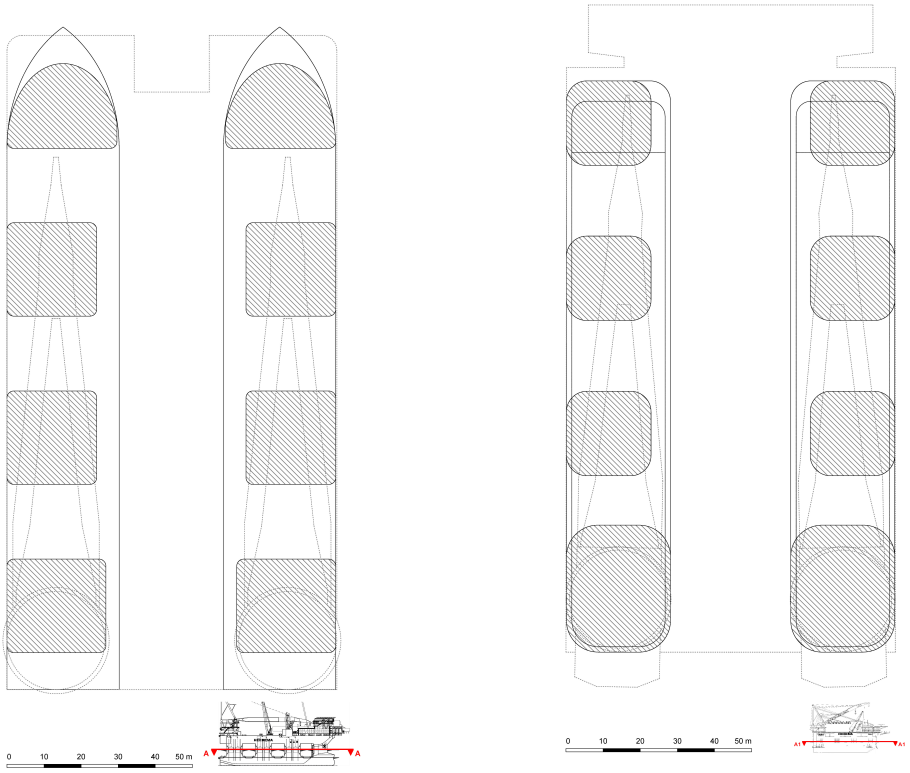

(a) NBV (b) SSCV Thialf

Figure 5.5: Vessel dimensions and indicated waterplane area at operational draft

	NBV				Thialf		
Tow Direction [deg]	Forward [m]	Middle [m]	Aft [m]	Full [m]	Other [m]	Aft [m]	Full [m]
0	29.00	25.00	28.00	87.00	22.80	28.00	88.4
15	29.57	30.48	33.38	124.01	27.52	35.30	124.82
30	30.22	33.53	36.13	152.23	29.38	38.72	151.74
45	28.91	33.70	35.82	169.46	27.52	36.94	166.6
60	27.39	33.53	35.03	177.12	29.38	40.99	175.72
75	25.22	30.48	31.25	172.09	27.52	39.68	171.13
90	22.00	25.00	25.00	155.00	22.80	34.20	153.90
105	25.22	30.48	31.25	172.10	27.52	39.68	171.13
120	27.39	33.53	35.03	177.12	29.38	40.99	175.72
135	28.91	33.70	35.82	169.46	27.52	36.94	166.6
150	30.22	33.53	36.13	152.23	29.38	38.72	151.74
165	29.57	30.48	33.38	124.01	27.52	35.30	124.82
180	29.00	25.00	28.00	87.00	22.80	28.00	88.4

Table 5.1: Measured effective column diameter in relation to tow direction for *NBV* and *Thialf*

As mentioned in section 2.4.1 the Strouhal number (St), which is required to determine the vortex shedding frequency (f_s), is dependent on the Reynolds number (Rn). Rn in return, is dependent on the flow velocity, the effective column diameter and the kinematic viscosity. Therefore, the Reynolds number must be determined first. The Reynolds numbers are determined for the effective column diameters and the full vessel footprint for NBV, Thialf and NBV model used in the tank tests. The model was built with a scale of 1:40 and the measurement results scaled with Froude scaling, which

means $\lambda_L = 40$. This means that to compute the Reynolds number, the effective diameter and the velocity must be scaled, according to [9]: $L_p = \lambda_L \cdot L_m$ and $V_p = \sqrt{\lambda_L} \cdot V_m$. Additionally, a kinematic viscosity of saltwater of $\nu_{salt} = 1.07854 \cdot 10^{-6}$ m^{2}s at a water temperature of 19°C is selected, as at this temperature saltwater has a density of $\rho_{salt} = 1025.0$ kg/m^3. The obtained Reynolds number for the full scale velocities of $V_C = 1.029 m/s = 2kn$ and $V_C = 2.058 m/s = 4kn$ is indicated in figure 5.6. To recall, the Reynolds number is defined as:

$$Rn = \frac{V \cdot D}{\nu} \tag{5.1}$$

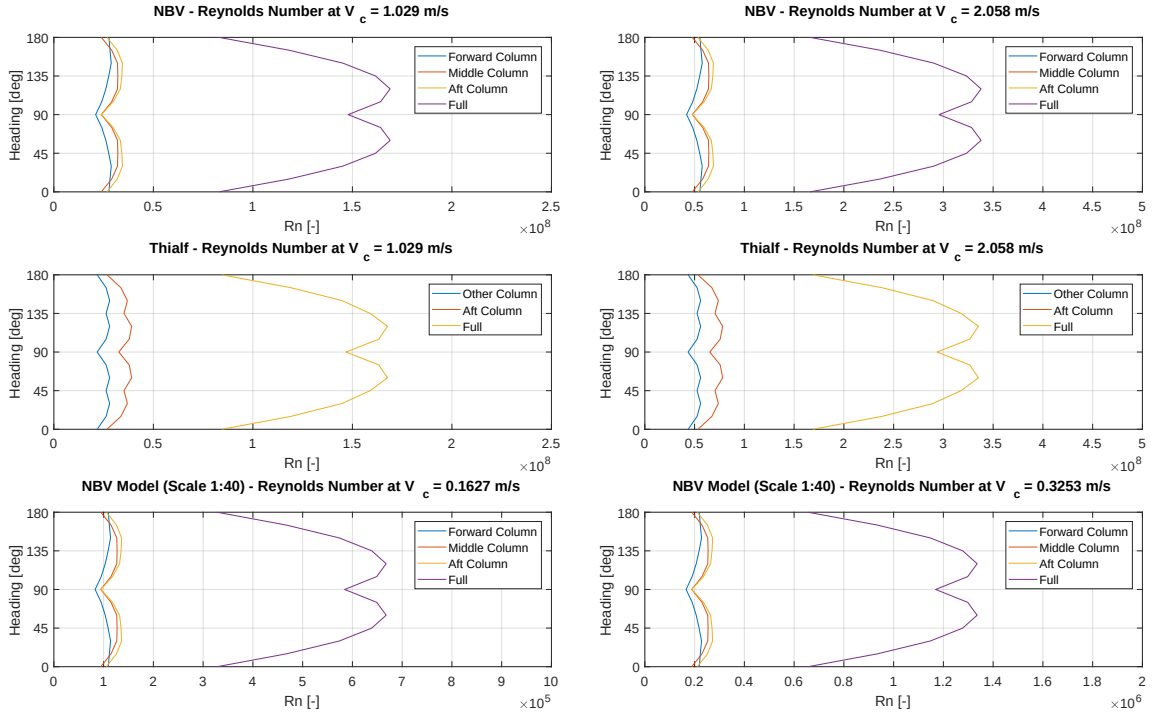

(a) V_c = 2 kn (b) V_c = 4 kn

Figure 5.6: Reynolds number for Thialf & NBV columns at full scale and NBV at model scale for 2 & 4 kn

The Reynolds numbers for the model scale dimensions range from $0.9 - 6.8 \cdot 10^5$ for 2 kn current velocity and $1.9 - 12.8 \cdot 10^5$ for 4 kn. For such a large square, rectangular and half circular shaped structures the Strouhal numbers cannot explicitly be identified. In [26] for instance, the Strouhal numbers were possible to determine for a Reynolds number of up to $2 \cdot 10^5$ for square and rectangular structures. In their experimental research, the Reynolds number range of $1 \cdot 10^4 - 2 \cdot 10^5$ the Strouhal number for square cylinder (width/height = 1.0) at an incidence angle of 0 degree were determined between 0.12 and 0.16. In addition, in [27] the Strouhal numbers for square cylinders with rounded edges at $Rn = 1 \cdot 10^4$ were $0.15 \leq St \leq 0.19$. The Strouhal number, however, is required to calculate the vortex shedding frequency, which is necessary to determine the frequency range in which vortex shedding on the columns of the hull or even the full vessels dimension take place. The vortex shedding frequency of these columns for full or model scale is difficult to be determined exactly, as they are also dependent on draft conditions, column and pontoon shapes, model details, et cetera [30]. For the model test, the Reynolds numbers for the columns are just in the range of the research of [26]. The full vessel dimension exceed these Reynolds numbers, leading to larger Strouhal numbers, when comparing it to the cylinder case (figure 2.6).

At this point, it must be noted that the intention of the determination of the Strouhal number is not to directly determine the vortex shedding frequency, but to provide an indication on the frequency band

where vortex shedding is most likely to occur. Therefore, for the following step, a Strouhal number of $St = 0.2$ and $St = 0.4$ are chosen. With the Strouhal number and the effective diameter, the vortex shedding frequency can be determined (figure 5.7) based on:

$$\omega_s = \frac{2\pi \cdot St \cdot U}{D} \tag{5.2}$$

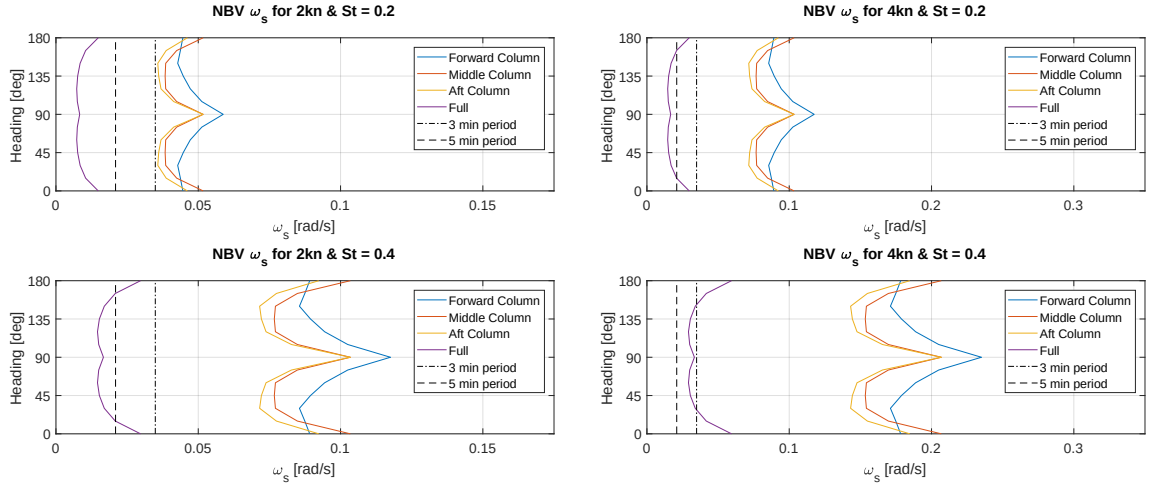

(a) V_c = 2 kn (b) V_c = 4 kn

Figure 5.7: Vortes shedding frequencies (ω_s) for NBV full scale dimension at current velocities of 2 & 4 kn and Strouhal numbers of 0.2 & 0.4

The conservative approach of a selected Strouhal number of $St = 0.4$ has been chosen to give an indication of the influence the Strouhal number has on the frequency band of the vortex shedding frequency. For lower Strouhal numbers, the vortex shedding frequencies would be even lower, which would not require further consideration as the lower limit for the selected frequency band is $\omega_{low} = 0 rad/s$. This signifies that possible Strouhal numbers of $0.15 \leq St \leq 0.19$ as reported in [27] would still be considered, but an upper limit must be selected.

Figure 5.7 indicates that the axis limit for the wave frequency is ω_{upper_s} = 0.15 rad/s for V_{c_s} = 2 kn and ω_{upper_f} = 0.3 rad/s for V_{c_f} = 4 kn. It should be noted that the subscripts s represent the 'slow' 2kn current load test and f the 'fast' 4 kn current load test. This is due to the fact that the vortex shedding frequency scales linear with respect to velocity (refer to equation 5.2). In order to observe the effect of vortex shedding for the two presented velocities, the frequency band for V_{c_s} = 2 kn is selected to ω_{fb_s} = 0 - 0.15 rad/s and for V_{c_f} = 4 kn ω_{fb_f} = 0 - 0.3 rad/s. This is further exemplified when analysing the results in the frequency domain (section 5.4) and the extrapolation of these current load test measurements (section 6.1).

Finally it must be mentioned that this estimation of the Strouhal numbers and the resulting vortex shedding frequencies does not take interaction between the different columns and columns shapes into account. Unfortunately, up to this point there are no simple methods to determine the vortex shedding frequency of such complicated multi column arrays.

5.4. Current Load Test Results

Depicted below in figure 5.8 are the EDS for the full scale forces and moments F_x, F_y & M_z at the current velocities of V_{c_s} = 2 kn at a frequency band of ω_{fb_s} = 0 - 0.15 rad/s and V_{c_f} = 4 kn at a frequency band of ω_{fb_f} = 0 - 0.3 rad/s. They are shown for all the measured heading directions from 0° to 180° and the energy content of the EDS is indicated by colours.

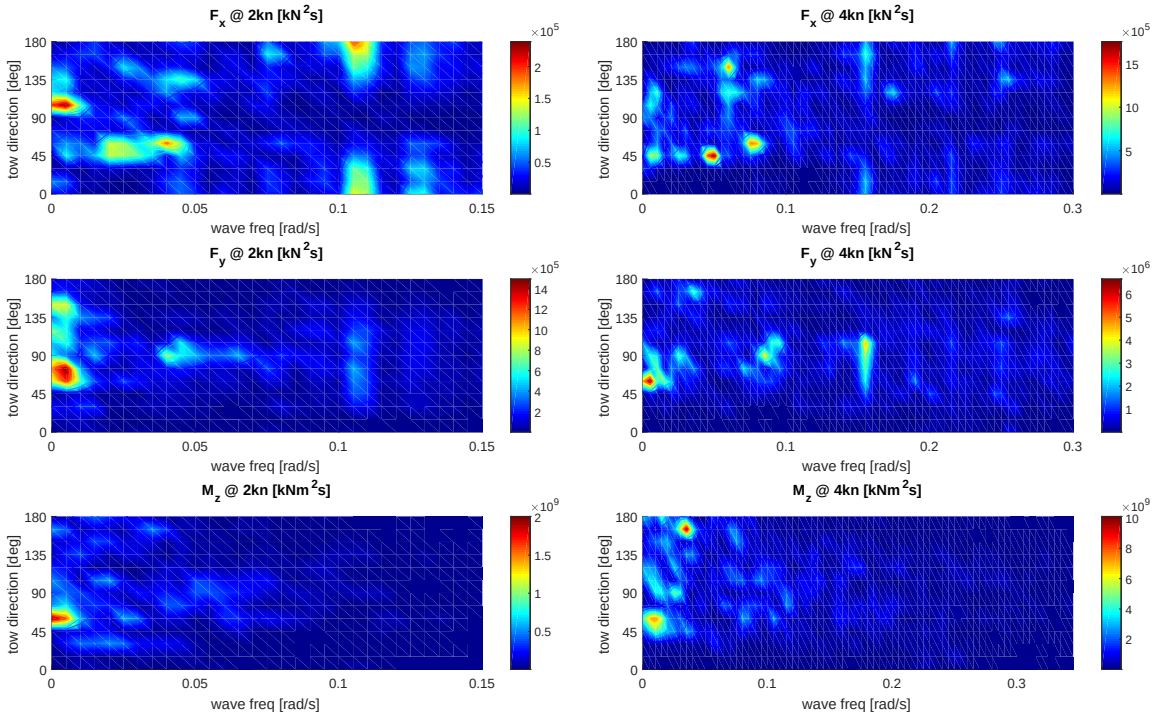

(a) V_c = 2 kn (b) V_c = 4 kn

Figure 5.8: F_x, F_y & M_z EDS for all headings at 2 & 4 kn for frequency ranges of ω_{fb_s} = 0 - 0.15 rad/s and ω_{fb_f} = 0 - 0.3 rad/s

With reference to figure 5.7 with St = 0.2, it can be observed in figure 5.8 for F_x at 2kn that in the frequency band of 0.01 to 0.05 rad/s that peaks in the EDS are present, which are in the frequency band as predicted by the vortex shedding frequency.

At the towing direction of 45° and 60 ° they appear dominant, which can be observed for the respective frequency band of 0.05 to 0.1 rad/s for F_x at 4kn. For F_x at 4kn also the 150° tow direction shows a peak.

Furthermore, for F_x at 2kn peaks are present at 0.105 rad/s, with the maxima at the tow directions of 0° and 180 °. Based on the direction convention (figure 5.4) F_x represents the longitudinal force acting in the sway direction of the vessel. This also explains the peak at the same frequency at 2kn for F_y. For 4 kn, a similar occurrence can be seen at 0.16 rad/s.

For F_y, at a tow direction of 90° a highlighted peak at 0.045 rad/s can be seen, which is for this heading in tow direction of the vessel. This is also evident at the respective frequency of 0.09 rad/s for the 4 kn measurement.

The very low frequent maxima at 0.005 - 0.01 rad/s for F_x at 105°, F_y at 60° and 75° plus for M_z at 60° have a significant energy content. These can be seen in part back at 4kn for F_y and M_z less so for F_x. Due to such low frequent alternating forces, the energy contribution to the EDS is large. Yet, particularly for the 60° tow direction, the maxima occur at 2kn and 4kn at their respective frequencies.

From these results it can be summarized that the 60° tow direction has a large energy contribution to all forces and moments F_x, F_y & M_z most notably at both tow velocities.

5.5. Effect of VIM on Station Keeping Behavior

From the previous section in which the current load test results were investigated, it is understood that from a constant current velocity, resulting time-varying forces are acting on the hull of the vessel. To assess whether these varying forces affect a SSCV during station keeping operations, the vessel must be exposed to these forces. This was conducted using the HSC, which, in comparison to an aNySIM Spring-Damper time domain simulation, provides insight to the thruster response. The simulations were carried out with the obtained full scale forces for the vessel headings of 60° and 90° at the current velocity of 2 kn, which results in a current direction (coming from) of 120° and 90° respectively, in the local vessel coordinate system. Resulting from the symmetry of the hull, they can be also represented as currents coming from 240° and 270°. For clarification, refer to figure 5.9 below.

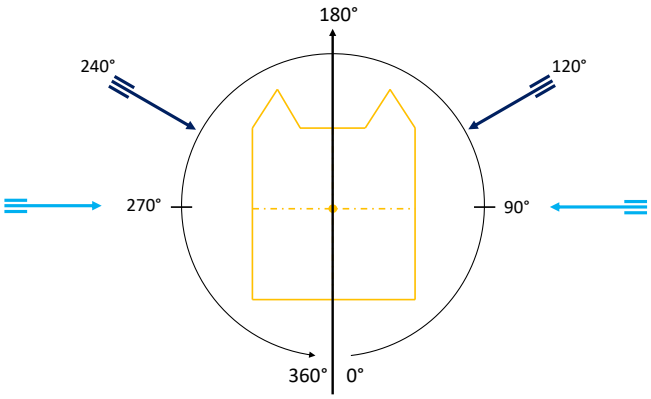

Figure 5.9: Direction convention for incoming currents as vessel was exposed to in current load tests. 60° heading (dark blue) and 90° heading (light blue) in the vessel coordinate system, as used in the current load tests (figure 5.4)

5.5.1. Simulation Setup

The setup for these simulations is similar and is applicable for both cases. The scenarios were set up where SSCV Thialf was located next to platform which is fixed in all 6 DOF and equipped with FanBeam reflectors. Furthermore, the procedure for real-time simulations in the HSC as outlined in section 4.2.2 was followed. Once the Kalman Filter & Controller Gain was selected, the forces and moments from the current load tests were added using the API. The force time traces used for these simulation runs were duplicated in time in order to account for the required stabilizing time of the vessel while in DP. Afterwards, only the second half of the time trace was used for the investigation.

		HSC Real-time Simulation
Vessel	Kalman Filter Gain	High
	Controller Gain	Medium
	Draft	26.6 m
	Position Reference System	Fanbeam 1 & 2 and LTW
Environment	Wind	-
	Waves	-
	Current	-
	External Forces & Moments	Time traces of 60° heading (fig C.2) and 90° heading (fig 5.11) current load test results
Duration	60° heading case	4744 s (of which 2372 s run-up)
	90° heading case	4934 s (of which 2467 s run-up)

Table 5.2: Vessel and environmental parameters

5.5.2. Simulation Results - 2kn & 90° heading

The input for this simulation was obtained from the 2kn and 90° current load test results and can be seen in figure 5.11. These forces and moments represent a current coming from 270° in both, the true North coordinate system as well as the coordinate system used by MARIN - see figure 5.10 below. Figure 5.12 to 5.14 show the results.

Note, that the results for the 2kn & 60° heading case can be found in Appendix C.

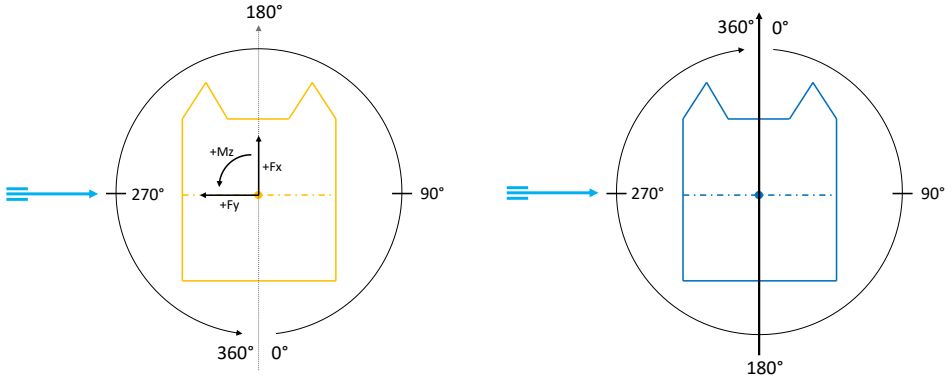

Figure 5.10: Direction convention for incoming currents, coming from 270° vessel coordinate system (left) and coming from 270° true North coordinate system (right)

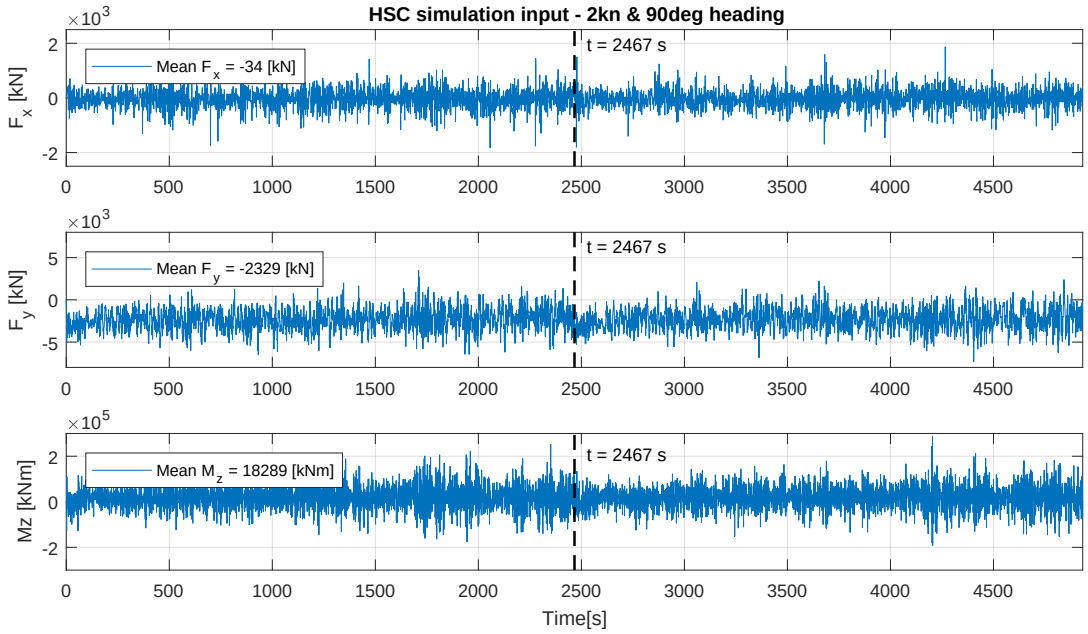

Figure 5.11: Simulation input - HSC - Normal Kalman Gain & Medium Controller Gain - 90° heading & 2 kn current load test measurements. The first half up to the black dashed line at $t = 2467s$ is the stabilizing time, from here the real measurement starts.

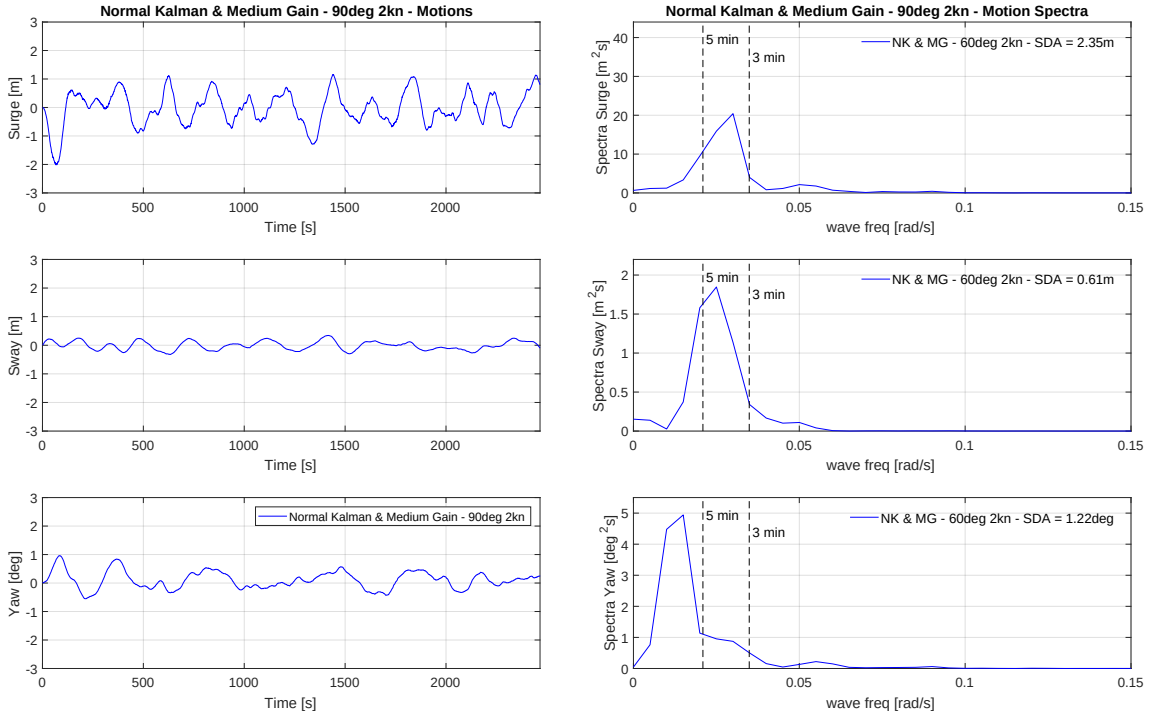

(a) Vessel Motions (b) Vessel Motions EDS

Figure 5.12: Vessel Motions - HSC - Normal Kalman Gain & Medium Controller Gain - exposed to 90° heading & 2 kn current load test measurements

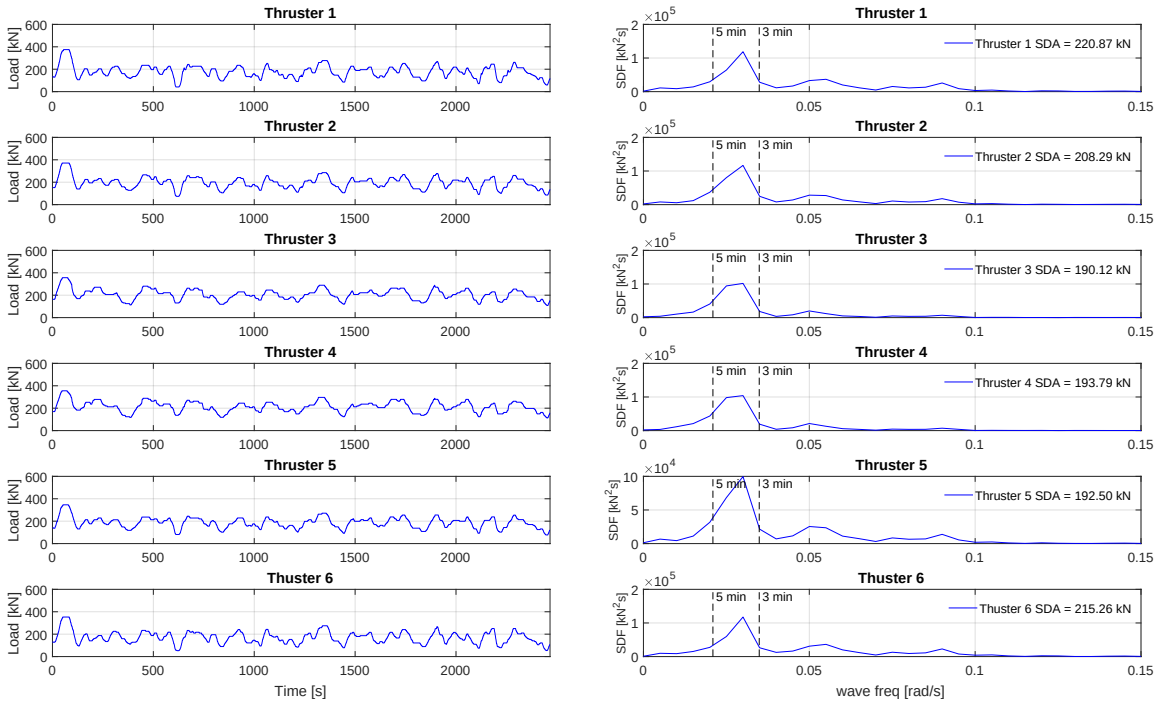

(a) Thruster Load (b) Thruster Load EDS

Figure 5.13: Thruster Load - HSC - Normal Kalman Gain & Medium Controller Gain - exposed to 90° heading & 2 kn current load test measurements

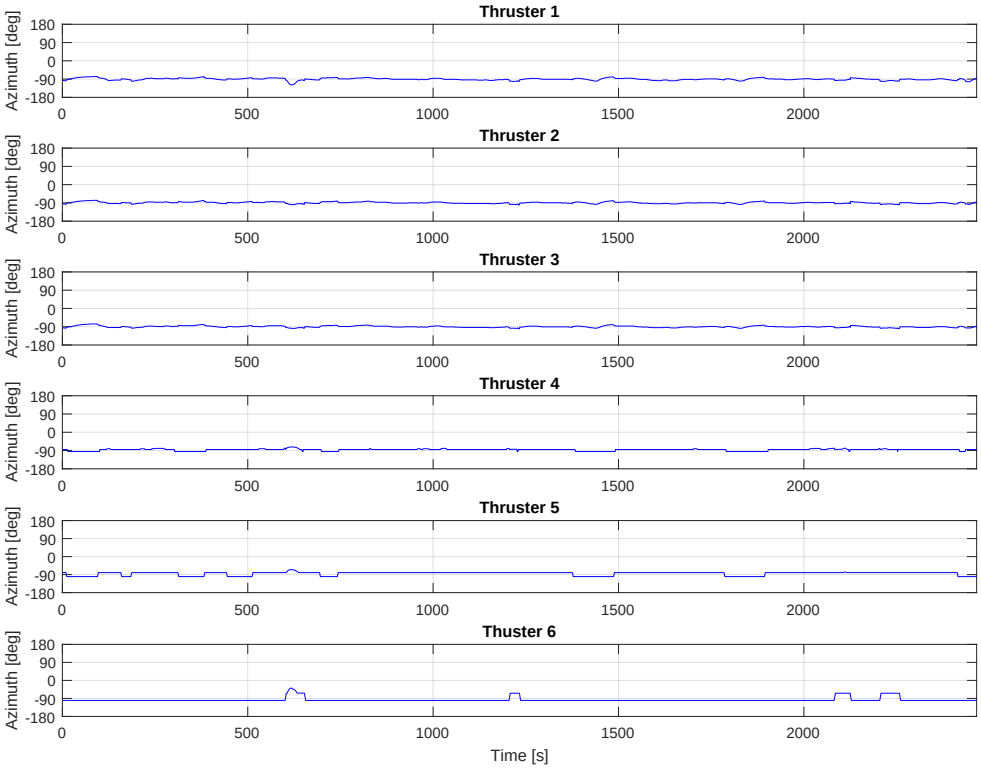

Figure 5.14: Thruster Azimuth - HSC - Normal Kalman Gain & Medium Controller Gain - exposed to 90° heading & 2 kn current load test measurements

5.5.3. Discussion

The 90° heading case represents the current in transverse direction of the vessel. This is also apparent with the force input of F_x, fluctuating around the with a mean of -34 kN. From figure 5.12b, it can be observed that the peaks of the energy content for surge and sway lays within the the relating frequencies of the periods of 3 and 5 minutes are indicated in the EDS. With their according SDAs of SDA_{Surge} = 2.35m and SDA_{Sway} = 0.61m. For Yaw, the peak frequency decreases even further, with a peak at approx. ω = 1.75 rad/s and its SDA_{Yaw} = 1.22°. However, what stands out is the deviation along the longitudinal axis. In this scenario according to the SDA, even 3.8 times more than transverse offsets, while the mean of F_y is 68.5 times as large as F_x.
In figure 5.14, the thruster azimuth for each individual thruster can be seen. The azimuth angle for Thruster 1 to 6 are varying around -90°, while Thruster 5 and 6 show periods of no azimuth angle variation and stay constat at -90°. During the simulation, the K-POS console gave azimuth prediction errors for Thruster 5 and 6, which results in 'freezing' of the thruster azimuth value and sudden jumps, as seen for Thruster 6 between 1000 and 1500 seconds. Despite those prediction errors, it can clearly be seen that the thrusters produce their thrust towards -90° in the local vessel K-POS coordinate system. This is also the direction where the current is coming from, see figure 5.15.

5.6. Subconclusion

From the current load tests, it can be concluded that from a constant current acting on the hull of a SSCV time-varying forces and moments occur. The peak frequencies of these varying forces are in the frequency range of the estimated vortex shedding frequencies for the columns and the full dimensions on the hull. Interaction between the different columns, shedding patterns and specific column shapes cannot be taken into account and complicate the estimation of the exact vortex shedding frequency. Nonetheless, by simply investigating the EDS and knowing that the vortex shedding frequency scales linearly w.r.t. velocity, it becomes evident that at the same respective frequency for the same heading, energy peaks are present. This strongly indicates that these time-varying forces indeed originate from vortex shedding.

With real-time simulations in the HSC, where the vessel was exposed to these measured time-varying forces from 2kn current load test, the vessel showed large offsets with peak periods between 3 to 5 minutes and lower.

Upon investigating the thruster response, peak periods in the load EDS also are between 3 to 5 minutes. The azimuth of the thrusters shows small variation, which was also observed in the DP Trials 2017 [4]. In addition, due to large mean force in transverse direction (and thrust generated transversely), force-variation in longitudinal direction cause large longitudinal offsets.

Finally, as 2kn represent a high current velocity for SSCV Thialf, an assessment method is required to investigate the effect at lower velocities, which is the main topic of the next chapter.

5.6.1. Thruster Response Observation

In the previous chapter an observation was mentioned on the thruster azimuth. In the given scenario the majority of the environmental forces were in longitudinal direction of the vessel. It was noted, that subsequently the thrusters are producing most thrust also in longitudinal direction to counteract these forces. This resulted in large transverse offsets.

In the present case, where the forces represent a current purely in transverse direction of the vessel this is further exemplified. Here, all 6 thrusters are directed towards -90° to provide an opposing force to the current, see figure 5.15 below.

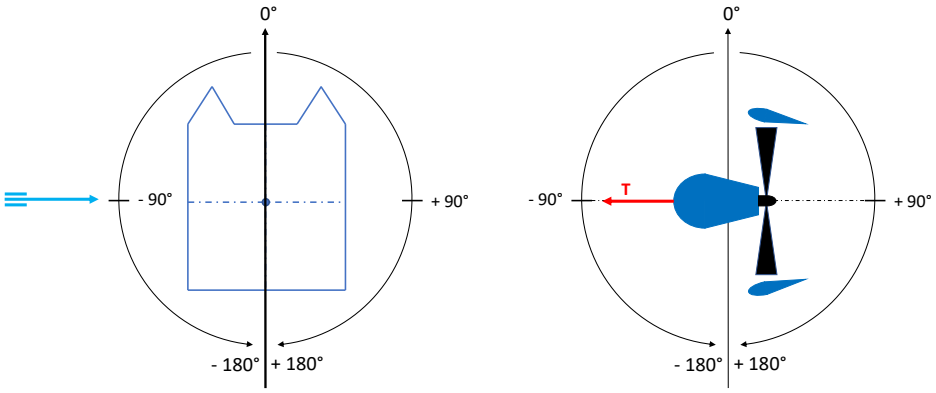

Figure 5.15: Azimuth orientation with indicated current direction

As the thrust is now directed completely in transverse direction of the vessel, the offsets in transverse direction decrease, because the thrusters can react fast to position errors in sway by only adapting the RPM per thrusters. This is can be observed clearly in the time trace of the thruster load (fig 5.13a). However, longitudinal variation of forces, caused by vortex shedding, then cause large surge offsets with an SDA of 2.35m.

Due to the large transverse mean load, the DP System uses all 6 thrusters to counteract this force. Meanwhile only small azimuth changes are applied to correct the surge offsets. In other words, the DP system gives priority of thrust being provided in transverse direction, but seems to 'neglect' the longitudinal offsets.

One hypothesis for this behavior can be the kind of forces in longitudinal direction. From figure 5.11 it can be seen that for F_x large fluctuations are present, but only a small mean load. This could mean that the DP System has no mean load to 'lean in' and provide an opposing force and thus prioritises the transverse direction.

Therefore one recommendation is to repeat the presented simulation, where an additional smaller constant force in longitudinal direction is added (eg. 5-30 % of F_y mean). The DP System should be provided with a constant load large enough to lean in yet small enough to still be affected by the fluctuations due to VIM. The intention of this is to figure out, how well the system will then react to longitudinal offsets due to VIM, as a recognisable constant force is present.

Additionally another approach is to bias 2 thrusters in longitudinal direction to counter the present forces and observe if the surge offsets can then be reduced. This can be tested in the HSC, but would affect the DP3 capability.

6 Extrapolation of Current Load Test

6.1. Introduction

The results of the current load test demonstrate the low frequent time-varying forces, which most likely originate from vortex shedding. With real time simulations is was possible to show the influence of these time-varying forces on the station keeping behavior of a SSCV.

The current load tests were executed at velocities of 2 and 4 knots at full scale. Especially for Thialf, current velocities above 2kn are considered too large. The range of interest, particularly for station keeping operations by means of DP are current velocities between 0 to 2 knots. In order to assess the effect of VIM on station keeping operations of an SSCV, the varying forces at each interested velocity must be known. To effectively utilise the data of the current load test, a method has been developed to extrapolate time varying current loads due to vortex shedding on the columns of the hull on a SSCV. With this method, the time-varying forces for lower velocities can be estimated and subsequently, the effect on a SSCV in during station keeping operations investigated. This is particularly important, as needs to be assessed whether vortex shedding and the resulting motions at lower velocities still represent a significant contribution to the low-frequency motion response of the vessel. The extrapolation will be done in the frequency domain. An exemplified procedure is depicted in figure 6.1 below.

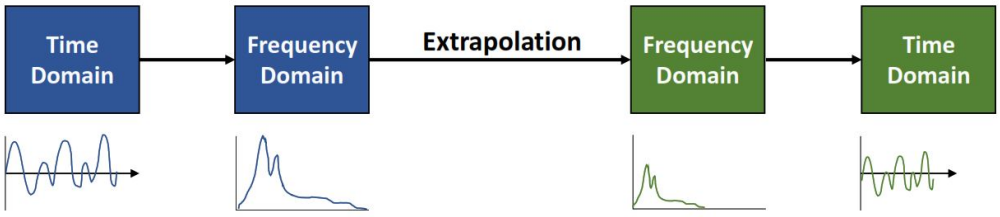

Figure 6.1: Extrapolation procedure in the frequency domain

6.2. Extrapolation Method

In section 2.3.1 the forces and moments based on current velocity were presented and are defined as:

$$F_{x,c} = \frac{1}{2}\rho \cdot V_c^2 \cdot C_{Fx,c}(\alpha_c) \cdot B \cdot T$$

$$F_{y,c} = \frac{1}{2}\rho \cdot V_c^2 \cdot C_{Fy,c}(\alpha_c) \cdot L \cdot T$$

$$M_{z,c} = \frac{1}{2}\rho \cdot V_c^2 \cdot C_{Mz,c}(\alpha_c) \cdot L^2 \cdot T$$

It can be ascertained that the forces in x and y, as well as the moment around z, scale quadratic with respect to the current velocity. The mean forces and moment due to the current load around which the forces and moments due to vortex shedding oscillate, will be extrapolated to lower current velocities based on quadratic scaling.

The vortex shedding frequency:

$$\omega_s = \frac{2\pi \cdot St \cdot U}{D}$$

scales linearly with respect to the velocity. This signifies that for higher velocities the frequency increases. However, even if the Strouhal number is affected by the Reynolds number, which in turn also depends on the current velocity; the vortex shedding frequency will still be considered to scale linear with respect to velocity.

The actual extrapolation of the fluctuating forces around the mean is done in the frequency domain. Based on the energy density spectra obtained from 2 and 4 kn measurement, the time-varying forces can be determined, as follows. From section 2.5.1 the energy density spectrum for each frequency component n, where A_n represents the amplitude for each frequency component is known to be:

$$S(\omega_n) = \frac{A_n^2}{2 \cdot d\omega}$$

As previously mentioned, the vortex shedding frequency scales linear with respect to velocity, as does $d\omega$. The amplitude is the amount of force or moment that the hull experiences. Section 2.4.1 introduced the drag force and lift force, which for a symmetrical shape alternates perpendicular to the flow due to the shedding of vortices to each side. For convenience they are mentioned below:

$$F_D = \frac{1}{2}\rho U^2 \cdot C_D \cdot D \cdot L$$

$$F_l = \frac{1}{2}\rho U^2 \cdot D \cdot C_L \cdot sin(2\pi f_s t + \epsilon_{Ft}) \cdot L$$

Both the lift and the drag component, scale quadratic with respect to the velocity. The frequency of the alternating lift force is dependent on the vortex shedding frequency. For the extrapolation in the frequency domain, this means that the amplitude (magnitude) of the forces and moments scales quadratic with respect to the velocity. For the following description, the subscripts e for extrapolation and m for measurement are used, which yields for the energy density spectra:

$$S_e(\omega_n) = \frac{A_{e_n}^2}{2 \cdot d\omega_e}$$

$$S_m(\omega_n) = \frac{A_{m_n}^2}{2 \cdot d\omega_m}$$

Additionally, a scaling factor x is introduced. This represents the current velocity to which the data intends to be extrapolated to, divided by the current velocity from the measurement data used for this extrapolation:

$$x = \frac{V_{c_e}}{V_{c_m}}$$

The amplitude of force scales quadratic:

$$A_e = A_m \cdot x^2$$

The frequency scales linear:

$$\omega_e = \omega_m \cdot x$$

$$d\omega_e = d\omega_m \cdot x$$

Putting the previous information together, a relation for extrapolating current load test results in different velocities in the frequency domain, under the assumption that the Strouhal number stays constant, is obtained:

$$S_e(\omega_n) = \frac{A_{e_n}^2}{2 \cdot d\omega_e} = \frac{(A_{m_n} \cdot x^2)^2}{2 \cdot d\omega_m \cdot x} = \frac{A_{m_n} \cdot x^3}{2 \cdot d\omega_m} = S_m(\omega_n) \cdot x^3$$

In appendix F the applicability of the presented extrapolation method is demonstrated with a theoretical base case of a circular cylinder.

6.2.1. Extrapolation from 4kn to 2kn current load test results

In this section, the full extrapolation process of 4kn current load test results to 2kn is presented and compared to the 2 kn current load test measurements. This outlines the principle of this method and demonstrates the accuracy. It is demonstrated for the 45 ° vessel heading. Note, that the subscripts s represents the 'slow' 2kn current load test and f the 'fast' 4 kn current load test.

As a first step, the full scale unfiltered current load test results of 2 and 4 knots were filtered with a Low-Pass Filter (LPF) at frequency of ω_{LPF_s} = 0.15 rad/s and ω_{LPF_f} = 0.3 rad/s. The reason for this low frequent filtering process is that with this extrapolation of the current load test, only the effect of vortex shedding is considered, as previously discussed in section 5.3. In figure 6.2, the low-pass filtered forces and moments for 2 & 4 kn can be seen. Additionally indicated is the mean current force / moment, which is required in the final step to determine the mean load for the intended extrapolation velocity.

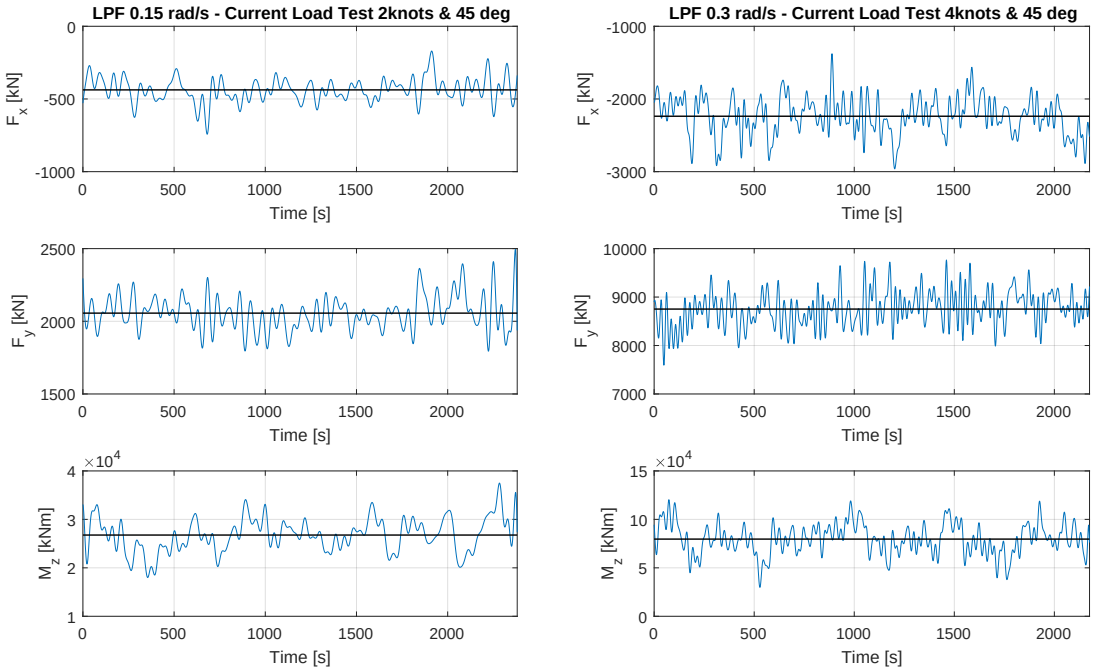

Figure 6.2: Low-pass filtered full scale current load test forces and moment at 45° heading and 2 & 4 kn current velocity

From these force and moment time traces, the EDS is obtained (figure 6.3). Furthermore, the vortex shedding frequencies based on a Strouhal number of St = 0.2 is depicted for the 3 different column shapes and the full vessel dimensions regarded as one. They are an indication to the forces and moments in a frequency band dominated by vortex shedding.

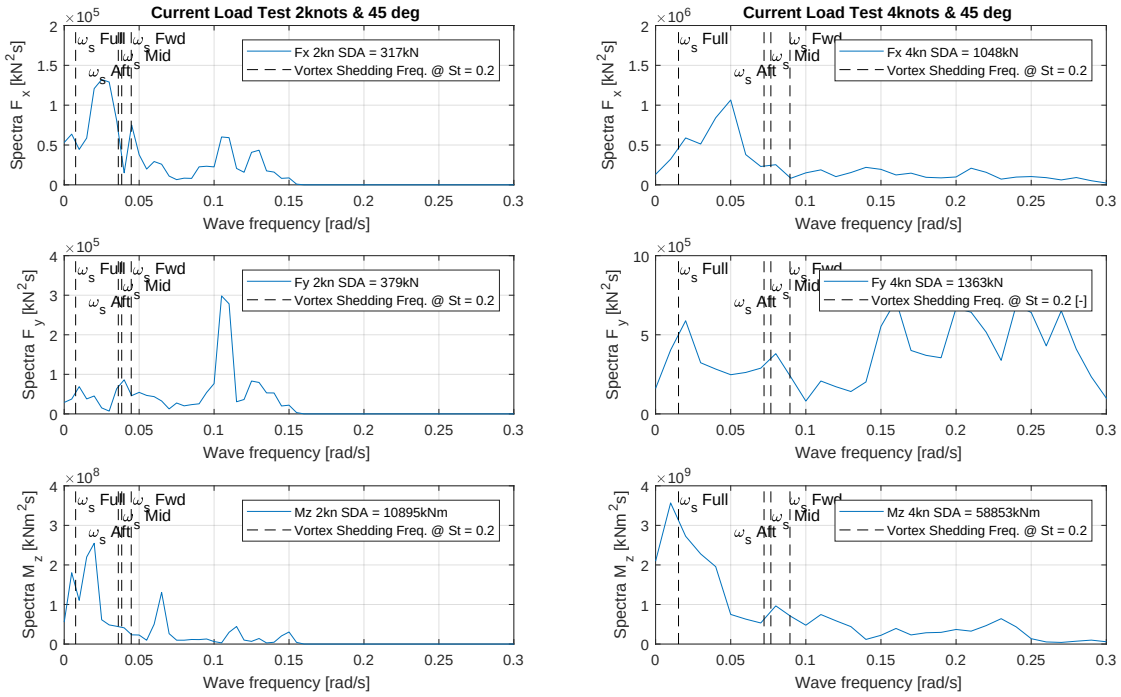

Figure 6.3: EDS of low-pass filtered full scale current load test forces and moment at 45° heading and 2 & 4 kn current velocity

The 4 kn EDS can now be extrapolated to a current velocity of 2 knots, by scaling it cubical with respect to velocity and the frequency range (including the vortex shedding frequencies) linear. The result can be seen in figure 6.4 and for extrapolating from 2kn to 4kn in figure 6.5.

Extrapolation from 4kn to 2kn

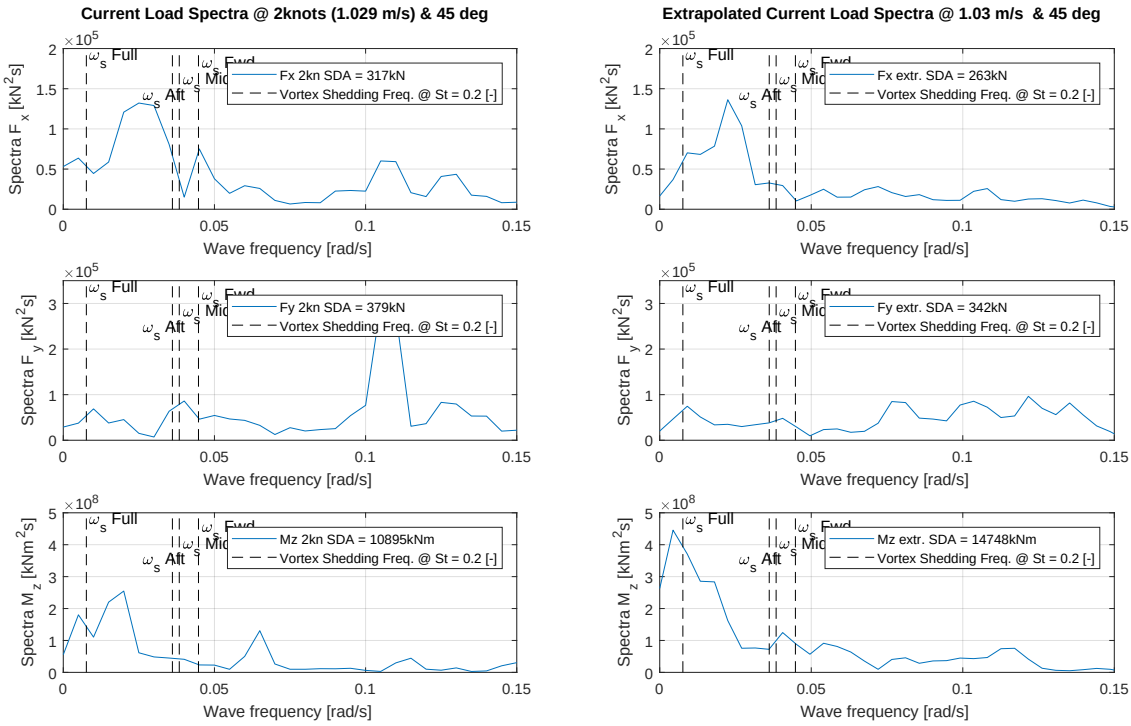

Figure 6.4: EDS of low-pass filtered full scale current load test forces and moment at 45° heading and 2 & extrapolated to 2 kn (from 4kn) current velocity

Extrapolation from 2kn to 4kn

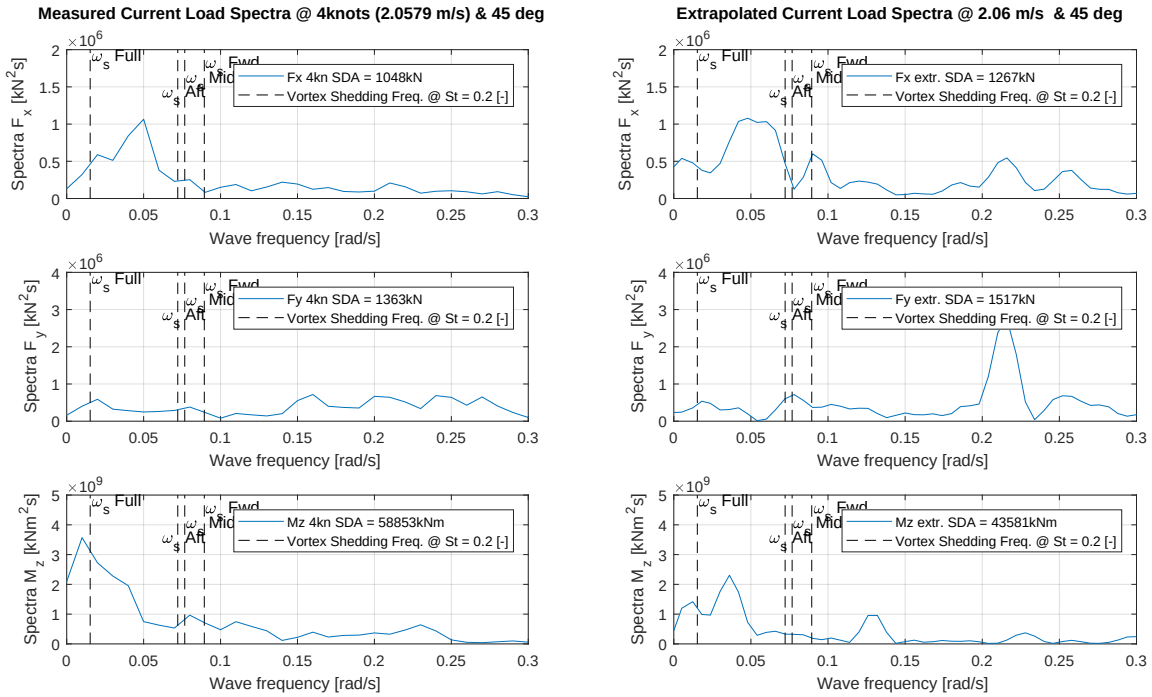

Figure 6.5: EDS of low-pass filtered full scale current load test forces and moment at 45° heading and 4kn & extrapolated to 4 kn (from 2kn) current velocity

Discussion

In the previous two figures, the result of extrapolating the 45 ° heading current load test results from 4kn to 2kn current velocity and from 2kn to 4kn are shown. For both figures, on the left is the measurement of 2kn and 4kn respectively and on the right are the extrapolations.
Overall a good match of the EDS is obtained and clear peaks, e.g F_x seen at both velocities. However, specific details, such as the peak for F_x at 0.11 rad/s for the measured 2kn are not seen back in the extrapolated 2 kn. Similarly, when extrapolating from 2 to 4kn, the same peak become visible at its respective frequency of 0.22 rad/s. The SDAs for surge and sway show, that the differences are minimal and for the 2kn relatively larger, whereas yaw has more energy content from the measured 4kn current load tests.

Considering the short duration of the time traces (approx. 2500s) and therefore resulting inaccurate EDS', this extrapolation method still shows a sufficiently accurate approach for extrapolating these current loads.

6.2.2. Transformation to Time Series

To utilise the extrapolated current load test, whether in the HSC or in time-domain simulation, a time record is required. Through the process of Fourier Series analysis, the phase information is discarded. This information has no further use, as the EDS contains the required information of energy per frequency; independent on the phase. To formulate the time record, the following formulas can be used [9]:

$$x(t) = \sum_{n=1}^{N} x_{a_n} cos(\omega_n \cdot t + \epsilon_n) \tag{6.1}$$

in which, for each component, n:

x_{a_n}	=	Amplitude component of forces / moment	[N] / [Nm]
ω_n	=	Circular frequency component	[rad/s]
ϵ_n	=	Random phase angle component	[rad]

The required amplitudes can be obtained by:

$$x_{a_n} = 2\sqrt{S_x(\omega) \cdot \Delta\omega} \tag{6.2}$$

In figure 6.2, the mean current load around which the fluctuating forces occur has been indicated. Knowing that the current loads (static and alternating) scale quadratic with respect to the current velocity, the mean current load similarly requires extrapolation. Obtaining the mean current forces and moments at any current velocity between 0 and 4 knots is based on the mean values per towing direction of the 2 & 4 kn current velocities and the three forces/moment (F_x, F_y & M_z). Additionally, it is known that at zero velocity, no current loads are present. The current loads, as described in equation 2.1, 2.2 and 2.3 can be reformulated:

$$F_{x,c} = X_c \cdot V_c^2 \qquad \text{where} \quad X_c = \frac{1}{2}\rho \cdot C_{Fx,c}(\alpha_c) \cdot B \cdot T$$

$$F_{y,c} = Y_c \cdot V_c^2 \qquad \text{where} \quad Y_c = \frac{1}{2}\rho \cdot C_{Fy,c}(\alpha_c) \cdot L \cdot T$$

$$M_{z,c} = Z_c \cdot V_c^2 \qquad \text{where} \quad Z_c = \frac{1}{2}\rho \cdot C_{Mz,c}(\alpha_c) \cdot L^2 \cdot T$$

The help constants X_c, Y_c and Z_c are assumed to be constant throughout the complete velocity range. However, as the forces are obtained from measurements and also the mean have been determined, they contain inaccuracies. To account for these inaccuracies, as well as not obtaining a negative mean force for positive directed forces or positive for negative directed forces, the average per each help constant of the *slow* 2kn and *fast* 4kn velocities is formed.

$$X_c = \frac{X_{c_s} + X_{c_f}}{2}$$

$$Y_c = \frac{Y_{c_s} + Y_{c_f}}{2}$$

$$Z_c = \frac{Z_{c_s} + Z_{c_f}}{2}$$

The relation for the mean current forces can now be obtained with the help constants X_c, Y_c and Z_c and is represented for the 45° heading below (figure 6.6).

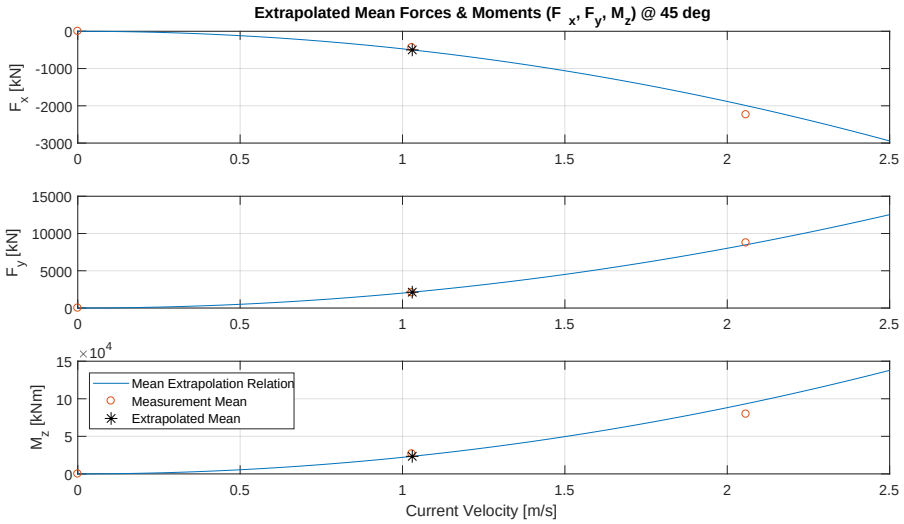

Figure 6.6: Relation of extrapolated mean current forces and moment (F_x, F_y & M_z) and indicated determined mean

As a final step, the complete time record is obtained by adding the alternating components and the mean component per time step with random phase angles.

$$F_x(t) = F_{x_{MEAN}} + \sum_{n=1}^{N} F_{x_{a_n}} cos(\omega_n \cdot t + \epsilon_n) \tag{6.3}$$

$$F_y(t) = F_{y_{MEAN}} + \sum_{n=1}^{N} F_{y_{a_n}} cos(\omega_n \cdot t + \epsilon_n) \tag{6.4}$$

$$M_z(t) = M_{z_{MEAN}} + \sum_{n=1}^{N} M_{z_{a_n}} cos(\omega_n \cdot t + \epsilon_n) \tag{6.5}$$

6.2.3. Extrapolation Results

The obtained time signals for F_x, F_y & M_z at the extrapolation current velocity of 1.03 m/s can be seen in figure 6.7. The extrapolated spectra (obtained from 4kn measurement) is plotted in blue for the frequency domain on the right. From this EDS, the timetrace was obtained, which can be seen also in blue for the time domain on the left. The measured 2kn current load test record and the according EDS are also depicted (orange). After the timetrace from the extrapolated EDS has been computed, another EDS based on the created time signal is obtained as a final check (yellow).

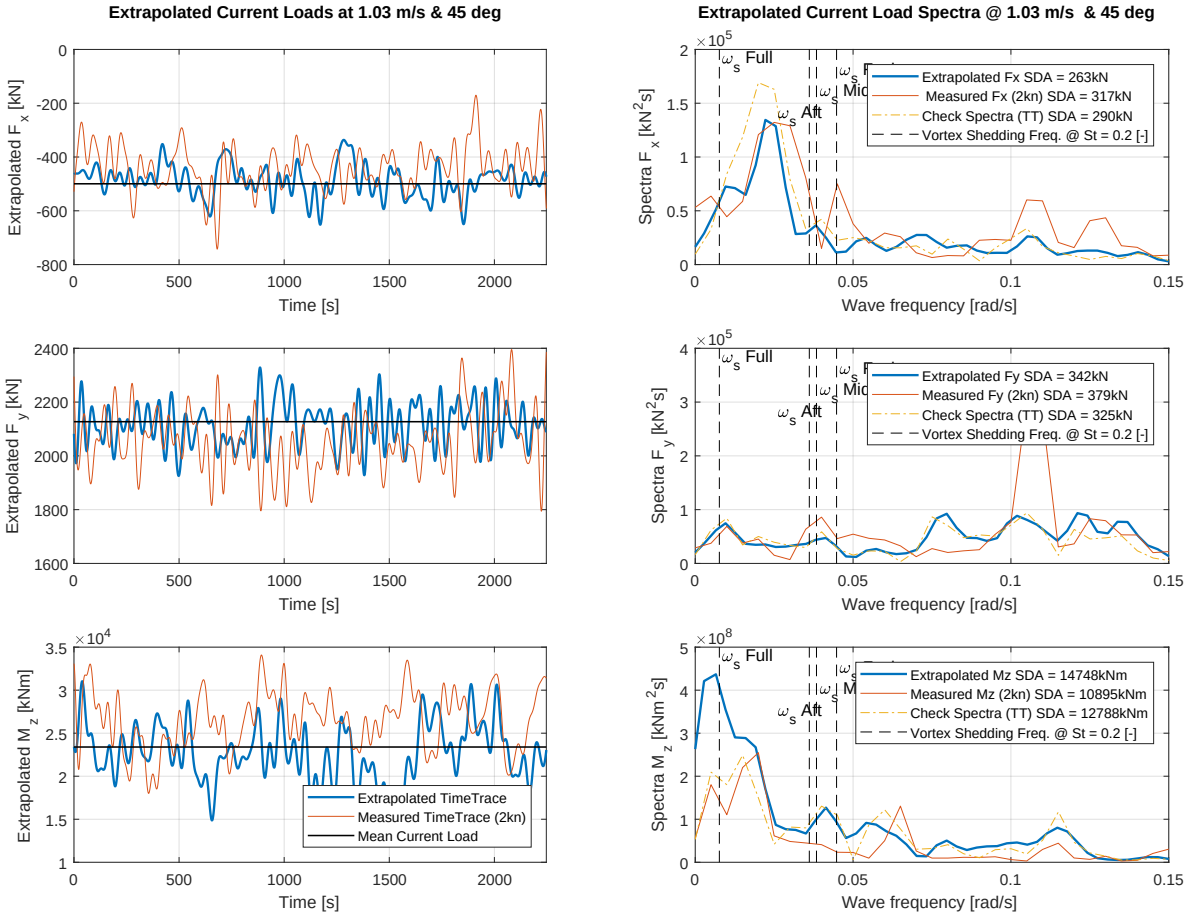

Figure 6.7: Result of 45 ° heading current load test extrapolation to 1.03 m/s (from 4 kn measurement) and comparison with the measured 2 kn current load test results

Accuracy & Remarks

From the obtained SDAs of the EDS' it can be seen that the extrapolation does estimate the fluctuating force, subjected to vortex shedding with sufficient accuracy.

The recurring issue of the duration of the measurement has an influence on the accuracy. From the obtained EDS, only a certain length of time trace can be computed. This means that in the present time trace for surge of 2300s and a peak frequency of approx. 0.02 rad/s (peak period of approx. 314s) only 7 cycli will be represented. The accuracy of the method itself, has been demonstrated for the single cylinder base case, but longer measurements are required in order to validate it against obtained data. Nevertheless, to assess the effect of VIM at lower velocities, resulting in longer time records, this method has shown a successful applicability and will be used for the estimating the time-varying forces at currents below 2kn.

6.3. Effect of VIM at lower velocities

Current velocities of 2kn and above can be considered very large for Thialf and therefore do not represent the 'typical' environmental working conditions. For this reason, the effect of vortex shedding in current velocities below 2 kn are of particular interest. Using the previous outlined method of extrapolating velocity dependent time-varying forces from the current load tests, time-varying forces in the velocity range of 0 to 2 kn can be obtained. With these obtained time traces, aNySIM simulations are carried out and the results investigated. This section presents the results of a SSCV in station keeping operation, while being exposed to current loads of 0.5kn, 1.0kn and 1.5kn for the vessel headings of 45°, 60°, 90° and 150°. These directions direction particularly shows large energy contents in the current load tests (recall figure 5.8) and are also in line with previous research. The current velocities that will be simulated are 0.5kn is $V_{0.5} = 0.2572 m/s$, 1kn is $V_{1.0} = 0.5144 m/s$ and 1.5kn is $V_{1.5} = 0.7716 m/s$. The aNySIM simulations were carried out using the spring-damper model and the ideal theoretical spring and damping terms as well as the not-ideal DP System (30% critical damping for Surge, Sway and Yaw). Both DP Systems represent a Medium Controller Gain.
In section 5.5, the obtained current loads of the measured 2 kn test with the headings of 60° and 90° have been used as simulation input for the real-time simulations in the HSC. Therefore, in order to effectively compare the results of the velocities of 0.5kn, 1.0kn and 1.5kn, aNySIM simulations with the measured 2.0kn, $V_{2.0} = 1.0288 m/s$ current loads are carried out for the mentioned headings as well.

6.3.1. Simulation Results

The results of these simulations for the 4 different current velocities can be seen below. Here only the results for the 60° and 150° vessel heading case for the Ideal and Not-Ideal DP System are presented. The results for heading cases of 45° and 90° can be found in Appendix G. They are presented separately per vessel heading and DP System, while the results from the 4 current velocities are plotted in the same figures. Note, that the duration for each velocity is different. This is due to the fact that the minimal possible $\Delta\omega$ was used to obtain the EDS from the measured data. When this data is now extrapolated to lower velocities, $\Delta\omega$ is decreased, resulting in more data points over the smaller frequency range and thus longer time traces.

60° heading - Ideal DP System

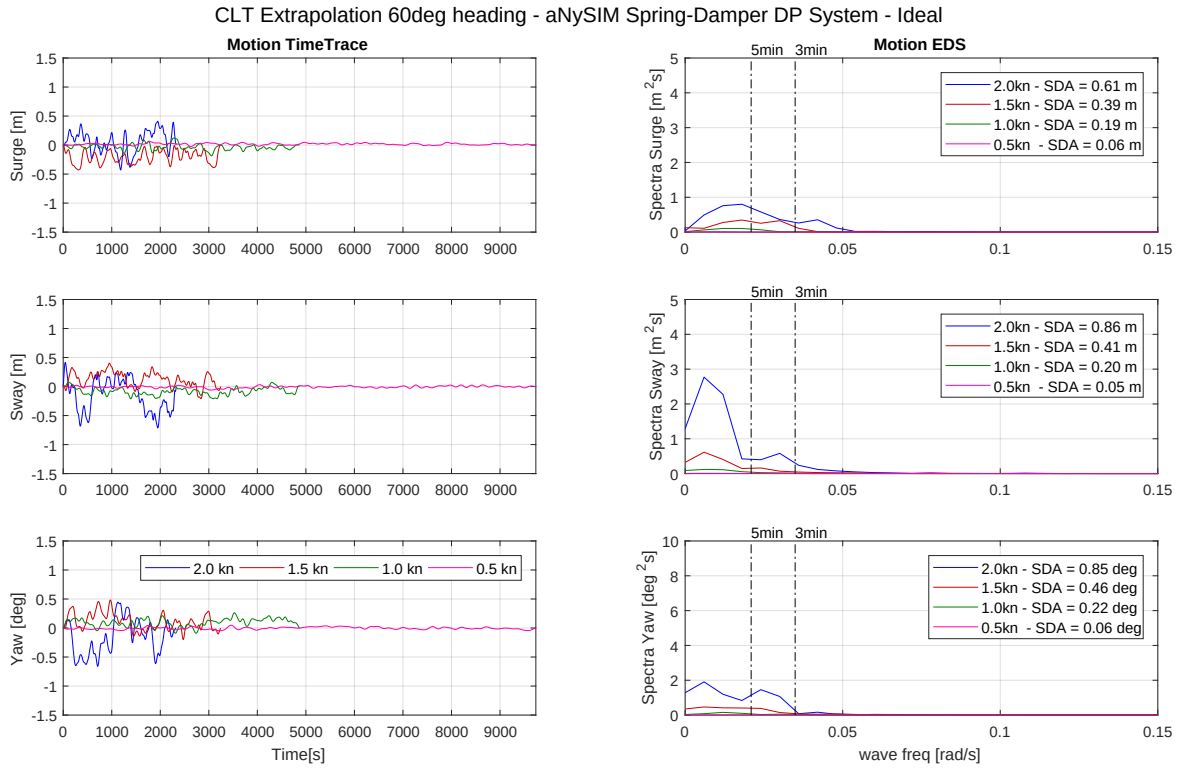

Figure 6.8: Result of 60° heading extrapolated and measured current load test aNySIM Spring-Damper simulation - Ideal

60° heading - Not Ideal DP System (30% critical damping)

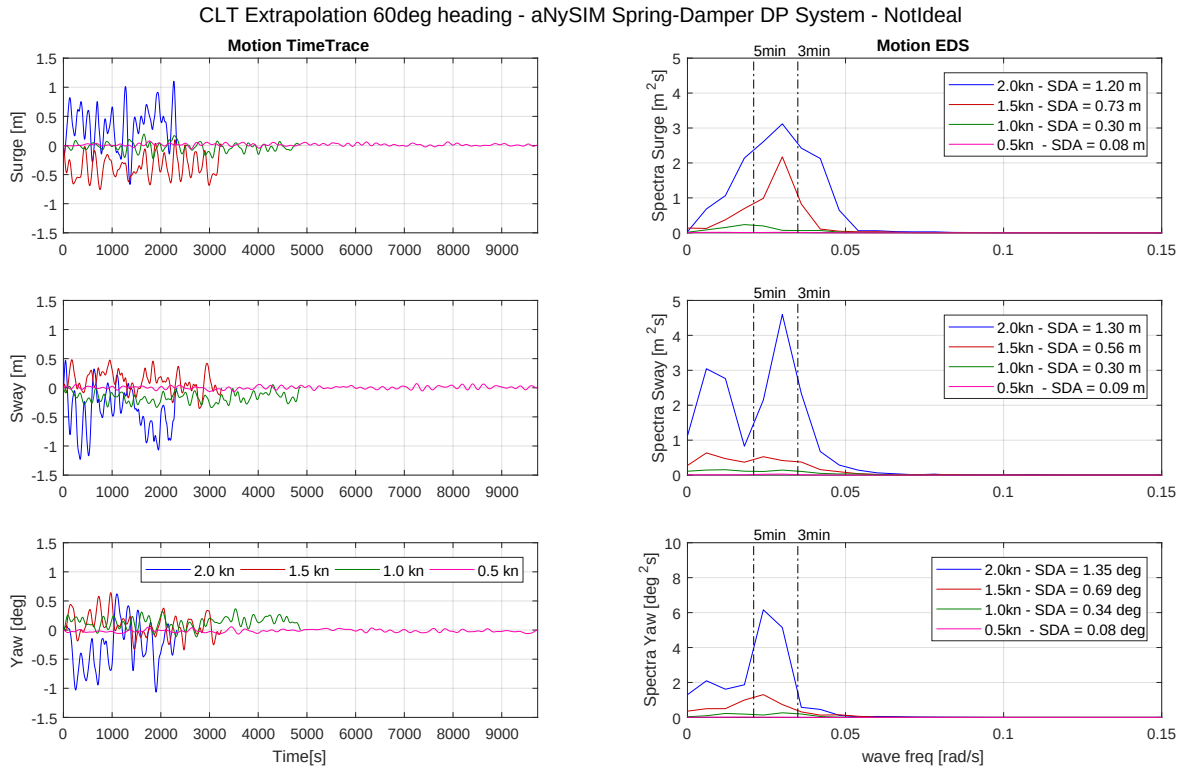

Figure 6.9: Result of 60° heading extrapolated and measured current load test aNySIM Spring-Damper simulation - Not Ideal

150° heading - Ideal DP System

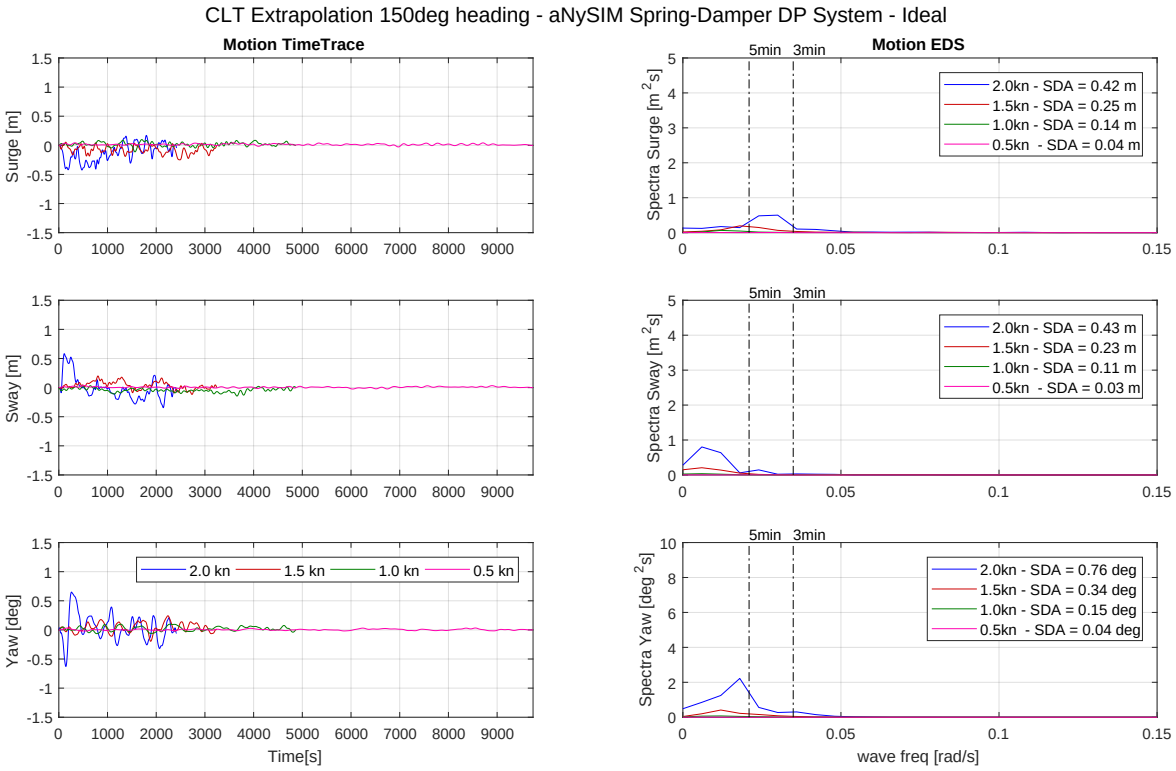

Figure 6.10: Result of 150° heading extrapolated and measured current load test aNySIM Spring-Damper simulation - Ideal

150° heading - Not Ideal DP System (30% critical damping)

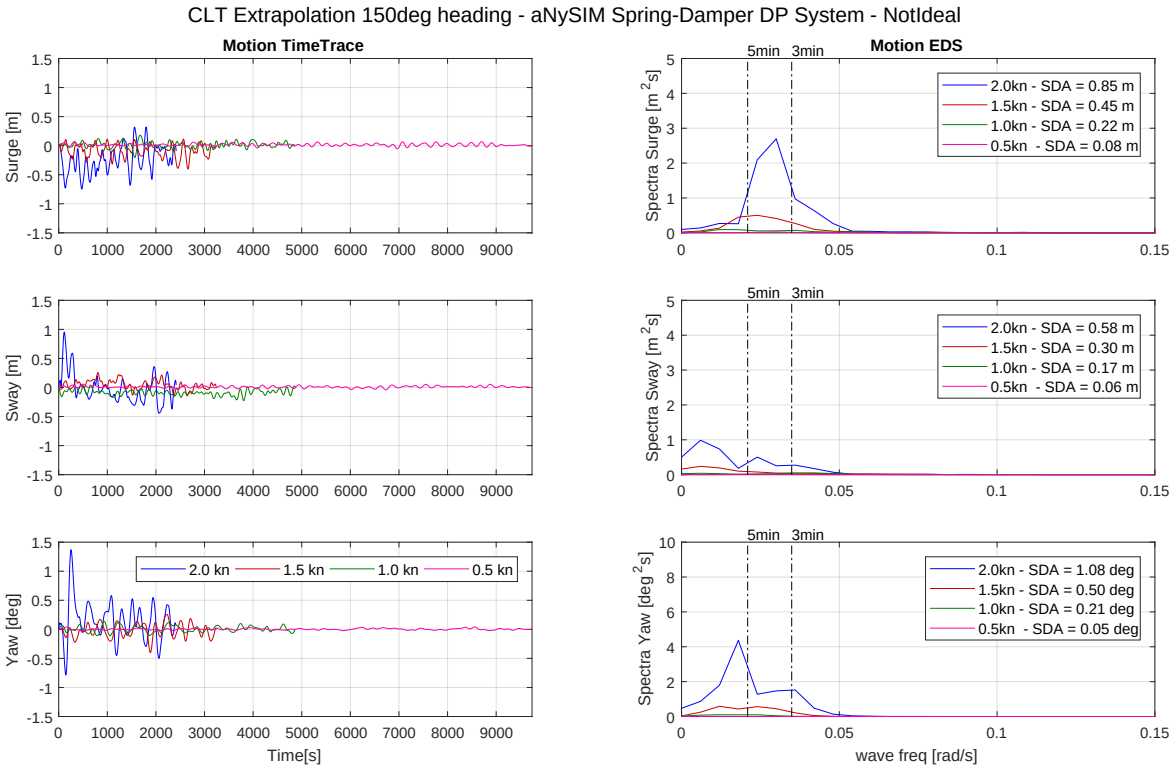

Figure 6.11: Result of 150° heading extrapolated and measured current load test aNySIM Spring-Damper simulation - Not-Ideal

6.3.2. Discussion

It is highly notable that the presented results of simulations with the extrapolated current loads to 0.5 kn, show offsets with a SDA in the range of 4 to 9 centimeters for the Ideal and Not-Ideal DP system. This clearly represents that at a current speed of $V_{0.5} = 0.2572m/s$, the energy decreases so drastically that the vessel motions are minimally influenced by VIM.

In the DP Trials, as presented in section 1.1, an increasing current from 0.5 to 0.9 m/s was present and low frequent vessel offsets with $SDA_{surge} = 0.2$ and $SDA_{sway} = 0.3$ were observed. The current direction in the DP Trials is comparable to the present 150° heading case figure 6.10 and 6.11. Considering the $V_{1.5} = 0.7716m/s$ results for the 150°heading case, for the Ideal DP System: SDA_{Surge} = 0.25m and SDA_{Sway} = 0.23m and SDA_{Yaw} = 0.34 deg. For the Not-Ideal DP System, these values become SDA_{Surge} = 0.45m and SDA_{Sway} = 0.30m and SDA_{Yaw} = 0.50 deg. Overall, a large increase of the SDAs are present for the Not-Ideal DP System in comparison with the Ideal System. This is distinctively present for 2.0kn, 1.5kn and 0.5kn, lesser so for 0.5kn as the energy decreases.

For the 60° and 15° heading case, it can be seen that for the Ideal DP System, the peak periods of the vessel motions are approx. 5 min or longer, apart from Surge for the 150° heading case for 2kn. For the Not-Ideal DP System the peak periods shift to the range of 3 to 5 minutes, especially for the 2kn current velocity and partially for 1.5kn. This is connected to the previous mentioned observation that the energy for lower velocities decreases plus the fact that the vortex shedding frequency de- & increases with respect to velocity. Nevertheless, the increase of the natural damped frequency (as first described in section 4.4.4) with decreasing damping can also be observed here, where the vessel is exposed to fluctuating forces of VIM.

The largest overall vessel motions are observed at the 60°and 90°heading case and not as previous research suggested for the 45°incident angle. Here lies also one of the significant differences between the present SSCVs and the semi-submersible platforms as described in VIM literature. The columns of a SSCV are closer to each other than for semi-submersible platforms. It is likely that this will result in different vortex patterns that could interact with each other and thus highlights the importance for required research specifically for SSCVs.

6.3.3. Subconclusion

Measured fluctuating current loads from constant current velocity, extrapolated to more realistic current velocities below 2kn cause the vessel to oscillate around its setpoint. For the extrapolated velocities of 0.5kn, 1.0kn and 1.5kn the vessel show a motion response with peak periods around 5 minutes and more. These periods tend to shift in the range of 3 to 5 minutes, when less damping and thus more realistic DP system characteristics are used. This signifies that for current velocities above 0.5kn VIM causes a SSCV during station keeping operations to fluctuate around its setpoint with periods as previously observed. Not only is the effect of VIM represented, but also the influence of a not-ideal DP system in under such environmental conditions.

With the presented extrapolation, a method is presented that enables to represent this effect using the time-domain simulation tool aNySIM.

7

Contribution to overall response

Until now, each of the contributing factors has only been investigated individually and the following findings made:

- With minimal information it is shown that a variation of current velocity & direction on a time scale of 1 to 5 minutes exists
- Damping is 'lost' in the control loop of the DP system
- VIM and 2nd order wave forces cause an increased unknown low-frequency excitation on a SSCV during DP-operations

This also shows that the effect of time-varying current loads on an SSCV during station keeping operations was not investigated. Furthermore, the relative contribution of each external influence (VIM, 2nd order waves and time-varying currents) as well as the internal influence of reduced damping, had not yet been addressed. This chapter presents two approaches to provide the missing answers.

7.1. Effect of time-varying currents on an SSCV in DP-Operations

The information on the presence of time-varying currents on a scale of 1 - 5 minutes is limited. Yet, with this limited information, a 45 min stationary current measurement with 1 Hz sampling rate, a variation on this time scale in velocity and direction can be seen. In section 4.4.6, the Ideal and Not-Ideal (30% critical damping) DP System for the Spring-Damper configuration in aNySIM have been introduced, which simulate a Normal Kalman Filter Gain with a Medium Controller Gain. For both system characteristics a simulation was carried out, where the vessel was exposed to the current as it was measured offshore (figure 7.1).

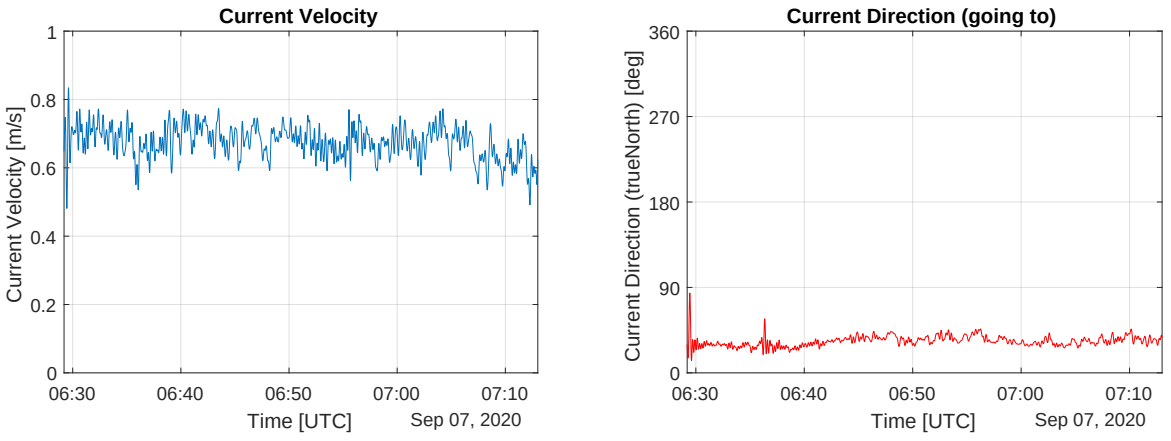

Figure 7.1: Stationary ADCP Current Measurement at Windpark HKZ

		aNySIM Simulation
Vessel	DP System	Ideal & Not-Ideal
	Sim. Kalman G.	Normal
	Sim. Controller G.	Medium
	Heading	0°
	Draft	26.6 m
Current	Direction (going to)	33 $\pm$ 15 ° (fig. 7.2)
	Velocity	V_c = 0.67 $\pm$ 0.2 m/s
Duration		2628 min (excluding run-up)

Table 7.1: Vessel and environmental parameters

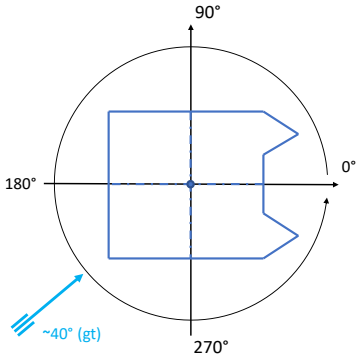

Figure 7.2: Current Direction - aNySIM coordinate system

Results

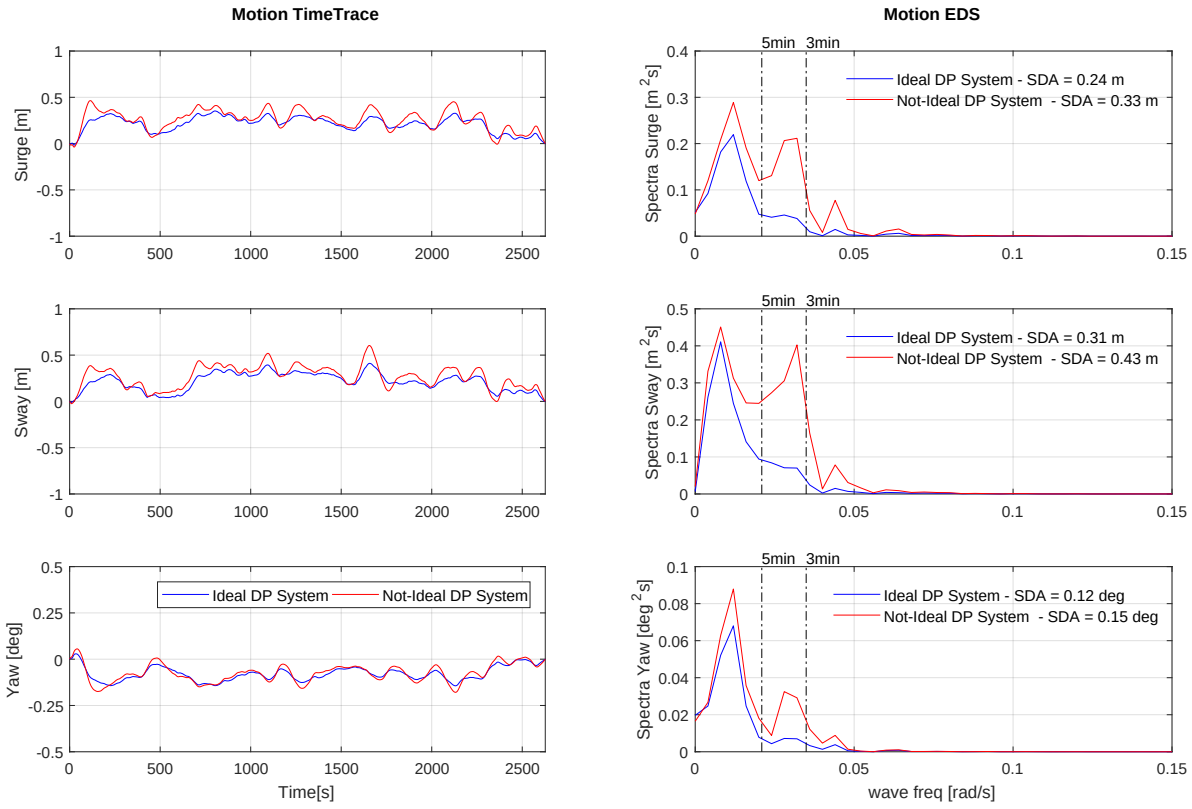

Figure 7.3: aNySIM Simulations with Ideal and Not-Ideal DP System exposed to measured time-varying currents

Discussion

The results presented in figure 7.3 indicate that indeed time-varying currents cause an increased vessel response. This is the case for the Not-Ideal as well as the Ideal DP System. The peak frequencies of the vessel motions, which can be seen for both simulations are at approx. $\omega = 0.01 rad/s$ and results in a period of approx. 10 min. This can be linked to the current measurement, where this peak period was observed in the EDS for velocity and direction, as in figure 3.6. What stands out is the increase of motions for the Not-Ideal DP System with periods between 3 to 5 min. For the Ideal DP System motions are also present in this 3 to 5 minute range. Due to the losses of damping and a resulting shift of the natural damped frequency, the magnitude of these motions increase, which in turn results in an energy increase in the EDS.

7.2. Relative contribution of external and internal influences

To determine the contribution of all the determined causes, a simulation environmental is selected that encompasses the external influeneces of time-varying currents, 2nd order waves and VIM. The same scenario is then selected to carry out simulations for the Ideal and Not-Ideal DP System. Additionally, for each environmental contribution and DP System, individual simulations were conducted.

		aNySIM Simulation
Vessel	DP System	Ideal & Not-Ideal
	Sim. Kalman G.	Normal
	Sim. Controller G.	Medium
	Heading	0°
	Draft	26.6 m
Current	Direction (going to)	33 $\pm$ 15 ° (fig. 7.4)
	Velocity	V_c = 0.67 $\pm$ 0.2 m/s
Waves	Direction (going to)	30° (fig. 7.4)
	Peak Period	T_p = 9s
	Sig. Wave Height	H_s = 2m
	Spectrum	JONSWAP
	gamma	γ = 3.3
VIM	from Cur. Dir. (gt)	30°
	Extrapolated Vel.	V_c = 0.67 m/s
Duration		5254s (excluding run-up)

Table 7.2: Vessel and environmental parameters

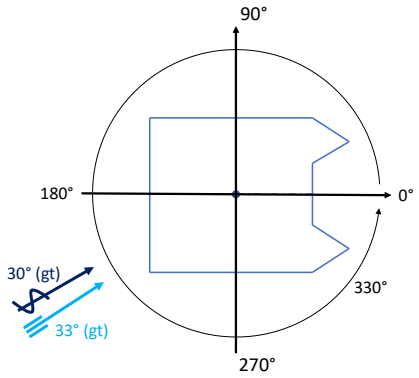

Figure 7.4: Environmental Directions - aNySIM coordinate system

Note, that unlike in the previous chapter, only the fluctuating part of VIM is extrapolated here, excluding the mean current load. The direction has been selected such, that it is represents a current going to 30° (aNySIM coordinates) and best in line with the direction of the current measurement of approx. 33°. Furthermore, the current measurement timetrace has been duplicated to obtain a longer measurement.

Results

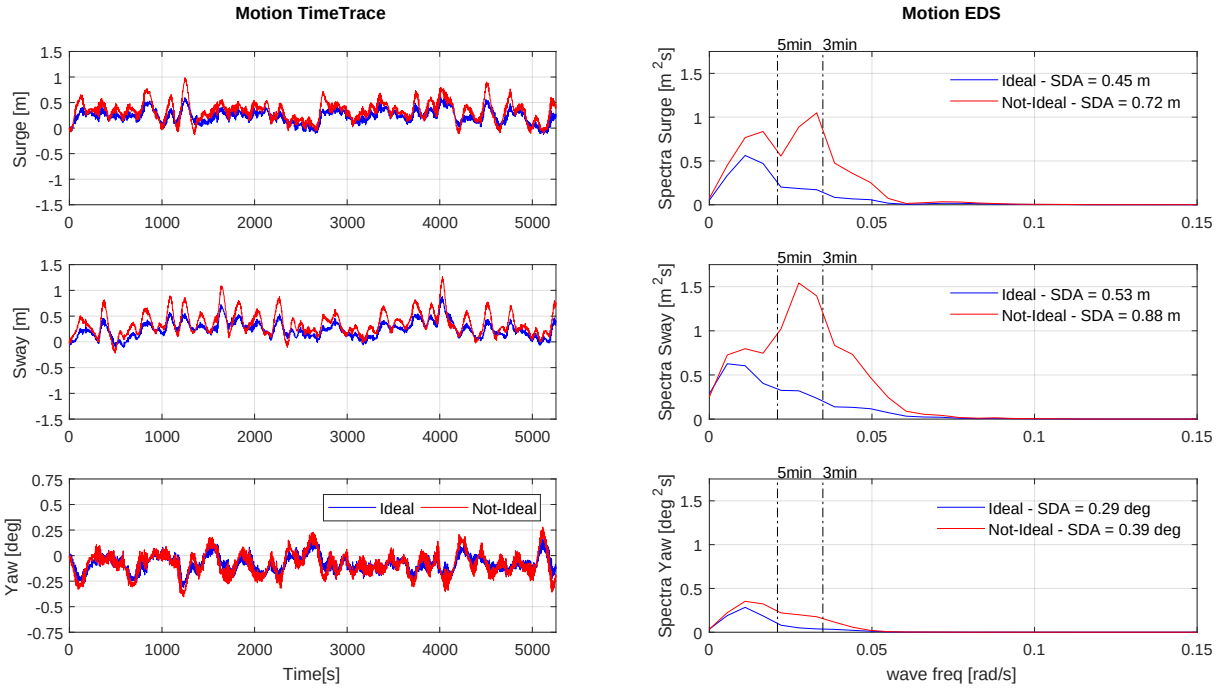

Figure 7.5: aNySIM Simulations with Ideal and Not-Ideal DP System exposed to measured time-varying currents, VIM and 2nd order waves

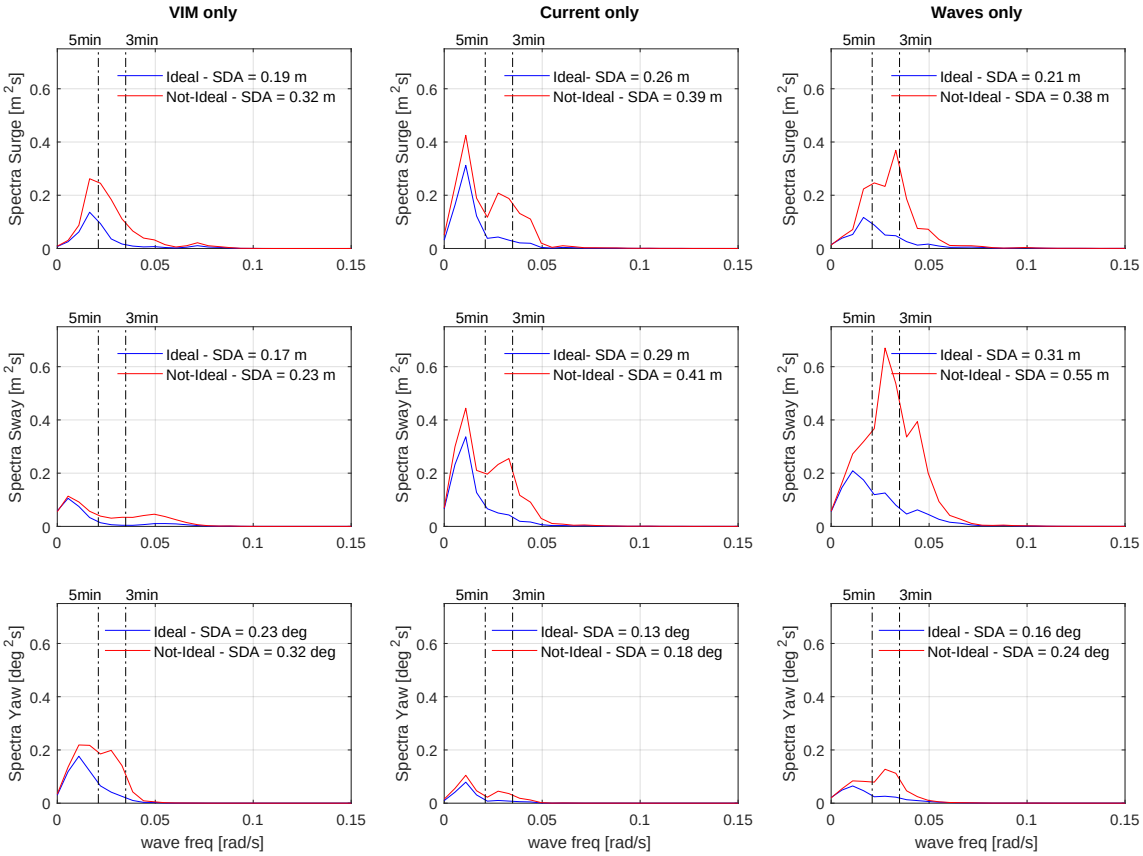

Figure 7.6: EDS of aNySIM Simulations with Ideal and Not-Ideal DP System exposed to VIM only, measured time-varying currents only and 2nd order waves only environment

Discussion

From figure 7.5 the contribution of the damping losses, when using the Not-Ideal DP System can be observed. For the Ideal DP System, especially for surge and sway, the peak periods are 5 minutes and longer. For the Not-Ideal DP System, the peak periods shift in the range of 3 to 5 minutes. Moreover, the SDAs increase with 60% for surge & sway and 30% for yaw.
Below in figure 7.6 the contribution of VIM, time-varying current and waves simulated individually for the Ideal and Not-Ideal DP System is depicted. This again shows the contribution of damping losses resulting in increased vessel motions with periods of 3 to 5 minutes. This effect is particularly dominant for 2nd order waves. Furthermore, the SDAs of the VIM and time-varying currents (for Ideal and Not-Ideal) show significant contributions to the overall response.

7.3. Subconclusion

With minimal available current data it was shown, that time-varying currents in fact cause a vessel response, formerly not known. The increase of vessel motions due to damping losses towards the previously observed period range of 3 to 5 minutes is further observed.

With the latter simulation it was possible to combine the determined causes contributing to an increased vessel response. This shows that the previously unknown contribution of VIM and time-varying current, significantly influence the overall response. While second order waves are captured in time-domain simulations, the contribution of damping losses amplifies the response notably. Lastly, a similar contribution of each external influence can be observed, highlighting the importance of each aspect.

The following limitations to these results need to be mentioned. For both simulations only one environmental direction was considered. In these simulations no wind was present. Additionally, the fluctuating forces of VIM do not account variability of currents velocity and direction.

8

Conclusions & Recommendations

8.1. Conclusions

First the sub-questions will be reassessed and answered, building up to complete this project by answering the main research question.

Does a variability of currents on the scale of 1 to 5 minutes exist?
Throughout this research it was not possible to find an explicit answer to this question. To ascertain this information, eight different research institutions were contacted and meetings with researchers were held. It became clear that finding suitable measurement data would pose a significant challenge. To be precise, finding measurement data with time steps in seconds. For oceanographic purposes, in-situ current measurements are typically conducted over a long time span and sampling rates are therefore kept low in order to save energy. Upon suggestion from Deltares, a month long current measurement in the north sea with a time step of 10 minutes was obtained. This data indicates that for the lowest possible frequencies, the current was not quasi-static. As further data was not accessible, this track was put on hold and the focus shifted towards the DP system.

In the finishing stages of this project, ADCP measurements were conducted in the North Sea with an ROV launched from Sleipnir and positioned motionless on the seabed. Only one 45min time trace with a sampling rate of 1Hz was obtained (as the ADCP was damaged the same day). According to this data, variation of currents in terms of velocity and direction on the scale of 1 to 5 minutes do, in fact, exist.

If yes, what would be the influence on the vessel response?
The limited available current measurement data showed that time-varying currents can cause an increased response of a SSCV during DP operations. Moreover, with a not-ideal DP system, which is closer to the real DP System, the vessel motions for surge, sway and yaw show peak periods in the previously observed range of 3 to 5 minutes.

What other possible causes can trigger the observed vessel response?
The potential origins were considered to be within the DP system itself or to come from external influences. The DP System, as installed onboard, and its exact behavior are not captured in aNySIM. Considered causes were the use of the High Kalman Filter Gain or characteristics of the control loop. Previous research has indicated that VIM affects multi column floaters. This highlights the fact that VIM could affect SSCVs during DP-operations.

How can these possible causes be assessed and simulated?
In the the DP Trials 2017, only the High Kalman Filter Gain was tested with the 3 Controller Gains of High, Medium and Low. It was noted that Normal Kalman Filter Gain was not used in these trials. For this reason, real-time simulations in the HSC have been conducted, where it was determined that the High Kalman Filter Gain performs better in comparison with the Normal Kalman Filter Gain. For all 3 Controller Gains, the High Kalman Filter Gain demonstrated a faster reaction time and increased performance with smaller offsets relative to Normal Kalman Filter Gain. This shows that the use of the High Kalman Filter Gain over the Normal Kalman Filter Gain does not cause the unexpected vessel response.

In order to obtain the DP System characteristics, a DP RAO assessment was conducted wherein the spring and damping terms were derived as demanded by the controller and as experienced by the vessel. This assessment showed that between 20% to 67% of the demanded critical damping is lost over the control loop (including Kalman Filter, Controller, Thruster Allocation and Thrusters). These damping losses cause the vessel to overshoot and the damped natural period to decrease. For critical damping ratios below 0.7 (for surge, sway and yaw) the damped natural period shifts to the range of 3 to 5 minutes. This results in increased oscillations in this period range and can be seen in the EDS of the vessel motions.
Based on these findings, spring and damper coefficients for an Ideal and Not-Ideal (30° of critical damping for surge, sway and yaw) DP system were deduced. The Not-Ideal DP System aims to represent the damping losses of the real DP system in aNySIM simulations.

To determine the effects of VIM on a SSCV during DP-operations vessel specific data is required. Current load test data available within HMC determined that from constant currents, time-varying fluctuating forces act on the hull of a SSCV. By estimating the vortex shedding frequency and relating the results to the velocities at which the measurements were conducted, it was determined that these fluctuating forces originate from vortex shedding. It should be noted that the potential interaction between the different columns and shapes was not taken into account.
With real-time simulations in the HSC, it was possible to verify that fluctuating forces from a constant current load cause the vessel to deviate from its setpoint with peak periods of 3 to 5 minutes.
A method was developed to extrapolate the current load test results to velocities below 2kn. Subsequently, in time-domain simulations the vessel was exposed to those forces. Data shows that for current velocities above 0.5kn, the vessel experienced forces and moments that caused it to fluctuate around its setpoint. In combination with the Not-Ideal DP System, the SDA of these motions increase and peak periods of 3 to 5 minutes are observed.

What causes the increased dynamic Vessel/Thruster response of a SSCV while station-keeping in operational conditions and is not captured in time-domain simulations?

- Even with limited information it was shown that time-varying current loads exist and cause an unexpected motion response of a SSCV.
- With the use of DP RAOs, it was possible to determine that the effective damping of the DP system decreases. Reduced damping causes larger offsets and longer oscillations with periods of 3 to 5 minutes.
- This research has demonstrated that VIM has an influence on a SSCV during station keeping operations. Strong currents on column type floaters can cause fluctuating forces and moments, which in turn can cause a SSCV to oscillate around its setpoint while operating on DP.

8.2. Recommendations

Variation of Currents
Until now, only one 45 minute current measurement has been conducted with a sampling rate of 1 Hz. This shows that time-varying currents on a time-scale of 1 to 5 minutes exist and cannot be assumed to be quasi-static. Further measurements are required to confirm the presence of such a current variability. This could be done by measurement as it was presented in this report, where the ADCP was installed on the ROV that was placed stationary on the seafloor. Such an arrangement depends on the project and the availability of the ROV, while the vessel remains on position. Another method would be to deploy a measurement frame with an upward looking ADCP, with a small enough sampling rate. Such a measurement frame can be equipped with a recovery buoy and an acoustic release for recovery.
Once more data becomes available, additional time-domain simulations can be carried out to verify the vessel response under such conditions. The most favourable option would be to include current time-traces in the HSC and observe the vessel and thruster response.

Vortex Induced Motion
In this research, VIM on the hull of a SSCV was determined based on current load tests carried out by MARIN. These tests were conducted at current velocities of 2kn & 4kn on the hull of a concept design vessel (NBV). Although many similarities are present between the hull of SSCV Thialf and NBV, the obtained forces from current load test measurements have been used for the research with Thialf. Furthermore, the potential interaction of specific shedding patterns between the columns has not been taken into account.
Specific data on vortex shedding for SSCV Thialf could be obtained by carrying out additional model tests or Computational Fluid Dynamics (CFD) calculations. This data could then be used to investigate its effect on DP-operations in more detail or to predict scenarios where VIM occurs and could affect the performance of the vessel.

Limitation of External Influences
The variation of currents and VIM represent external influences acting on the hull of the vessel. This means that their occurrence and the forces they exert on the vessel cannot be influenced. With the suggested recommendations regarding variation of currents and VIM it is possible to gain a better understanding and to assess the effect on the motion response in more detail. Hence, it is suggested to take this into consideration for the future when making the trade off between 'how much additional research will be carried out' and 'how will this improve the DP performance'.

Damping Losses
In this research it has been shown that the effective damping of the DP system decreases, causing larger offsets and longer oscillations. This was achieved by identifying RAOs of different stages of the control loop of the DP System. While the method in itself is still under development within HMC, the application as carried out in this research can also be improved. In this thesis, the duration of the measurements in the HSC, from which the DP RAOs were obtained, was 2 hours. For instance, a natural period of $T_n = 200s$ will result in 36 cycli, which in return affects the accuracy of the RAOs. Therefore, it is suggested to carry out measurements of 6 hours and more. This can be done in the HSC, where environmental influences can be controlled. Offshore data where no setpoint changes were applied can also be taken into consideration.

Unlike the external influences of time-varying current and VIM, the internal influence of lost damping can be addressed. This line of research could lead to an additional student graduation project. First of all, it must be fully understood as to why damping is 'lost' in the control loop. In the present thesis the estimation of the vessel velocity was mentioned as one possible cause. Another possibility could be introduced delays in the thruster response (Azimuth, RPM) or Kalman Filter. However, this is unknown and therefore additional research is required, for example by deriving the critical damping per RAO at each stage of the control loop.
Furthermore, it needs to be investigated how the estimation of the vessel can be improved. It is strongly advised to contact Kongsberg on this matter in order to determine the extent to which the estimation of vessel velocity within Kalman Filter can be altered and to hear their opinion on the present losses of damping.

Bibliography

[1] Howard Shatto. Histroy of DP (accessed: 04/03/2020), 2011. URL https://dynamic-positioning.com/history-of-dp/.

[2] Ivan Van Winsen and Radboud R.T. Van Dijk. Quad lift: Enabling lifting of larger integrated topsides. In *Proceedings of the International Conference on Offshore Mechanics and Arctic Engineering - OMAE*, volume 1, 3 2019. ISBN 9780791858769. doi: 10.1115/OMAE2019-95375.

[3] Eelco Harmsen, Radboud Van Dijk, and Petter Stuberg. DP-stability during heavy lift operations using a modified Kalman filter. In *Proceedings of the International Conference on Offshore Mechanics and Arctic Engineering - OMAE*, volume 1, Madrid, Spain, 2018. ISBN 9780791851203. doi: 10.1115/OMAE2018-77901.

[4] Arman Hakim. VAL-MAE-024 Software Validation Report. Technical report, Heerema Marine Contractors, 2017.

[5] Herrera Marine Contractors. Parkwind, Heerema and MHI Vestas announce a revolutionary construction methodology for Arcadis Ost 1 (accessed: 10/06/2020), 2019. URL https://heerema-production-content.s3.amazonaws.com/HMC/PressReleasespdf/2019-11-26-PressReleaseParkwind_Heerema_MHIVestas.pdf.

[6] Kongsberg Maritime. Dynamic positioning - basic principles (accessed: 20/02/2020), 2012. URL https://www.kongsberg.com/maritime/support/themes/dynamic-positioning-basic-principles/http://www.km.kongsberg.com/ks/web/nokbg0240.nsf/AllWeb/BD306BBB3E7DA73FC1256DAB00353083?OpenDocument.

[7] Heerema Marine Contractors. Fleet (accessed: 14/03/2020), 2020. URL https://hmc.heerema.com/fleet/.

[8] Sif OFFSHORE FOUNDATIONS. Größter Schwimmkran der Welt bringt Piles zum Johan-Sverdrup-Feld (accessed: 08/06/2020), 2018. URL https://sif-group.com/de/aktuelles/projekt-updates/590-groesster-schwimmkran-der-welt-bringt-piles-zum-johan-sverdrup-feld.

[9] J.M.J. Journee and W.W. Massie. *Offshore Hydromechanics*. Delft University of Technology, Delft, first edit edition, 2001.

[10] Williard J. Pierson, Gerhard Neumann, and Richard W. James. Observing and Forecasting Ocean Waves by Means of Wave Spectra and Statistics. *Hydrographic Office Publication*, 603:284, 1955.

[11] John H. Lienhard. Synopsis of lift, drag, and vortex frequency data for rigid circular cylinders, 1966.

[12] MARIN. aNySIM XMF - Time Domain Simulations for Multi Body Dynamics for Offshore Operations (accessed: 10/10/2020), 2014. URL https://www.marin.nl/storage/uploads/3569/files/aNySIM_XMF.pdf.

[13] Jorrit Jan Serraris. Time domain analysis for DP simulations. In *Proceedings of the International Conference on Offshore Mechanics and Arctic Engineering - OMAE*, volume 1, pages 595–605, 2009. ISBN 9780791843413. doi: 10.1115/OMAE2009-79587.

[14] Andreas Malcherek. *Gezeiten und Wellen*. Springer Verlag, 2 edition, 2010. doi: 10.1007/978-3-8348-9764-0.

[15] Arve Berg. Supply of Meteorological and Oceanographic data at Ten Norden van den Waddeneilanden. Technical report, Fugro Norway, RVO.nl, 2019.

[16] Nicholas C. Flemming, Jan Harff, and Delminda Moura. Non-Cultural Processes of Site Formation, Preservation and Destruction. In *Submerged Landscapes of the European Continental Shelf: Quaternary Paleoenvironments*, pages 51–82. WILEY Blackwell, 2017. ISBN 9781118927823. doi: 10.1002/9781118927823.ch3.

[17] C. A. Willemse, H.T. Grimmelius, and A.R. Tjallema. *OE 5663 Dynamic Positioning*. Delft University of Technology, 2008.

[18] Thor I. Fossen. *Handbook of Marine Craft Hydrodynamics and Motion Control*. John Wiley & Sons, 2011. ISBN 9781119991496. doi: 10.1002/9781119994138.

[19] Olivier Cadet. Introduction to Kalman Filter and its use in Dynamic Positioning Systems. *Proceedings of Dynamic Positioning*, pages 1–33, 2003. URL http://www.dynamic-positioning.com/dp2003/design_cadet.pdf.

[20] Greg Welch and Gary Bishop. An Introduction to the Kalman Filter. *In Practice*, 7(1):1–16, 2006. ISSN 10069313. doi: 10.1.1.117.6808. URL http://citeseerx.ist.psu.edu/viewdoc/download?doi=10.1.1.79.6578&rep=rep1&type=pdf.

[21] Thor I. Fossen and Tor A. Johansen. A survey of control allocation methods for ships and underwater vehicles. In *14th Mediterranean Conference on Control and Automation, MED'06*, 2006. ISBN 0978672003. doi: 10.1109/MED.2006.328749.

[22] Ramamoorthy Jeyasenthil and Jyotisman Dasgupta. Thrust allocation logic of dynamically positioned offshore vessel. *Ships and Offshore Structures*, 5(3):243–251, 2010. ISSN 17445302. doi: 10.1080/17445300903439215.

[23] D. E. Fry. The use of Cross-Correlation and Power Spectral Techniques for the Identification of the Hunter Mk.12 Dynamic Response. *Ministry of Technology - Aeronautical Research Council Current Papers*, 1970.

[24] Radboud van Dijk. DEV80833 Dual SSCV Test Lift - Assessment of DP-RAOs. Technical report, Heerema Marine Contractors, 2018.

[25] Colin Dr. Mercer. Acceleration, Velocity and Displacement Spectra - Omega Arithmetic. *Prosig Signal Processing Tutorials*, 2006. URL http://prosig.com/wp-content/uploads/pdf/blogArticles/OmegaArithmetic.pdf.

[26] Mustafa Sarioglu and Tahir Yavuz. Vortex shedding from circular and rectangular cylinders placed horizontally in a turbulent flow. *Turkish Journal of Engineering and Environmental Sciences*, 24 (4):217–228, 2000. ISSN 13000160.

[27] Dennis Gambarine, Arjen Koop, Gustavo Assi, Fabiano Rampazzo, and Rodolfo T. Gonçalves. Force measurements and stationarity analysis on the flow around a single square column with rounded edges. In *Proceedings of the International Conference on Offshore Mechanics and Arctic Engineering - OMAE*, volume 9, 10 2019. ISBN 9780791858882. doi: 10.1115/OMAE2019-95353.

[28] Radboud Van Dijk, Allan Magee, Steve Perryman, and Joe Gebara. Model test experience on vortex induced vibrations of truss spars. In *Proceedings of the Annual Offshore Technology Conference*, volume 2003-May, pages 1585–1591, 2003. ISBN 9781555632502.

[29] Olaf J. Waals, Amai C. Phadke, and Stephen Bultema. Flow induced motions of multi column floaters. In *Proceedings of the International Conference on Offshore Mechanics and Arctic Engineering - OMAE*, volume 1, pages 669–678, San Diego, 2007. ISBN 0791842673. doi: 10.1115/OMAE2007-29539.

[30] Oriol Rijken, Steve Leverette, and Kent Davies. Vortex Induced Motions of Semi Submersible with Four Square Columns. In *Deep Offshore Technologies*, 2004.

[31] Chia Rong Chen and Hamn Ching Chen. Simulation of vortex-induced motions of a deep draft semi-submersible in current. *Ocean Engineering*, 118:107–116, 5 2016. ISSN 00298018. doi: 10.1016/j.oceaneng.2016.04.005. URL https://www.sciencedirect.com/science/article/pii/S0029801816300580.

[32] J.W. Serraris, R. Bergevoet, and D.H.C. Beks. Heerema Offshore Services: New Heavy Lift Vessel - Current Load and Thruster Interaction Tests. Technical report, MARIN, 2009.

[33] Jianfeng Yao, Wenjuan Lou, Guohui Shen, Yong Guo, and Yuelong Xing. Influence of inflow turbulence on the flow characteristics around a circular cylinder. *Applied Sciences (Switzerland)*, 9(17), 2019. ISSN 20763417. doi: 10.3390/app9173595.

A

Simulation Center Test Series Detection of GPS noise

At the early stage of this project, the aim was to investigate the vessel behavior at different environmental conditions in order to potentially highlight any environmental conditions as the cause of those unexpected motions. Due to the COVID-19 pandemic and the resulting lockdown in the first half of 2020 and special arrangements by HMC, it was possible to frequently use the HSC for this research. The environmental scenarios in which the vessel behavior was to be investigated, consisted of one singular environmental force at a time, such as waves only, wind only or current only. The emphasis lay on comparing the vessel settings of Controller Gain and Kalman Filter Gain . For every environmental condition, 6 simulations of at least 2 hours were carried out. These 6 simulation runs consisted of High Kalman Filter Gain, as used in DP Trials, with Low, Medium & High Controller gain as well as Normal Kalman Filter Gain with Low, Medium & High Controller Gain.

After a total of more than 64 hours of real-time simulations in the HSC, an increased low frequency vessel response in the period range of 3-5 minutes was observed for all simulations. At this stage, it was believed that these observed motions form the unexpected vessel response as observed offshore. However, the deterministic pattern of these vessel oscillations raised doubts and soon showed that this origin of the oscillations in the HSC was traceable. The following results show the discovery and origin of this repetitive pattern.

In figure A.1, the motions of Thialf during DP operation can be seen, when the vessel was exposed to a constant current of 1kn going to 300° (true North). Below, in figure A.2, the motions of Thialf on DP in zero environmental forces are presented. In both figures the results of Normal (blue) and High (red) Kalman Filter Gain at Medium Controller Gain are shown. For all 4 simulations, the vessel has a draft of 26.6m, heading of 0° and GPS for position reference.

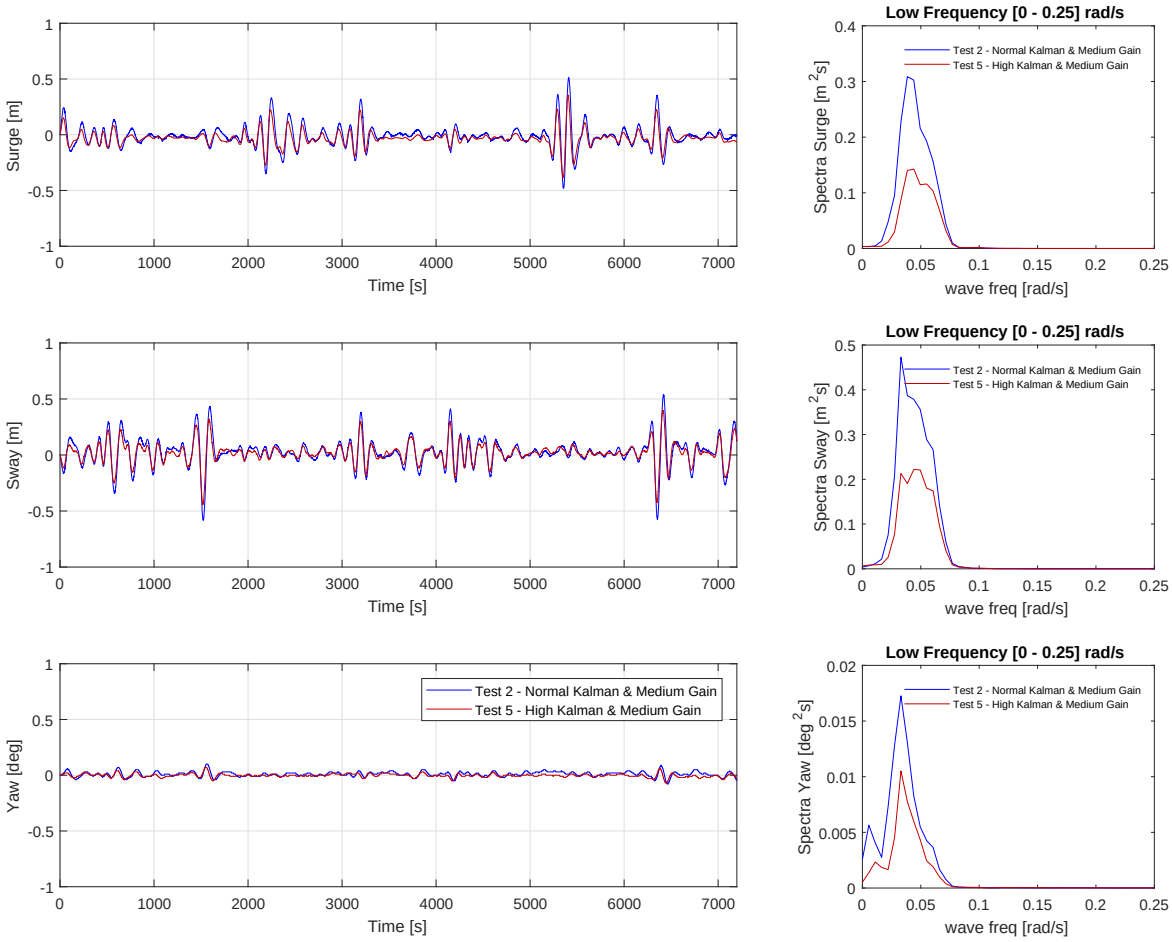

(a) Motion Time Traces

(b) EDS and SDA

Figure A.1: HSC run with SSCV Thialf - Heading: 0 deg, Draft 26.6 m, Current Dir: 300 deg (going to), Current Velocity: 1 kn, Kalman Gain: Normal (blue) & High (red), Controller Gain: Medium, Duration: 2 hrs, Position Reference: GPS

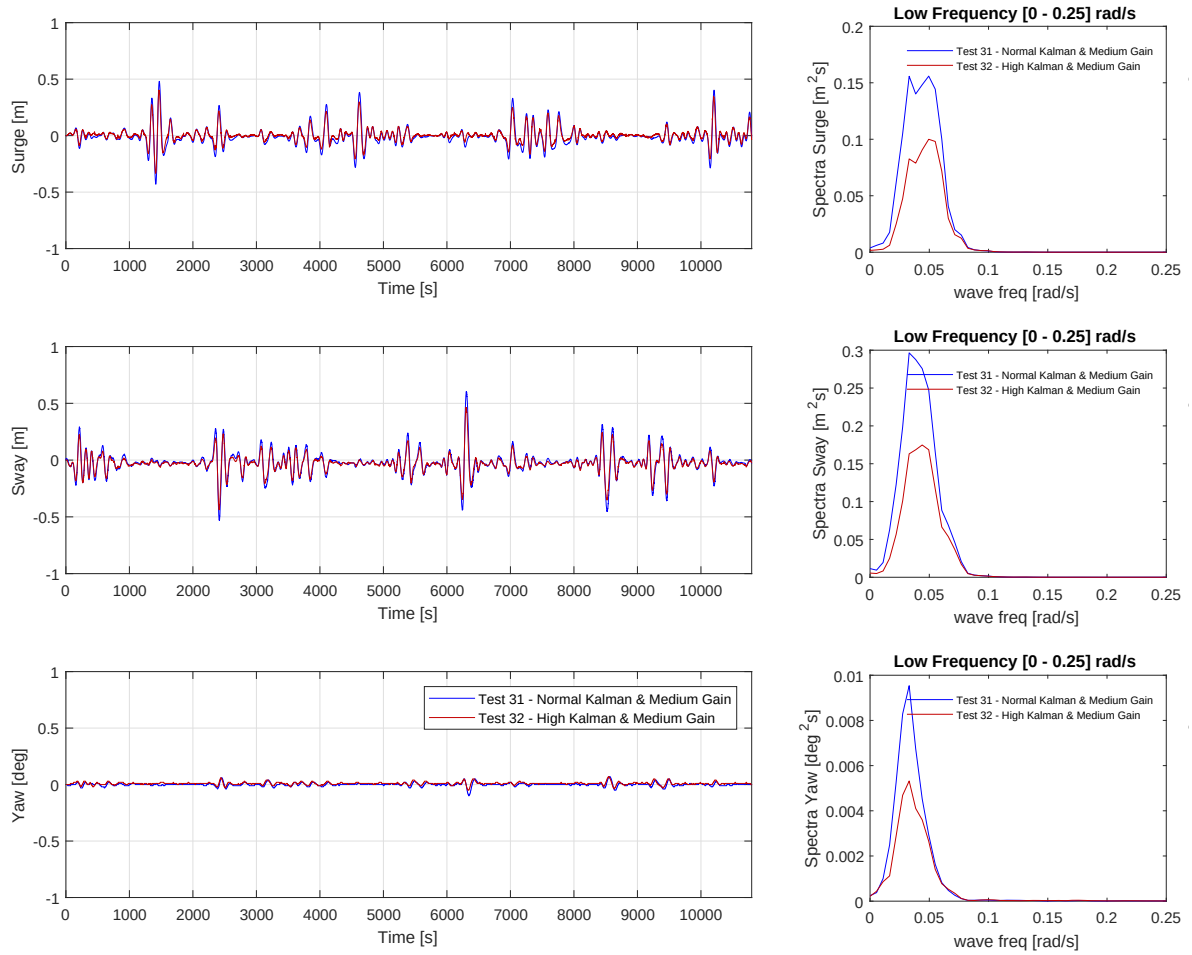

(a) Motion Time Traces

(b) EDS and SDA

Figure A.2: HSC run with SSCV Thialf - Heading: 0 deg, Draft 26.6 m, No environmental forces, Kalman Gain: Normal (blue) & High (red), Controller Gain: Medium, Duration: 3 hrs, Position Reference: GPS

The previous two figures demonstrate that for each environmental scenario, the High and Normal Kalman Filter simulation run, follow the same pattern, where for the High Kalman filter the excitations are less. More surprising, is the fact that each of the 4 runs were conducted at different times in the HSC. They have been plotted such that the pattern matches to highlight its repetitiveness.

As a result of this unusual vessel response with zero environmental forces, the following simulation was carried out. For this simulation, Thialf was fixed in all 6 DOF using the API. The thrusters were disabled and only the GPS was used as a reference system. Figure A.3 presents the results.

It is evident that for surge and sway the vessel shows oscillations with SDAs of up to 0.25m. Nevertheless, the vessel did not move in any of its 6 DOF, signifying that this deterministic oscillation must be introduced into the control loop of the DP system. The most obvious sources are the positioning sensors.

The data from the 3 utilised GPS sensors during the simulation in which Thialf was fixed in 6DOF, revealed the answer shown in figure A.4. The sensor weight in this figure represents the weighting factor that the DP system associates to each sensor when calculating its position. When looking at the UTM Easting and Northing, it is evident that all 3 sensors show the same signal, with the same noise. Note, that no additional noise was added from the instructor station, which can be undertaken in order to avoid a sensor freeze detection. The sensor freeze detection of the DP system disregards a sensor that has not changed its value over a period of time and thus considered to be too constant or even

faulty. However, this feature was not applied in the presented simulations.

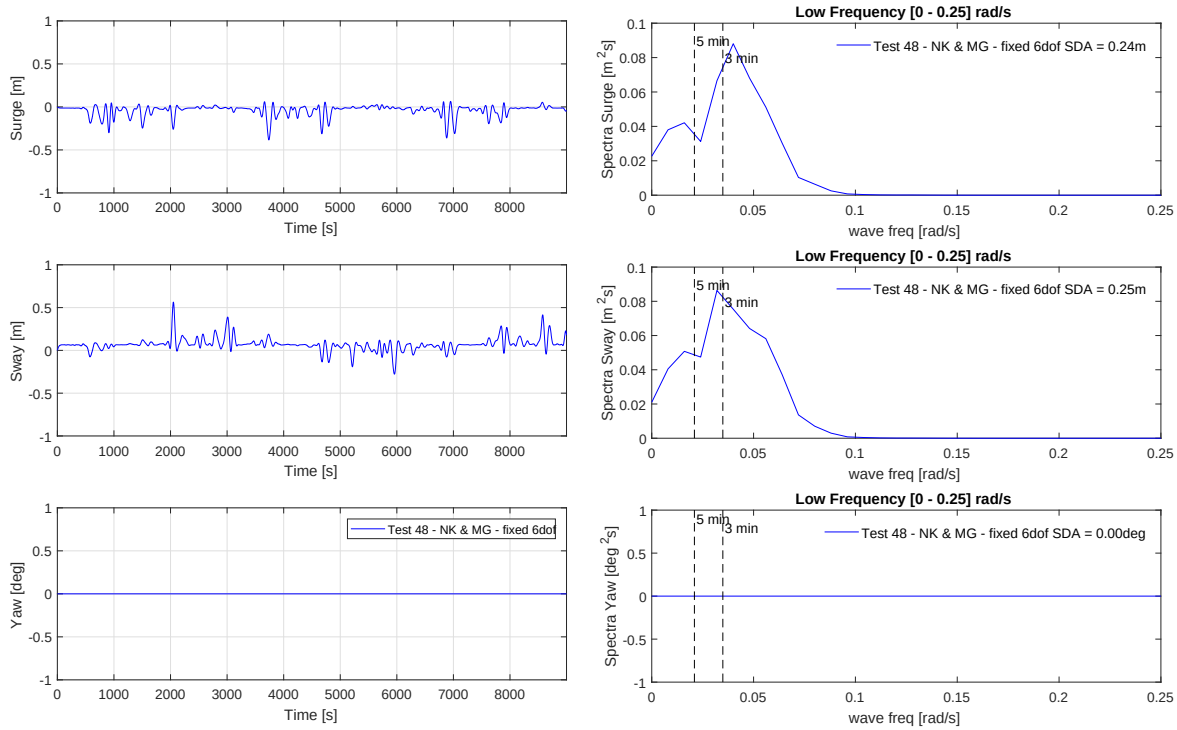

(a) Motion Time Traces (b) EDS and SDA

Figure A.3: HSC run with SSCV Thialf - Heading: 0 deg, Draft 26.6 m, No environmental forces, Fixed in 6 DOF via API, Kalman Gain: Normal (blue), Controller Gain: Medium, Duration: 2.5 hrs, Position Reference: GPS

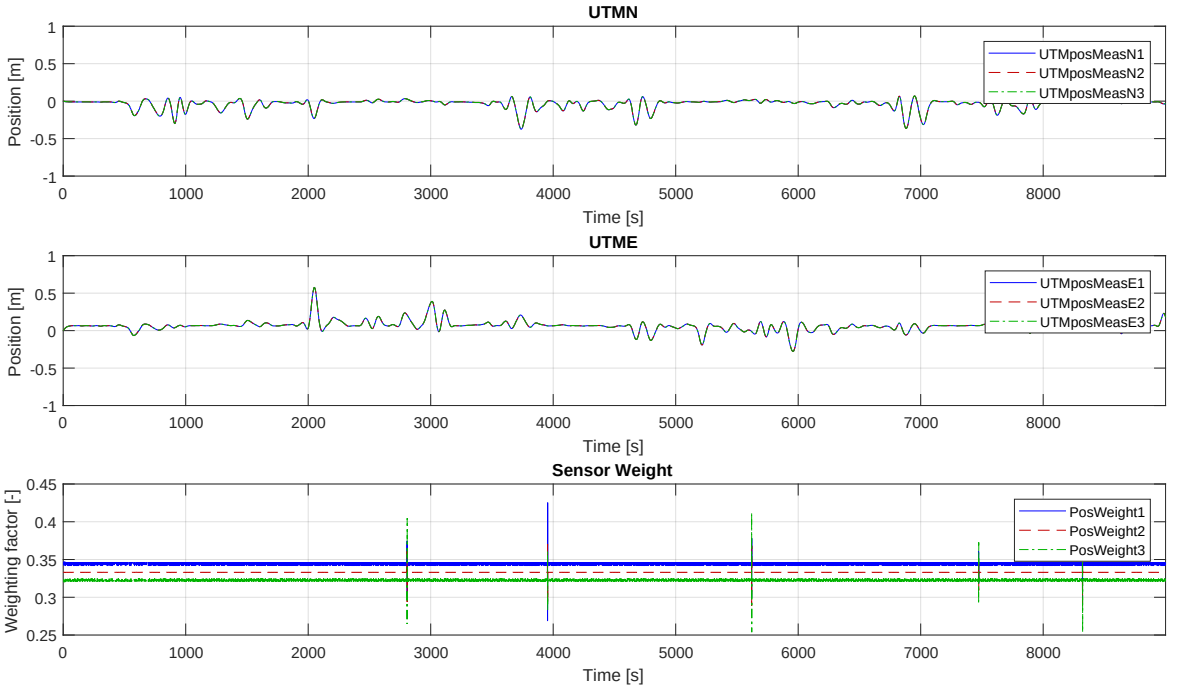

Figure A.4: SensorNoise per sensor

GPS & FanBeam Comparison

Further research required the use of an accurate positioning system without any unknown sensor noise. The comparison between using FanBeam and GPS, as selected reference systems, can be seen below. As FanBeam requires reflectors, Thialf was positioned with its aft (where the FanBeam sensors are installed) towards a platform, which is equipped with FanBeam reflectors. The platform itself was fixed in 6 DOF. The results in figure A.6 provide evidence that the FanBeam sensor indeed does now show the noisy pattern.

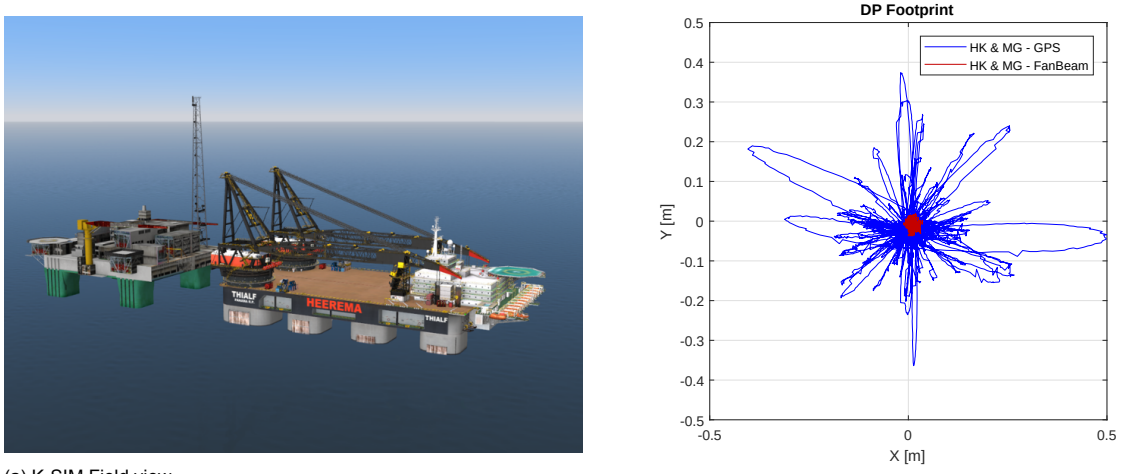

(a) K-SIM Field view

(b) Footprint

Figure A.5: HSC run with SSCV Thialf - Heading: 0 deg, Draft 26.6 m, No environmental forces, Fixed in 6 DOF via API, Kalman Gain: Normal (blue), Controller Gain: Medium, Duration: 2.5 hrs, Position Reference: GPS

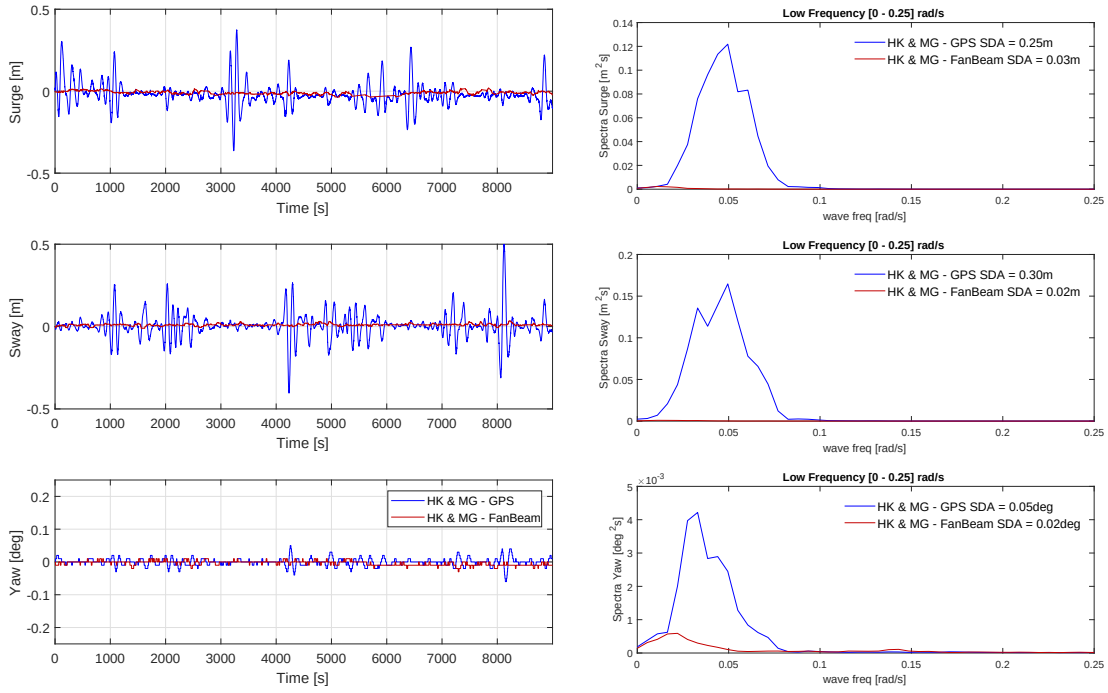

(a) Motion Time Traces

(b) EDS and SDA

Figure A.6: HSC run with SSCV Thialf - Heading: 0 deg, Draft 26.6 m, No environmental forces, Fixed in 6 DOF via API, Kalman Gain: Normal (blue), Controller Gain: Medium, Duration: 2.5 hrs, Position Reference: GPS

Thialf moored in Calandkanaal

The observed noise pattern for all 3 GPS sensors raised the concern that this might be the case for the real vessel as well. For this reason, a 4 hour window of offshore data from Thialf was selected, where the vessel was moored alongside in the 'Calandkanaal' in December 2019. In figure A.7, the time trace and EDS are shown.

These results demonstrate that the signal for each sensor show a SDA of <0.05m and, more importantly, every sensor does not display an identical signal. The peak periods of the measured positioning signal in the EDS, which can be a result of real measurement noise, first order wave forces or vessel motions (which can be influenced by the mooring lines or the fenders) do, in fact, occur at different frequencies than observed in the HSC.

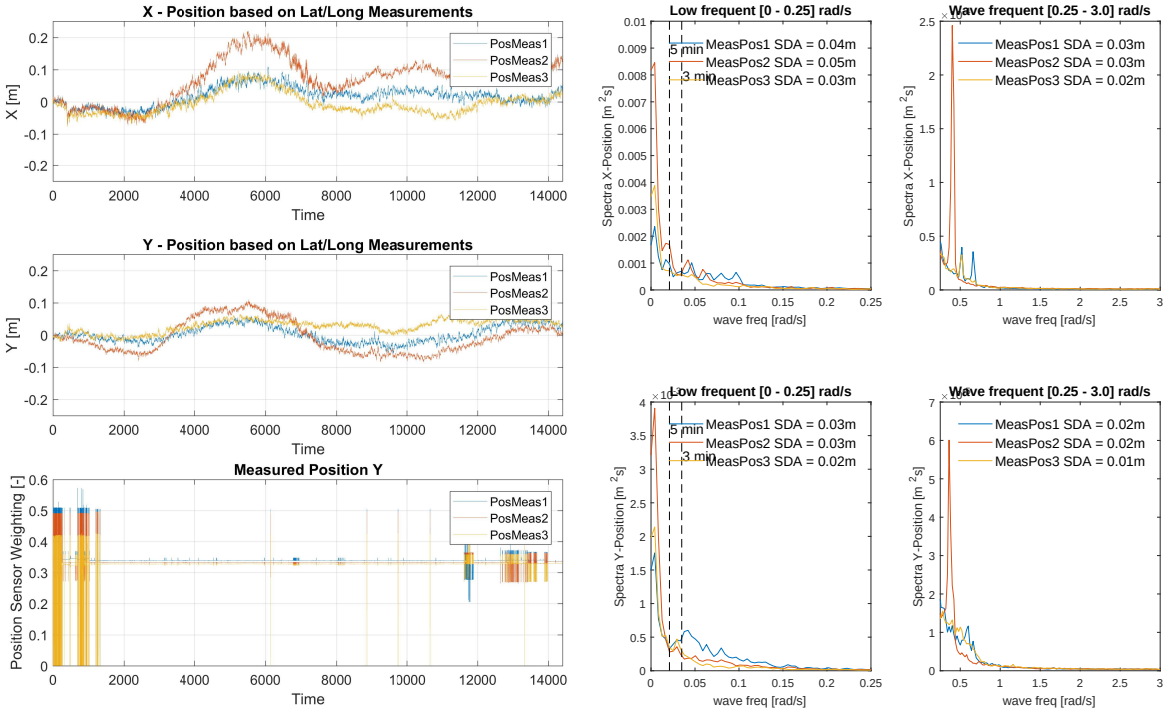

(a) Positioning Time Traces

(b) EDS and SDA

Figure A.7: Offshore data SSCV Thialf - Moored in Calandkanaal, 02-12-2019 9:00 - 13:00 UTC, GPS Position Measurement Sensor 1 (blue), 2 (orange) and 3 (yellow), Duration of observation: 4 hrs

A.1. Conclusion

Based on the presented results, it becomes clear that noise is present in the position measurement of the GPS sensors in the HSC. This becomes particularly apparent when the offshore data from Thialf, moored in the Calandkanaal is studied. Here, it can be seen that the offshore measurement shows different peak noise frequencies with a SDA of less than 0.05m and differences between all sensors. The noise observed in the HSC is more significant, with SDA of approx. 0.25m and a large proportion of its energy at approx. 3 minutes ($\omega = 0.0349 rad/s$) and equal for all sensors. This matter has been forwarded to Kongsberg and further tests have been carried out by the HSC-team to address this. Unfortunately to this date, Kongsberg has not been able to confirm why this sensor noise occurs.

B

Effect of Kalman Filter and Controller Gain Simulation Results

B.1. Normal Kalman Filter Gain

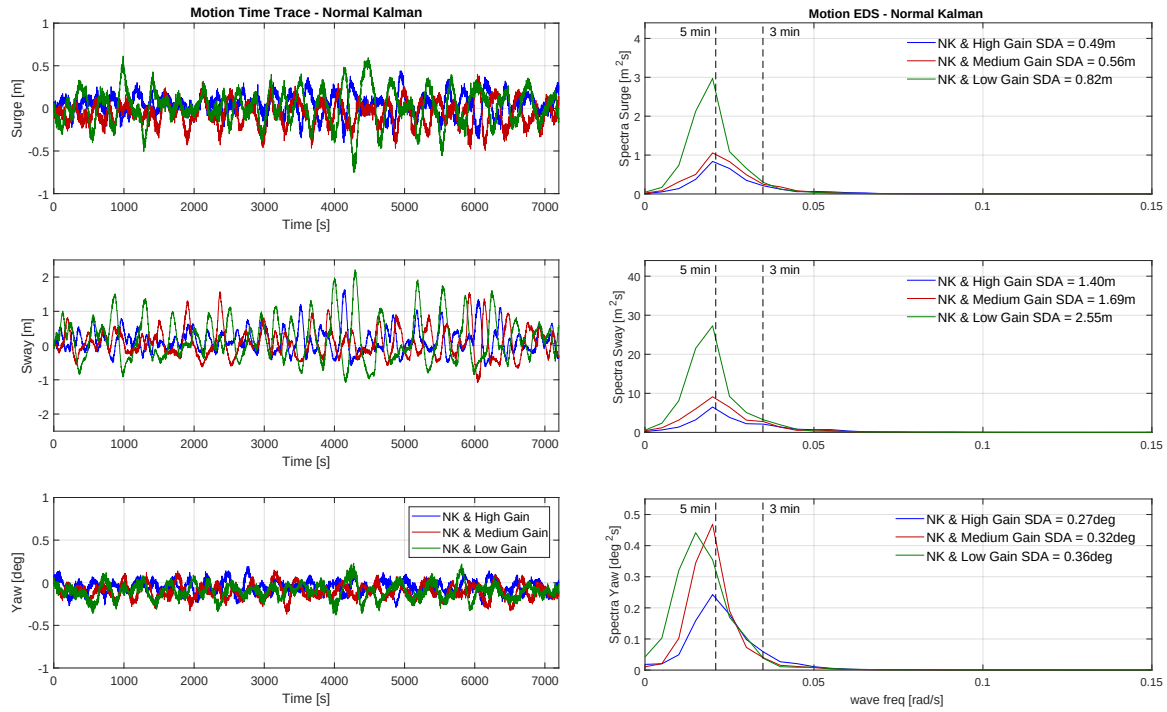

(a) Time Trace

(b) EDS

Figure B.1: HSC run with SSCV Thialf - Motions - Heading: 90 deg, Draft 26.6 m, Waves (Dir=300(coming from), $T_p = 9s$, $H_s = 2m$, JONSWAP, $\gamma = 3.3$), Kalman Gain: Normal, Controller Gain: High, Medium, Low

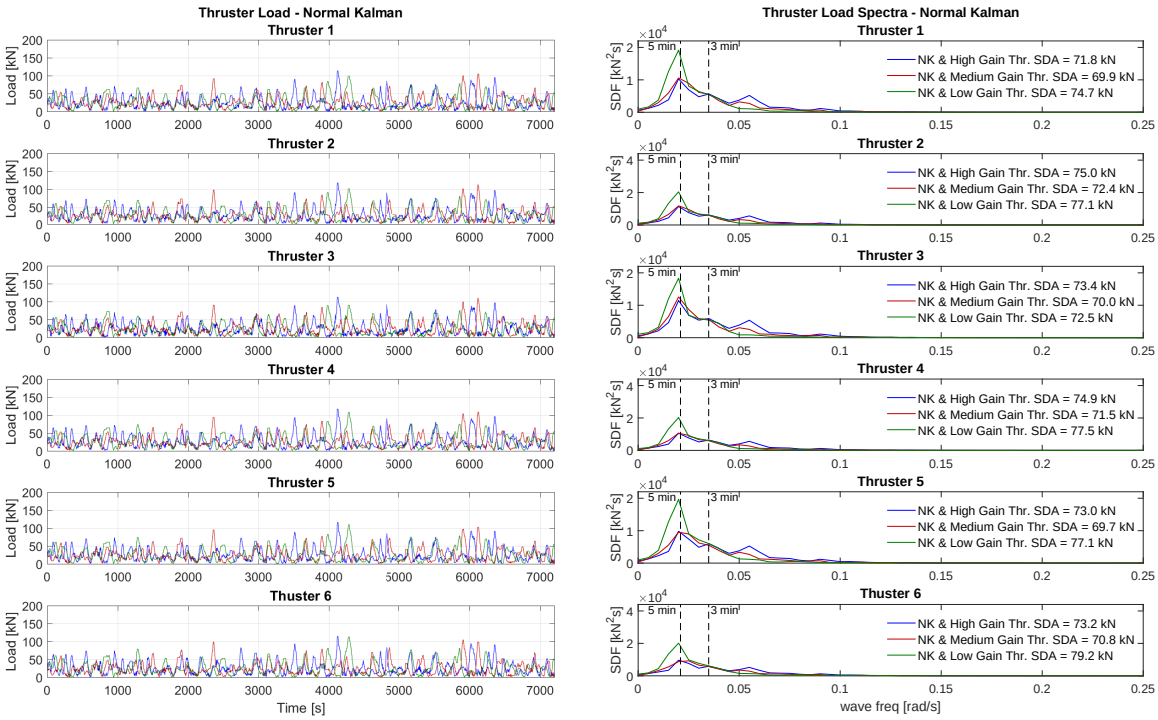

(a) Time Trace (b) EDS

Figure B.2: HSC run with SSCV Thialf - Thruster Load - Heading: 90 deg, Draft 26.6 m, Waves (Dir=300(coming from), $T_p = 9s$, $H_s = 2m$, JONSWAP, $\gamma = 3.3$), Kalman Gain: Normal, Controller Gain: High, Medium, Low

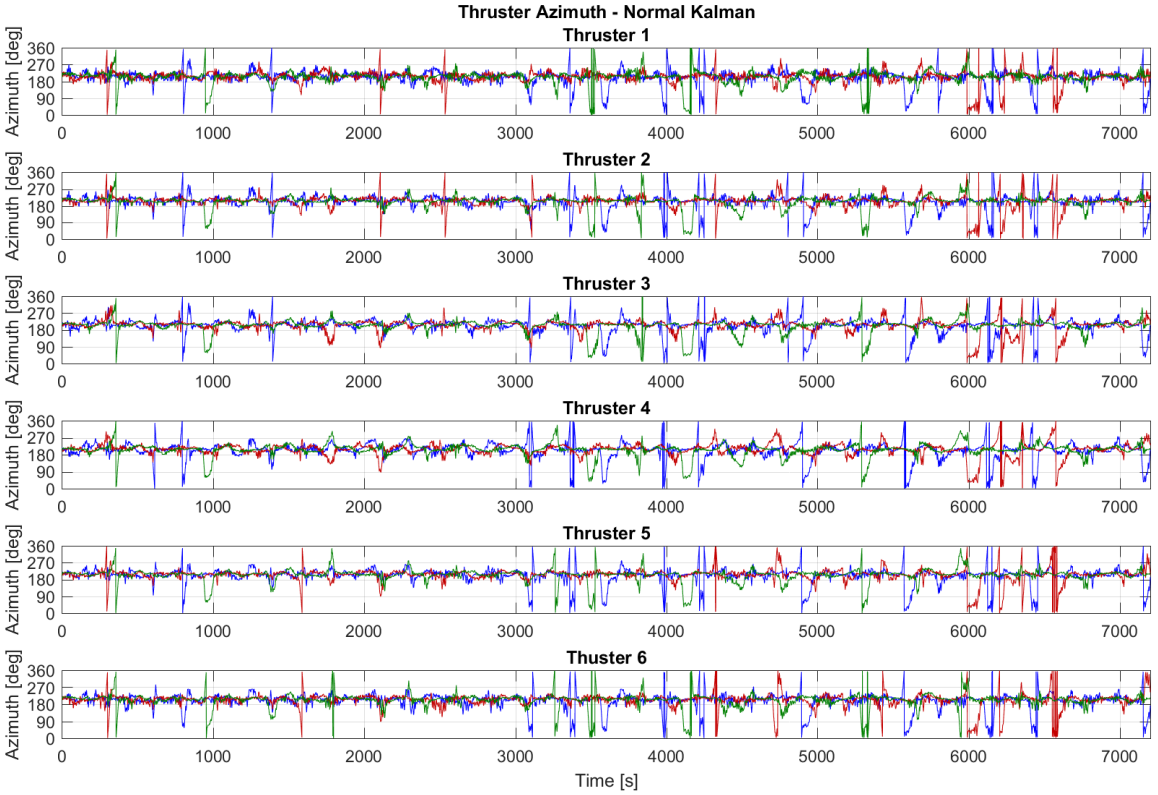

Figure B.3: HSC run with SSCV Thialf - Thruster Azimuth - Heading: 90 deg, Draft 26.6 m, Waves (Dir=300(coming from), $T_p = 9s$, $H_s = 2m$, JONSWAP, $\gamma = 3.3$), Kalman Gain: Normal, Controller Gain: High, Medium, Low

B.2. High Kalman Filter Gain

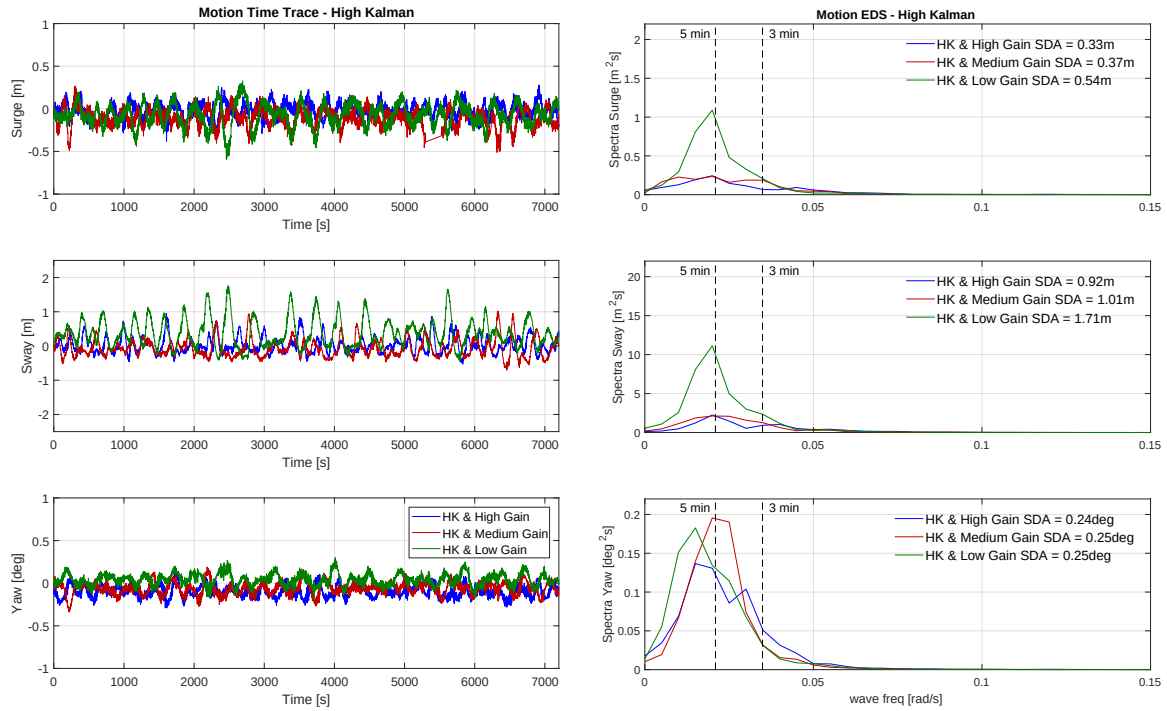

(a) Time Trace (b) EDS

Figure B.4: HSC run with SSCV Thialf - Motions - Heading: 90 deg, Draft 26.6 m, Waves (Dir=300(coming from), $T_p = 9s$, $H_s = 2m$, JONSWAP, $\gamma = 3.3$), Kalman Gain: High, Controller Gain: High, Medium, Low

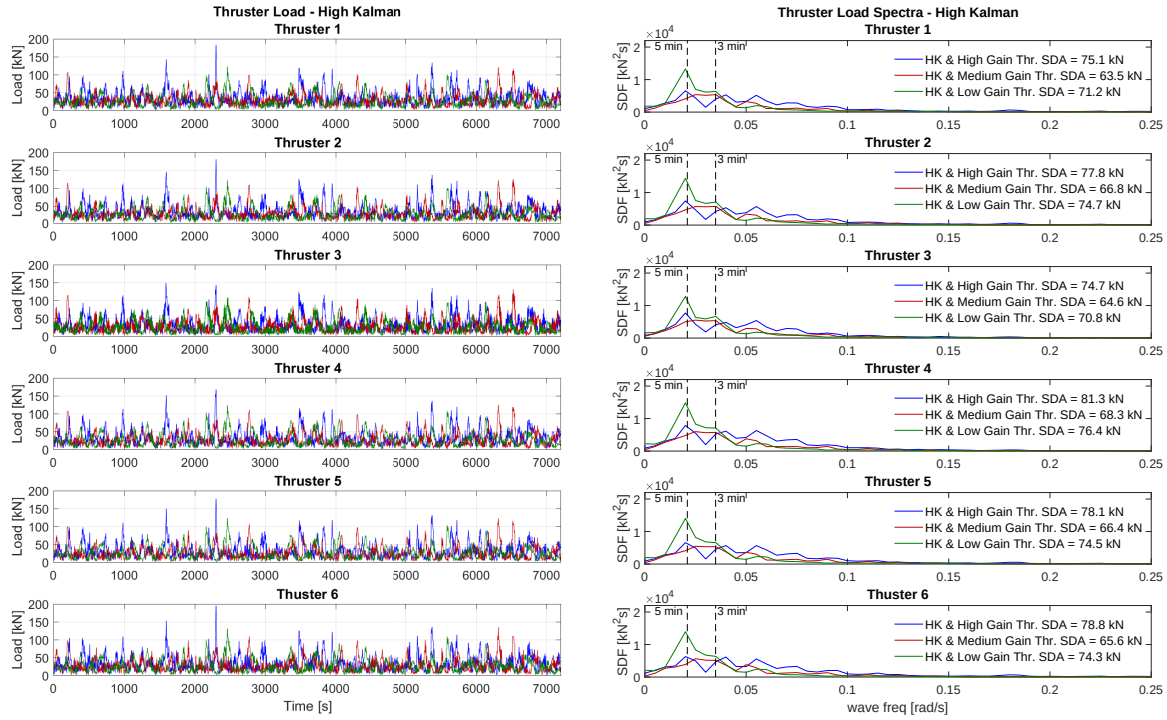

(a) Time Trace (b) EDS

Figure B.5: HSC run with SSCV Thialf - Thruster Load - Heading: 90 deg, Draft 26.6 m, Waves (Dir=300(coming from), $T_p = 9s$, $H_s = 2m$, JONSWAP, $\gamma = 3.3$), Kalman Gain: High, Controller Gain: High, Medium, Low

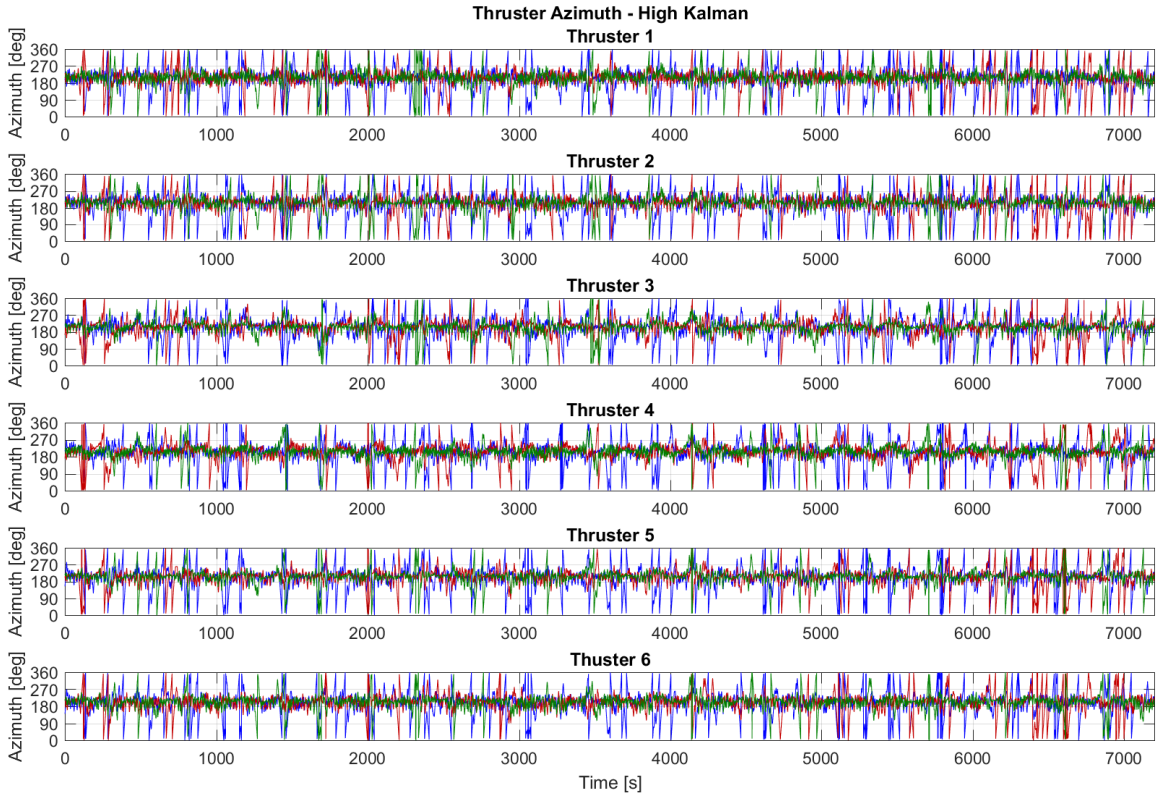

Figure B.6: HSC run with SSCV Thialf - Thruster Azimuth - Heading: 90 deg, Draft 26.6 m, Waves (Dir=300(coming from), $T_p = 9s$, $H_s = 2m$, JONSWAP, $\gamma = 3.3$), Kalman Gain: High, Controller Gain: High, Medium, Low

C

Effect of VIM Simulation Results 2kn & 60° heading

Input for the simulation, the forces and moment time trace, which was obtained from the 2kn and 60° heading current load test results are shown in figure C.2. These represent a current coming from 240° in the coordinate system as used by MARIN and a current coming from 300° in the true North clockwise positive coordinate system where the bow is North, see below (figure C.1). The results of the simulation, vessel motions and thruster response, can be seen in figure C.3, C.4 and C.5.

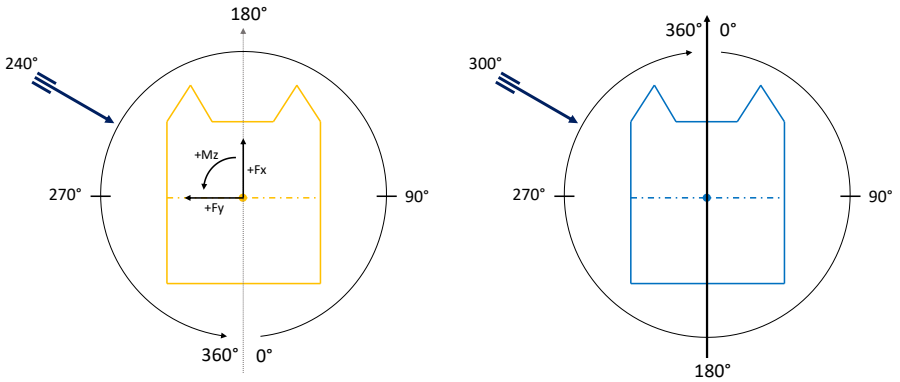

Figure C.1: Direction convention for incoming currents, coming from 240° vessel coordinate system (left) and coming from 300° true North coordinate system (right)

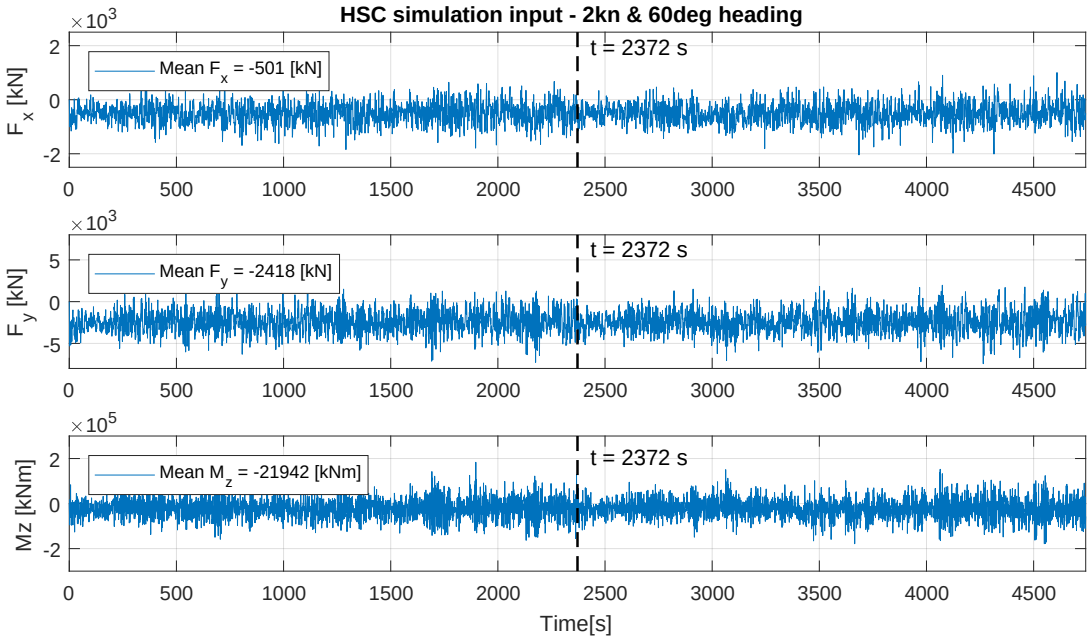

Figure C.2: Simulation input - HSC - High Kalman Gain & Medium Controller Gain - 60° heading & 2 kn current load test measurements

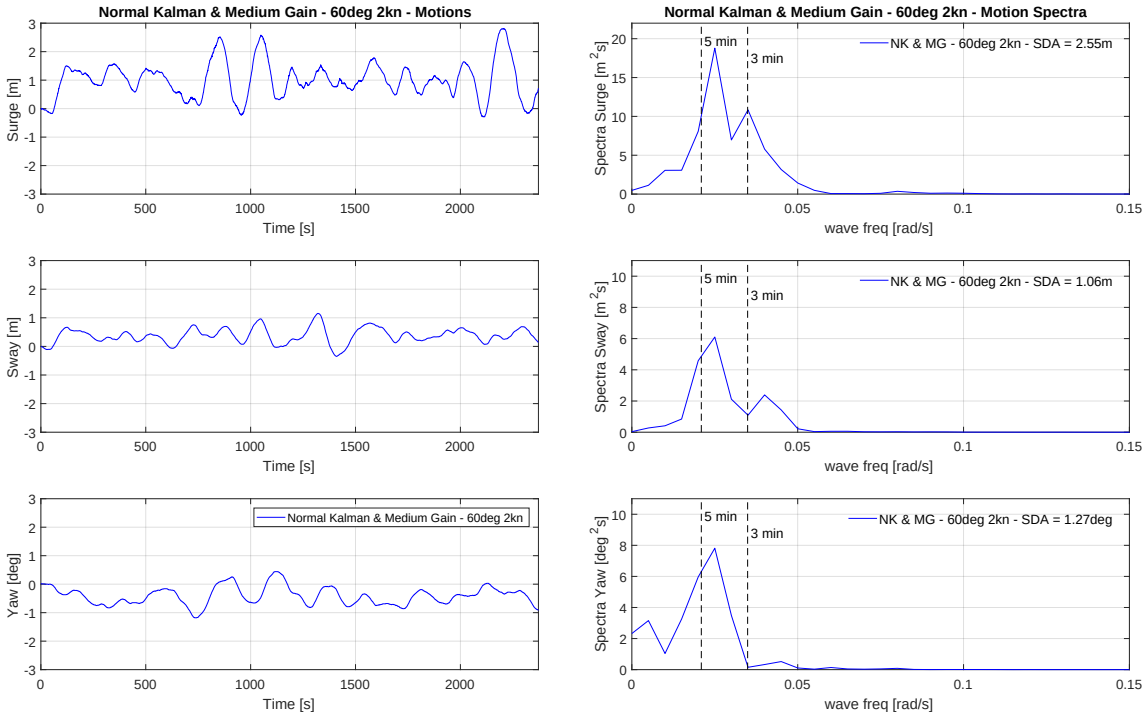

(a) Vessel Motions

(b) Vessel Motions EDS

Figure C.3: Vessel Motions - HSC - Normal Kalman Gain & Medium Controller Gain - exposed to 60° heading & 2 kn current load test measurements

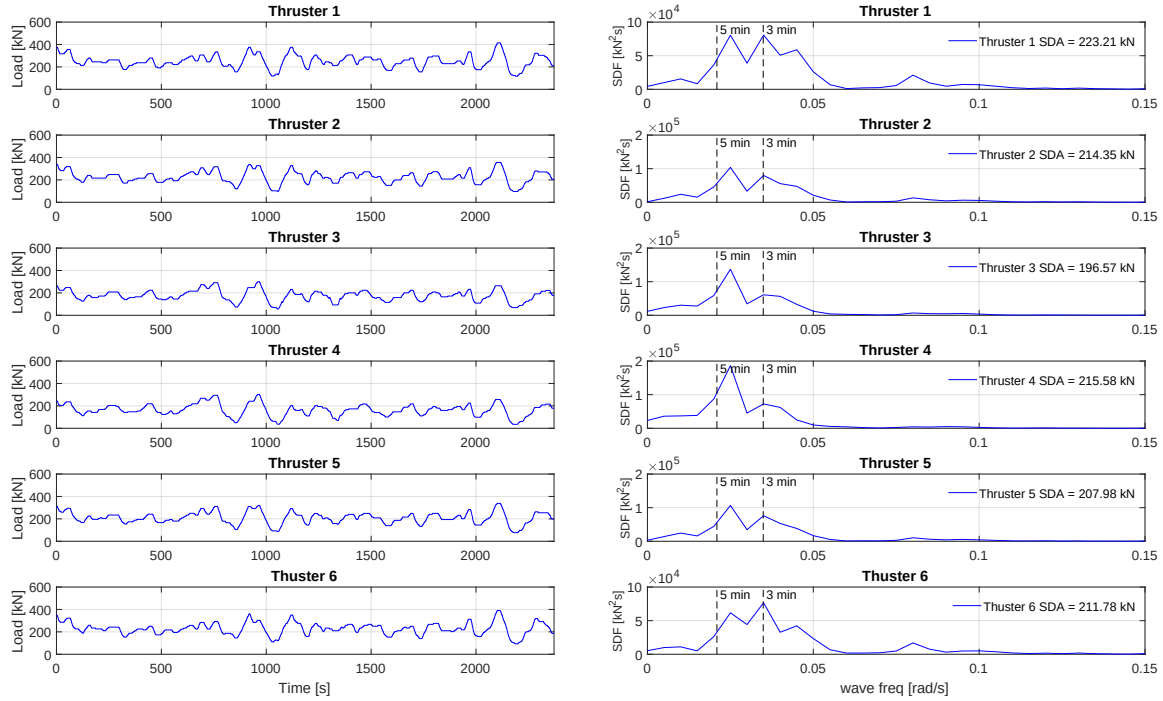

(a) Thruster Load

(b) Thruster Load EDS

Figure C.4: Thruster Load - HSC - Normal Kalman Gain & Medium Controller Gain - exposed to 60° heading & 2 kn current load test measurements

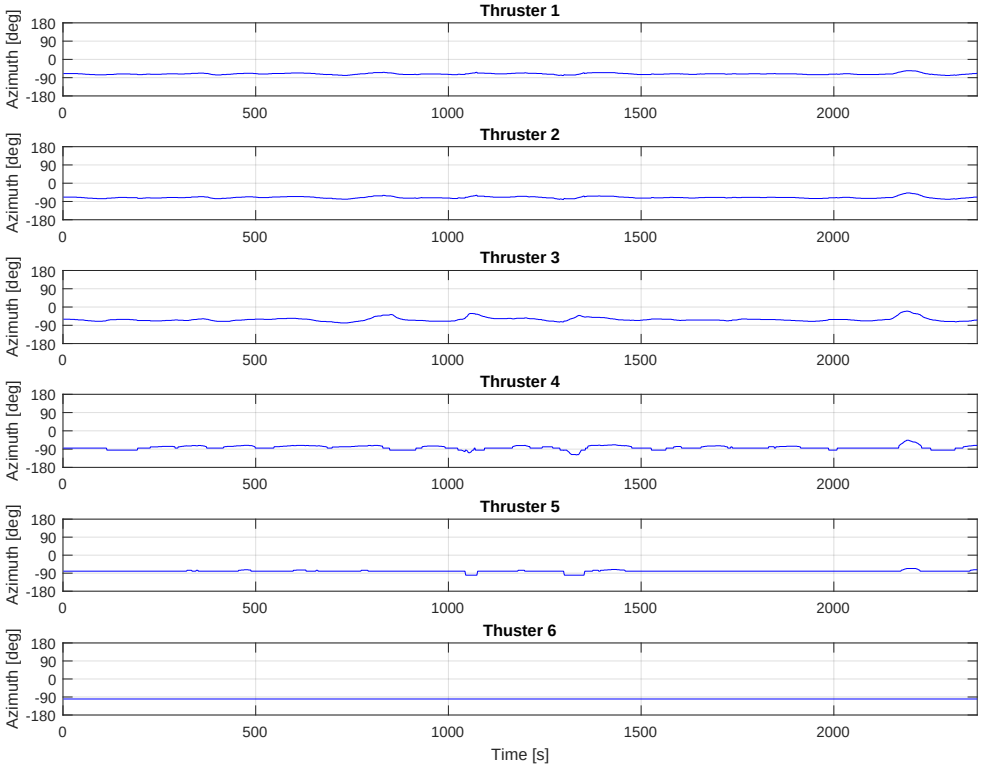

Figure C.5: Thruster Azimuth - HSC - Normal Kalman Gain & Medium Controller Gain - exposed to 60° heading & 2 kn current load test measurements

Discussion

Figure C.3 demonstrates that the time-varying forces and moments obtained from 2kn current velocity cause the vessel to fluctuate around the set-point and heading. The SDA indicated in figure C.3b (computed based on equation 2.15) show values of SDA_{Surge} = 2.55m, SDA_{Sway} = 1.06m & SDA_{Yaw} = 1.27°. The low frequency excitation of the vessel entails periods in the range of 3 & 5 min as marked in the EDS. This is also the case for the thruster response, where the thruster load indicates a reaction at a similar low frequency band.

Despite an increased force acting on the vessel in y- / sway-direction (refer to figure C.2), the vessel shows larger offsets in x- / surge-direction. According to the SDA, the offsets in surge are 2.4 times larger than the sway offsets. While the mean of forces acting on the vessel, F_x is 4.8 times smaller than F_y. This can be explained by assessing the thruster azimuth.

In figure C.5, the thruster azimuth for each individual thruster can be seen. The azimuth angle for Thruster 1 to 3 are varying around -60°, while Thruster 4 to 5 are varying around -90° and Thruster 6 does not change its azimuth angle and stays constant at -100°. During the simulation, the K-POS console gave azimuth prediction errors for Thruster 5 and 6, which results in 'freezing' of the thruster azimuth value and sudden jumps, as seen for Thruster 5 between 1000 and 1500 seconds. Despite those prediction errors, the majority of thrust is generated towards the directions between -60° and -90° in the local vessel K-POS coordinate system for azimuth angles. In figure C.6 below, the local vessel K-POS coordinate system for azimuth angles is shown and the coming from current direction indicated. From a thruster point of view, the direction in which thrust is generated is indicated.

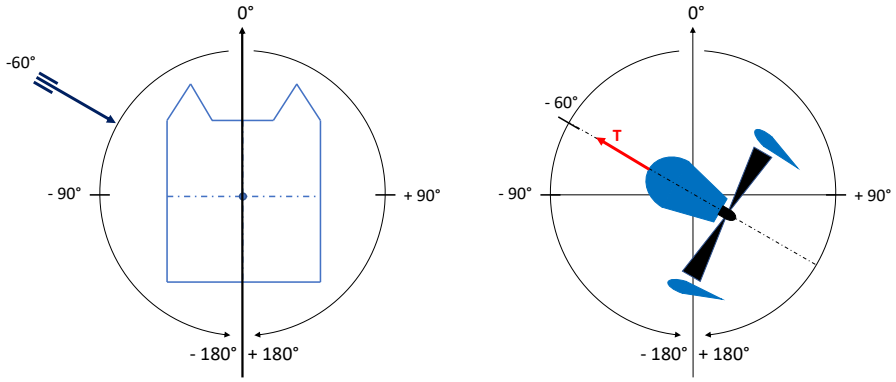

Figure C.6: Coming from current direction and generated thrust direction for local vessl K-POS coordinate system for azimuth angles -60° coming from current direction represents the true North 300° coming from current direction (refer to figure C.1)

This means, the thrusters are generating thrust opposite to the direction of the current loads. The greater part of current loads is acting transversely on the vessel, in y- / sway-direction and therefore the transverse generated thrust is greater. Smaller current loads which are then acting longitudinal on the vessel, in x- / surge-direction, requires the DP system to keep counteracting the larger transverse content while adjusting the thrusters to also counteract the smaller longitudinal forces. This is the function of a DP system.

However, when fluctuations of forces are present in longitudinal direction of the vessel, which is the case here, the vessel cannot counteract these forces effectively, causing large longitudinal offsets.

D

DP RAO Assessment - Normal & High Kalman Filter - Medium Gain

Inputfile: 200903_NormalKalmanGain(2020-09-03 14.55.02)Variables
AnalysisRange: 03-Sep-2020 08:00:00 to 03-Sep-2020 10:00:00 (UTC)
DP-controller Spring & Damping Coefficients (26.6m Draft / Medium Gain / High Precision Controller Mode)

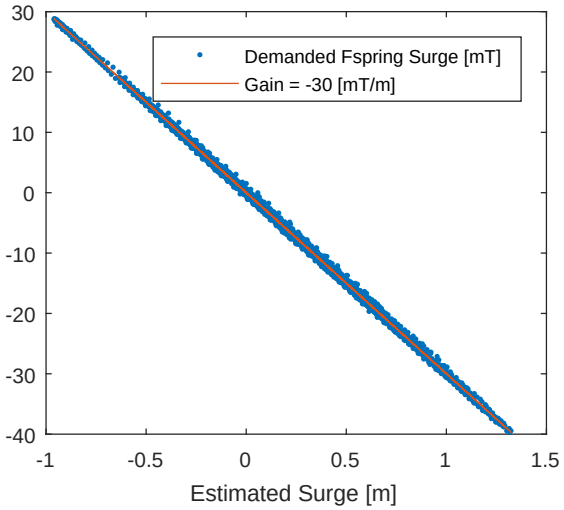

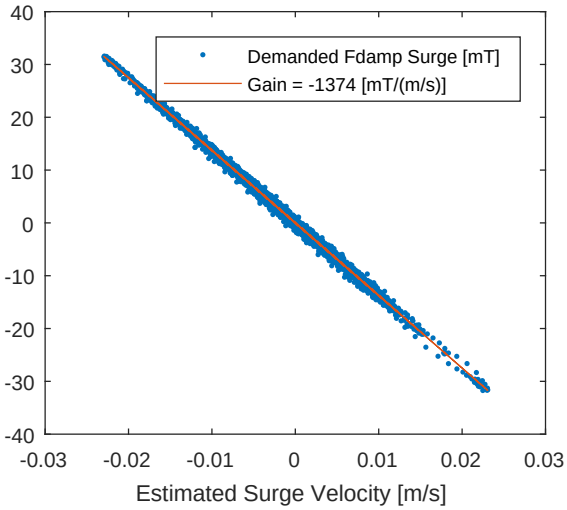

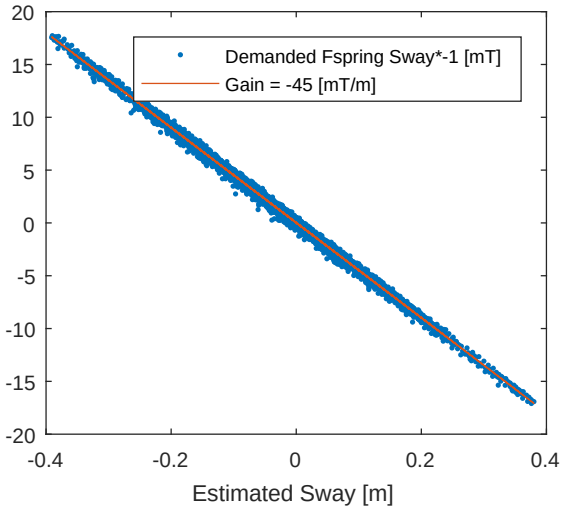

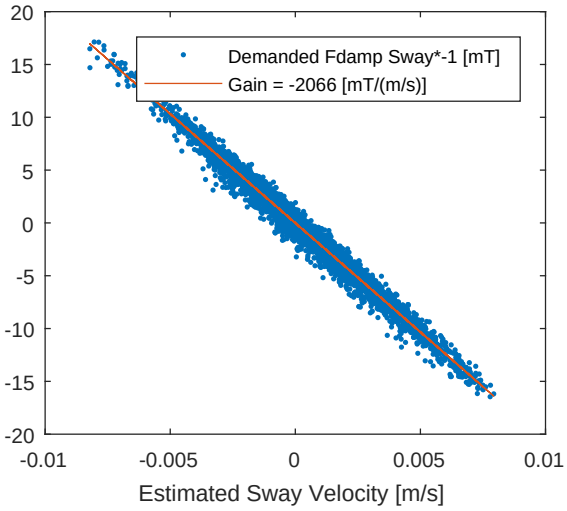

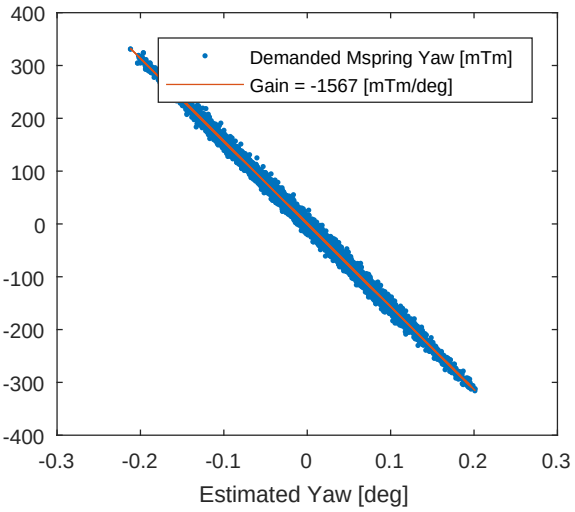

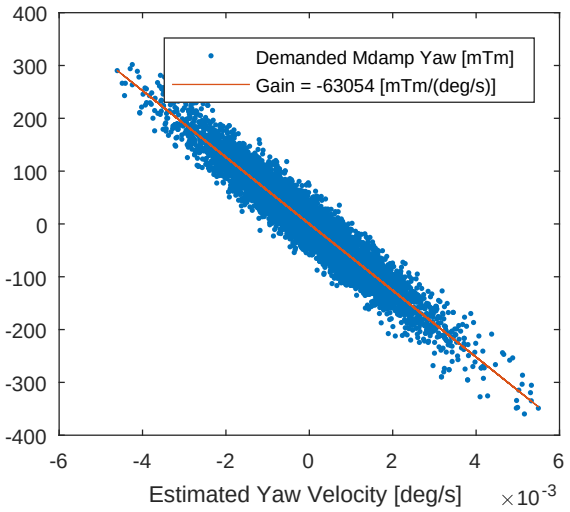

Inputfile: 200903_NormalKalmanGain(2020-09-03 14.55.02)Variables
AnalysisRange: 03-Sep-2020 08:00:00 to 03-Sep-2020 10:00:00 (UTC)
DP-RAO (Spring & Damper)

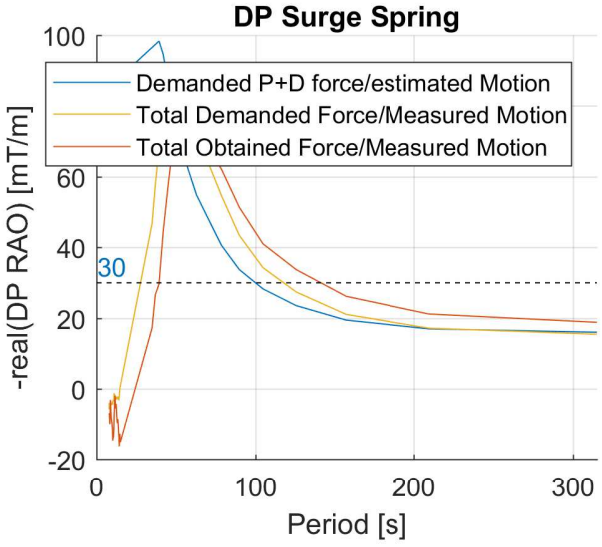

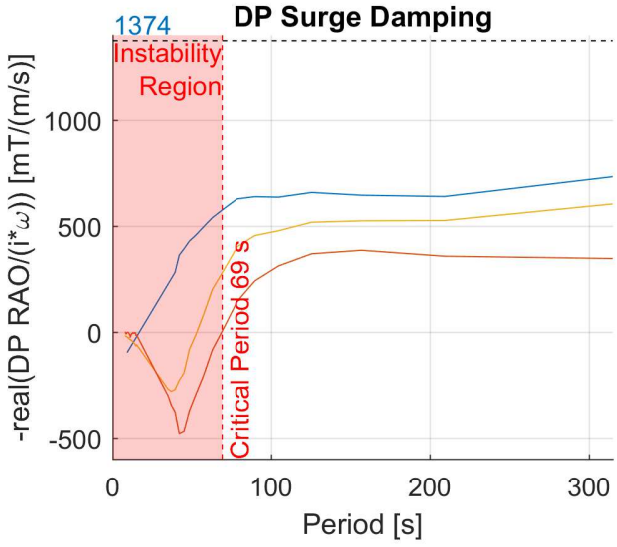

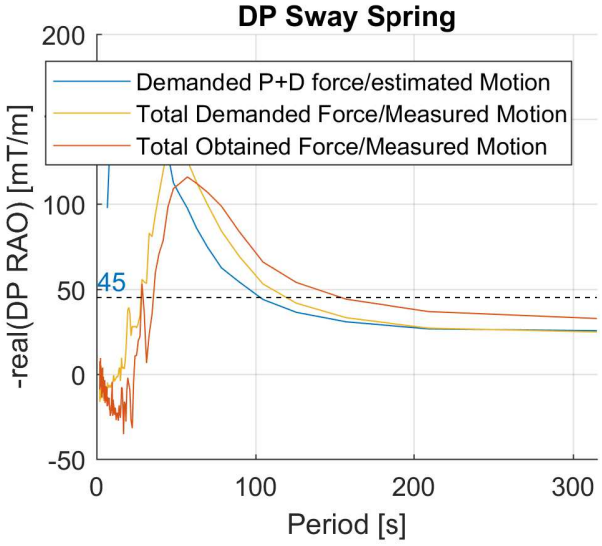

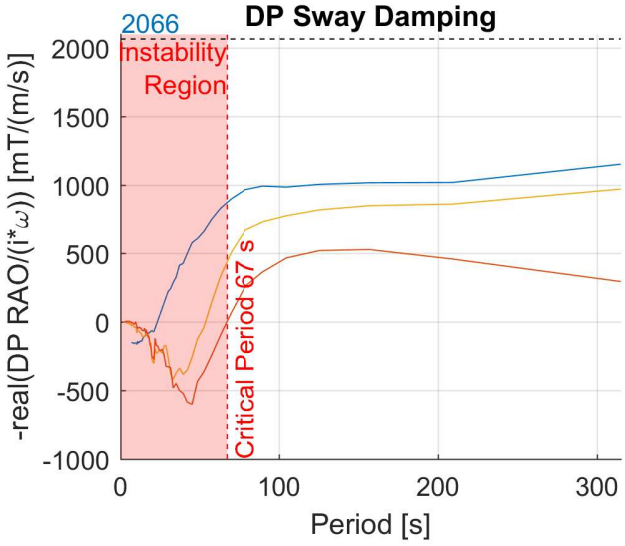

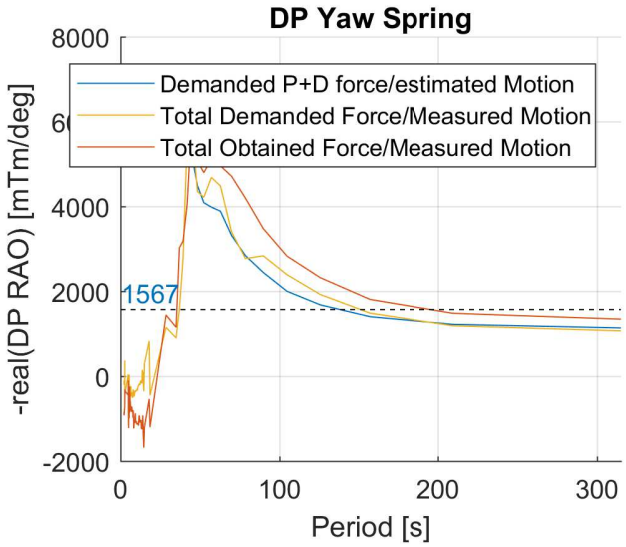

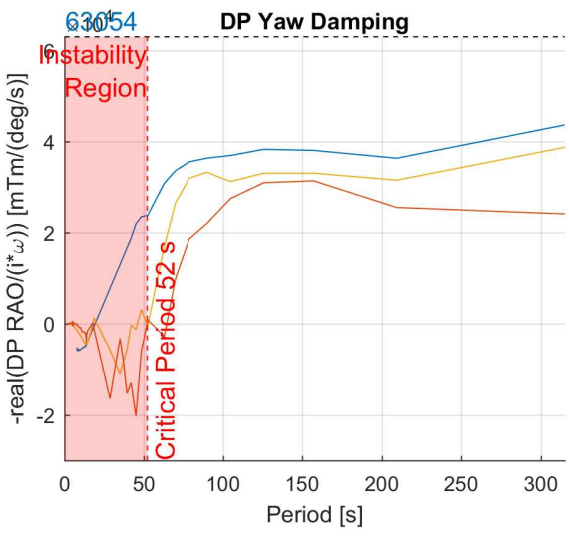

Inputfile: 200904_HighKalmanGain(2020-09-04 14.37.57)Variables
AnalysisRange: 04-Sep-2020 07:05:00 to 04-Sep-2020 09:00:00 (UTC)
DP-controller Spring & Damping Coefficients (26.6m Draft / Medium Gain / High Precision Controller Mode)

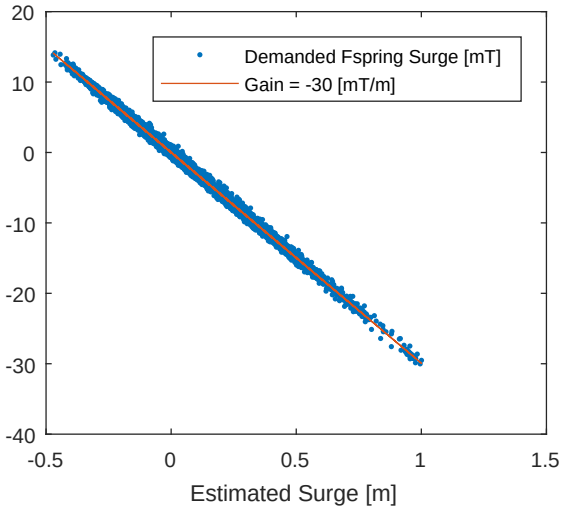

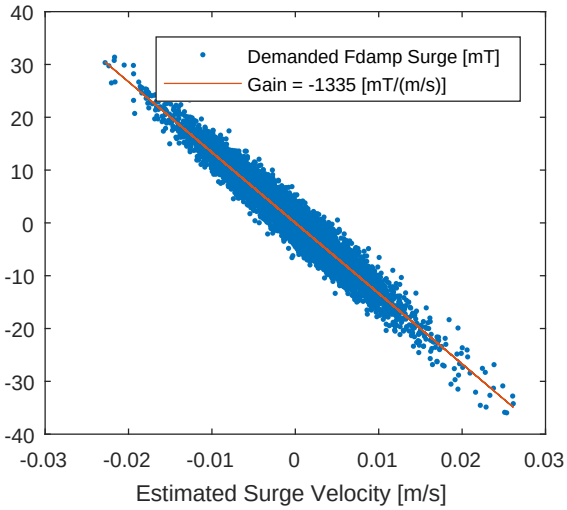

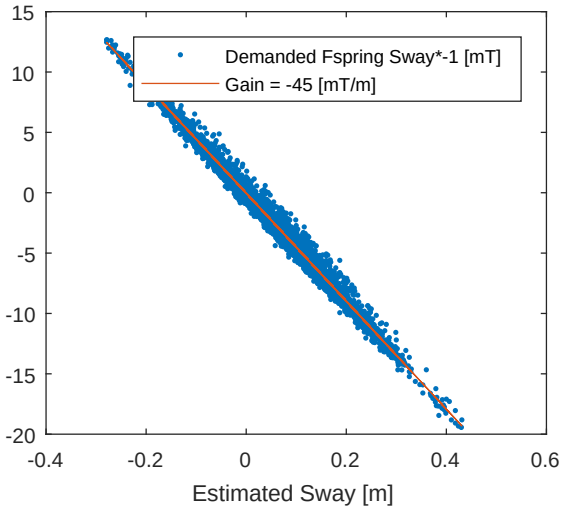

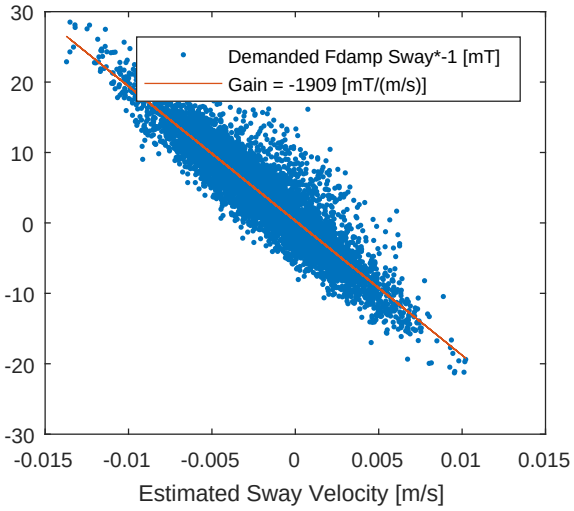

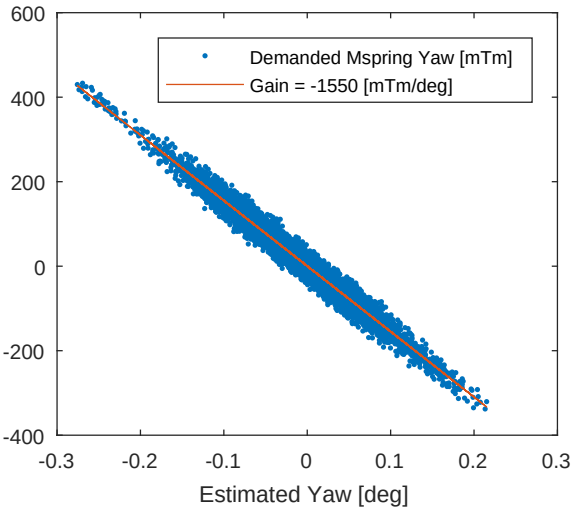

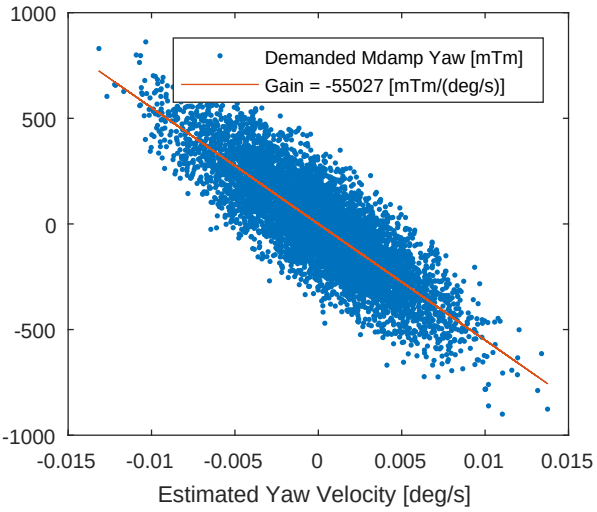

Inputfile: 200904_HighKalmanGain(2020-09-04 14.37.57)Variables
AnalysisRange: 04-Sep-2020 07:05:00 to 04-Sep-2020 09:00:00 (UTC)
DP-RAO (Spring & Damper)

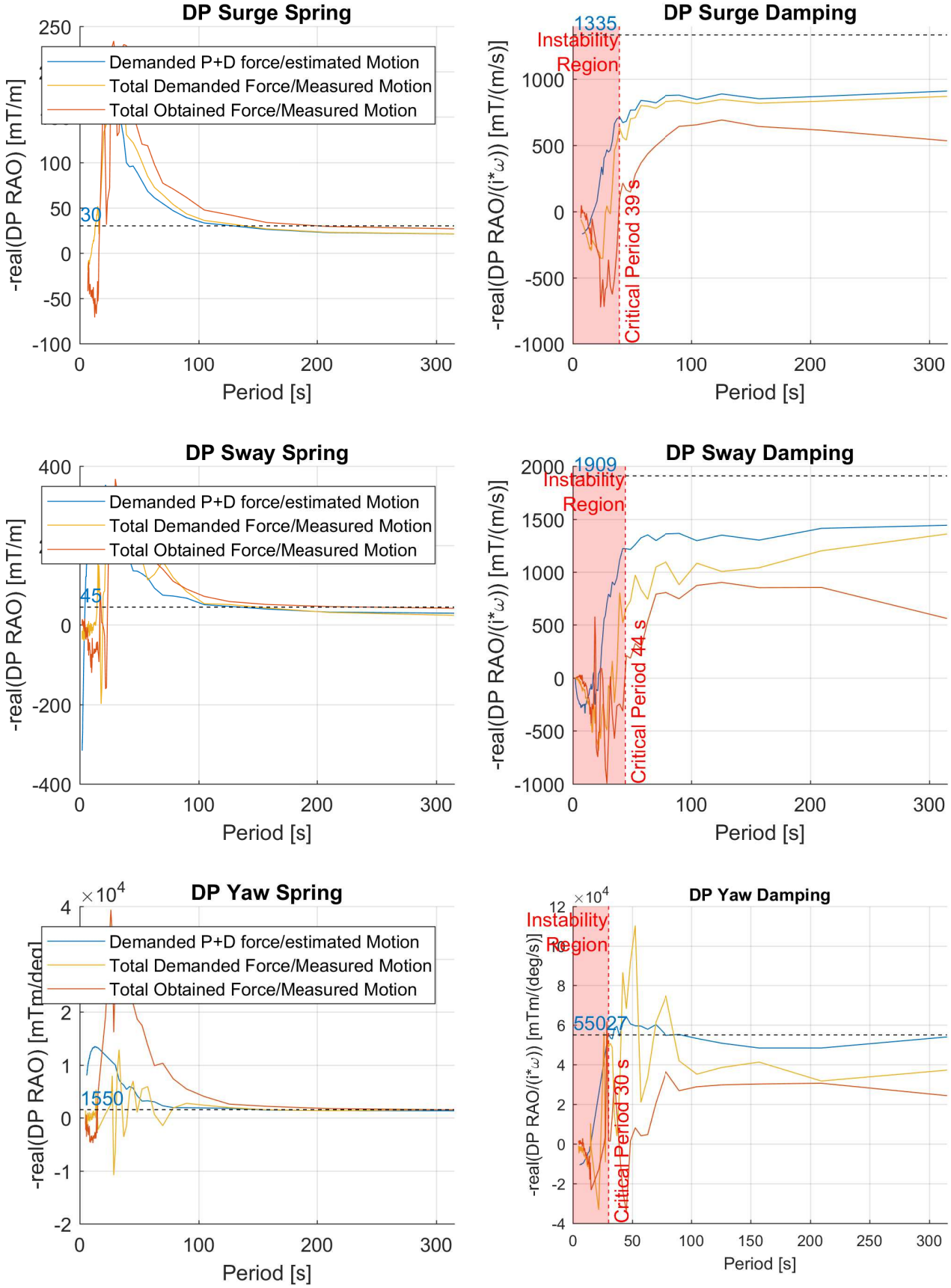

E

Effect of Reduced Damping - aNySIM Damping Series

aNySIM & HSC Comparison - Normal Kalman & Medium Gain - Waves: Hs=2m, Tp=9s, Dir=330deg (going to - aNySIM)
aNySIM - Spring: Obtained from HSC, Damping: β_{Surge} = 90%, β_{Sway} = 90%, β_{Yaw} = 70%

Motion TimeTrace

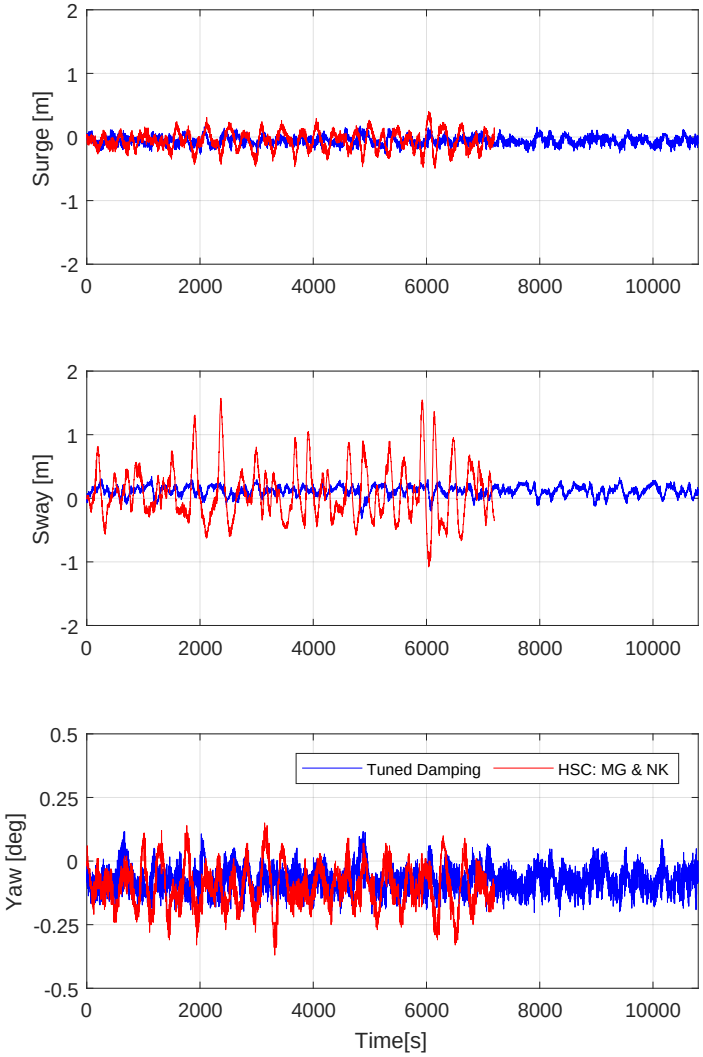

Motion EDS

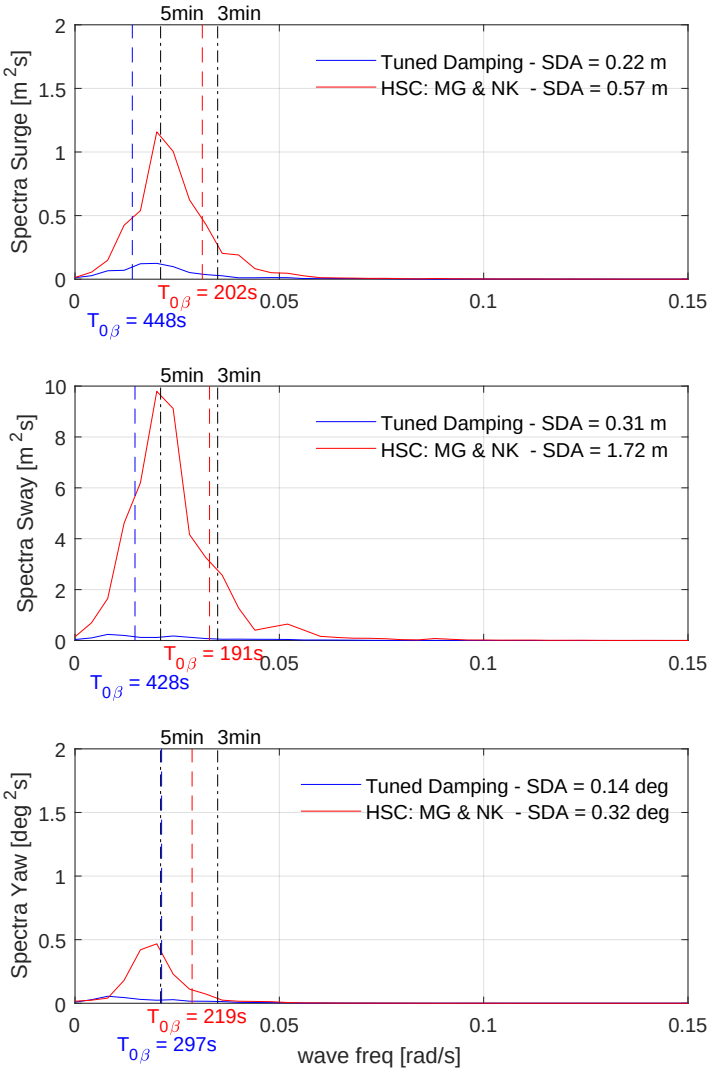

aNySIM & HSC Comparison - Normal Kalman & Medium Gain - Waves: Hs=2m, Tp=9s, Dir=330deg (going to - aNySIM)
aNySIM - Spring: Obtained from HSC, Damping: β_{Surge} = 80%, β_{Sway} = 80%, β_{Yaw} = 65%

Motion TimeTrace

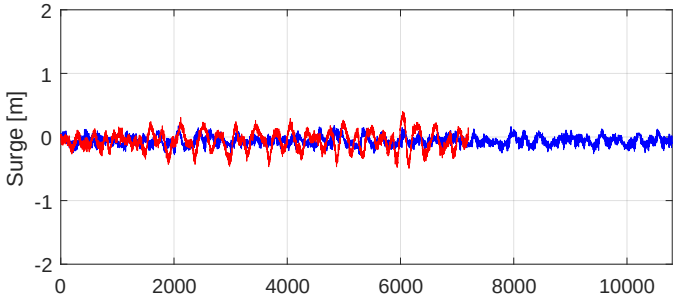

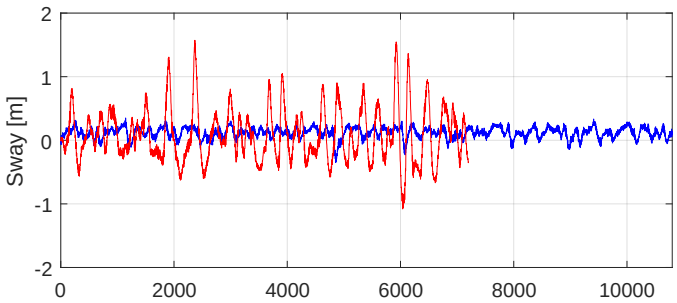

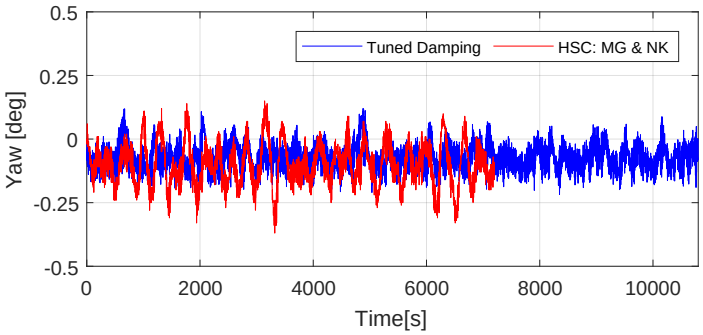

Motion EDS

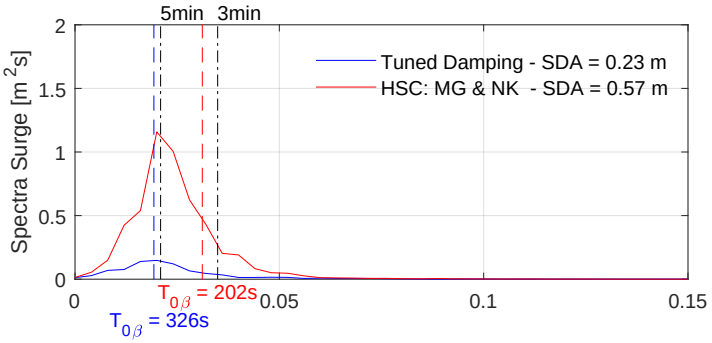

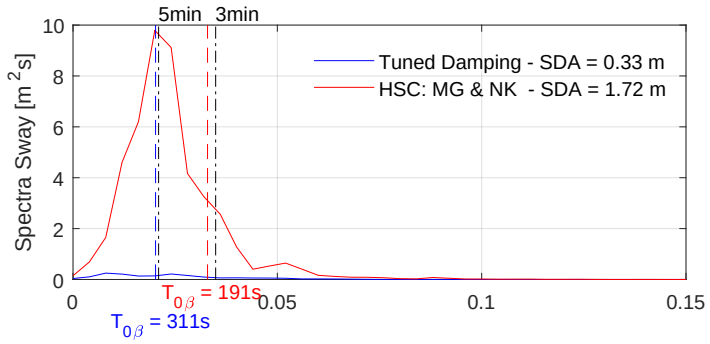

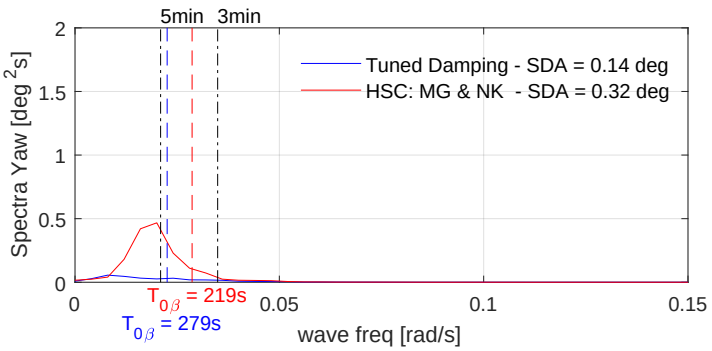

aNySIM & HSC Comparison - Normal Kalman & Medium Gain - Waves: Hs=2m, Tp=9s, Dir=330deg (going to - aNySIM)
aNySIM - Spring: Obtained from HSC, Damping: β_{Surge} = 70%, β_{Sway} = 70%, β_{Yaw} = 50%

Motion TimeTrace

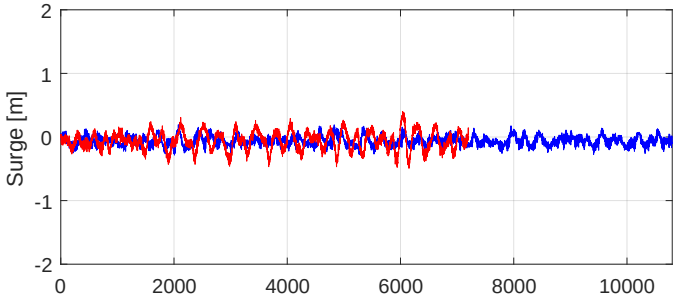

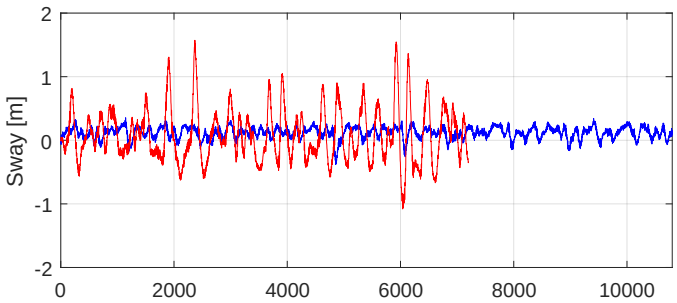

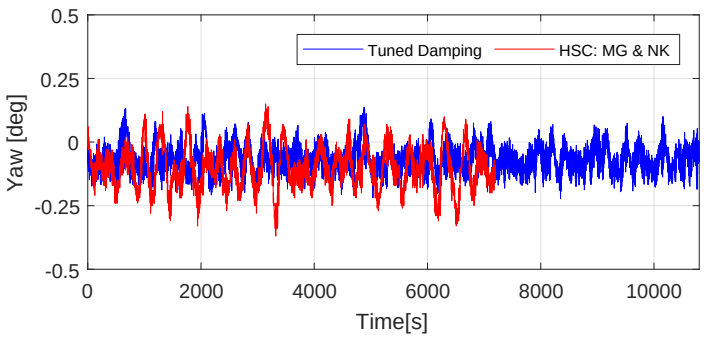

Motion EDS

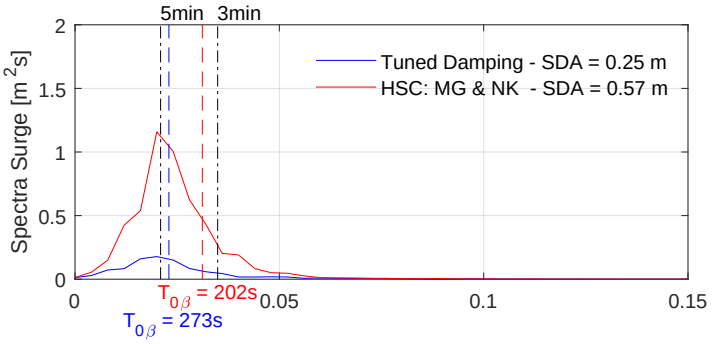

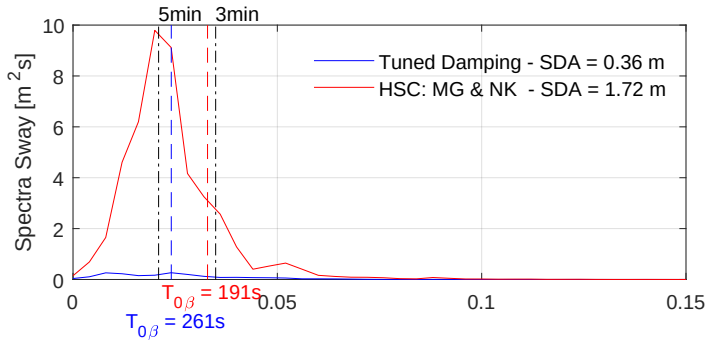

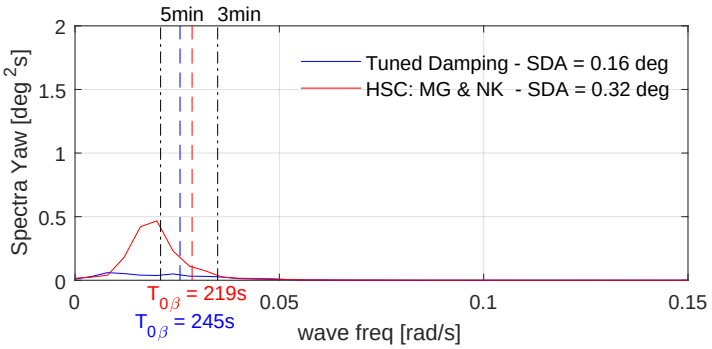

aNySIM & HSC Comparison - Normal Kalman & Medium Gain - Waves: Hs=2m, Tp=9s, Dir=330deg (going to - aNySIM)
aNySIM - Spring: Obtained from HSC, Damping: β_{Surge} = 60%, β_{Sway} = 60%, β_{Yaw} = 45%

Motion TimeTrace

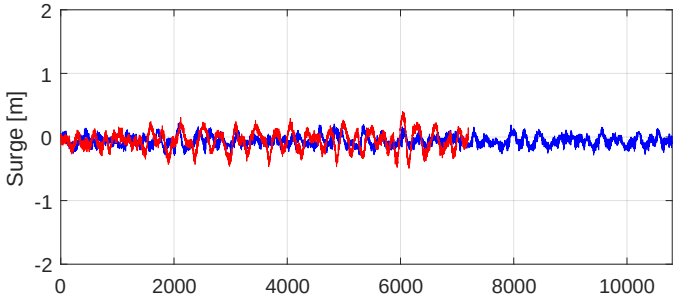

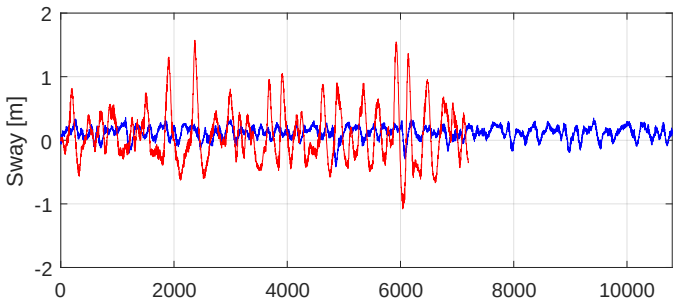

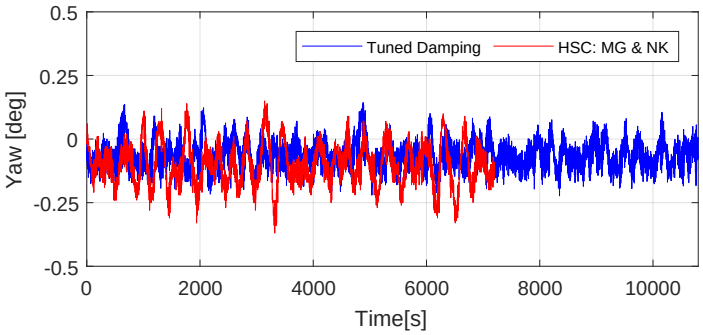

Motion EDS

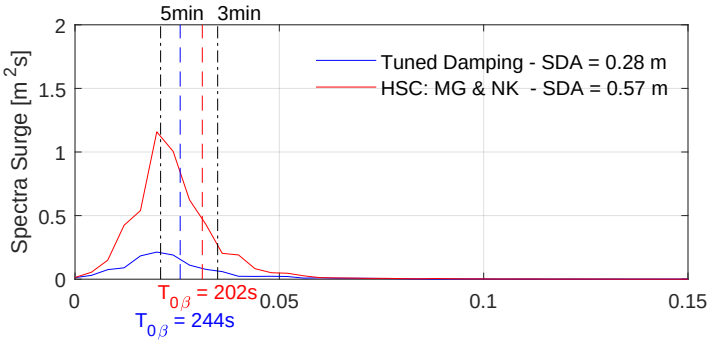

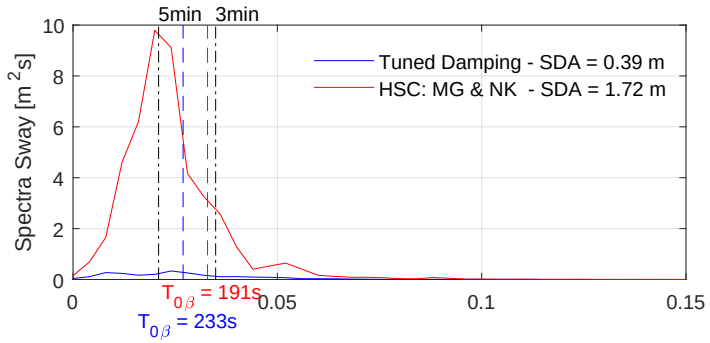

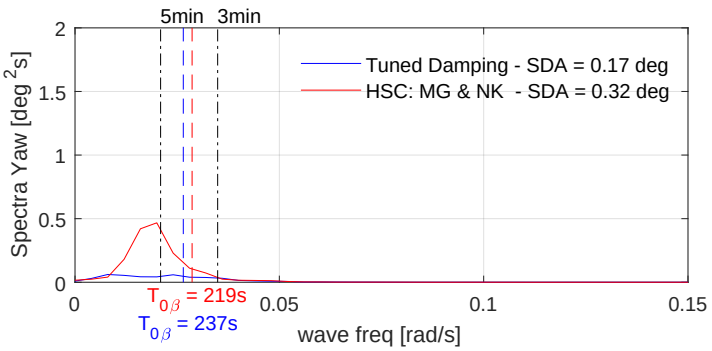

aNySIM & HSC Comparison - Normal Kalman & Medium Gain - Waves: Hs=2m, Tp=9s, Dir=330deg (going to - aNySIM)
aNySIM - Spring: Obtained from HSC, Damping: β_{Surge} = 50%, β_{Sway} = 50%, β_{Yaw} = 40%

Motion TimeTrace

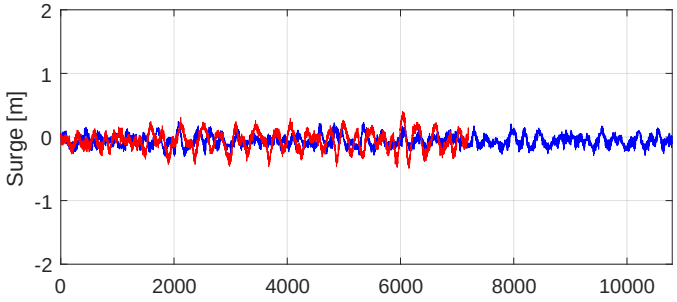

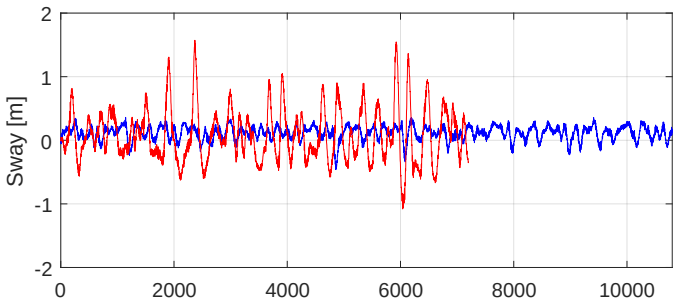

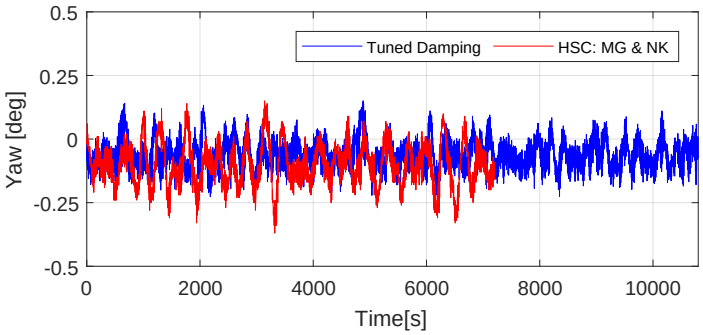

Motion EDS

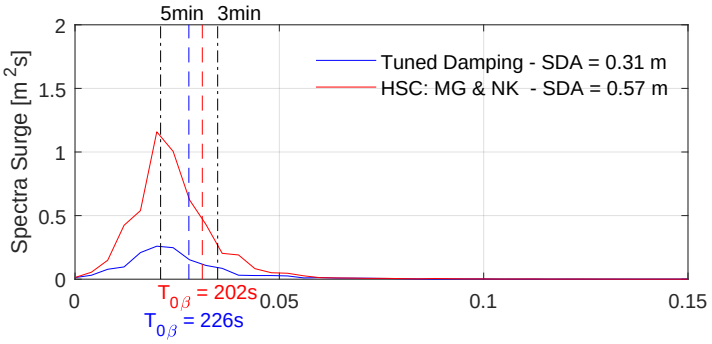

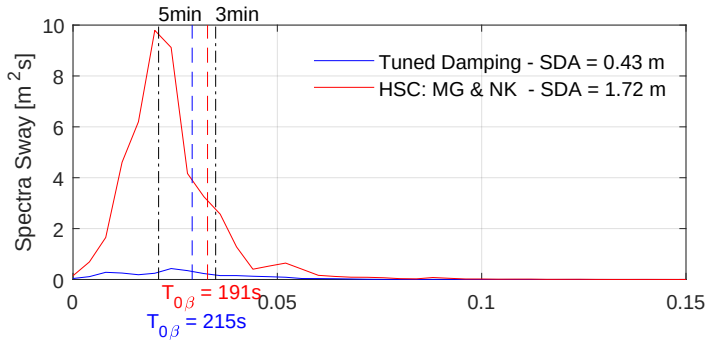

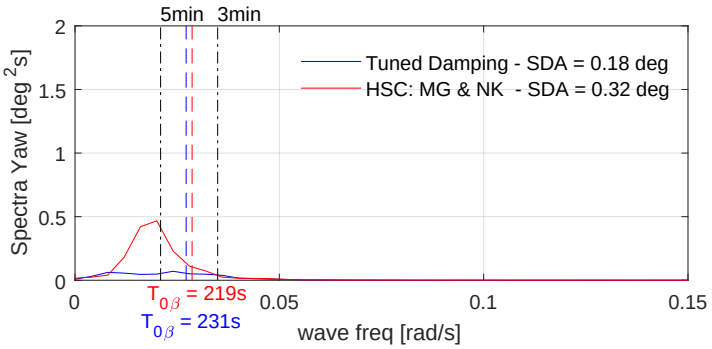

aNySIM & HSC Comparison - Normal Kalman & Medium Gain - Waves: Hs=2m, Tp=9s, Dir=330deg (going to - aNySIM)
aNySIM - Spring: Obtained from HSC, Damping: β_{Surge} = 40%, β_{Sway} = 40%, β_{Yaw} = 35%

Motion TimeTrace

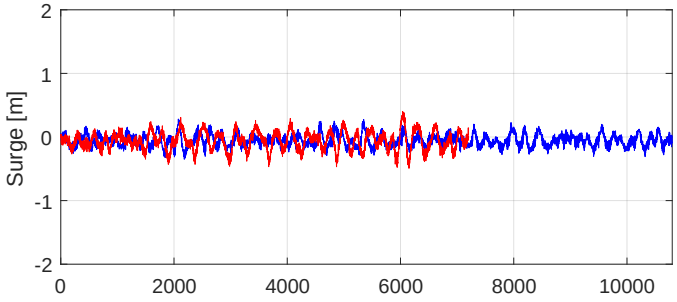

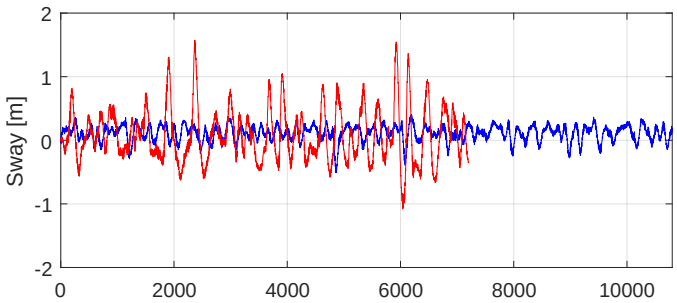

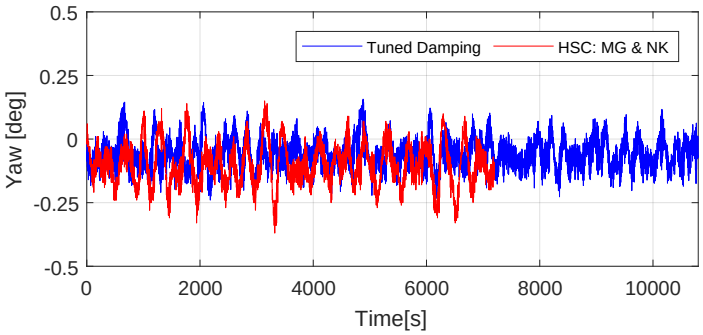

Motion EDS

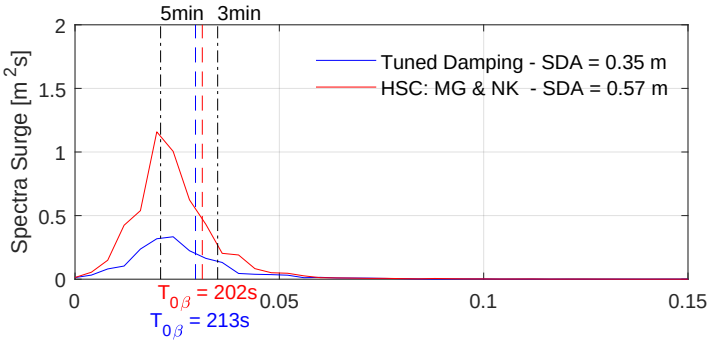

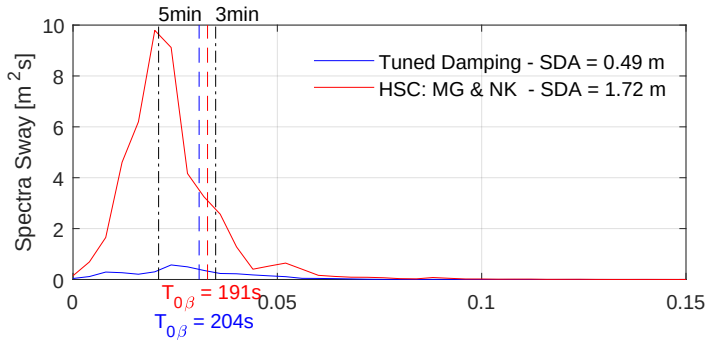

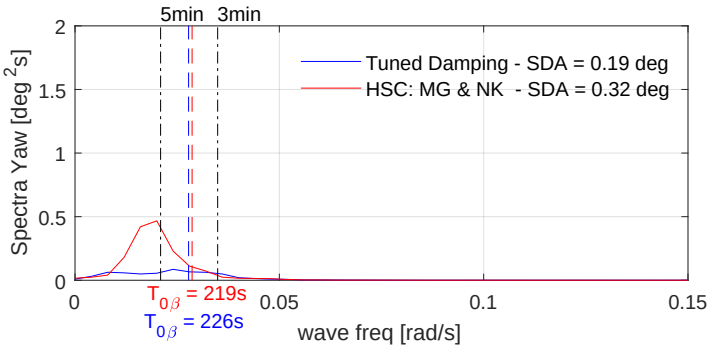

aNySIM & HSC Comparison - Normal Kalman & Medium Gain - Waves: Hs=2m, Tp=9s, Dir=330deg (going to - aNySIM)
aNySIM - Spring: Obtained from HSC, Damping: β_{Surge} = 30%, β_{Sway} = 30%, β_{Yaw} = 30%

Motion TimeTrace

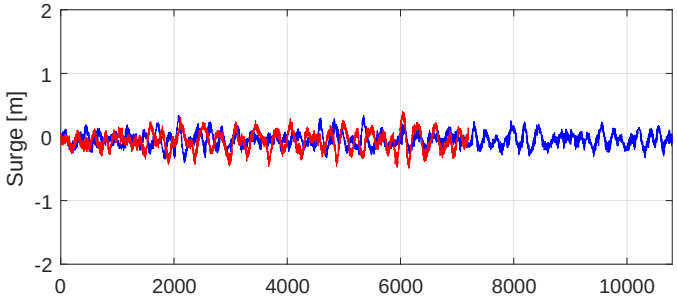

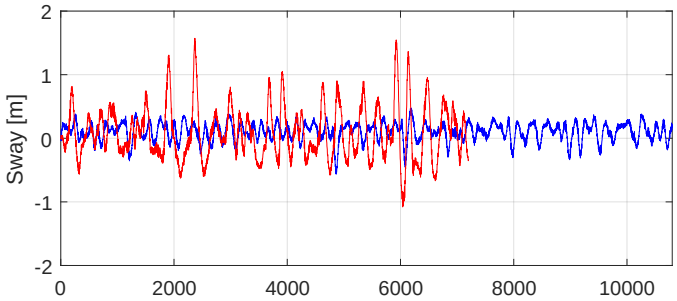

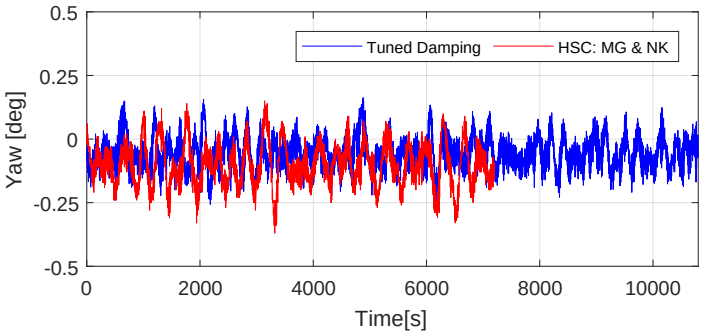

Motion EDS

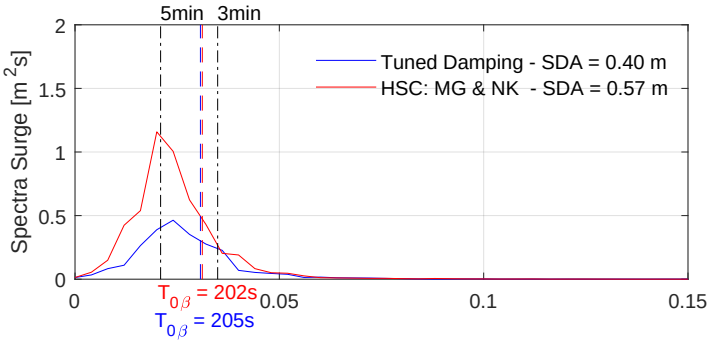

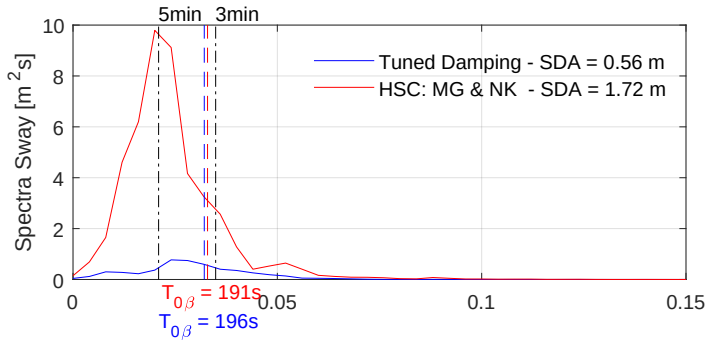

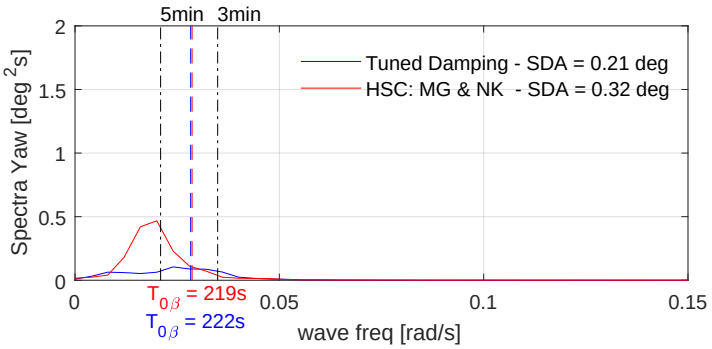

aNySIM & HSC Comparison - Normal Kalman & Medium Gain - Waves: Hs=2m, Tp=9s, Dir=330deg (going to - aNySIM)
aNySIM - Spring: Obtained from HSC, Damping: β_{Surge} = 20%, β_{Sway} = 20%, β_{Yaw} = 20%

Motion TimeTrace

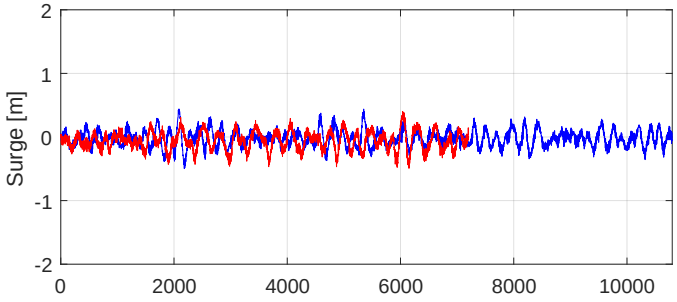

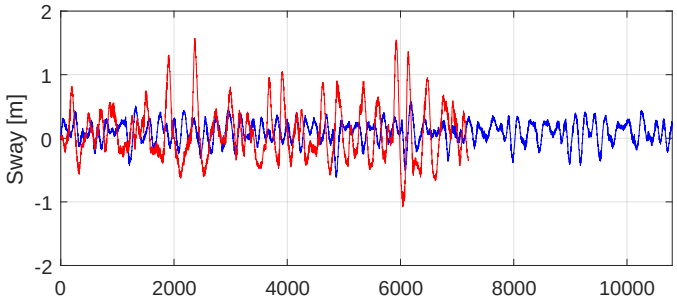

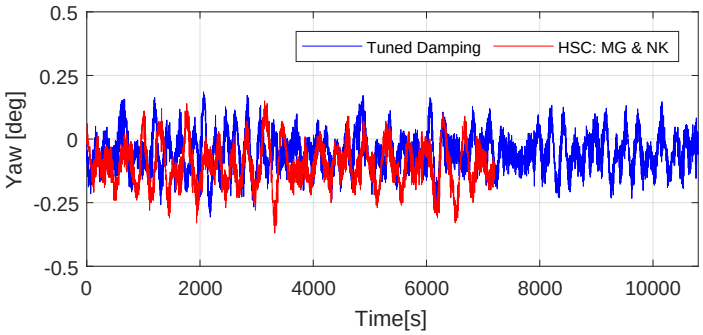

Motion EDS

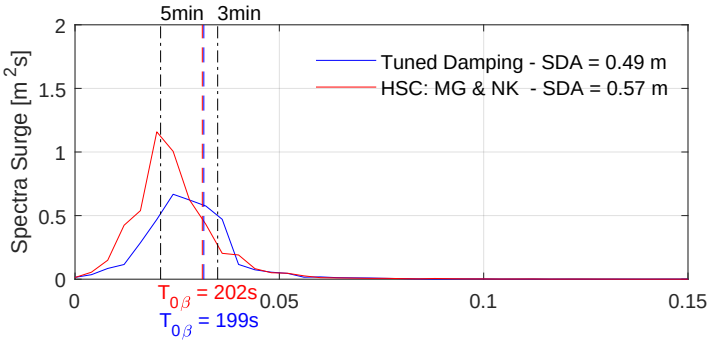

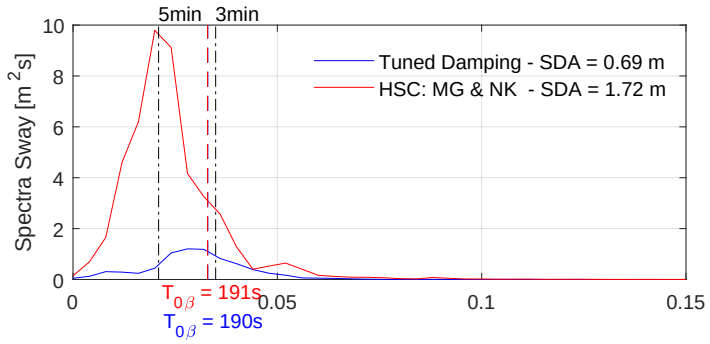

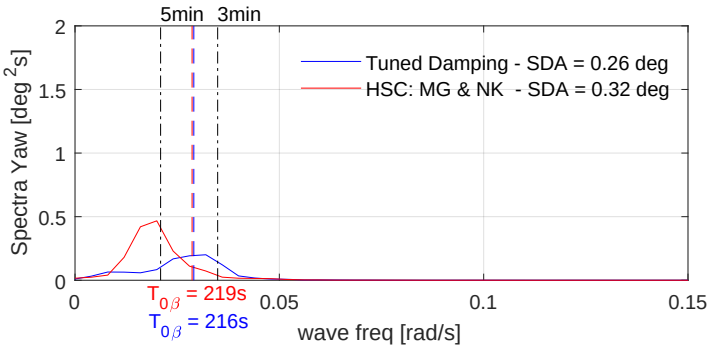

aNySIM & HSC Comparison - Normal Kalman & Medium Gain - Waves: Hs=2m, Tp=9s, Dir=330deg (going to - aNySIM)
aNySIM - Spring: Obtained from HSC, Damping: β_{Surge} = 15%, β_{Sway} = 15%, β_{Yaw} = 15%

Motion TimeTrace

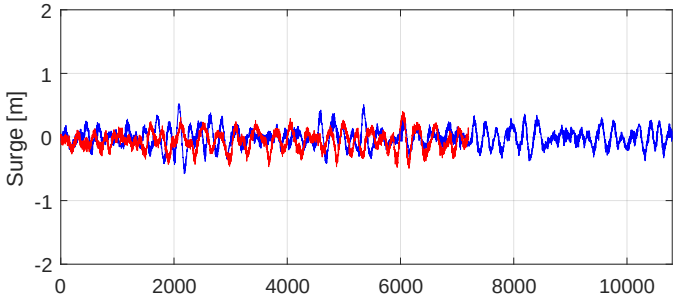

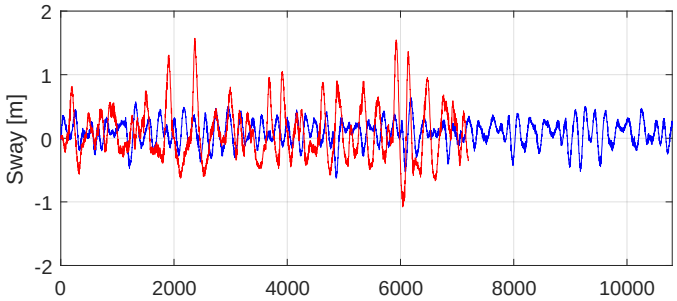

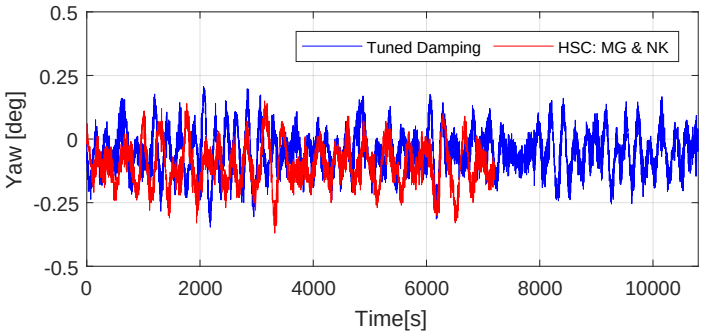

Motion EDS

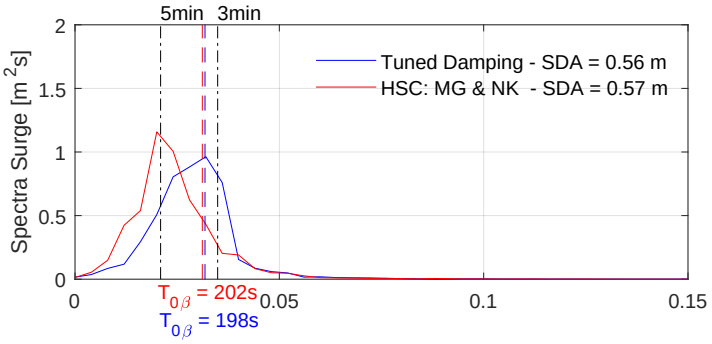

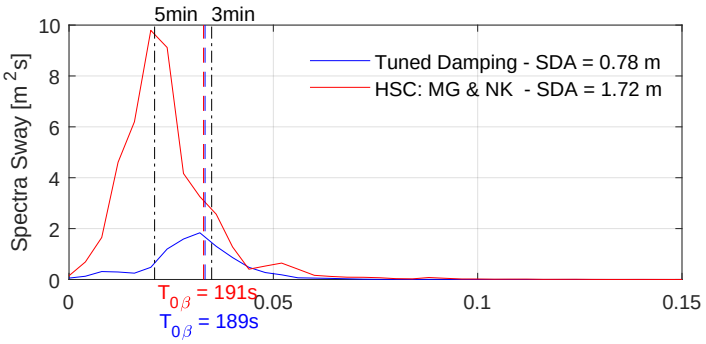

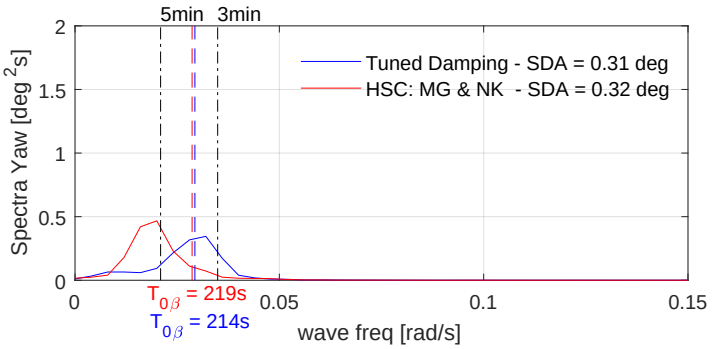

aNySIM & HSC Comparison - Normal Kalman & Medium Gain - Waves: Hs=2m, Tp=9s, Dir=330deg (going to - aNySIM)
aNySIM - Spring: Obtained from HSC, Damping: β_{Surge} = 10%, β_{Sway} = 10%, β_{Yaw} = 10%

Motion TimeTrace

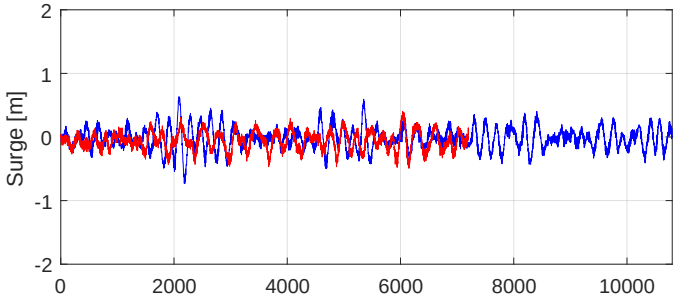

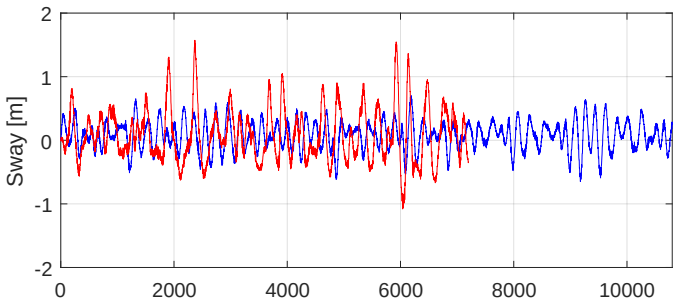

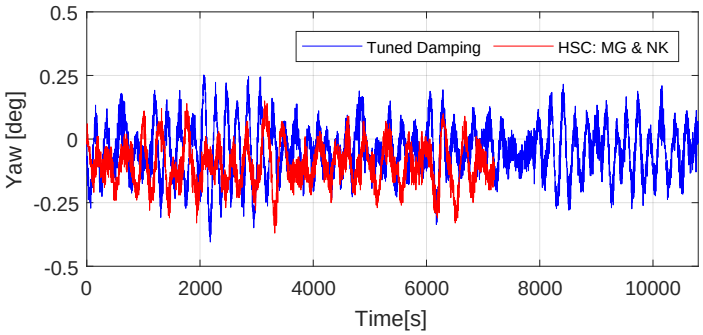

Motion EDS

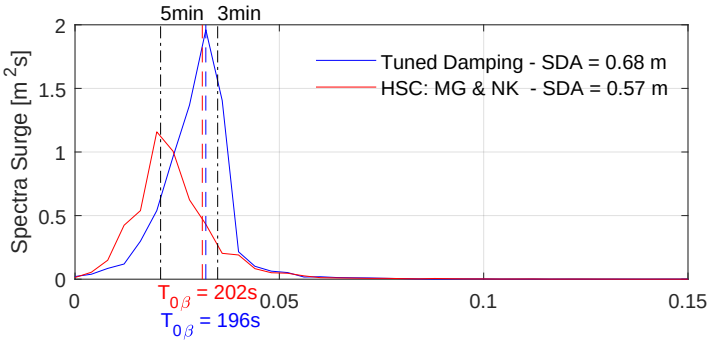

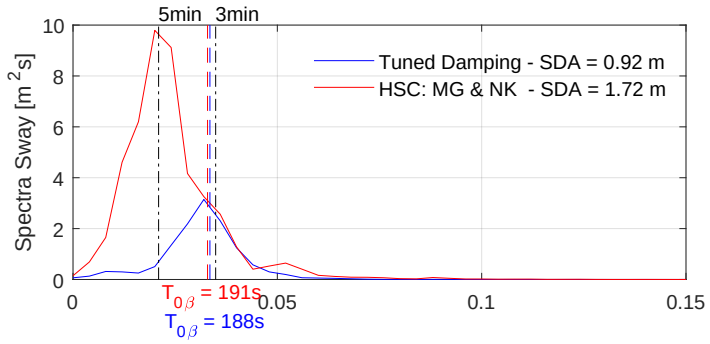

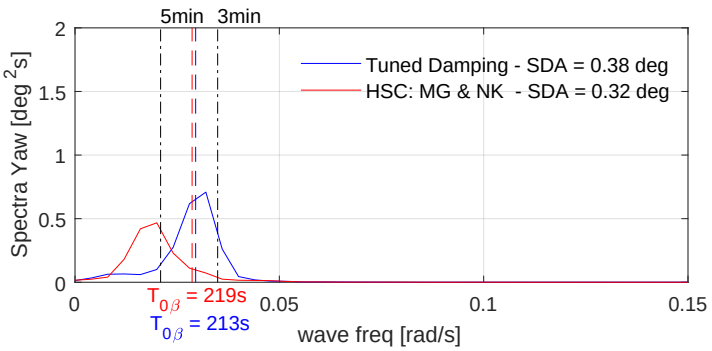

aNySIM & HSC Comparison - Normal Kalman & Medium Gain - Waves: Hs=2m, Tp=9s, Dir=330deg (going to - aNySIM)
aNySIM - Spring: Obtained from HSC, Damping: β_{Surge} = 5%, β_{Sway} = 5%, β_{Yaw} = 5%

Motion TimeTrace

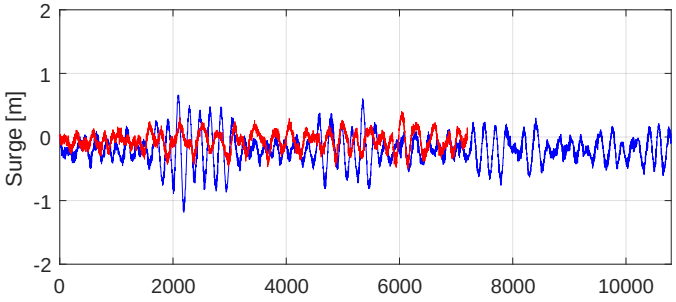

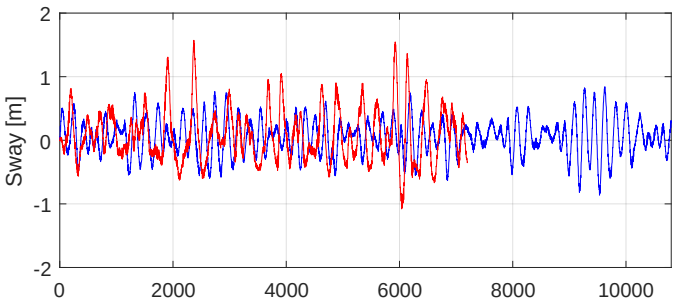

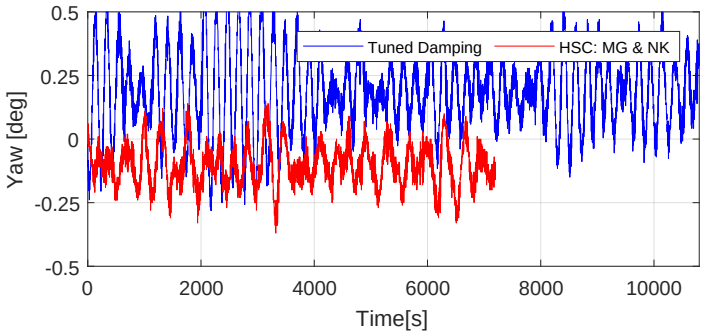

Motion EDS

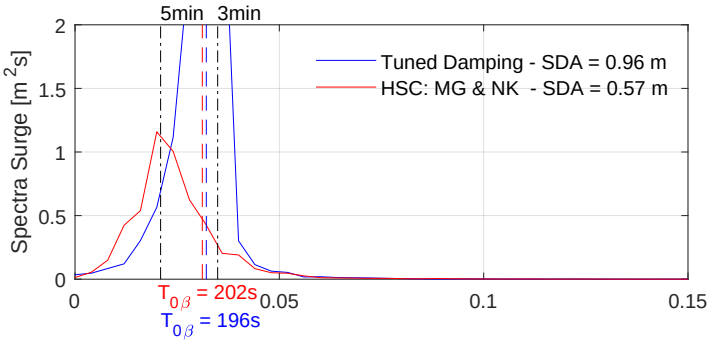

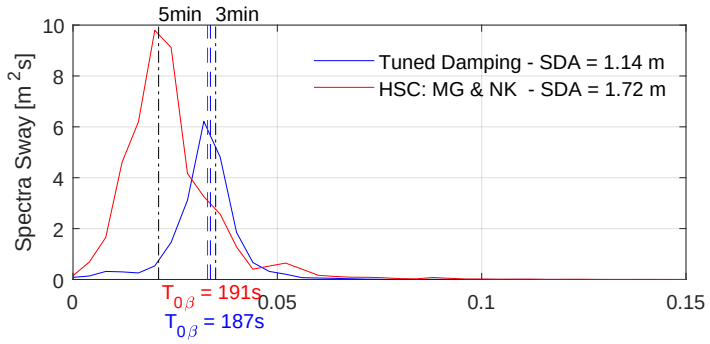

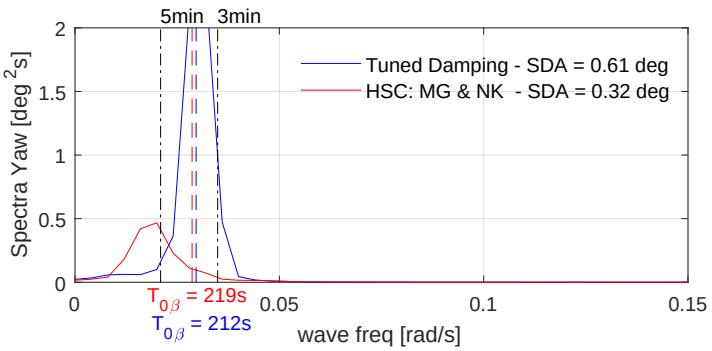

Extrapolation Method Proof Single Cylinder Case

The applicability of the extrapolation method will be demonstrated with a theoretical base case of a circular cylinder. A cylinder with a diameter of 0.2 m and a length of 1 m that is exposed to current flow. As previously specified, it will experience drag and for Rn >65 alternating lift forces due to vortex shedding. In this case, the interest lies on the alternating lift force. For this example, the cylinder is assumed to be exposed to 2 flow velocities, V_1 = 1 m/s and V_2 = 2 m/s. First, the Reynolds number must be determined, for which a kinematic viscosity of fresh water at 20 °C, $\nu = 1.00374 \cdot 10^{-6}$m^{2}s is selected, at which ρ = 1000 kg/m^3. This yields the following, where the subscripts 1 and 2 relate to the flow velocities of 1 and 2 m/s respectively.

$$Rn_1 = \frac{V_1 \cdot D}{\nu} = \frac{1m/s \cdot 0.2m}{1.00374 \cdot 10^{-6}m^2s} = 1.99 \cdot 10^5$$

$$Rn_2 = \frac{V_2 \cdot D}{\nu} = \frac{2m/s \cdot 0.2m}{1.00374 \cdot 10^{-6}m^2s} = 3.98 \cdot 10^5$$

From figure 2.6 for Rn_1 and Rn_2 a Strouhal number of St=0.2 is selected. This results in the following vortex shedding frequencies:

$$fs_1 = \frac{St \cdot V_1}{D} = \frac{0.2 \cdot 1m/s}{0.2m} = 1Hz$$

$$fs_2 = \frac{St \cdot V_2}{D} = \frac{0.2 \cdot 2m/s}{0.2m} = 2Hz$$

Based on [33], a dimensionless lift coefficient of C_L=0.03 was selected for this case. For a duration of t_{end} = 60 s, the alternating lift forces for V_1 = 1 m/s and V_2 = 2 m/s, which can be seen in figure F.1 for a length of L = 1 m is obtained by:

$$F_{l_1} = \frac{1}{2}\rho \cdot V_1^2 \cdot D \cdot C_L \cdot sin(2\pi \cdot fs_1 \cdot t) \cdot L$$

$$F_{l_2} = \frac{1}{2}\rho \cdot V_2^2 \cdot D \cdot C_L \cdot sin(2\pi \cdot fs_2 \cdot t) \cdot L$$

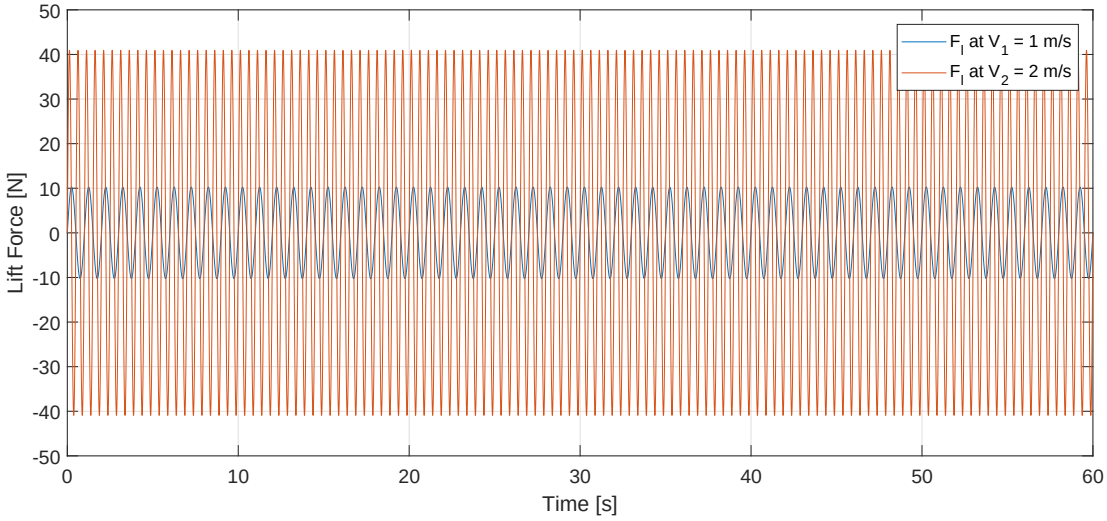

Figure F.1: Alternating lift forces on cylinder for V_1 = 1 m/s and V_2 = 2 m/s

The according EDS of these time traces can be seen below in figure F.2. In this figure, the peak of the energy content can be seen at the vortex shedding frequencies of $\omega s_1 = 2\pi \cdot fs_1 = 2\pi$ and $\omega s_2 = 2\pi \cdot fs_2 = 4\pi$. According to the previously presented method, the EDS of the lift force from V_2 = 2 m/s has been extrapolated in the frequency domain to the V_1 = 1 m/s. This extrapolated EDS can also be observed with the black dotted line. Moreover, the SDA, based on equation 2.15, was obtained from the already extrapolated spectra and indicates the same magnitude as the measured EDS at V_1 = 1m/s.

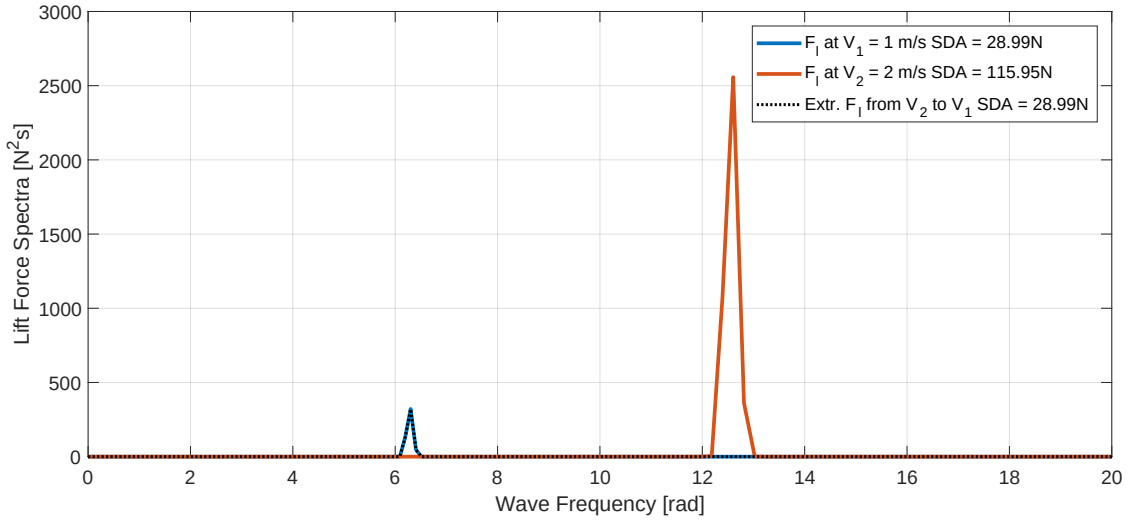

Figure F.2: Energy density spectrum of alternating lift forces on cylinder for V_1 = 1 m/s, V_2 = 2 m/s and extrapolated from V_2 to V_1

In this base case per velocity only one vortex shedding frequency is present. The result shows, that the extrapolated forces have the same frequency than the theoretical and represents the successful extrapolation of the energy content per frequency in the frequency domain. It also represents well the decrease of energy of the EDS, due to the established cubic relation.

G

Current Load Test Extrapolation Station Keeping Simulation Results

G.1. Ideal DP System

45° heading

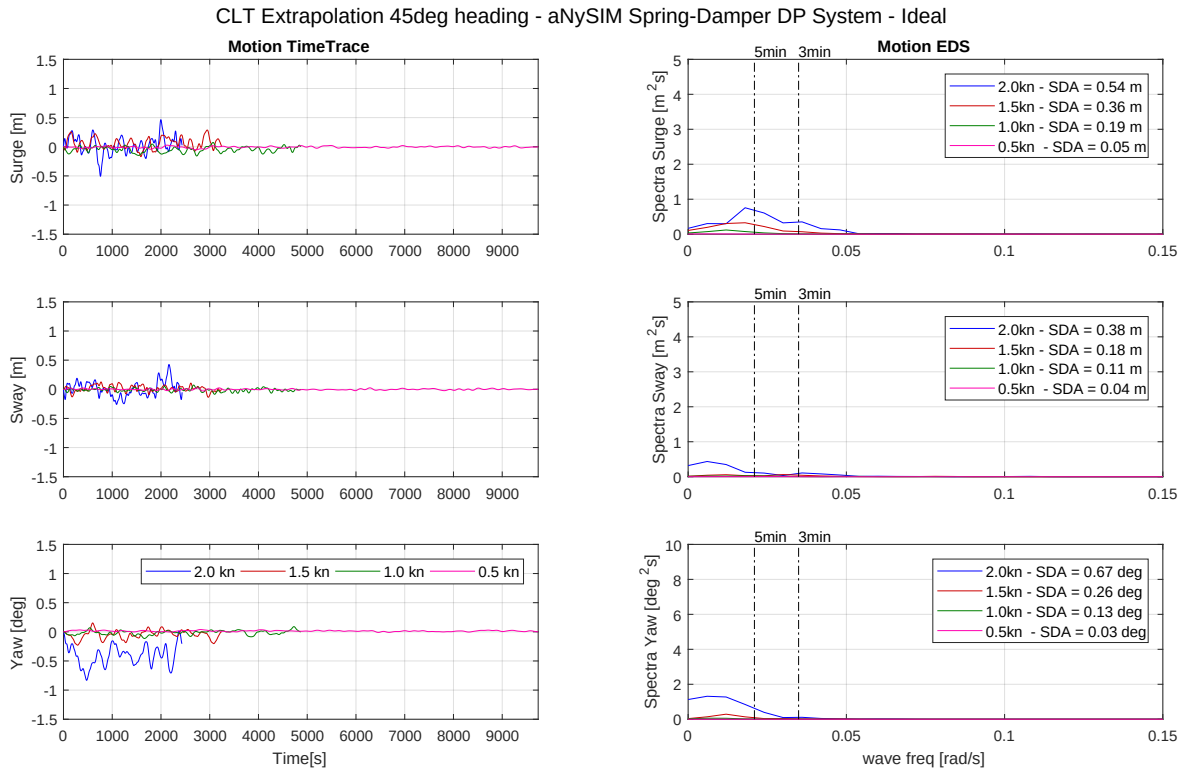

Figure G.1: Result of 45° heading extrapolated and measured current load test aNySIM Spring-Damper simulation - Ideal

60° heading

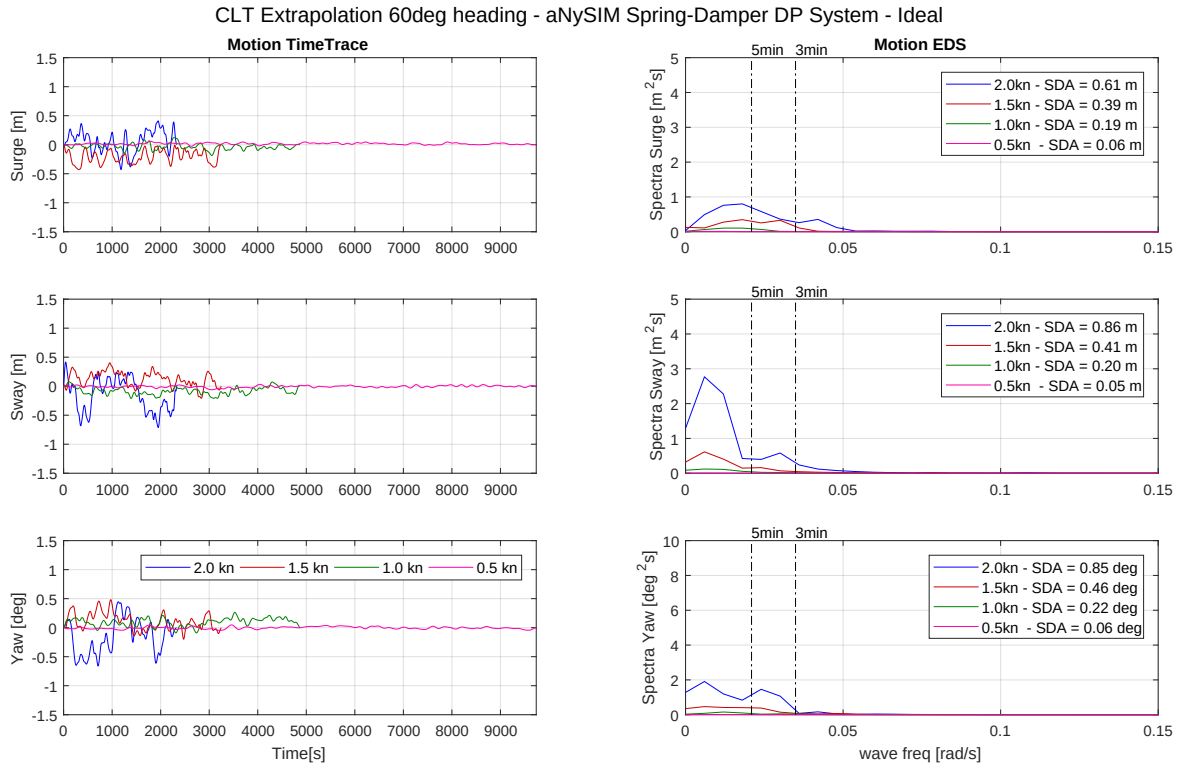

Figure G.2: Result of 60° heading extrapolated and measured current load test aNySIM Spring-Damper simulation - Ideal

90° heading

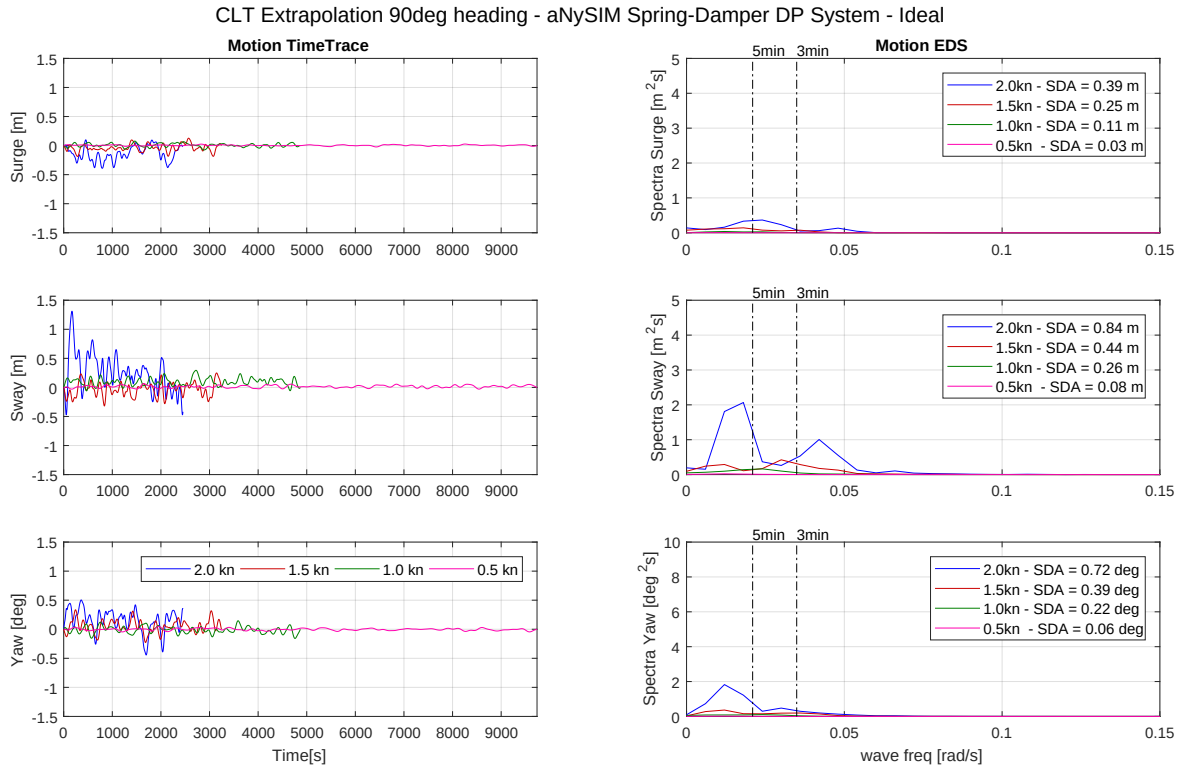

Figure G.3: Result of 90° heading extrapolated and measured current load test aNySIM Spring-Damper simulation - Ideal

150° heading

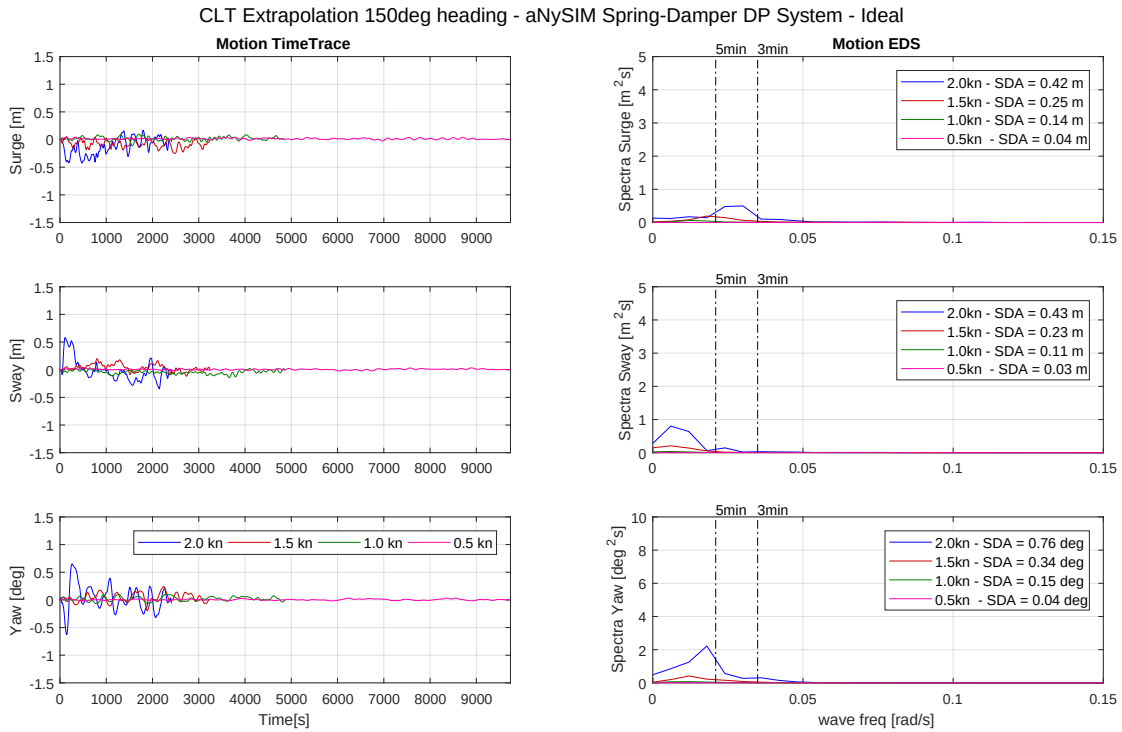

Figure G.4: Result of 150° heading extrapolated and measured current load test aNySIM Spring-Damper simulation - Ideal

G.2. Not-Ideal DP System

45° heading

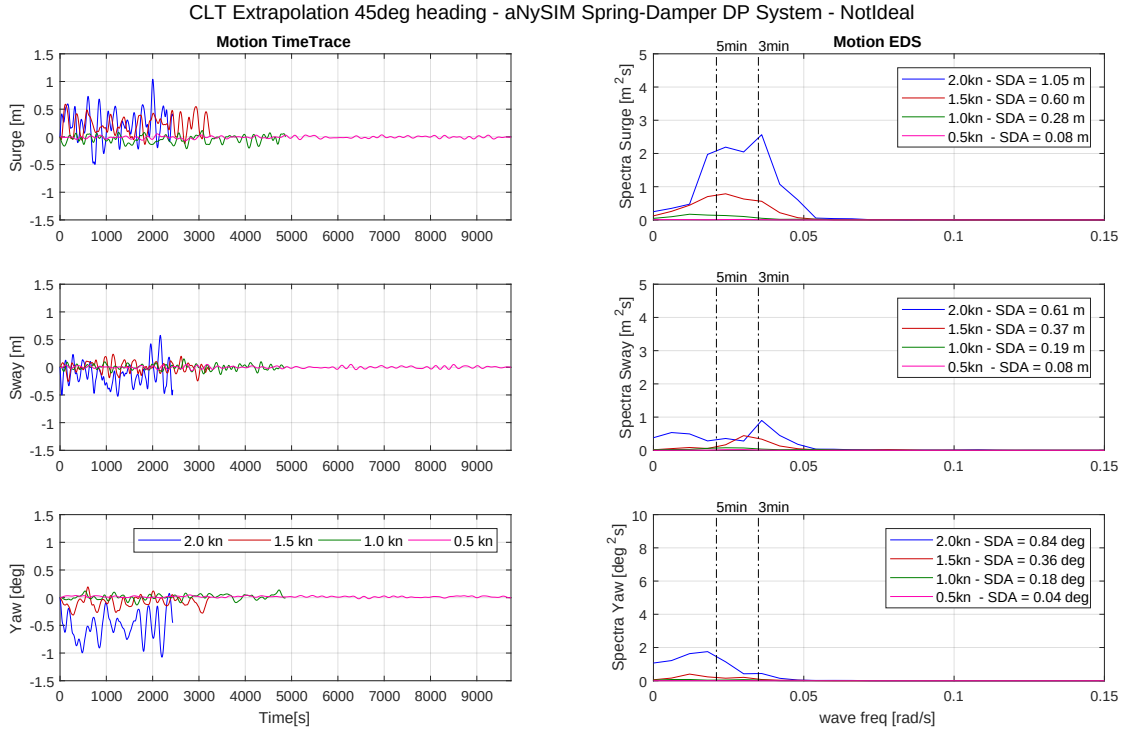

Figure G.5: Result of 45° heading extrapolated and measured current load test aNySIM Spring-Damper simulation- NotIdeal

60° heading

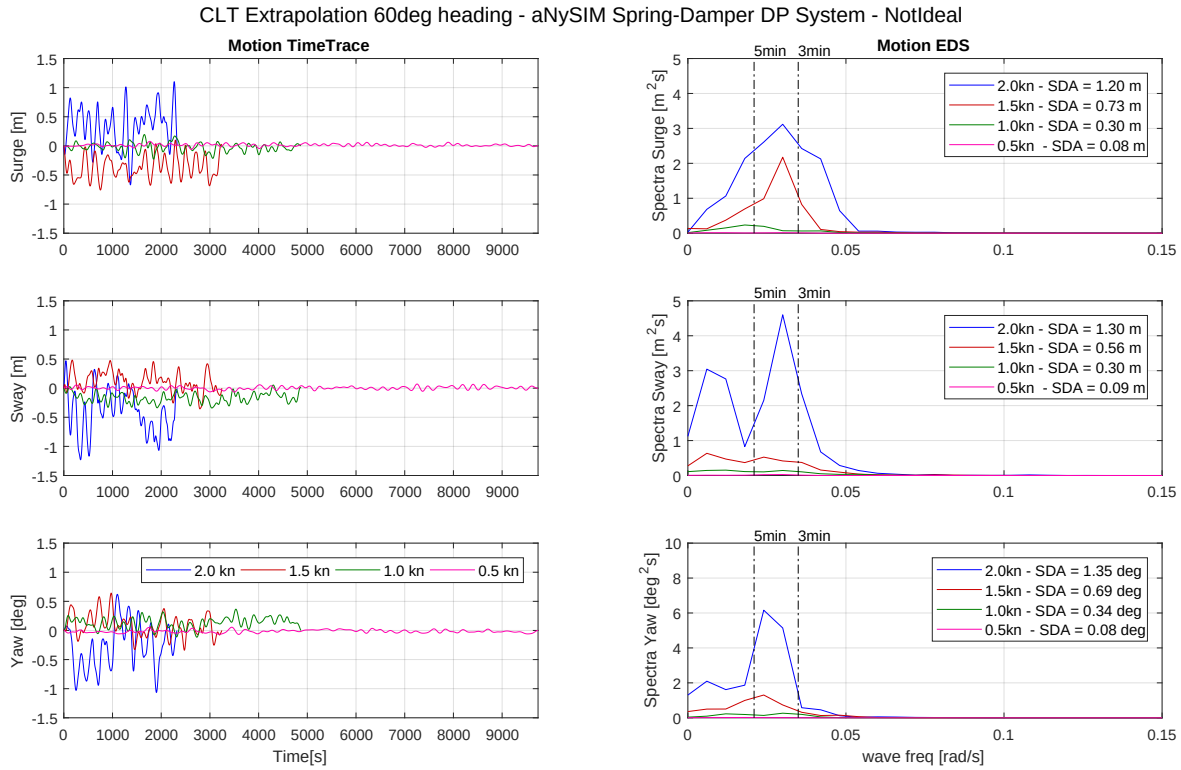

Figure G.6: Result of 60° heading extrapolated and measured current load test aNySIM Spring-Damper simulation- NotIdeal

90° heading

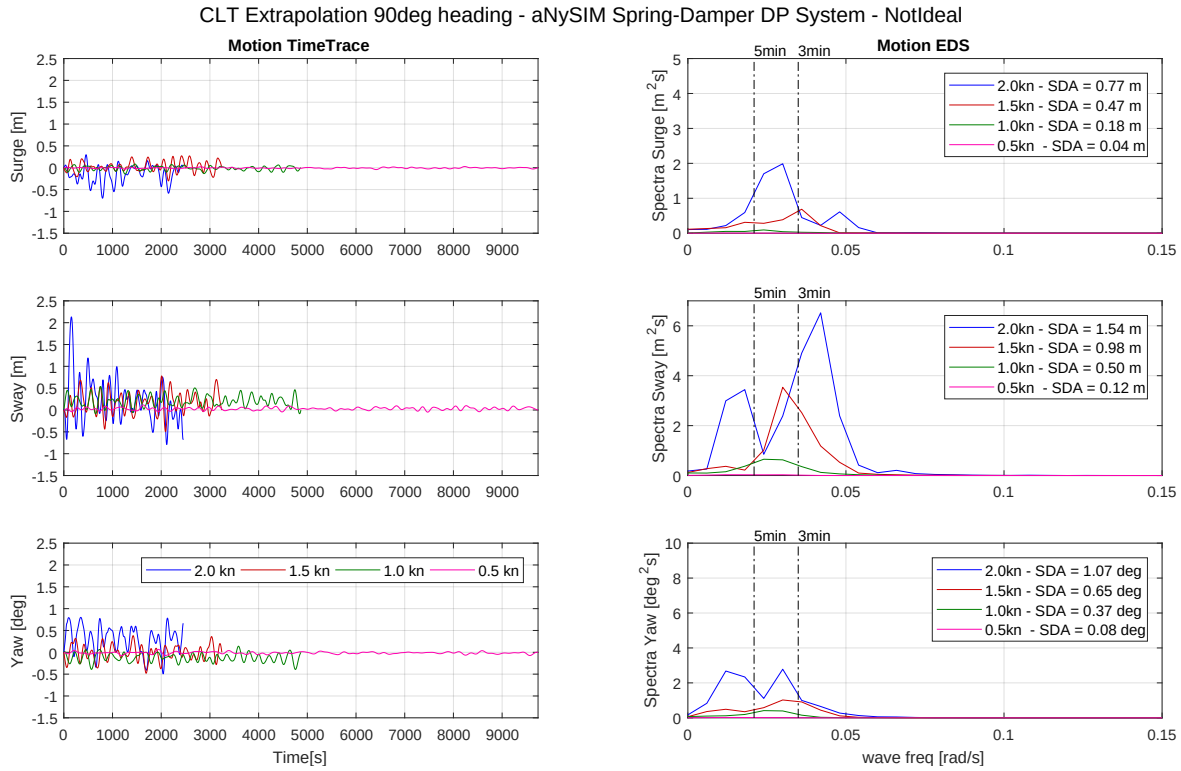

Figure G.7: Result of 90° heading extrapolated and measured current load test aNySIM Spring-Damper simulation- NotIdeal

150° heading

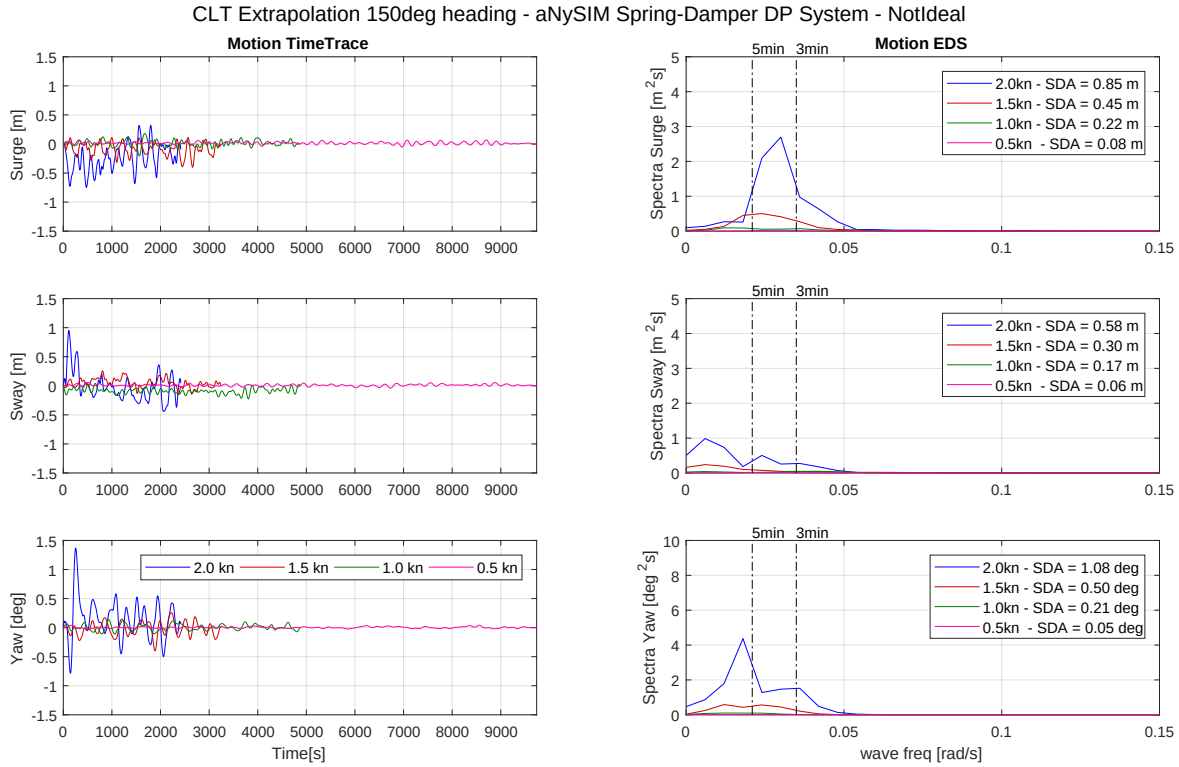

Figure G.8: Result of 150° heading extrapolated and measured current load test aNySIM Spring-Damper simulation - NotIdeal